Investigation of pathophysiological mechanisms in clinically isolated syndrome using advanced imaging techniques

Sara Collorone MD

Queen Square MS Centre

Department of Neuroinflammation

UCL Institute of Neurology

London WC1N 3BG

Thesis submitted to University College London for the degree of Doctor of Philosophy May 2020

I, Sara Collorone confirm that the work presented in this thesis is my own. Where information has been derived from other sources, I confirm that this has been indicated in the thesis.

Dr Niamh Cawley contribute to the cohort recruitment and assessment. Dr Ferran Prados and Dr Baris Kanber assisted with the imaging analysis presented in Chapters 5, 7 and 8. Dr Carmen Tur assisted with statistical analysis for Chapter 7. Dr Indran Davagnanam helped with the inter-rater agreement for multiple sclerosis lesions in Chapter 7. Dr Dan Altmann assisted with the statistical analysis presented in Chapter 8.

London, 22.06.2020 Signed

Abstract

This thesis concerns an observational study of patients recruited after their first episode of neurological symptoms suggestive of demyelination in the central nervous system and diagnosed either with clinically isolated syndrome or relapsing-remitting multiple sclerosis.

In multiple sclerosis, brain tissues can exhibit extensive neuroaxonal microstructural and metabolic abnormalities, but little is known about their presence and significance at the time of the first demyelinating episode. I used a novel multi-parametric quantitative MRI approach, combining neurite orientation dispersion and density imaging (NODDI), which gives information about tissue microstructure, and ^{23}Na MRI, which estimates total sodium concentration, a marker of metabolic dysfunction, in the brains of clinically isolated syndrome patients. I found microstructural and sodium homeostasis alterations in cortical areas of patients that showed clinical relevance. Within the diffuse axonal dispersion found in the normal-appearing white matter, the corpus callosum shared with lesions, signs of axonal damage and metabolic dysfunction, thus emerging as a possible target for early neuroprotective interventions.

Structural cortical networks (SCNs) represent patterns of coordinated morphological modifications in cortical areas and they have shown pathophysiological changes in many brain disorders, including multiple sclerosis. I investigated alterations of SCNs at the individual level in this early cohort. Patients showed altered small-world topology, an efficient network organization combining dense local clustering with relatively few long-distance connections. These disruptions were worse for patients with higher lesion load and worse cognitive processing speed indicating that pathophysiological changes in the cortical morphology can influence clinical outcomes.

Finally, I hypothesised that the patients in the cohort presenting with ON may have disturbances in neuropsychological functions related to visual processes. I found that cognitive visuospatial processing is affected after unilateral ON

and improves over time with visual recovery, independently of the structural damage in the visual and central nervous system.

Impact statement

Benefits inside academia.

MRI studies in both the brain and spinal cord are generally rare due to the long acquisition times and the difficulties in adapting MRI models to two different structures. Here, I have shown the possible application of a novel diffusion technique, neurite orientation dispersion and density imaging (NODDI), in the neuroaxis of multiple sclerosis patients demonstrating clinically relevant alterations in both the brain and spinal cord. This accomplishment has already had an impact in the academic world interested in the discovery of new biomarkers for multiple sclerosis: in one year, three review papers in the field have cited the paper derived from this project (Lakhani *et al.*, 2020; Rocca *et al.*, 2020; Tavazzi *et al.*, 2020). Furthermore, this project's novel methodology opens the doors to future researchers interested in the application of quantitative MRI in the neuroaxis of neurological disorders besides multiple sclerosis.

The findings reported in my thesis have given me the basis for post-doctoral fellowship applications. For the first time in early MS patients, I found microstructural and metabolic alterations in the normal-appearing brain tissues and white matter lesions. The presentation of the preliminary findings of this project received interest from the multiple sclerosis scientific community and it was awarded a poster prize at the annual ECTRIMS meeting in 2018.

In the future fellowship, I will move forward and investigate individual lesion features and determine which features are associated with disease activity (i.e., gadolinium-enhancing) and disability accrual.

For the first time, I have shown that it is possible to investigate retrospectively structural cortical networks from already acquired anatomical scans in a multi-centre setting. The dataset I have used was from the Magnetic Resonance Imaging in Multiple Sclerosis (MAGNIMS), a consortium that has made a significant contribution to defining the role of MRI in diagnosis and monitoring treatments in multiple sclerosis. Hence, the technique I have used can now be extended to other MAGNIMS datasets with different disease phenotypes.

Benefits outside academia.

The discoveries presented in my thesis also have possible impacts in the clinical setting.

In the short-medium term, I will contribute to the Quantitative Neuroradiology Initiative (QNI) that aims to translate the latest advances in neuroimaging analysis into clinical applications using radiological reports.

In the long term, my findings will contribute to the use of novel biomarkers in multiple sclerosis patients. Clinical trials in advanced multiple sclerosis patients are employing the advanced MRI techniques used in this thesis, i.e., NODDI and 23Na MRI. Therefore, the knowledge arisen from this thesis will provide a future reference for interventions in early patients. Specifically, I have identified the corpus callosum as a vulnerable structure that can be the target for neuroprotective trials.

Finally, I have provided evidence that the impaired visual function in optic neuritis patients can influence the cognitive performance in the brief cognitive assessment for multiple sclerosis (BICAMS), a battery specifically designed for clinical applications. Therefore, clinicians are encouraged to assess visual acuity when testing BICAMS in patients with optic neuritis.

Acknowledgements

This research would not have been possible without the financial support of the Rosetrees Trust, the ECTRIMS-MAGNIMS fellowship programme and the United Kingdom Multiple Sclerosis Society.

I'm sincerely grateful to all the people who have participated in this research, travelling long distances to attend the appointments and giving up their time for MRI scans and clinical assessments. Without their help and dedication this work would have been impossible.

I would like to express my profound gratitude to my supervisors for their constant support and their expert guidance throughout my PhD. They have been inspirational mentors over these years and helped me secure the funding for my PhD. I would like to thank Dr Ahmed Toosy for teaching me the neuro-ophthalmology skills and for providing me so much encouragement and motivation. The recruitment of patients at the onset of multiple sclerosis is a long and challenging process. He has always been supportive and helpful in dealing with the setbacks this project has presented. It is thanks to Prof Olga Ciccarelli if I developed my interest in the application of advanced MRI in multiple sclerosis and started a PhD at UCL. She has been a constant source of inspiration as a thriving academic woman and always gave me valuable advice and kind help for my career. I would like to thank Prof Frederik Barkhof whose insight and knowledge into the MRI and multiple sclerosis field guided me through this research and his great help with ECTRIMS-MAGNIMS fellowship.

I would like to thank Prof Alan Thompson. I have had the privilege to work in his clinic and I am thankful for his expert clinical teaching about MS management.

I would like to thank the physics team and their leader Prof Claudia Gandini Wheeler-Kingshott, who have developed the MRI protocols used in this thesis. Particularly, Prof Claudia Gandini Wheeler-Kingshott for helping me in the understanding of the MRI physics behind these techniques, Dr Ferran Prados, whose IT expertise and knowledge has been fundamental for the imaging post-

processing, Dr Baris Kanber for his help with Xnat, Dr Francesco Grussu and Dr Bhavana Solanky, the NODDI and ^{23}Na MRI “gurus”, respectively.

I would like to thank the radiographers who have worked at our 3 T scanner, particularly Marios Yiannakas for his patient support during the endless MRI sessions.

I feel I have been privileged to work in a wonderful and supporting team such as the one of the Queen Square MS Centre. I would like to thank Tina Holmes, Charlotte Burt, Marie Braisher and Jon Steel, for their indispensable administrative and technical support. I would like to thank my colleagues for their support and friendship during these years in London: Rosa Cortese, Floriana De Angelis, Alberto Calvi, Anisha Doshi, Karen Chung, Alessia Bianchi, Sarah Alexander, Nevin John, Arman Eshaghi, Becky Samson, Marco Battiston, Elisa Colato, Vanessa Bassan, Tiggy Beyene.

I am indebted to Prof Dan Altmann and Dr Carmen Tur who take the time to teach me statistical methods and answer my many questions.

I would like to thank my friends. Fabrizia and Francesca, I have planned and started this journey with them, and their friendship has been vital during these years. Felice, who provided me with the London “starter pack” to set up here. My friends in Italy and abroad (Martina, Giulia, Corinna, Marianna e Isabella): the distance has only tightened our bonds.

I would like to thank my family. My mother and my father, who have sustained me throughout this long journey with their unconditioned love and born the distance, particularly during this difficult time. Leonardo, for his endless patience, help and support over the years, deadline after deadline, stress after stress. I do not know how I would have survived without him during this lockdown-writing up period.

Finally, I would like to dedicate this thesis to my grandmother, a modern woman who has always supported my choices with her infinite love and whose memory will always give me guidance and reassurance during my life.

Publications associated with this thesis

Collorone S, Prados F, Hagens MH, Tur C, Kanber B, Sudre CH, et al. Single-subject structural cortical networks in clinically isolated syndrome. Mult Scler J 2019: 135245851986573.

Collorone S, Cawley N, Grussu F, Prados F, Tona F, Calvi A, et al. Reduced neurite density in the brain and cervical spinal cord in relapsing–remitting multiple sclerosis: A NODDI study. Mult Scler J 2019: 135245851988510.

Collorone S., Prados F., Kanber B., Cawley N., Tur C., Grussu F., et al. Brain microstructural and metabolic alterations detected in vivo at the onset of the first demyelinating event. *Internal revisions*

Collorone S., Kanber B., Hashem L., Cawley N., Prados F., N., Davgnanam I., et al. Visual Function and Brief Cognitive Assessment for Multiple Sclerosis (BICAMS) in Optic Neuritis Clinically Isolated Syndrome Patients. *Submitted to Journal of Neuroopthalmology*

Cortese R*, **Collorone S***, Ciccarelli O, Toosy AT. Advances in brain imaging in multiple sclerosis. Ther Adv Neurol Disord 2019; 12: 175628641985972. *Joint first authors

Index

List of Tables

List of figures

Abbreviations

AD: axial diffusivity

APC: antigen-presenting cell

ART: automatic real-time

ATP: adenosine triphosphate

BBB: blood-brain barrier

BICAMS: brief cognitive assessment for multiple sclerosis

BVMTR: brief visuospatial memory test-revised

CGM: cortical gray matter

CI: confidence interval

CIS: clinically isolated syndrome

CNS: central nervous system

CSA: cross-sectional area

CSF: cerebrospinal fluid

CVLTII: California verbal learning test-II

DT: diffusion tensor

DTI: diffusion tensor imaging

DWI: diffusion-weighted imaging

EAE: experimental autoimmune encephalomyelitis

EDSS: expanded disability status scale

ETDRS: early treatment diabetic retinopathy study

FA: fractional anisotropy

GCIPL: combined ganglion cell- inner plexiform layer

GCL: ganglion cell layer

HADS: hospital anxiety and depression scale

HCLA: high-contrast letter acuity

INL: inner nuclear layer

IPL: inner plexiform layer

ISOVf: fractional isotropic volume

LCLA: low-contrast letter acuity

LogMar: logarithm of minimum angle of resolution

MAGNIMS: magnetic resonance imaging in multiple sclerosis

MD: mean diffusivity

MHC: major histocompatibility complex

MRI: magnetic resonance imaging

MSFC: multiple sclerosis functional composite

NDI: neurite density index

NO: nitric oxide

NODDI: Neurite orientation dispersion and density imaging

OCT: optical coherence tomography

ODI: orientation dispersion index

ON: optic neuritis

PASAT: paced auditory serial addition test

PD: proton density

RD: radial diffusivity

RNFL: retinal nerve fiber layer

ROS: reactive oxygen species

SCN: structural cortical network

SD: standard deviation

SDMT: symbol digit modalities test

STIR: short-tau inversion-recovery

TBSS: tract-based spatial statistics

TES: total error score

TNF: tumour necrosis factor

TSC: total sodium concentration

Chapter 1 Thesis rationale

This thesis concerns an observational study of patients recruited after their first episode of neurological symptoms suggestive of demyelination in the central nervous system and diagnosed either with clinically isolated syndrome (CIS) or relapsing-remitting multiple sclerosis.

At this stage, the main tool routinely used to stratify the severity of the disease and formulate short-medium term decisions, such as the initiation of a treatment, is the magnetic resonance imaging (MRI) scan of brain and spinal cord. The metrics used are the number and location of the white matter lesions and their possible enhancement after contrast administration. Also, the presence of atrophy can be assessed, but its presence is rare at the onset of first symptoms. These parameters are not specific for pathological substrates and do not provide quantitative measures of the damage in the central nervous system. As a consequence, they give an incomplete picture of the patient status and show limited correlation with the clinical manifestation of the disease.

Furthermore, *post mortem* studies have demonstrated that inflammation, demyelination, and neuro-axonal loss can extensively involve the central nervous system, beyond the conventional MRI visible plaques. These processes may be present since the onset, but we can only have a limited evidence from pathological studies since in early cases they are, understandably, very rare.

Advanced imaging techniques can help measuring *in vivo* microstructural changes, thereby contributing to the understanding of multiple sclerosis from its early phases (Cortese et al., 2019).

In this thesis, I have assessed patients at their first neurological episode suggestive of demyelination with the following aims (i) to quantify the damage in the central nervous system and investigate the possible pathological processes behind it by using quantitative MRI techniques; (ii) to assess the clinical relevance, in terms of physical and cognitive disability, of the possible alterations detected with these techniques; (iii) to explore if pathophysiological changes in the cortical morphology can influence clinical outcomes; (iv) to determine if the presence of structural and functional damage in the visual pathway can affect the assessment of cognitive performances.

In the first three chapters I give a background for this thesis. In Chapter 2, I outline the clinical aspects of CIS, the criteria used to diagnose relapsing-remitting multiple sclerosis and the prognostic factors for further clinical attacks and disability accrual. In Chapter 3, I summarise the pathophysiological mechanisms behind the disease examining their correlation with conventional MRI metrics. In Chapter 4, I give a background and rationale for the use of the advanced imaging techniques chosen in this thesis to investigate pathophysiological mechanisms in early patients. In Chapter 5, I report the clinical characteristics of the cohort studied in this thesis and methods used. Chapter 6 is a preliminary work done in established relapsing-remitting multiple sclerosis patients on one of the imaging techniques used in this thesis, Neurite Orientation Dispersion and Density Imaging (NODDI). In Chapter 7, I investigate the presence of microstructural and metabolic alterations in the brain of the cohort recruited in this study using NODDI and ^{23}Na MRI. In Chapter 8, I examine if early patients present pathophysiological alterations in cortical morphology that can influence the physical and cognitive disability. Finally, in Chapter 9, I examine if functional and structural alterations in the visual pathways can influence the assessment of cognitive disability in patients at their onset.

Chapter 2 Introduction to clinically isolated syndrome and multiple sclerosis

This thesis concerns an observational cross-sectional study of patients recruited within three months from the onset of their first episode of neurological symptoms suggestive of central nervous system demyelination. This project is still ongoing, and the cohort has been further followed up over time, but the main results presented in this thesis concern the baseline observations and, for the last chapter, part of the six months observations.

At the time of presentation of these first symptoms, patients are diagnosed either with a CIS, or, if they fulfil the 2017 revision of the McDonald Diagnostic Criteria, with relapsing-remitting multiple sclerosis. The presence of a typical CIS is a prerequisite for the diagnosis of relapsing-remitting multiple sclerosis.

Therefore, in this chapter, I first characterise the clinical features of a typical CIS and the possible challenges in the diagnosis. Secondly, I report the criteria used to diagnose a patient with multiple sclerosis. Finally, I summarise the risk factors at onset for developing a second attack or physical disability over time.

2.1 Clinically isolated syndrome

2.1.1 Clinical presentation

The CIS is an isolated episode of sub-acute neurological symptoms indicative of the presence of a demyelinating lesion in the central nervous system. The symptoms last more than 24 hours and usually evolve over the course of 2-3 weeks before completely or partially recovering. A CIS should not be associated with fever, infection or encephalopathy (Miller *et al.*, 2012).

The CIS has a higher prevalence in female than male with a ratio of 2.5F:1M. For the 70% of CIS patients, the age of onset is between 20 and 40 years (mean 30 years). However, approximately 0.5% of adults have symptom onset at the age of 60 years or older (Miller *et al.*, 2012).

The CIS is by definition isolated in time (i.e., first neurological episode imputable to demyelination) and it is also usually isolated in space, in a specific location within the central nervous system. The inflammatory demyelinating lesion can affect the optic nerve, the cerebral hemispheres, the brainstem, the cerebellum or the spinal cord. Rarely, symptom presentation is multi-focal with evidence of involvement of more than one central nervous system area simultaneously.

Depending on the area affected, patients may suffer from variable symptoms from motor or sensory disturbances to balance problems or double vision.

Table 2.1 summarises typical presentations and possible red flags.

Table 2.1 Typical and Atypical Clinical Presentations

Site	Typical Features	Atypical Features
Optic Nerve	Unilateral optic neuritis	Simultaneous Bilateral optic neuritis
	Mild pain on eye movement	Painless or very severe pain
	Reduced visual acuity with reduced colour vision	No perception of light
	Normal disc or mild disc swelling	Severe haemorrhages and exudates Vitritis and neuroretinitis
	Improvement begins within 3 weeks from onset	Extended loss of vision
Cerebral Hemispheres	Hemiparesis Hemisensory disturbance	Severe hemiplegia Encephalopathy Epilepsy Cortical blindness
Brainstem and Cerebellum	Bilateral internuclear ophthalmoplegia	Complete external ophthalmoplegia Fluctuating ocular weakness
	Ataxia and gaze-evoked nystagmus	Acute ataxia onset with severe postural instability
	Sixth nerve palsy (in patients <40 years)	
	Paroxysmal phenomena (occurring for at least 24 h)	Movement disorders

Site	Typical Features	Atypical Features
	Multifocal signs (e.g., nerve and long tract)	Vascular territory signs Progressive trigeminal sensory neuropathy Isolated trigeminal neuralgia
Spinal Cord	Incomplete transverse myelitis	Complete transverse myelitis Complete Brown-Séquard syndrome Cauda equina syndrome Anterior spinal artery territory lesion Sharp level to all sensory modalities
	Lhermitte's syndrome	Localised or radicular spinal pain
	Sphincter symptoms	
	Asymmetric limb weakness	Progressive and symmetrical spastic paraparesis or progressive sensory ataxia Areflexia
	Deafferented hand	

Table adapted from (Miller *et al.*, 2012)

A common CIS is optic neuritis (ON), which is worthy of a separate section for its specific features and differential diagnosis. Moreover, although the presence of a marked cognitive disturbances should address the neurologist towards a different diagnosis, CIS patients can present with cognitive disturbances. Therefore, cognition in CIS patients is briefly discussed in the paragraph 2.1.1.2.

2.1.1.1 Optic neuritis

One in five CIS presents as ON (Jenkins and Toosy, 2017). In CIS-ON, the inflammatory-demyelinating lesion is localised to the optic nerve, typically unilaterally although there could be a sub-clinical involvement of the fellow eye. This syndrome usually has onset with periocular pain, worsened by eye

movements and moderate in intensity. After a few days, the pain is followed by a subacute onset of visual disturbances characterised by blurred vision, often more evident in the central visual field than in the periphery. While the decrease in visual acuity can vary from a subtle blurriness to loss of perception of light, a constant feature is the presence of dyschromatopsia and a decrease in contrast sensitivity. Another key finding is the presence of a relative afferent pupillary defect, although if patients have subclinical demyelination in the other eye this sign may not be present. Fundoscopy usually shows a normal optic disc but it is swollen in a third of patients. In the first few weeks after the onset, patients can report Uhthoff's and Pulfrich's phenomena: the former is a transient worsening of vision with elevation of body temperature; the latter a difficulty judging the trajectory of moving objects.

ON itself is a benign condition as >95% of patients recover in the first year after the onset, 93% by five weeks (Cleary *et al.*, 1997).

However, although visual function returns to the near normality, patients often present residual visual problems characterised by deficits in colour vision (Cole *et al.*, 2000), contrast sensitivity (Balcer *et al.*, 2017) and quality of life (Sabadia *et al.*, 2016).

Two autoantibody-mediated conditions affecting the optic nerve are important differential diagnoses of multiple sclerosis-related ON.

In 2004, the discovery of anti-aquaporin-4 autoantibodies helped to identify a neuroinflammatory disease: the neuromyelitis optica (Lennon *et al.*, 2004). This is now a well-established disease phenotype characterised by the involvement, often bilateral, of long segments of the optic nerves, and by poor visual recovery. Other areas of the CNS, such as the spinal cord and the brainstem, can also be involved (Wingerchuk *et al.*, 2015).

In 2012, researchers discovered that about 25–33% of anti-aquaporin-4-negative patients had antibodies to myelin oligodendrocyte protein (MOG) (Kitley *et al.*, 2012). These patients have a similar phenotype to neuromyelitis optica, but they are usually males, in the fourth decade and have a monophasic course of the disease with a better prognosis than anti-aquaporin-

4 patients. The optic nerve involvement usually spares the chiasma and is not extensive as in patients with anti-aquaporin-4 ON. The CNS is usually involved in the caudal segment (lumbar spinal cord) or the brainstem. Furthermore, anti-MOG antibodies have also been associated with acute disseminated encephalomyelitis, particularly in children. MOG antibody disease (MOG-AD) is now recognised as a nosological entity with specific clinical and paraclinical features (Wynford-Thomas *et al.*, 2019).

2.1.1.2 Cognition in CIS

In clinical practice, CIS patients are not routinely assessed with neuropsychological tests. However, researchers have documented the presence of cognitive impairment in CIS patients, defined as a score below 1.5-2 standard deviations (SD) from the normative means in at least two cognitive tests. The prevalence of cognitive impairment varied across the studies with an average frequency of 27% (Brochet and Ruet, 2019). This variability can be due to different test batteries and inclusion criteria (i.e., time from onset, presence of white matter lesions) as well as from the thresholds used to define the cognitive impairment.

Even when focusing on studies with a similar population to the ones recruited in this study, CIS patients at their onset, we can observe different findings.

Feuillet and colleagues (Feuillet *et al.*, 2007) reported the highest prevalence of cognitive impairment: about 57% of their patients. They recruited 40 patients by 3 months from onset, including only patients with more than two white matter lesions. Patients and controls underwent the Rao's Brief Repeatable Battery of Neuro-psychological Testing and they used a threshold of two standard deviations to define cognitive impairment. Uher and colleagues (Uher *et al.*, 2014) observed the lowest prevalence of cognitive impairment, about 12.3%, even though they assessed a similar cohort (81 patients with at least two white matter lesions and less than four months from onset) and used a less conservative threshold (1.5 SD). The reason of this discrepancy may be partly attributed to the different populations, sample sizes and batteries, the Rao's Brief Repeatable Battery of Neuro-psychological Testing (BRB-N) in the first study as opposite to the more specific Minimal Assessment of Cognitive

Function in Multiple Sclerosis (MACFIMS) in the second one. On the other hand, one can speculate that different pathophysiological mechanisms, not accounted by the white matter lesion load and investigated in these studies, can affect cognitive performances, even in early patients.

Interestingly, regarding the neuropsychological domains affected, the findings consistently reported in CIS deficits in information processing speed, episodic verbal and visuospatial memory (Reuter *et al.*, 2011; Viterbo *et al.*, 2013; Ruano *et al.*, 2017).

Assessment of multiple sclerosis patients often is heavily weighted towards physical disability. As we will see in Paragraph 5.4, the main tool to assess disability, which is routinely used in clinical trials, is the Kurtzke Expanded Disability Status Scale (EDSS), whose score is mainly determined by ambulation (Kurtzke, 1983). However, cognitive aspects have a significant impact on multiple sclerosis patients' quality of life (Campbell *et al.*, 2017). As cognitive impairment in multiple sclerosis has a prevalence of 40 to 65% of patients (Chiaravalloti and DeLuca, 2008), it is crucial to understand if cognitive abnormalities began at the onset of the disease. Furthermore, a correct understanding of the prevalence of cognitive dysfunction at this stage may help interventions since the early phases of the disease for personalised care.

2.1.2 CIS diagnosis and red flags

The diagnosis of CIS relies on the integration of clinical, imaging, and laboratory findings. This complex diagnostic approach is fundamental because there is no single pathognomonic clinical feature or diagnostic test. Therefore, the neurologist must carefully consider signs, symptoms or diagnostic test results suggesting an alternative diagnosis, so-called red flags (Thompson *et al.*, 2018).

In patients with CIS, the MRI of the brain and spinal cord represents the main tool to support the diagnosis, exclude other conditions, stratify the risk for developing multiple sclerosis and eventually diagnose multiple sclerosis. Therefore, the International Panel on Diagnosis of Multiple Sclerosis has

recommended that an MRI, at least of the brain, is performed in all the patients with a CIS.

In CIS, the MRI should evidence the presence of a typical demyelinating lesion in the central nervous system area responsible for the neurological symptoms and signs. Besides the presence of the single symptomatic lesion, about 50-70% of CIS patients have multiple demyelinating white matter lesions in central nervous system detectable by T2-weighted sequences at the MRI (Fisniku *et al.*, 2008).

Demyelinating lesions are hyper intense on MRI T2-weighted sequences and may have a low-intermediate MRI T1 signal.

In the brain, lesions appear as oval/round areas with sharp margins. They should be at least 3 mm in long axis (Rovira *et al.*, 2015). In the acute inflammatory phase of CIS, the symptomatic lesion can present either as a nodular/homogeneous or with ring-like enhancement after gadolinium administration. Demyelinating lesions in the supratentorial compartment are usually located in periventricular (i.e., in the trigonum, corpus callosum, temporal horns) and juxtacortical (i.e., involving the U fibers) regions. Due to the perivenular origin of the inflammatory-demyelinating process, they are usually perpendicular to the ventricular surface. In the posterior fossa, they are usually located in the cerebellar peduncles, at the pial and ventricular surface of the pons, in the medulla oblungata, around the fourth ventricle and in the intra-axial segment of the trigeminal nerve (Aliaga and Barkhof, 2014).

In the spinal cord, demyelinating lesions are less than two vertebral segments in length and less than half of the diameter of the spinal cord in thickness. They are usually localised to the periphery (lateral and dorsal columns) in the cervical segment or conus medullaris. Acute lesions may enhance and exhibit focal swelling.

In the optic nerve, the lesion usually has a short length and can be identified as focal hyperintensity of the optic nerve with dedicated T2-weighted sequences of the orbits. MRI of the optic nerves is challenging due to the high intrinsic signal of the fatty tissue in the orbits. Spectral fat suppression

techniques or short T1 inversion recovery (STIR) pulsed sequences are used in clinical practice to detect ON. Recently, double inversion recovery (DIR) is emerging due to its superior performance in revealing inflammatory lesions of the optic nerve. Table 2.2 summarises typical radiological features and red flags. Figure 2.1 shows typical MRI findings from the cohort studied in this thesis.

Table 2.2 Typical and Atypical MRI Findings and Possible Alternative Diagnosis

	Typical findings	Atypical findings	Possible alternative diagnosis
Signal intensity	T1: Intermediate-low T2: Hyperintense Black holes: Signal intensity lower than the gray matter on T1	Lacuna	Hypertensive ischemic disease; CADASIL; Susac syndrome
Enhancement	Nodular/homogeneous or ring-like Frequent coexistence of enhancing/non-enhancing lesions Tumefactive demyelinating lesions: incomplete ring (open-ring pattern)	Persistence of contrast enhancement or continued enlargement of lesions	Lymphoma; glioma; vasculitis; sarcoidosis Vasculitis;
		Simultaneous enhancement of all lesions T2-hyperintensity	Vasculitis; lymphoma; sarcoidosis
		Meningeal enhancement	Chronic meningitis; sarcoidosis; lymphomatosis; vasculitis
Location			
Supratentorial	Juxtacortical (involvement U-fibers); periventricular (corpus callosum, trigonum, temporal horns); cortical. Basal ganglia infrequent	T2-hyperintensity dentate nucleus	Cerebrotendinous xanthomatosis
		T1-hyperintensity in the pulvinar	Fabry disease; hepatic encephalopathy; manganese toxicity
		Predominance of lesions at the corticosubcortical junction	Embolic infarction; vasculitis; progressive multifocal leukoencephalopathy
		Selective involvement anterior temporal, inferior frontal	CADASIL

	Typical findings	Atypical findings	Possible alternative diagnosis
		Cortical infarcts	Embolic disease; thrombotic thrombocytopenic purpura; vasculitis Cysticercosis;
		Haemorrhage or microbleed	Amyloid angiopathy; Moyamoya disease; CADASIL; vasculitis
		Corpus callosum central fibers with sparing of the periphery	Susac syndrome
Infratentorial	Fourth ventricle, cerebellar peduncles, medulla oblongata, intra-axial segment of the trigeminal nerve and the pial and ventricular surface of the pons	Large and infiltrating brainstem lesions	Behc¸et's disease; pontine glioma; embolic infarction; vasculitis; progressive multifocal leukoencephalopathy
Spinal cord	Short segment Less than half of the diameter	Spinal cord: longitudinal extensive; entire diameter	NMOSD
Optic Nerve	Short segment Anterior or posterior Punctate enhancement	Extensive Anterior segment Perioptic gadolinium enhancement	NMOSD-MOG
		Extensive lesion involving the posterior segment and the optic chiasm Bilateral	NMOSD-AQP4

CADASIL: cerebral autosomal dominant arteriopathy with subcortical infarcts and leukoencephalopathy; NMOSD: Neuromyelitis optica spectrum disorder; MOG: myelin oligodendrocyte glycoprotein; AQP: aquaporin-4

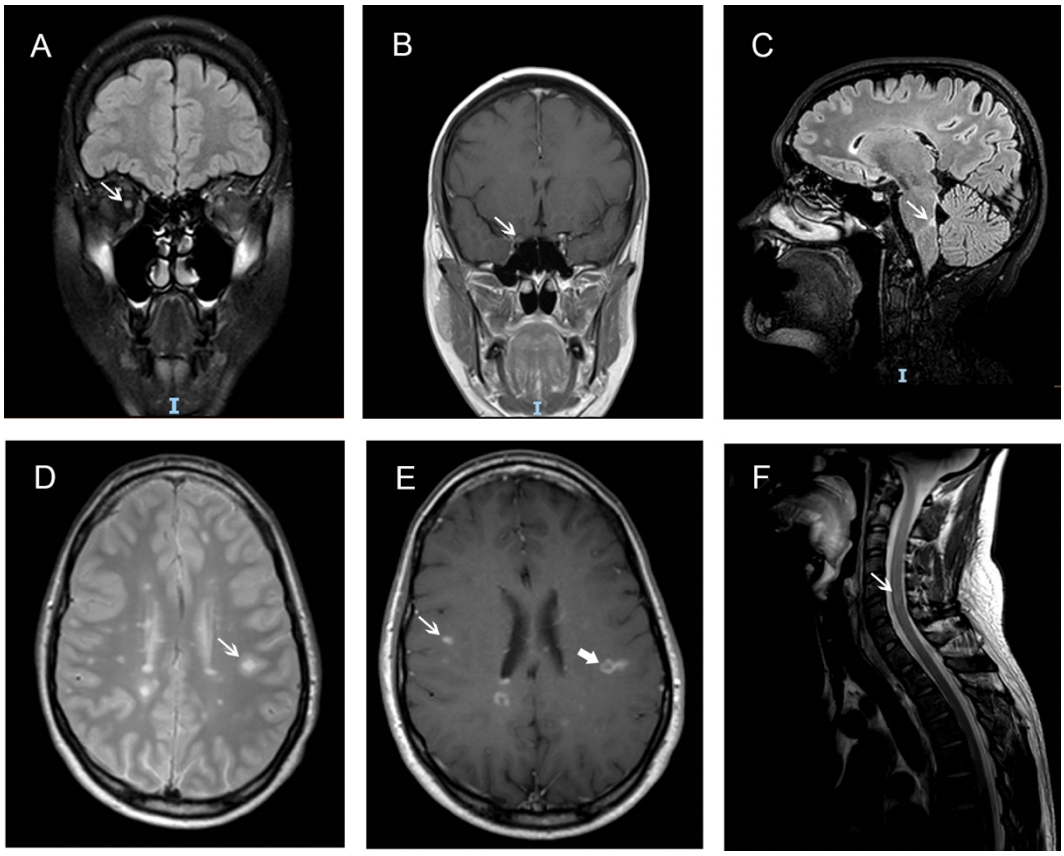

Figure 2.1 MRI findings from this cohort

(A) Right optic neuritis; (B) Same patient, enhancement in the pre-chiasmatic portion of the optic nerve; (C) patient with brainstem onset; (D) multifocal CIS patient with several white matter lesion; (E) the same patient presents nodular and open-ring enhancement (bold arrow) of the white matter lesions; (F) patient with myelitis onset,

White matter lesions fulfil the criteria for “dissemination in space” if they are found in at least two of four areas of the central nervous system: 1) periventricular, 2) cortical/juxtacortical, 3) infratentorial brain regions, 4) spinal cord). “Dissemination in time” is fulfilled if there is the simultaneous presence of gadolinium-enhancing and non-enhancing lesions (Thompson *et al.*, 2018) in CIS.

In the presence of an atypical clinical or radiological presentation, the examination of the cerebrospinal fluid (CSF) can be used to exclude other diagnoses. Atypical findings include elevated protein concentration of >100 mg/dL, pleocytosis with >50 cells per mm^3, presence of neutrophils, eosinophils, or atypical cells. Whereas, in a CIS patient with a typical clinical presentation, if the CSF examination shows evidence of intrathecal antibody

synthesis (unmatched oligoclonal bands), it provides evidence of dissemination in time.

At the onset of a typical CIS, if the imaging and laboratory findings demonstrate the presence of dissemination in space and time and exclude alternative diagnosis, the neurologist can formulate a diagnosis of multiple sclerosis according to the 2017 revision of McDonald criteria.

2.2 Multiple sclerosis diagnosis

The diagnostic criteria for multiple sclerosis have changed over time. On the one hand, the technology has evolved so that more paraclinical tests have been developed to support clinical findings and allow a more sensitive and more specific diagnosis. On the other hand, new treatments have become available for patients with multiple sclerosis at their onset and earlier diagnosis is now fundamental.

The prerequisite for the application of the latest criteria (Thompson *et al.*, 2018) for multiple sclerosis diagnosis is a typical clinical presentation. Care should be taken when applying the criteria to non-Caucasians, children or elderly patients as the criteria have not been formally validated in these cohorts.

In typical CIS, clinical, imaging and laboratory findings can be used to diagnose multiple sclerosis by demonstrating the presence of dissemination in space and time but should also exclude alternative diagnoses.

In early revisions of the diagnostic criteria, two neurological episodes or two MRI scans were needed to diagnose multiple sclerosis. The 2010 revision of the McDonald criteria modified this requirement: for the first time it was possible to diagnose multiple sclerosis at the time of the first neurological episode, the CIS (Polman *et al.*, 2011). Supported by retrospective analyses by the Magnetic Resonance Imaging in multiple sclerosis (MAGNIMS) consortium (Montalban *et al.*, 2010), these criteria simplified the previous requirements for dissemination in space and time, such that they could both be demonstrated at the time of the first MRI scan in a typical CIS patient. The simultaneous presence of asymptomatic gadolinium enhancing and non-

enhancing lesions in the first MRI scan was a sufficient requirement for the dissemination in time while, in comparison to previous criteria, fewer lesions were required for dissemination in space.

Three years ago, the International Panel on Diagnosis of Multiple Sclerosis released the 2017 McDonald criteria, which are a revision of the 2010 version (Thompson *et al.*, 2018). This version further increased diagnostic sensitivity whilst maintaining specificity.

At the beginning of this study, which spans from 2014 to present, the patients recruited were diagnosed with CIS or multiple sclerosis according to the 2010 revision of the McDonald criteria. As a consequence, they were not routinely offered a lumbar puncture. Then, the 2017 revision took place, changing how patients recruited in this cohort were diagnosed. Lumbar puncture, not included in this study, was routinely offered to patients by referring clinicians when the MRI scan showed demyelinating lesions in the central nervous system (CNS). However, patients were not always keen on undergoing this invasive procedure.

This application of the 2017 McDonald criteria in a real-world setting highlights how imaging still has a tremendous importance as patients may not always accept a lumbar puncture procedure. Furthermore, as we will see in 2.3.1.4 and 2.3.2.4, MRI features can help stratify the risk of future relapses and disability.

Another reflection comes from the increased sensitivity of McDonald revisions over time. It concerns the disappearing of CIS as a distinct clinical entity that used to define all those patients with an isolated first demyelinating episode. From 2010 onwards, as diagnosing multiple sclerosis from the first event has become possible, the CIS diagnosis has been applied to fewer patients. At present, CIS now only define those patients whose MRI shows white matter lesions that are either too few or in an atypical location for multiple sclerosis or patients who do not show signs of active inflammation, defined as the enhancement of white matter lesions after contrast or the presence of unmatched oligoclonal bands in the CSF.

I decided to adopt the 2017 revision of the McDonald criteria in this cohort as it was the latest version available when I started the analysis for this thesis. Furthermore, this would have allowed the comparison between my study results and the contemporary and future scientific literature.

Consequently, in the research setting, studies like this one, focusing on the onset of a first demyelinating event, have now included both CIS and multiple sclerosis patients. Considering that, as discussed before, patients with typical imaging features for multiple sclerosis at onset may not always wish to undergo a lumbar puncture, this determines a subtle boundary between the two conditions at the onset.

Table 2.3 summarises the concepts of dissemination in space and time according to the new McDonald criteria and includes a comparison with the 2010 revision. Figure 2.2 is a flow chart of the four possible scenarios applying to this cohort of patients at their first episode of neurological symptoms suggestive of demyelination according to the 2017 revision criteria. Figure 2.3 shows the MRI scan of a patient from this cohort diagnosed with multiple sclerosis according to the 2017 revision of McDonald criteria at her first scan.

Table 2.3 Dissemination in Space and Time according to the McDonald Criteria 2010 and 2017 Criteria

Criteria	Method	McDonald 2010 criteria	McDonald 2017 criteria
Dissemination in Space	MRI	≥ 2 T2-hyperintense lesions characteristics for MS in four sites: - Periventricular - Juxtacortical - Infratentorial - Spinal cord	≥ 2 T2-hyperintense lesions characteristics for MS in four sites: - Periventricular - Juxtacortical and cortical - Infratentorial - Spinal cord
		Lesions in the symptomatic region excluded	Lesions in the symptomatic region included
Dissemination in Time	1st MRI	Simultaneous presence of asymptomatic gadolinium-enhancing and non-enhancing lesions	Simultaneous presence of gadolinium-enhancing and non-enhancing lesions
		Symptomatic lesions excluded	Symptomatic lesions excluded
	CSF	-	Unmatched Oligoclonal Bands
	Follow-up MRI	≥ 1 new T2-hyperintense and/or gadolinium-enhancing lesion	≥ 1 new T2-hyperintense and/or gadolinium-enhancing
	Follow-up visit	Second clinical attack	Second clinical attack

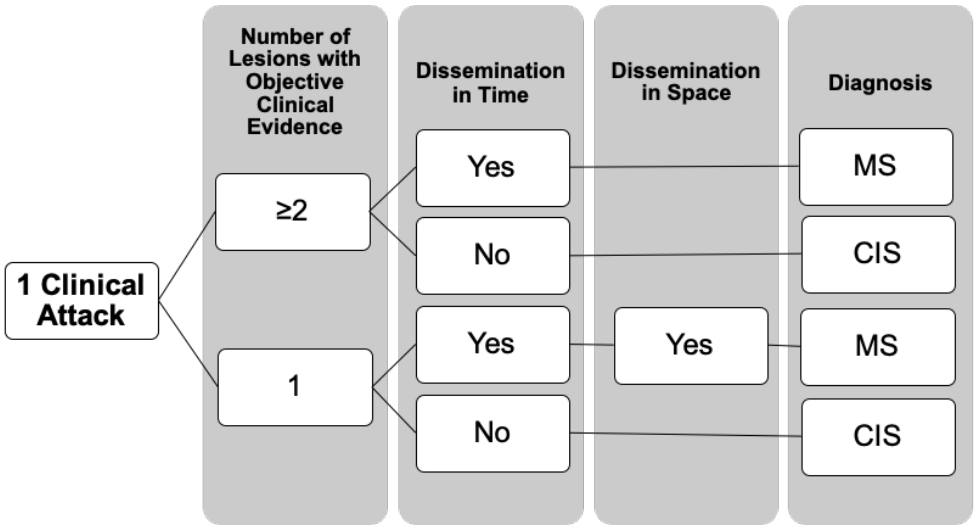

Figure 2.2 Flow chart of the four possible scenarios applying to this cohort

Abbreviations: MS: multiple sclerosis; CIS: clinically isolated syndrome.

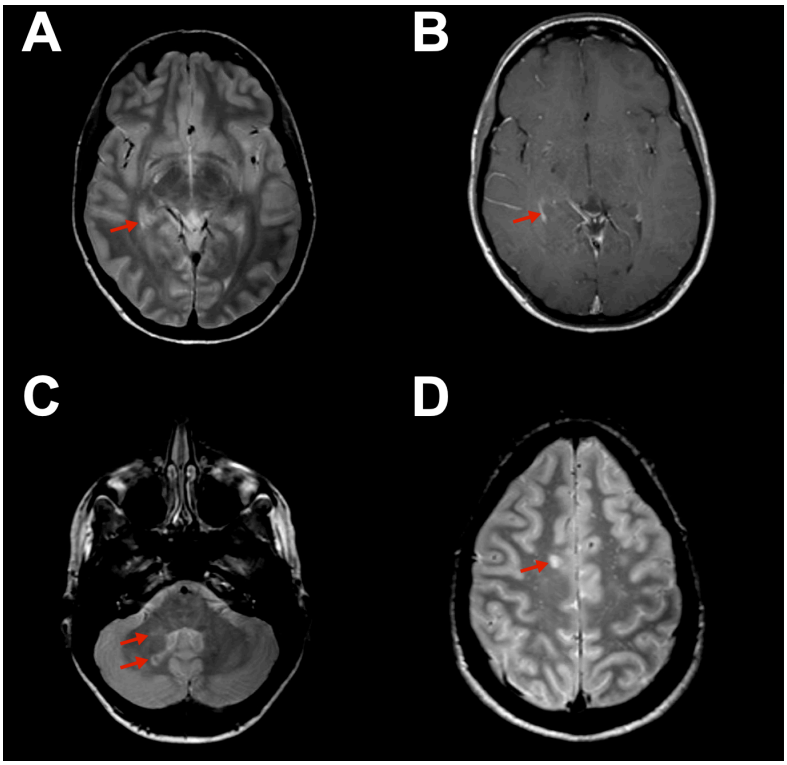

Figure 2.3 MRI scan of a patient of this cohort diagnosed with multiple sclerosis according to McDonald Criteria 2017 revision

Patient had onset with optic neuritis. (A) A periventricular lesion showing nodular enhancement (B) after contrast, thus fulfilling the dissemination in time criteria. Posterior fossa lesions (C) and juxtacortical lesion (D) that contribute to the dissemination in space criteria.

2.3 Prognostic factors in CIS

2.3.1 Disease activity

Several prospective observational and natural history studies in CIS cohorts have investigated which factors can predict a second neurological episode. This event would have marked the conversion to multiple sclerosis, as most of these studies used the diagnostic criteria for multiple sclerosis published before the 2010 McDonald revision, so that patients with distributed enhancing and non-enhancing lesions at the baseline MRI were still classified as CIS.

Robust predictors for conversion to multiple sclerosis have emerged, such as the presence of multiple demyelinating lesions, and they have been taken into account by clinical guidelines. In 2015, the Association of British Neurologists, revised the guidelines for disease-modifying treatments in multiple sclerosis allowing the prescription of selected disease modifying drugs (β-interferons and glatiramer acetate) to CIS patients with MRI evidence of demyelinating lesions because of their high risk of developing multiple sclerosis. These guidelines have now been adopted by the National Health Service (https://www.england.nhs.uk/). Other risk factors, such as the presence of oligoclonal bands in the CSF, have helped the revisions of the McDonald Criteria to achieve a better sensitivity.

At present, the risk factors identified in previous studies for a second attack find some applications to the clinical scenarios depending on the question asked, such as chances of having a second clinical attack despite disease modifying drug administration or precise figures for multiple sclerosis conversion in patients with limited number of lesions. In future, follow-up of this new cohort of CIS patients may help provide these answers.

In this section, I briefly summarise the prognostic factors for developing a second clinical attack in patients at their onset that have emerged from previous studies. Table 2.4 summarises observational studies of untreated CIS patients including only studies including MRI data, as MRI has now a fundamental role in the multiple sclerosis diagnosis.

Table 2.4 Risk of a second attack in observational studies of untreated CIS patients

Study	CIS Patients	Follow-up Period	Risk Factors	Non-Risk Factors
Hauser et al., 2000	178[a]	5 yrs	HLA-DRB1*1501 Presence of asymptomatic T2 lesions	
Jacobs et al., 2000	383	3 yrs	-	CIS subtype Number of T2 lesions
Tintorè et al., 2001	112[b]	5 yrs	OCB Number (≥9) and location (infratentorial, juxtacortical and periventricular) of T2 lesions Gadolinium-enhancing lesions	
Beck et al., 2003	160[a]	10 yrs	Presence of asymptomatic T2 lesions Female sex Normal optic disc at fundoscopy Typical optic neuritis	
Tintorè et al., 2005	320	3 yrs	CIS subtype (Non-optic neuritis) T2 lesions	
Tintorè et al., 2006	175	7 yrs	Number and location of T2 lesions	
Di Paoli et al., 2008	129[c]	3 yrs	Smoking	
Polman et al., 2008	176[d]	2 yrs	Younger age (<30yrs) OCB Number of T2 lesions Gadolinium-enhancing lesions	CIS subtype
Optic Neuritis Study Group, 2008	389[a]	15 yrs	Sex (female) Presence of asymptomatic T2 lesions [e]	Number of T2 lesions
Fisniku et al., 2008	107	20 yrs	Presence of asymptomatic T2 lesions	CIS subtype Number of T2 lesions

Study	CIS Patients	Follow-up Period	Risk Factors	Non-Risk Factors
Mowry et al., 2009	330	1 yr.	Younger age Non-white ethnicity Incomplete recovery Low number of functional systems affected [f]	CIS subtype
Tintorè et al., 2010	246	7.7 yrs	Location of asymptomatic T2 lesions (infratentorial)	
Swanton et al., 2010	142[a]	5 yrs	Sex (female) Location of asymptomatic T2 lesions (periventricular) Gadolinium-enhancing lesions	
Lunemann et al., 2010	147	7 yrs	Epstein-Bar Virus IgG	
Sombekke et al., 2013	121	5 yrs	Location of asymptomatic T2 lesions (spinal cord)	
Martinelli et al., 2014	100	9 yrs	Low 25-hydroxyvitamin D levels	
Ascherio et al., 2014	465[g]	5 yrs	Low 25-hydroxyvitamin D levels	
Tintorè et al., 2015	1015	7 yrs	Younger age CIS subtype (Non-optic neuritis) OCB Number of T2 lesions (>10)	Sex
Kuhle et al., 2015	1047	2 yrs	Younger age OCB Number of T2 lesions (>9)	Sex Epstein-Bar Virus IgG CIS subtype
Munger et al., 2015	468[g]	5 yrs	-	Epstein-Bar Virus IgG Smoking

[a]only optic neuritis included; [b] only optic neuritis, myelitis and brainstem syndromes included; [c] disseminated T2 lesions on brain MRI, and positive OCB; [d] the placebo arm of the BENEFIT study; [e] baseline non-contrast-enhanced MRI of the brain; [f] functional systems defined as visual, brainstem,

pyramidal, sensory, cerebellar, bowels and bladder and mental according to the Expanded Disability Status Scale score; [g] both the placebo and the treatment (Betaferon) arm of the BENEFIT study.

Clinical trials on β-interferons and glatiramer acetate in CIS patients provide another source of information about potential risk factors for a second clinical attack. They only included CIS patients with MRI evidence of asymptomatic T2 lesions and subgroups analyses assessed if demographic, clinical and MRI factors could have influenced the treatment effect. Clinical trials are summarised in Table 2.5.

Table 2.5 Risk of a second attack in clinical trials in CIS patients

Clinical Trial	CIS Patients Recruited	Treatment arms	Follow-up Period	Factors increasing the treatment effect	Factors non-increasing the treatment effect
ETOMS	309	Interferon beta-1a vs placebo	2 yrs	CIS subtype (multi-focal) Number of T2 lesions (>8)	-
CHAMPS	383 [a]	Interferon beta-1a vs placebo	2 yrs	Gadolinium-enhancing lesions	CIS subtype [a] Sex Age T2 lesion volume
CHAMPS	192 [b]	Interferon beta-1a vs placebo	2 yrs	-	Sex Age T2 lesion volume Gadolinium-enhancing lesions
CHAMPION	203 [a]	Interferon beta-1a: early vs delayed treatment	5 yrs	T2 lesion volume Gadolinium-enhancing lesions	-
BENEFIT	468	Interferon beta-1b vs placebo	2 yrs	-	CIS subtype (mono-focal vs multi-focal) Number of T2 lesions Gadolinium-enhancing lesions
BENEFIT	418	Interferon beta-1b: early vs delayed treatment	3 yrs	CIS subtype (multi-focal) Number of T2 lesions (≥9)	Gadolinium-enhancing lesions

Clinical Trial	CIS Patients Recruited	Treatment arms	Follow-up Period	Factors increasing the treatment effect	Factors non-increasing the treatment effect
PReCISE	481	Glatiramer acetate vs placebo	3 yrs	Sex (female) Younger age Gadolinium-enhancing lesions	Number of T2 lesions
Clinical Trial	**CIS Patients**	**Treatment**	**Follow-up Period**	**Risk Factors**	**Non-risk Factors**
CHAMPIONS	203 [a]	Interferon beta-1a or placebo	5 yrs	Younger age	-
BENEFIT	468	Interferon beta-1b or placebo	5 yrs	Low 25-hydroxyvitamin D levels	
BENEFIT	468	Interferon beta-1b or placebo	5 yrs	-	Epstein-Bar Virus IgG Smoking

[a] only unifocal CIS included; [b] only optic neuritis patients.
ETOMS (Comi *et al.*, 2001) ; CHAMPS (Jacobs *et al.*, 2000; CHAMPS STUDY GROUP, 2001; Beck *et al.*, 2002); CHAMPION (CHAMPIONS STUDY Group, 2006); BENEFIT (Kappos *et al.*, 2006, 2007; Ascherio *et al.*, 2014; Munger *et al.*, 2015); PReCISE (Comi *et al.*, 2009) ;

2.3.1.1 Demographics

Younger age at onset is a risk factor for conversion to multiple sclerosis (CHAMPIONS STUDY Group, 2006; Polman *et al.*, 2008; Mowry *et al.*, 2009; Tintoré *et al.*, 2015; Kuhle *et al.*, 2016). While the CHAMPS clinical trial did not report any significant effect of the age on the treatment effect (Beck *et al.*, 2002), the PReCISE trial showed that patients entering the trial at a younger age were better responders than the older patients (Comi *et al.*, 2013). This could be because younger patients have more T2 lesions (Filippi *et al.*, 2001), a possible manifestation of inflammatory activity, and are more responsive to treatment with DMDs.

Early studies showed that females were at higher risk of a second attack than males (Optic Neuritis Study Group, 2008*a*; Swanton *et al.*, 2010). However, the higher prevalence of CIS in women than men (Dobson *et al.*, 2012) could have influenced this finding and, indeed, recent studies did not identify the sex as a risk factor (Kuhle *et al.*, 2015; Tintoré *et al.*, 2015).

2.3.1.2 Genetic and environmental factor

The gene variant HLA-DRB1*1501 is associated with an increased risk of a second attack in CIS (Hauser *et al.*, 2000). We have also strong evidence that low 25-hydroxyvitamin D levels can be a risk factor (Ascherio *et al.*, 2014; Martinelli *et al.*, 2014). Whereas the role of an Epstein-Bar Virus past infection and of smoking habit is less clear (Lünemann *et al.*, 2010; Kuhle *et al.*, 2015; Munger *et al.*, 2015).

2.3.1.3 CNS location

The different type of onset does not seem to have an effect on the risk of a second attack (Jacobs *et al.*, 2000; Fisniku *et al.*, 2008; Polman *et al.*, 2008; Mowry *et al.*, 2009). Originally the studies on the Barcelona cohort report a better outcome for ON patients (Tintoré *et al.*, 2006), however this effect disappeared in the multi-variate analysis when T2 lesions are included.

In clinical trials, β-interferons seems to have more effect in the presence of a multi-focal onset than of a mono-focal one (Comi *et al.*, 2001; Kappos *et al.*,

2007). Again, this can be a consequence of the presence of more inflammatory activity.

2.3.1.4 White matter lesions

The presence of asymptomatic T2 lesions is an established risk factor for conversion to multiple sclerosis. So far, longitudinal studies with follow-up of 7, 15 and 20 years reported conversion to clinically definite multiple sclerosis in 56%, 72% and 82% of CIS patients with evidence of demyelinating lesions at baseline (Fisniku *et al.*, 2008, Optic Neuritis Study Group, 2008*b*; Tintoré *et al.*, 2015). The same studies reported a conversion of 7%, 25% and 21% of CIS patients without white matter lesions at the MRI, respectively.

As regards lesion characteristics, studies have assessed if lesion number or location could help to stratify the risk of a second attack.

The number of white matter lesions is a risk factor for converting to multiple sclerosis (Tintoré *et al.*, 2001, 2006, 2015; Polman *et al.*, 2008; Kuhle *et al.*, 2015). Studies have usually divided patients in categories according to the lesion number using a cut-off of nine or ten: patients with nine, ten or more lesions were at higher risk of developing a second attack than the others in the lower categories (Tintoré *et al.*, 2001, 2015; Kuhle *et al.*, 2015). However, the number of T2 lesions seems to have a marginal effect on the risk of conversion in the long term (Fisniku *et al.*, 2008, Optic Neuritis Study Group, 2008*a*).

The lesion location as well represents a risk factor for multiple sclerosis conversion. Since the first MRI studies, periventricular, juxtacortical and infratentorial areas were identified as specifically affected in multiple sclerosis and included in the MRI criteria. Presently, they are used to demonstrate dissemination in space. Not surprisingly, the presence of asymptomatic T2 lesions in these areas increase the risk of CIS patients of having a second attack (Tintoré *et al.*, 2010).

Similarly, the presence of gadolinium-enhancing lesion, a factor that now determines the presence of dissemination in time, is a risk factor for multiple

sclerosis conversion (Tintoré *et al.*, 2001; Polman *et al.*, 2008; Swanton *et al.*, 2010).

2.3.1.5 Cerebrospinal fluid

The presence of unmatched oligoclonal bands in CSF is now employed as a marker for dissemination in time and supports diagnosis of multiple sclerosis (Thompson *et al.*, 2018). Studies have reported that finding unmatched oligoclonal bands in CIS patients with 0-1 white matter lesions increase the risk of multiple sclerosis conversion at 5 years from 31% to 70% (Kuhle *et al.*, 2015).

2.3.2 Disability accumulation

Besides the risk of a second attack, other studies have investigated prognostic factors for long-term disability. The longest period of observation comes from the London CIS cohort, which was followed up for over 30 years (Chung *et al.*, 2020). Their findings are very informative as they represent long-term natural history data, from mainly untreated patients.

Although several risk factors have emerged, the more robust ones are determined in the first years of follow-up rather than at onset (Fisniku *et al.*, 2008; Chung *et al.*, 2020). Furthermore, studies showed divergence in possible multiple sclerosis outcomes independently from the presence of these risk factors (Fisniku *et al.*, 2008; Chung *et al.*, 2020). In Table 2.6 I summarise the risk factors at the onset of CIS that have been related to disability accrual over time. Moreover, lesion volume and its change at earlier time points are correlated with disability after 20 years (Fisniku *et al.*, 2008).

Table 2.6 Risk factors for disability accumulation in CIS patients

Study	CIS Patients	Follow-up Period	Risk Factors	Non-Risk Factors
O'Riordan et al., 1998 Sailer et al., 2000	81 [a]	10 yrs	Number of asymptomatic T2 lesions (>10) [b] T2 Lesion Volume	CIS subtype
Brex et al., 2002	71[a]	14 yrs	Number of asymptomatic T2 lesions [b] T2 Lesion Volume	-
Optic Neuritis Study Group, 2004	127 [c]	10-12 yrs	-	Number of asymptomatic T2 lesions Presence of asymptomatic T2 lesions
Minneboo et al., 2004	42	8.7 yrs	Number of T2 lesions (>9) Location of T2 lesions	Gadolinium-enhancing lesions Hypo-intense T1 lesions
Tintorè et al., 2006	175	7 yrs [d]	Number of T2 lesions (>10) Location and number of T2 lesions [e]	-
Fisniku et al., 2008	107	20 yrs	Number of T2 lesions (>10)	CIS subtype

Study	CIS Patients	Follow-up Period	Risk Factors	Non-Risk Factors
Swanton et al., 2009	100 [f]	5 yrs	Location of T2 lesions Number of infratentorial T2 lesions Gadolinium-enhancing lesions	Sex Age
Tintorè et al., 2010	246	7.7 yrs	Location of asymptomatic T2 lesions (infratentorial)	-
Ascherio et al., 2014	468[g]	5 yrs	Low 25-hydroxyvitamin D levels	-
Munger et al., 2015	468 [g]	5 yrs	-	Epstein-Bar Virus IgG Smoking
Tintorè et al., 2015	1015	7 yrs	CIS subtype (non-optic neuritis) OCB Number of T2 lesions (>10)	Sex Age
Brownlee et al., 2017	131[h]	5 yrs	Number of spinal cord T2 lesions	Age Sex
Brownlee et al., 2019	178	15 yrs	Location of T2 lesions (spinal cord) Gadolinium-enhancing lesions	Brain and spinal cord atrophy Number of supratentorial T2 lesions Presence of infratentorial lesions

Study	CIS Patients	Follow-up Period	Risk Factors	Non-Risk Factors
Chung et al., 2020	120	30 yrs	Number of T2 lesions Location of T2 lesions (infratentorial)	Age Sex

[a] only optic neuritis, myelitis and brainstem syndromes included; [b] post-contrast T1 images not performed; [c] optic neuritis patients who have already developed clinically defined multiple sclerosis due to a second relapse; [d] disability measured at 5 yrs; [e] Barkhof Criteria: Presence of gadolinium enhancement, juxtacortical lesions, periventricular lesions or infratentorial lesions; [f] only optic neuritis patients included; [g] treated and untreated patients from the BENEFIT trial; [h] non-spinal CIS;

2.3.2.1 Demographics

No effect of age or sex has been identified (Swanton *et al.*, 2009; Tintoré *et al.*, 2015, Brownlee *et al.*, 2019*a*; Chung *et al.*, 2020) . Early studies showed that older and male patients were getting more disable over time than younger ones, but these studies were retrospective natural-history studies, including both progressive as well as relapse onset patients (Eriksson *et al.*, 2003), not assessing patients systematically at their onset (Confavreux *et al.*, 2003) and without MRI data (Confavreux *et al.*, 2003; Eriksson *et al.*, 2003)

2.3.2.2 Genetic and environmental factor

Low 25-hydroxyvitamin D levels are a risk factor for future disability (Ascherio *et al.*, 2014), whereas there is no evidence for Epstein-Bar Virus infection (Munger *et al.*, 2015) and smoking habit (Munger *et al.*, 2015). HLA-DRB1*1501 has not been investigated yet longitudinally in CIS patients, but cross-sectionally it was not associated with disability measures in multiple sclerosis (Masterman *et al.*, 2000; Hensiek *et al.*, 2002; Moutsianas *et al.*, 2015).

2.3.2.3 CNS location

The different type of onset does not seem to have an effect on disability accrual (O'riordan *et al.*, 1998; Sailer *et al.*, 1999; Fisniku *et al.*, 2008).

2.3.2.4 White matter lesions

The presence of asymptomatic T2 lesions at onset is moderately correlated with future disability (Brex *et al.*, 2002; Tintoré *et al.*, 2006, 2015; Fisniku *et al.*, 2008).

The number of T2 lesions, greater than nine (Minneboo *et al.*, 2004) or ten (O'riordan *et al.*, 1998; Tintoré *et al.*, 2006, 2015), has been associated with a higher disability over time. However, in the London cohort, one-third of CIS patients with more than 10 T2 lesions at baseline had low disability at 20 years (Expanded Disability Status Scale score ≤3) (Fisniku *et al.*, 2008), whilst at 30 years, the location of the lesions was more predictive of disability than their number (Chung *et al.*, 2020). Furthermore, the change in T2 lesion volume

over time was a better predictor of disability than baseline T2 lesion count (O'riordan *et al.*, 1998).

The lesion location seems to be a strong predictor of disability. In particular, the presence and the number of T2 lesions in the brainstem and spinal cord are associated with greater disability at 5, 7, 15 and 30 years after CIS onset (Minneboo *et al.*, 2004; Swanton *et al.*, 2009; Tintoré *et al.*, 2010; Brownlee *et al.*, 2017, 2019*a*; Chung *et al.*, 2020).

In the medium term, the presence of gadolinium-enhancing lesions is related to increased disability in CIS patients, but not in patients who have already developed multiple sclerosis (Swanton *et al.*, 2009) suggesting that MRI activity is related more to the risk of relapses than to disability. This has been corroborated in studies in multiple sclerosis (Kappos *et al.*, 1999). In the long term, however, recent studies on the same cohort have shown correlations with disability (Brownlee *et al.*, 2019*a*; Chung *et al.*, 2020). The presence of gadolinium-enhancing lesions at baseline may be a marker of future disease activity and an increased number of relapses in the first years after a CIS has been related with worse disability outcomes in natural history study.

Although brain and spinal cord atrophy is related to disability in multiple sclerosis (Simon, 2000), the presence in CIS at onset seems to not influence the disability outcome in the long term (Dalton *et al.*, 2004; Swanton *et al.*, 2009). The rate of atrophy, instead, seems to correlate with disability accumulation (Brownlee *et al.*, 2017).

2.3.2.5 Cerebrospinal fluid

Oligoclonal bands in the CSF increased the risk of disability at 7 years independently of the MRI findings (Tintoré *et al.*, 2015).

2.4 Summary

At the time of the first neurological episode suggestive of demyelination, patients may be diagnosed either with CIS or multiple sclerosis on the basis of clinical, imaging and laboratory findings. The diagnosis is not devoid of

challenges as other conditions may mimic, clinically or radiologically, multiple sclerosis.

Robust predictors for a second clinical attack have emerged from observational studies and clinical trials and they have contributed to the achievement of higher specificity in the diagnostic criteria and earlier treatment options. An important role is played by MRI measures that are mainly related to the presence, number, location and activity of the demyelinating plaques.

However, when looking at disability, the strongest predictors are derived from the observation of patients over time while the initial MRI characteristics have a less important effect. One of the possible reasons is that conventional MRI metrics are not specific for the pathological substrates behind the damage in the central nervous system.

In the next chapter, I examine the complex pathophysiological mechanisms involved in multiple sclerosis pathology and their correlation with conventional MRI metrics.

Chapter 3 Pathophysiological mechanisms and their pathological correlates in multiple sclerosis

In this chapter, I highlight the pathophysiological mechanisms behind CNS damage in multiple sclerosis. I subsequently discuss how conventional MRI (cMRI) correlates with these pathological features.

3.1 Pathophysiological mechanisms

Multiple sclerosis was originally considered a disease characterised almost exclusively by focal demyelination in the white matter. Although the presence of demyelinating plaques still represents the hallmark of multiple sclerosis pathology, in reality damage to the CNS is widespread and results from heterogeneous processes. These pathophysiological processes comprise dynamic cascade of inflammation, demyelination and neuroaxonal damage occurring to varying degrees during the course of multiple sclerosis

3.1.1 Inflammation

Multiple sclerosis is considered an autoimmune disease primarily mediated by CD4+ T lymphocytes, which are responsible for a multifactorial attack on myelin components, oligodendrocytes, axons and neurons (Sospedra and Martin, 2005). The animal model of multiple sclerosis, experimental autoimmune encephalomyelitis (EAE), can be induced, by *in vitro* activated CD4+ T cells (Ben-Nun *et al.*, 1981). Over the past two decades, however, researchers have also demonstrated the important role of CD8+ T cells and B lymphocytes in the multiple sclerosis pathogenesis(Corcione *et al.*, 2005; Friese and Fugger, 2005).

3.1.1.1 The precursors of inflammation

Multiple sclerosis is a multifactorial disease: genetic and environmental risk factors influence susceptibility to disease manifestations.

The most important genetic component is the polymorphic variant of the human leukocyte antigen (HLA) class II gene: the HLA-DR15 haplotype, which accounts for 15-50% of the genetic susceptibility (Hafler *et al.*, 2007).

CD4+ T cells recognise peptides bound on the major histocompatibility complex (MHC) II expressed in antigen-presenting cells (APCs), such as dendritic cells and B lymphocytes. Furthermore, under inflammatory conditions, the MHC II can be also expressed by monocytes, macrophages and T cells (Reith *et al.*, 1995). DR15 alleles presenting peptides from organ-specific self-proteins to T cells promote a break of tolerance and the selection of an autoreactive CD4+ T cell repertoire.

However, the presence of autoreactive T cells alone is not sufficient to generate the autoimmune cascade responsible of the CNS damage in multiple sclerosis. This reaction has to be triggered by the exposure of an antigen in the CNS.

Therefore, infections, particularly viral, are thought to play a fundamental role in producing and maintaining the inflammatory reaction (Steiner *et al.*, 2001) although a single pathogen has not been identified.

Epstein–Barr virus is one of the possible candidates, since researchers have found association between multiple sclerosis susceptibility and the presence of T cells and antibodies reactive against this virus (Pender, 2011). In multiple sclerosis, studies have demonstrated the presence of intrathecal antibodies against Epstein–Barr virus antigens (Cepok *et al.*, 2005) and of EBNA1-specific T cells cross-reacting with myelin (Lünemann *et al.*, 2008). Other infections, such as the ones promoted by endogenous retroviruses, may facilitate the inflammatory reaction in the CNS (Perron and Lang, 2010).

Myelin specific CD4+ lymphocytes may originate from two processes. One is molecular mimicry, the cross-activation of T cells derived from the similarity between auto-antigens (self) and pathogens' peptides (Libbey *et al.*, 2007). The other process is bystander activation in which non-specific inflammatory events, such as viral and bacterial infections, increase cytokines and chemokine levels activating T cells against self-antigens (Andersen *et al.*,

1993). Other environmental factors can disturb the balance between pro-inflammatory and anti-inflammatory/protective components of the immune system. Specifically, low levels of vitamin D and reduced exposure to sunlight are implicated in multiple sclerosis pathogenesis (Hart *et al.*, 2011). Vitamin D is involved in a variety of immune functions, such as cell proliferation, differentiation and immunomodulation (Cantorna, 2000; Nagpal *et al.*, 2005).

The selection and activation of autoreactive T cells are the precursors of the autoimmune reaction. T lymphocytes mature in the thymus where autoreactive T cells are usually suppressed. Even in physiological conditions, however, in normal conditions, T cells against foreign antigens may also have low avidity for self-antigens. Therefore, even in healthy subjects, we can find T cells reactive to myelin components. In multiple sclerosis, however, patients have myelin-specific T cells with a higher avidity and state of activation than healthy controls (Bielekova and Martin, 2004).

3.1.1.2 The inflammatory cascade

Myelin-specific CD4+ T cells are activated outside the CNS, becoming encephalitogenic (Bielekova *et al.*, 2000) and, guided by chemotactic substances, they move into the CNS compartment where they cross the blood-brain barrier (BBB) interacting with adhesion molecules on the endothelium (Charo and Ransohoff, 2006). Once in the CNS they are re-activated by local APCs, such as dendritic cells, presenting myelin antigens (Greter *et al.*, 2005). At this point, they start a complex immune attack directed against the myelin and they recruit other immune cells from outside the CNS, such as B lymphocytes, plasma cells and macrophages, and they activate local cells such as microglia (Brosnan and Raine, 1996).

3.1.1.3 T cells

Among the CD4+ T cells, the Th1 subtype was thought to be the main effector of this cascade, but now there is evidence that supports a major role for the Th17 lymphocytes (Cua *et al.*, 2003). Th17-type T cells can drive tissue damage through the local upregulation and release of harmful cytokines, such

as IFN-g and molecules of the tumour necrosis factor (TNF) family, and the complement activation (Hemmer *et al.*, 2002; Zipp and Aktas, 2006).

However, although responsible for the initial steps of this auto-immune cascade, CD4+ T cells tend to accumulate in the venular perivascular spaces and only in the parenchyma during the second stage infiltrate (Babbe *et al.*, 2000). Instead, MHC class I restricted CD8+ T lymphocytes represent the major components in the lesions ranging from 60% to more than 85% of the T cells (Lassmann, 2011). MHC class I molecules are exhibited by all cells, although, under physiological conditions, neurons have very low expression of MHC class I (Neumann *et al.*, 1995). CD8 + T cells mediate the tissue injury not only through an antigen-specific cytotoxic action (Evans *et al.*, 1996), but also through antigen-independent mechanisms involving, for instance, the TNF receptors (Aktas *et al.*, 2006).

Therefore, in active lesions, there are typically two stages of inflammation: an initial inflammatory reaction with predominantly CD8+ T cells, and then a second wave of immune cell infiltration, after demyelination and tissue damage, characterised by a broader spectrum of inflammatory cells, including CD4+ T cells together with macrophages and B cells (Lassmann, 2011).

This inflammatory cascade not only directly damages the myelin sheath, but also the oligodendrocytes; neurons undergo apoptosis and demyelinated axons are dissected (Peterson *et al.*, 2001; Frohman *et al.*, 2006). This widespread damage is mainly caused by collateral antigen-independent processes driven by both CD4+ as well as by CD8+ cells (Meuth *et al.*, 2009). Three main processes may be identified. First, a consequence of demyelination and macrophage activation is the alteration of the ion channel homeostasis and mitochondrial failure (Waxman, 2008) (see paragraph 2.1.1.6). Secondly, there is “epitope spreading”: new immunological antigens are released during tissue damage and they can activate other clones of auto-reactive T cells (McMahon *et al.*, 2005). Finally, in a process of “cumulative autoimmunity”, the primary attack against myelin antigens may redirect T cells against other self-antigens of the axon cytoskeleton that are now exposed (Krishnamoorthy *et al.*, 2009).

3.1.1.4 B cells

In health, B cells derive from the lymphopoietic stem cells in the bone marrow where they mature and, similarly to the T cells in the thymus, they are negatively selected if auto-reactive (i.e., responding to self-antigens). Subsequently, B cells undergo an antigen-dependent maturation in the lymphoid organs, where naive B cells differentiate into memory B cells. Activated B cells exert three main functions: presentation of specific antigens on to an MHC II complex to CD4 + T cells (Lanzavecchia, 1990); secretion of various inflammatory and regulatory cytokines (Duddy *et al.*, 2004); differentiation into plasma cells that, in turn, secrete antibodies.

Similarly to T cells, low-affinity autoreactive B cells can be found in physiological conditions in the peripheral blood where they serve as scavengers cells, whilst B cells escaping the negative selection in the bone marrow or becoming reactive towards self-antigens through molecular mimicry, can initiate autoimmune reactions (Wucherpfennig and Strominger, 1995). In multiple sclerosis, this reaction is against the CNS myelin sheath and one of the putative auto-antigen is MOG (myelin oligodendrocyte glycoprotein). However, while active immunization with MOG or transfer of anti-MOG antibodies in animal models can induce EAE (Von Büdingen *et al.*, 2001), results in multiple sclerosis are not the same and anti-MOG antibodies have not been validated as disease markers in multiple sclerosis (Sospedra and Martin, 2005).

Even if multiple sclerosis does not represent a classical B-cell autoimmune disease, there is a strong evidence that B cells play a fundamental role in multiple sclerosis pathogenesis. In multiple sclerosis, B cells clonally expand and differentiate inside the CNS following an intrathecal stimulus(Krumbholz *et al.*, 2005). These processes take place in the ectopic lymphoid follicle-like structures in the meninges where clones of B cell aggregate (Serafini *et al.*, 2004). Interestingly, they are predominant in the chronic phase of multiple sclerosis (Magliozzi *et al.*, 2007). Additionally, there is also increased transmigration of active B cells towards the BBB as they are attracted by inflammatory chemokines (Krumbholz *et al.*, 2006).

In the CNS, activated B cells also differentiate into plasma cells secreting antibodies. The presence of intrathecal IgG production is associated with multiple sclerosis and the presence of oligoclonal bands is a well-recognised hallmark of the disease (Reiber *et al.*, 1998). However, specificity for these antibodies have not yet been found. IgG and activated complement contribute to the inflammatory reactions and they can be found deposited within the myelin sheath in more than half of demyelinating lesions (Lucchinetti *et al.*, 2000).

3.1.1.5 Macrophages and microglia

Macrophages and activated microglia represent the vast majority of the cells in demyelinating lesions (Frischer *et al.*, 2009), with microglia dominating the phagocytic population within active lesions (Lassmann, 2011).

Furthermore, they are present before the establishment of the demyelinating plaque: in the so-called “prephagocytic phase” of the lesion, there is an increase in activated microglia associated with initial myelin and oligodendrocyte damage (Henderson *et al.*, 2009). This is also supported by the finding of an activation gradient of microglia from the normal-appearing white matter surrounding the active lesion to the lesion itself (Lassmann, 2011). Figure 3.1 shows the evolution of the inflammatory-demyelinated lesion.

Macrophages and activated microglia are found adhered to myelin sheaths (Babinski, 1885) and dystrophic axons (Ferguson *et al.*, 1997). On the one hand, they remove tissue debris, particularly myelin fragments (Brück *et al.*, 1995). On the other hand, they actively contribute to myelin damage and neuro-axonal damage by secreting TNF-alpha (Probert *et al.*, 2000), proteases (Cuzner and Opdenakker, 1999) and reactive oxygen species (ROS) or nitric oxide (NO) (Smith and Lassmann, 2002). ROS and NO induce oxidative axonal injury through direct effects on axonal cytoskeleton and indirect effects trough mitochondrial dysfunction affecting neurons and oligodendrocytes (Smith and Lassmann, 2002; Nikić *et al.*, 2011)(Smith and Lassmann, 2002; Nikic et al., 2011).

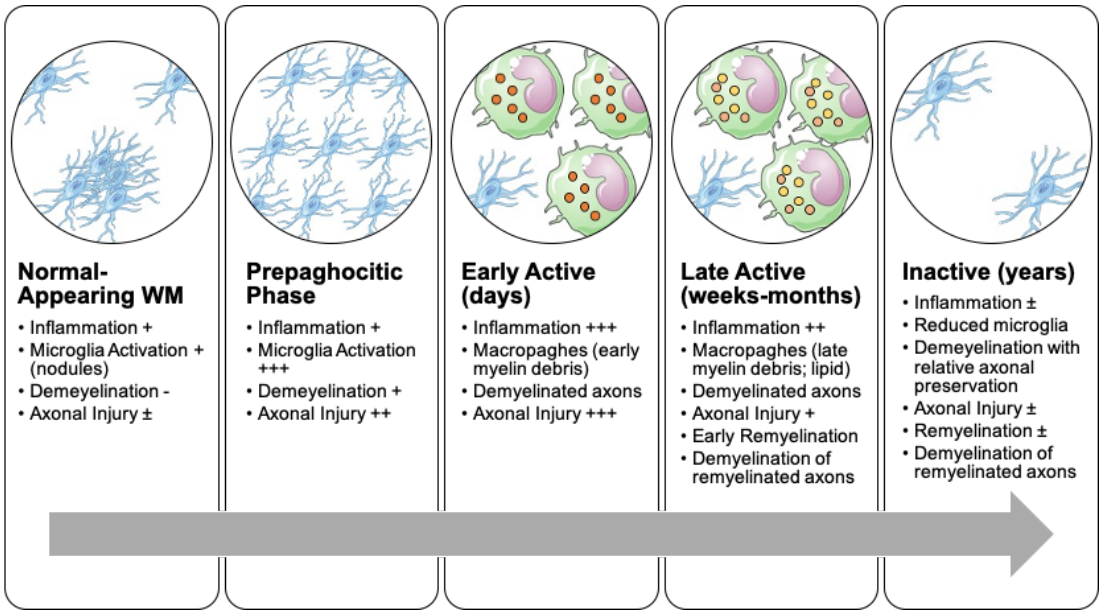

Figure 3.1 White matter lesion evolution

Adapted from (Kutzelnigg and Lassmann, 2014). Abbreviations: WM: white matter.

3.1.1.6 Oxidative injury and channelopathy

Our CNS is particularly sensitive to oxidative damage because of its high oxygen consumption (Halliwell, 2006). Thus, not surprisingly, oxidative stress is one of the principal pathogenetic mechanisms in multiple sclerosis, causing disturbed ion channel homeostasis at the point that, from a neurobiological perspective, multiple sclerosis has be described as an "acquired channelopathy" (Waxman, 2008).

ROS (reactive oxygen species) and NO (nitric oxide), produced by phagocytes, inactivate proteins of the mitochondrial respiratory chain and induce deletions in mitochondrial genes (Campbell and Mahad, 2012). This mitochondrial dysfunction causes energy failure with adenosine triphosphate (ATP) depletion that results in the impairment of ATP-dependent ion channels, such as the Na-K ATPase, leading to intracellular Na accumulation (Waxman, 2003). The increased axoplasmic Na concentration, together with membrane depolarization, promotes a reversal of the Na^{+}-Ca^{++} exchange and an influx of calcium. Calcium overload activates the Ca^{++}-dependent enzymes that damage the axon (Waxman, 2003). This process is exacerbated by the concurrent hypoxia, caused by inflammatory damage of the vessels

(Wakefield *et al.*, 1994) and the compressive effects of the oedema on the local microcirculation (Shi and Blight, 1996), as well as by the increased energy demand on the demyelinated axons where saltatory nerve conduction is no longer possible.

This energy failure is particularly evident in acute multiple sclerosis lesions (Lucchinetti *et al.*, 2000), particularly in thin-calibre axons that have few mitochondria and high energy demand (Trapp and Stys, 2009). Moreover, mitochondrial dysfunction has also been found in the cortex of progressive multiple sclerosis patients (Dutta *et al.*, 2006).

The increase in the Na influx is also caused by a redistribution and phenotypic modification of Na channels during demyelination (Waxman *et al.*, 2004). On one hand, the demyelinated axons express Na channels along the naked internodal axolemma to maintain the propagation of the action potential (Coman *et al.*, 2006). On the other hand, they switch to different Na channel isoforms responding to the demyelination and degeneration of axons. In physiological conditions, Nav 1.6 is the predominant sodium channel in the CNS, and is clustered at the node of Ranvier, where the saltatory conduction happens. In the demyelinated lesion, there is redistribution of Nav 1.6, causing an increased sodium concentration with consequent toxic Ca influx, but there is also a switch towards the Nav 1.2 isoform. The Na 1,2 is an immature channel, usually expressed in the axon before their myelination during the CNS development, and produces a less persistent Na current (Waxman *et al.*, 2004). Interestingly, in multiple sclerosis, specific cells such as the Purkinje cells of the cerebellum, during the demyelination express another isoform, the Nav1.8 channel, that is been associated with cerebellar dysfunction (Shields *et al.*, 2012). Figure 3.2 summarises the events leading to axonal injury.

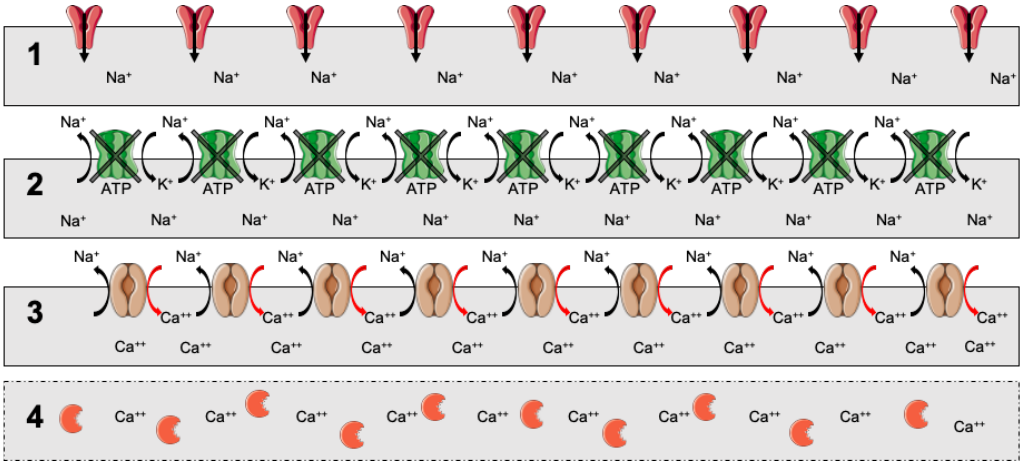

Figure 3.2 Axonal injury after demyelination and hypoxic injury

1. Demyelination causes Na^+ channel redistribution along the axon and increases energy demand; 2. As a consequence of mitochondrial dysfunction and increased energy demand, there is failure of the Na^+/K^+ ATPase with increased Na^+ influx; 3. Increased intra-axonal Na^+ concentration reverses the Na^+/Ca^{++} exchanger; 4. Increased intra-axonal Ca^{++} activates proteolytic enzymes that destroy the axons

3.1.2 Demyelination

The presence of primary demyelination is the hallmark of multiple sclerosis lesions (Babinski, 1885). The inflammatory reactions described above, remove myelin from axons in a segmental manner: myelinated axons enter the plaque from the peri-plaque white matter, lose the myelin sheath at the nodes of Ranvier, then traverse the entire plaque embedded in a dense astroglial scar (Charcot, 1880).

The role of oligodendrocytes, the cells responsible for myelin production in the CNS, have been instead controversial for many years. Originally, researchers believed that oligodendrocytes were completely lost with demyelination and, consequently, remyelination was absent (Lumsden, 1970). When specific oligodendrocyte markers become available, they revealed that these cells are present in multiple sclerosis lesions although their density can be highly variable between lesions (Lucchinetti *et al.*, 1999).

Oligodendrocytes can be destroyed to various degrees as a consequence of the inflammatory mechanisms previously discussed. Some lesions can even show a predominant oligodendroglial pathology, particularly in patients with

short disease duration (Lucchinetti *et al.*, 2000). Some researchers have suggested that oligodendroglial damage is the first event of the inflammatory cascade. Barnett and Prineas (Barnett and Prineas, 2004) found that oligodendrocyte apoptosis occurred prior to macrophage phagocytosis of myelin debris, suggesting that the earliest event in lesion formation might be oligodendroglial death, which recruits the macrophages and activates the local microglia and finally trigger the adaptative immune response of the T cells. In support of this hypothesis, there is the evidence in genetic demyelinating diseases (leukodystrophies) that oligodendrocytes abnormalities induce immune reactions against the myelin (Berger *et al.*, 2001).

The oligodendrocytes that have survived the attack can be found in lesions, but they are not able to synthesise myelin and they probably incur apoptosis (Wolswijk, 2000). However, in some lesions, there are also glial progenitor cells that can differentiate into myelinating cells (Wolswijk, 2002). They seem to be responsible for the remyelination process, although they can fail to differentiate and produce myelin (Chang *et al.*, 2002). This could explain why remyelination is effective only in some lesions.

In multiple sclerosis, spontaneous remyelination can occur after lesion formation, when active demyelination is still present (Lassmann, 1983). Remyelination can be restricted to small areas of the plaque but may also lead to the repair of the whole plaque (Lassmann, 1983). In pathology, remyelinated lesions are known as “shadow plaques” and contain very thin myelin sheaths and shortened internodes (Frischer *et al.*, 2015).These lesions, however, can still suffer from further demyelinating attacks to which they are more susceptible than the normal-appearing white matter because of the thin myelin sheath (Bramow *et al.*, 2010).

About 20-30 % of multiple sclerosis patients can show extensive remyelination, irrespective of the clinical course of disease (relapsing, primary, or secondary progressive) (Patrikios *et al.*, 2006). Although many explanations have been proposed, it is still not known why some patients and some lesions remyelinate and others do not.

Outside the demyelinated plaques, in the normal-appearing white matter, primary demyelination is almost absent and restricted to microscopic peri-venous areas (Allen and McKeown, 1979). Within the cerebral cortex, instead, demyelination is extensive, particularly in patients with progressive disease (Peterson *et al.*, 2001). It seems to develop independently of white-matter plaques (Kutzelnigg *et al.*, 2005) and is associated with meningeal inflammation (Magliozzi *et al.*, 2007).

3.1.3 Neuro-axonal loss

Although demyelination is considered the hallmark of CNS damage in multiple sclerosis, neuro-axonal loss is extensively present in white matter plaques, cortical lesions normal-appearing white and grey matter (Trapp and Nave, 2008).

Axonal loss is a consistent feature of white matter lesions (Kornek and Lassmann, 1999), but it can be highly variable between lesions and patients: in some lesions only the 10–20%, in others more than 90% of axons are lost (Mews *et al.*, 1998; Bjartmar *et al.*, 2000).

In acute plaques, axonal damage occurs immediately after demyelination and, in some cases, it can even precede myelin destruction (Marik *et al.*, 2007). Axons are in close contact with macrophages and activated microglia cells, suggesting that axonal injury is mediated by the inflammatory reaction (Kornek and Lassmann, 1999). In patients with “tumefactive” lesions in the brain there is a fulminant axonal injury leaving the tissue with cystic cavities (Bjartmar *et al.*, 2000). In these lesions cytotoxic CD8+ T cells can be found adherent to degenerating axons (Neumann *et al.*, 2002).

In chronic plaques, the axonal loss is profound, arriving up to 90%. However, the acute axonal injury, as promoted by inflammation, is rare, although still greater than in normal-appearing white matter. Instead, there is progressive axonal loss consequent to the lack of trophic support and to the existing demyelination (Pitt *et al.*, 2000). As discussed before, the thin demyelinated axons are more susceptible to oxidative stress and energy failure. Glutamate excitotoxicity as well seems to play a role in axonal injury (Pitt *et al.*, 2000).

In cortical demyelinating lesions, axons and neurons are also affected (Peterson *et al.*, 2001). Specifically, axons, dendrites, and synapses, seem to be more severely affected than neuronal cell bodies (Wegner *et al.*, 2006).

The normal-appearing white matter in multiple sclerosis is highly abnormal and characterised by diffuse axonal damage with consequent myelin destruction (Kutzelnigg *et al.*, 2005). This reduction in the density of myelinated fibers is most prominent in periventricular white matter and causes expansion of the extracellular space (Seewann *et al.*, 2009). Moreover, it can be a consequence of axonal transection within white matter plaques that causes secondary Wallerian degeneration of local fibres (Dziedzic *et al.*, 2010) This occurs particularly in areas where fibre tracts are highly compacted and lesions are frequent, such as the spinal cord (Lovas *et al.*, 2000) and corpus callosum (Dziedzic *et al.*, 2010).

Wallerian degeneration of tracts connected to plaques only partially contribute to this process, as demonstrated by the lack of significant correlations between the axonal injury in the normal-appearing white matter and the white matter lesion load (Kutzelnigg *et al.*, 2005).

A state of diffuse inflammation, trapped inside the CNS by an intact or repaired BBB, may contribute to axonal injury as shown by Kutzelnigg and colleagues in their study on advanced patients (Kutzelnigg *et al.*, 2005). Furthermore, these authors found a significant, correlation between axonal loss in normal-appearing white matter and cortical demyelinating lesions. They hypothesised that activated lymphocytes from meningeal nodules may cause not only cortical demyelination but also, through parenchymal infiltration, axonal injury in normal-appearing white matter (Kutzelnigg *et al.*, 2005; Androdias *et al.*, 2010).

Similar mechanisms may occur in the cortex. On the one hand, there is evidence of retrograde or anterograde damage of the neurons from the axonal transection in white matter plaques, particularly if they are located subcortically. On the other hand, diffuse neuronal loss can be observed, both in demyelinated as well as in myelinated cortical areas, suggesting a primary

neurodegenerative process (Kutzelnigg *et al.*, 2007). An oxidative injury, related to the presence of meningeal inflammation, may be one of the causes (Haider *et al.*, 2016).

3.2 Brain pathology

3.2.1 Lesions

3.2.1.1 White matter lesions

In 2000, Lucchinetti and colleagues classified white matter lesions into four pathological categories based on the patterns of demyelination (Lucchinetti *et al.*, 2000). The study was performed on 51 biopsies and 32 autopsies of patients with histologically proven active multiple sclerosis. Interestingly, they did not find any evidence of intra-subject heterogeneity: the lesion pattern was the same within each patient.

Pattern I and II showed active demyelination with lymphocyte T and macrophage infiltrations associated with activated microglia. Patterns II, in addition, also had IgG deposited on the disintegrating myelin sheath. Both patterns of lesions were typically centred on small veins and venules and had sharp edges with perivenous extensions. In some patients these patterns were associated with a high incidence of remyelinated shadow plaques.

Pattern III and IV, instead, showed primary oligodendroglial dystrophy with subsequent inflammation characterised by T lymphocytes, macrophages and activated microglia. These lesions were not centred on a vein.

In type III lesions, the authors found diffuse apoptosis of the oligodendrocytes extending from the border of the lesion to the normal-appearing white matter of the periplaque. Oligodendrocytes were absent in the inactive center of the plaque and there was no association with remyelination. These aggressive lesions showed a pattern of demyelination, oligodendrocyte destruction, and neurodegeneration closely similar to the one (hypoxia-like) present in the initial stages of stroke lesions (Aboul-Enein *et al.*, 2003).

In type IV, instead, there was a center of active myelin destruction surrounded by a rim of oligodendrocytes with signs of cellular death, but not apoptosis. These lesions had usually a sharply demarcated border with radial expansion of the lesion.

Some overlap between these patterns, however, has been observed in another study (Barnett and Prineas, 2004). These authors suggest that multiple sclerosis lesions start with pattern III changes and, when they further actively expand, develop into a pattern of complement-mediated demyelination (pattern II). Furthermore, a study on established multiple sclerosis cases, including also inactive lesions, found only a pattern of antibody- and complement-mediated myelin phagocytosis without hypoxia-like damage and oligodendrocyte apoptosis (Breij *et al.*, 2008).

We do not know if these immunopathologic patterns remain stable in a given patient and if in active early patients there is an overlap of the four patterns because longitudinal biopsies or autopsies are very rare at this disease stage. Table 3.1 summarises this classification.

Table 3.1 White matter lesions classification

Lesion Type	Cells	IgG and Complement Deposition	OG	Demyelination	Remyelination	Perivenular	Edges
I	T cells, macrophages, activated microglia	-	± (periplaque rim)	+ (synchronous myelin destruction)	+	+	Sharp
II	T cells, macrophages, activated microglia	+	± (periplaque rim)	+ (synchronous myelin destruction)	+	+	Sharp
III	T cells, macrophages, activated microglia	-	++ (apoptosis)	± (absent around intra-plaque vessels)	-	-	III- defined
IV[a]	T cells, macrophages	-	++ (death)	+ (synchronous myelin destruction)	-	±	Sharp Radial expansion

[a] found only in primary-progressive multiple sclerosis patients. Abbreviations: OG: oligodendrocytes .
Adapted from (Lucchinetti *et al.*, 2000)

Active lesions can be further classified according to their structure. Kutzelnigg and colleagues (Kutzelnigg *et al.*, 2005) distinguished between acute active, chronic active, and slowly expanding lesions. In early multiple sclerosis, patients can present acute or chronic active lesions. Acute lesions show synchronous myelin destruction across the entire lesion with infiltrating macrophages containing early myelin degradation products. Chronic active lesions have an inactive lesion center surrounded by a rim of macrophages digesting early myelin degradation products. In progressive multiple sclerosis phases, these two categories of lesions are rare and, instead, slowly expanding lesions can be found. They also consist of an inactive lesion center surrounded by a rim of macrophages and activated microglia, but these phagocytes contain late myelin degradation products, or they have even finished the digestion.

3.2.1.2 Cortical lesions

In multiple sclerosis, demyelination in the cortex is diffuse and, similarly to the white matter, different patterns of cortical lesions can be identified.

The first type of lesion, present at every stage of multiple sclerosis, is the leukocortical lesion: mixed white matter–grey matter involvement that from the juxtacortical white matter extends into the deep cortical layers.

The second type of cortical lesion, which is also present at all stages of multiple sclerosis, is the small perivascular intra-cortical lesion.

The third and fourth types of lesions are subpial. These plaques have a band-like shape and affect the outer portions of the cortex penetrating into the cortex. Type IV lesions extend for the whole width if the cortex, until the white matter border, and have a large extension involving often several adjacent gyri and sulci. Both type of lesions are associated with meningeal inflammation and become more prominent in patients with progressive multiple sclerosis (Kutzelnigg *et al.*, 2005).

3.2.2 Normal-appearing tissues

3.2.2.1 White matter

The normal-appearing white matter in multiple sclerosis patients is mainly characterised by inflammation and axonal loss.

Inflammation is present areas of microglia activation that can precede the lesion formation and as parenchymal lymphocytes infiltrate, more prominent in progressive patients (Kutzelnigg *et al.*, 2005).

Primary demyelination, instead, is almost absent and only present as microscopic peri-venular lesions. We can only observe a secondary decrease in the myelin content relative to the loss of large myelinated axons.

As discussed before, axonal loss can be prominent in this tissue. It can be consequent to secondary Wallerian degeneration of nerve fibres crossing lesions(Pitt *et al.*, 2000), but it also occurs independently of lesions, possibly triggered by other inflammatory mechanisms. Axonal loss is more prominent in progressive than in early relapsing-remitting multiple sclerosis (Kutzelnigg *et al.*, 2005). However, as discussed previously, little is known about the extension and aetiology of axonal loss in the normal-appearing white matter in early disease, where insights into this process come mainly from advanced MRI (e.g., De Stefano *et al.*, 2002).

3.2.2.2 Grey matter

Inflammatory infiltrates can be found in the cortex originating from ectopic lymphoid structures in the meninges (Serafini *et al.*, 2004).

In the cortex, subpial band lesions are mainly responsible for demyelination and they are not captured by conventional MRI (see paragraph 2.3.2.1). They mainly occur in enfoldings of the cortex, such as cortical sulci and indentations (Kutzelnigg *et al.*, 2005). These areas include: insular cortex, cingulate cortex, frontobasal, temporobasal cortex, and cerebellum. The limbic circuit, including the hippocampus (Geurts *et al.*, 2007), seems to be particularly affected by demyelination (Kutzelnigg and Lassmann, 2008) .

Besides demyelination, axonal and neuronal loss occur in the cortex. The neurodegeneration is only partly related to cortical demyelination (Wegner *et al.*, 2006) or to anterograde or retrograde degeneration from subcortical white matter plaques (Haider *et al.*, 2016). As discussed, it is also a consequence of primary or secondary effects of the inflammation.

As a result, cortical atrophy can be profound in multiple sclerosis patients, even at early stages of the disease. The reduction in cortical volume is probably a result of the presence of cortical demyelinating lesions, axonal loss from white matter plaques and primary neurodegeneration.

In the deep grey matter of multiple sclerosis patients, there are often demyelinated lesions which are associated with a variable degree of neuro-axonal loss (Cifelli *et al.*, 2002). Moreover, there can be diffuse axonal damage mainly due to secondary Wallerian degeneration from connected white matter lesions (Haider *et al.*, 2016).

3.3 Spinal cord pathology

In the spinal cord white matter, particularly the cervical portion, demyelinating lesions are frequently observed. These lesions present severe axonal loss, with studies reporting a reduction of axon numbers of 60– 70% compared with healthy spinal cord tissue (Bjartmar *et al.*, 2000). This axonal transection affects nerve fibers even in distant segments.

In spinal cord grey matter, similar to the brain, there is demyelination, which is associated with neuro-axonal loss (Gilmore *et al.*, 2009*b*) that is also present in non-demyelinated grey matter affecting motor- and inter-neurons (Gilmore *et al.*, 2009*a*). Axonal loss in the spinal cord can be present from the early phases of multiple sclerosis (Schirmer *et al.*, 2009). Table 3.2 summarises pathological abnormalities in the brain and spinal cord normal-appearing tissues.

Table 3.2 Pathological abnormalities in brain and spinal cord

	Inflammation	Demyelination	Axonal Loss
Brain			
Normal-Appearing White Matter	++ Microglia activation and nodules T (CD8+) and B-cell infiltration	-	++ Active axonal injury ++ Secondary Wallerian Degeneration from Plaques +
Cortex	++ T (CD8+) and B-cell infiltration from meningeal lymphoid-like structures	++	++ Active axonal injury ++ Secondary Wallerian Degeneration from Subcortical Plaques +
Deep Grey Matter	++ Microglia activation T (CD8+) and B-cell infiltration	++	++ Active axonal injury + Secondary Wallerian Degeneration from Plaques ++
Spinal Cord			
Normal-Appearing White Matter	++ Microglia activation T (CD8+) and B-cell infiltration	-	++ Active axonal injury ++ Secondary Wallerian Degeneration from Plaques and Brain Tracts ++
Grey Matter	Microglia activation T (CD8+) and B-cell infiltration	++	++ Active axonal injury ++ Secondary Wallerian Degeneration from Plaques++

3.4 Alterations in the CNS network

The CNS can be pictured as a network in which grey matter neurons, performing different functions, share information between each other through their connections via white matter tracts. As such, in multiple sclerosis, the structural damage in the CNS previously described can result in functional changes in the CNS: some neurons may have to work more or differently than in healthy conditions because other cells have been damaged or information has to be shared through different routes as white matter tracts are interrupted by plaques (Filippi and Rocca, 2009). These functional changes can be present from the earliest stages (Rocca *et al.*, 2005).

Most researchers believe that multiple sclerosis patients initially develop a compensatory strategy that can partly limit the consequences of structural damage. As the disease progresses, however, this compensatory plasticity plateaus, it cannot compensate any further for the damage accrual, and this eventually results in clinical consequences, disability (Tomassini *et al.*, 2012). In this context, differences in brain reserve as well as the location of the damage can play a key role in determining the success of the compensatory strategy in each patient (Sumowski *et al.*, 2014). These individual differences can contribute to the disease heterogeneity: while some patients may functionally withstand considerable amounts of brain tissue damage, others already suffer from severe disability (Strasser-Fuchs *et al.*, 2008).

Alterations in the CNS network can be particularly relevant for cognition. We have seen in Paragraph 2.1.1.2 that cognitive function can be impaired since the early stage of the disease. In CIS, cognitive deficits seem to be independent of structural MS damage, i.e, cognitive performance has not showed significantly correlations with white matter lesion volume (Glanz *et al.*, 2007) Instead, changes in CNS networks have been related cognitive performance (Roosendaal *et al.*, 2010).

3.5 Conventional MRI correlates

3.5.1 White matter

3.5.1.1 Gadolinium-enhancing lesions

Intravenous gadolinium enhancement provides a measure of focal active inflammation. Gadolinium is a paramagnetic molecule of 400-800 Dalton that can cross the BBB when tight junctions are destroyed by the provoked inflammatory reaction. As such, gadolinium-enhancing lesions pathologically correspond to active plaques with T cells and macrophage infiltration (Nesbit *et al.*, 1991).

Gadolinium, once it has crossed the BBB, accumulates in the interstitium where it shortens the T1-relaxation time of water molecules such that they appear brighter than the surrounding tissue in T1 sequences. The lesion enhancement seen with gadolinium lasts about 2-3 weeks (Cotton *et al.*, 2003).

Small lesions usually enhance homogeneously, and later, may progress to a ring enhancement pattern. Large lesions can begin as ring-enhancing lesions (Cotton *et al.*, 2003). The ring enhancement pattern has been associated with macrophage infiltration, more severe tissue destruction and longer duration of enhancement than solid enhancement (Morgen et al., 2001).

Although gadolinium enhancement may be used as a “snapshot” of focal macroscopic inflammation, this phenomenon is not pathologically specific. It does not capture other pathological processes in active lesions: demyelination, remyelination and axonal loss. Furthermore, although gadolinium enhancement indicates inflammation, inflammation is not always associated with gadolinium enhancement. Firstly, as discussed before, the white matter has inflammatory infiltration and microglia activation before lesion formation. Additionally, it is not known how often these microscopic alterations evolve in a macroscopic acute lesion. Secondly, the paracellular route through the disruption of the BBB tight junctions is not the only way lymphocytes infiltrate the CNS parenchyma: they may also use trans-cellular routes (Engelhardt and Wolburg, 2004) and there can be BBB alterations without the macroscopic

leakage detected by gadolinium (Plumb *et al.*, 2006) . Finally, particularly in the progressive phases of multiple sclerosis, inflammation can be present hindered by an intact BBB (Kutzelnigg *et al.*, 2005).

3.5.1.2 Hyper-intense T2 lesions

White matter lesions exhibit increased T2 signal compared with adjacent white matter tissue. T2-weighted images are dominated by long transverse relaxation time of relatively free water, therefore both the CSF as well as the demyelinated lesions appear bright. Fluid attenuated inversion recovery (FLAIR) imaging adds a T1 inversion pulse to the long TR and TE of the T2-weighted image suppressing the CSF signal and helping the detection of periventricular lesions.

CIS patients present with an average T2-hyperintense lesion volume of 2-5 cc (Jacobs *et al.*, 2000; Comi *et al.*, 2001). Most T2-hyperintense lesions reach their maximum size at 2-8 weeks and then usually shrink over weeks or months when the vast majority remain stable as chronic lesions. An exception to this are the slowly expanding lesions that are present in the secondary progressive phase of the disease.

T2-hyperintense lesions are pathologically nonspecific: the signal can include demyelination, remyelination, and axonal loss. Furthermore, up to 48% of T2-hyperintense lesions are not seen by macroscopic inspection of *post mortem* brain (De Groot *et al.*, 2001). These lesions may represent early stages of myelin reduction and microglia activation as well as remyelinated shadow plaques or areas of secondary Wallerian degeneration (De Groot *et al.*, 2001; Barkhof *et al.*, 2003).

3.5.1.3 Hypo-intense T1 lesions

About 5-20% of T2-hyperintense lesions are hypo-intense in T1 and are called “black holes”. They represent lesions with marked tissue destruction, so they are more closely associated than T2 hyperintensities to axonal loss (JH *et al.*, 1999). Furthermore, lesions remaining T1-hypointense lack of remyelination (Bitsch *et al.*, 2000).

The volumes of T1-hypointense lesions usually increase during the course of the disease, but patients present with a heterogeneous ratio of T2-hyperintense/T1-hypointense volumes.

Enhancing lesions appear T1-hypointense because of oedema. Whilst the majority of these lesions recover T1 signal after the resolution of oedema and partial remyelination (Barkhof *et al.*, 2003; Brück *et al.*, 2003), about 14–41% of these lesions may remain hypointense (van Walderveen *et al.*, 1998; Ciccarelli *et al.*, 1999; Brex *et al.*, 2002; Dalton *et al.*, 2004; Minneboo *et al.*, 2004), particularly ones showing prolonged, ring enhancement (Ciccarelli *et al.*, 1999). Table 3.3 summarises the conventional MRI correlates for white matter lesions.

Table 3.3 MRI correlates for the white matter lesions

MRI Signal	Inflammation	Demyelination	Remyelination	Axonal Loss
Gadolinium-enhancing	Present (macro BBB leakage)	?	?	? Ring enhancement associated with tissue destruction
T2-Hyperintense	?	Present	?	?
T1-Hypointense	?	Present	Absent	Present (> T2-Hyperintense lesions)

3.5.2 Grey matter

3.5.2.1 Cortical lesions

Among the four patterns of cortical lesions, only the first type, the leukocortical lesions may be seen in T2 images. The others are undetected by T2 and T1 sequences.

Other sequences have been developed in the past decade to improve the detection of cortical lesions. They include double inversion recovery (DIR), which relies on T2-hyperintensity combined with white-matter and CSF suppression, and phase-sensitive inversion recovery (PSIR), which relies on T1 signal combining negative and positive longitudinal magnetisation to achieve a greater range of signal intensity than standard T1-weighted sequences. PSIR provides a high contrast between white and grey matter and it has been superior to DIR in detecting intra-cortical lesions (Sethi *et al.*, 2012). Furthermore, ultra-high field (7 T) MRI seem to be a suitable gold-standard for detecting *in vivo* cortical lesions, particularly the pial-cortical ones (type III and IV) (Nielsen *et al.*, 2012).

As discussed before, cortical demyelination is associated with meningeal inflammation. Several studies have showed that post-contrast 3D T2-FLAIR MRI, acquired at least 10 minutes after intravenous gadolinium administration, can detect leptomeningeal contrast enhancement.

3.5.2.2 Brain and spinal cord atrophy

High-resolution structural MRI sequences, such as the 3D-MPRAGE, can be used to compute brain atrophy. Registration-based techniques measuring the percentage brain volume changes (PBVC)(De Stefano *et al.*, 2010), are considered the most robust method to assess brain atrophy. The reduction in brain volume during multiple sclerosis, however, is a complex measure in terms of pathological substrates. On the one hand, both demyelination as well as neuro-axonal loss can result in the decrease in brain volume, on the other hand, inflammation, oedema, and remyelination processes can contrast this phenomenon.

In multiple sclerosis, since the initial studies, researchers have showed that there is a greater rate of grey matter volume loss than white matter (Bermel *et al.*, 2003; Dalton *et al.*, 2004), although specific white matter structures, such as the corpus callosum, may be early atrophy indicators (Dietemann *et al.*, 1988). Furthermore, grey matter atrophy has stronger correlations to disability measures than white matter (Fisniku *et al.*, 2008). Regional grey matter atrophy seems to spread involving more regions over time in a specific sequence (Eshaghi *et al.*, 2018*a*). Deep grey matter is involved from the CIS phase (Eshaghi *et al.*, 2018*a*) and its volume loss seems to drives disability accumulation in multiple sclerosis (Eshaghi *et al.*, 2018*b*).

Spinal cord atrophy is a reflection of secondary fibre tract degeneration and, similarly to the brain, local damage including demyelination and neuro-axonal loss. As discussed before, due to the anatomy of the spinal cord, neuro-axonal loss can be extensive and, not surprisingly, it is reported to be higher than the rate of brain atrophy (Moccia *et al.*, 2019*b*). Spinal cord atrophy is generally measured as the cross-sectional area at the cervical level, usually at C1–C2 and C2–C3, using 3D structural sequences. Furthermore, recently, registration-based methods, more standardisable than segmentation-based ones, have recently become available(Moccia *et al.*, 2019*a*).

CIS patients converting to multiple sclerosis in the future have been found with spinal cord atrophy (Hagström *et al.*, 2017).

3.6 Summary

In conclusion, a dynamic cascade of inflammation, demyelination, and neuro-axonal loss lead to damage in the CNS of multiple sclerosis patients. Other processes, such as remyelination or immune regulation, may influence the final pathological outcome. As a consequence, heterogenous pathophysiological changes occur in different tissues, phases of the disease, and different patients.

However, conventional MRI techniques offer a range of metrics that are not specific for these processes and their pathological manifestations. Consequently, conventional MRI metrics show only a low to moderate

correlations with clinical parameters. Furthermore, the conventional techniques available are unable to detect abnormalities in the normal-appearing (i.e., free from demyelinated lesions) tissues, although widespread alterations can be present since the early phase of multiple sclerosis.

Therefore, several quantitative MRI techniques have been developed to better account for the different pathological substrates of the multiple sclerosis damage. In the following chapter, I summarise the techniques used in this thesis.

Chapter 4 Advanced imaging techniques

4.1 Neurite orientation dispersion and density imaging (NODDI)

4.1.1 Diffusion-weighted imaging

Diffusion-weighted imaging (DWI) measures the microscopic Brownian motion of water molecules in biological tissues from which information about tissue microstructure can be derived (Le Bihan *et al.*, 1986).

In tissues, such as white matter, water diffusion is hindered by cellular structures (e.g., cell membranes and axonal cytoskeletons). Therefore, researchers developed a model of water molecules movement according to trivariate Gaussian dispersion pattern along a tensor matrix, the diffusion tensor (DT) (Basser *et al.*, 1994). DT has three axes perpendicular to each other that cross at the centre point: a principal axis and two smaller axes describing the depth and width of an ellipsoid. Three eigenvalues, lambda1, lambda2, and lambda3, can be extracted and combined to compute the magnitude of the diffusion, mean diffusivity (MD), and the degree of anisotropy, fractional anisotropy (FA). Conventionally, the diffusivity along the principal axis is called parallel or axial diffusivity (AD); the diffusivities along the two small axes are called radial diffusivity (RD).

Since its development, over 300 studies have employed DT imaging (DTI) in multiple sclerosis. Table 4.1 summarises the main DTI findings in CIS. Only studies including patients within six months from onset have been included.

Table 4.1 DTI findings in CIS patients at onset

Author	Design	Population	Findings
(Ranjeva *et al.*, 2003)	Cross-sectional	46 CIS Vs. 24 HCs	Patients' callosal NAWM: ↑MD ↑ MD correlated with ↓magnetization transfer ratio
(Gallo *et al.*, 2005)	Longitudinal (1 yr.; only structural scans)	45 CIS Vs. 22 HCs	Patients' NAWM: ↑MD ↓FA No correlation with lesion accumulation
(Rovaris *et al.*, 2008)	Longitudinal (3 yrs)	30 CIS	GM: ↑MD over time No correlations with relapse rate and brain volume change
(Bester *et al.*, 2008)	Longitudinal (1 yr.)	24 CIS-ON Vs. 15 HCs	Patients' callosal NAWM: ↓FA Over time, ↓FA ↓ADC
(Henry *et al.*, 2009)	Cross-sectional	24 CIS Vs. 18 HCs	Patients' thalamocortical NAWM: ↑MD ↓FA ↑ MD correlated with ↓thalamic volume
(Raz *et al.*, 2010)	Cross-sectional	34 CIS Vs. 16 HCs	Patients' NAWM: ↓FA in most tracts
(Lin *et al.*, 2011)	Cross-sectional	19 CIS Vs. 19 HCs	Patients' callosal NAWM: ↑MD ↓FA ↑RD DTI metrics correlated with lesion volume
(Cappellani *et al.*, 2014)	Cross-sectional	45 CIS Vs. 52 HCs	Patients' NAWM and GM: = MD ↓ FA NAWM ↓FA correlated with ↑lesion load

Author	Design	Population	Findings
(Kolasa *et al.*, 2015)	Longitudinal (4 yrs)	9 CIS non-converting Vs. 11 CIS converting Vs. 10 HCs	Patients' NAWM: ↑MD ↓FA. Converting patients' higher rate of MD decrease over time than non-converting. No correlation with MS conversion
(Moroso *et al.*, 2017)	Cross-sectional	37 CIS Vs. 32 MS Vs. 36 HCs	CIS patients' cerebellum: =FA MS patients' cerebellum: ↓FA than CIS patients
(Planche *et al.*, 2017)	Cross-sectional	37 CIS Vs. 32 MS Vs. 36 HCs	CIS patients' hippocampus: ↓FA than HCs. MS patients' hippocampus: ↑MD and ↓FA than CIS and HCs. In CIS, MD discriminated memory-impaired from memory-preserved persons
(Kugler and Deppe, 2018)	Longitudinal (MRI FU at 6 months; clinical FU 4.5 yr.)	46 CIS Vs. 26 HCs	Patients' cerebellum: ↓FA. Over time ↓FA In 16 patients converting to MS , ↓FA correlated with ↓latency conversion
(Koubiyr *et al.*, 2018)	Longitudinal (1 yr.)	56 CIS Vs. 38 HCs	Patients' hippocampus: ↑MD Over time ↑MD Over time, ↑ MD correlated with ↓hippocampal volume

Author	Design	Population	Findings
(Huang *et al.*, 2018)	Cross-sectional	36 CIS Vs. 36 MS Vs. 36 HCs	Patients' NAWM: ↑ MD ↓FA ↓AD than HCs, more widespread in MS than CIS patients In CIS patients = RD and no correlations between DTI metrics and disability
(Bommarito *et al.*, 2018)	Cross-sectional	27 CIS 24 HCs	Patients' NAWM (corticospinal tracts, corpus callosum, optic radiations): ↑MD,=FA
(Schneider *et al.*, 2019)	Cross-sectional sub-group analysis	51 CIS Vs. 55 MS Vs. 49 HCs	NAWM: = FA and =MD between CIS and MS

CIS: clinically isolated syndrome; HCs: healthy controls; MS: multiple sclerosis; NAWM: normal-appearing white matter; MD: mean diffusivity; FA: fractional anisotropy; GM: grey matter; FU: follow-up; RD: radial diffusivity; AD: axial diffusivity

In general, axonal damage has been associated with increased AD and demyelination with increased RD (Pierpaoli *et al.*, 2001). However, in several CNS areas, characterised by low anisotropy, such as grey matter, areas of crossing fibres or voxels affected by partial volume, the DT does not describe the tissue microstructure adequately, and so there is not a direct correspondence between eigenvalues and pathological substrates (Wheeler-Kingshott and Cercignani, 2009).

Furthermore, according to the DT assumption, in the presence of axonal loss, the diffusive behaviour of water molecules is increased, resulting in increased MD and decreased FA (Pierpaoli *et al.*, 2001). However, pathological correlates of DWI in *post mortem* multiple sclerosis studies showed that increased MD and decreased FA correlated more strongly with myelin content than with axonal loss (Schmierer *et al.*, 2007).

A possible reason that may affect the specificity of DT metrics to CNS pathology is that the model of Gaussian diffusion oversimplifies the diffusive behaviour of water in complex media. MD and FA can correlate with major tissue damage (i.e., stroke), but they lack sensitivity and specificity to more subtle pathological changes as the ones taking place in MS.

Therefore, over the years, different diffusion models have been developed to achieve a better correlation with potential biological substrates (Cercignani and Gandini Wheeler-Kingshott, 2019).

Some frameworks, such as q-space imaging, use a model-free approach to overcome the limitations of the DT model (Assaf and Cohen, 1999). Others, such as diffusion kurtosis imaging, measure the deviation from Gaussian behaviour (Jensen *et al.*, 2005). Finally, others divide the CNS into compartments that differ for water diffusion behaviour (Ferizi *et al.*, 2014). Among them, a three-compartment model seems to be more specific to the tissue substrates than the two-compartment or DT model (Ferizi *et al.*, 2014).

In this study, therefore, I have adopted a three-compartment model, developed at University College London (Zhang *et al.*, 2012) (Zhang et al., 2012): NODDI.

4.1.2 NODDI

The NODDI model assumes that water molecules in the CNS are divided into three different compartments (Figure 4.1):

- The intracellular compartment is the space delimited by the neurite membranes. Using Watson's distribution, this space is modeled as dispersed sticks, representing dendrites and axons, in which the water diffusion is restricted and depending on the sticks (neurites) orientation, which can vary from highly parallel to highly dispersed.

- The extracellular compartment is the space around neurites. In this space, water diffusion is anisotropically hindered within glial cells, neuronal cell bodies and the extracellular environment (anisotropic Gaussian diffusion)

- The free-water compartment is modeled as isotropic Gaussian diffusion, such as the areas with CSF

In the NODDI model, after the DW data are acquired, parametric maps describing the properties of these three compartments are obtained. They represent indices such as:

• Orientation Dispersion Index (ODI): measures the tortuosity of axons and dendrites (0, neurites completely aligned; 1, neurites completely dispersed)

• Neurite Density Index (NDI): measures the density of neurites (0, absence of neurites; 1, the maximum density of neuritis)

• Fractional Isotropic Volume (ISOVf): measures CSF presence (0, absence of CSF; 1, maximum presence of CSF)

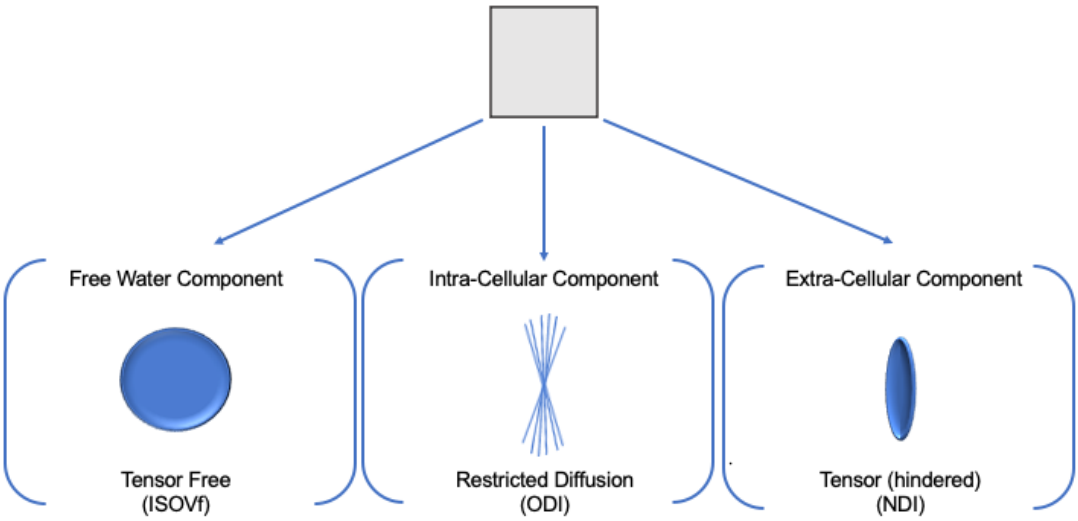

Figure 4.1 NODDI Model

The NODDI parametric maps reproduce the spatial pattern of CNS anatomy. The NDI map, for example, follows the neurite density: it is lower in grey matter than in white matter, where reaches the highest levels in the major tracts, such as the corpus callosum. The ODI map, instead, has higher values in the grey matter than in the white matter, with the lowest values in the corpus callosum where fibres are highly parallel. Finally, the ISOVf map has the highest values in the CSF compartment, as expected. Furthermore, NODDI parameters demonstrated higher specificity to tissue structure than FA in complex brain regions like the centrum-semiovale, where FA has grey-matter values, whilst NDI is comparable to other white matter regions (Chung *et al.*, 2016).

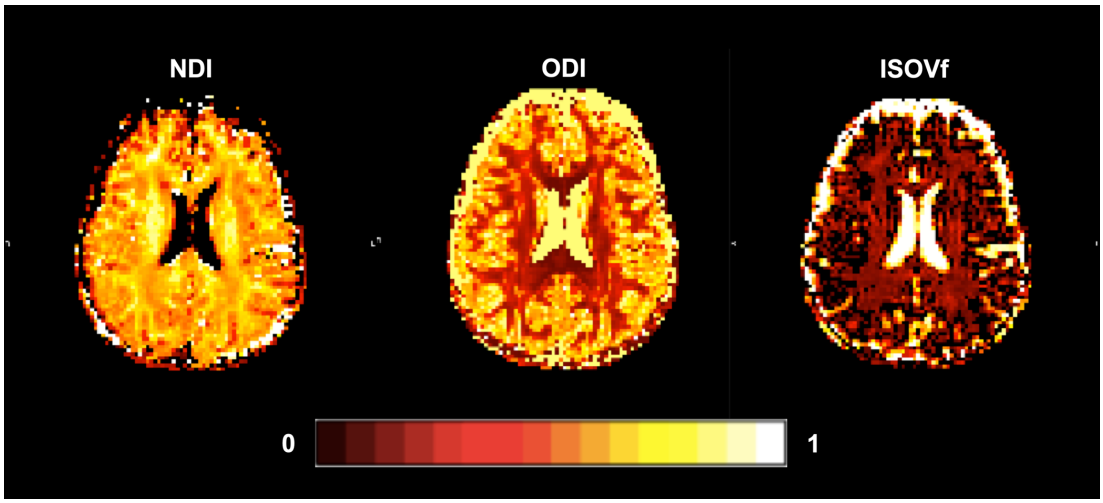

Figure 4.2 NODDI maps in the brain

Example of NODDI maps from a patient of the cohort analysed in this thesis. Abbreviations: NDI: neurite density index; ODI: orientation dispersion index; ISOVf: fractional Isotropic Volume

In multiple sclerosis, NODDI metrics better characterise tissue alterations than DTI (Schneider *et al.*, 2017; De Santis *et al.*, 2019) and show a higher specificity and sensitivity to neurodegeneration than FA (De Santis *et al.*, 2019). However, in comparison with DTI, NODDI, with its higher specificity to tissue microstructure and a more complex model, is more susceptible to noise. This determines a higher between-subject and between-vendor variability and lower within-subject reproducibility than DTI (Chung *et al.*, 2016; Andica *et al.*, 2020). Therefore, comparisons between different studies need cautious interpretations.

4.1.2.1 Histopathological correlations

There is evidence that NDI and ODI of brain and spinal cord tissues are reasonably correlated with histology-based neurite density and orientation dispersion, respectively (Sepehrband *et al.*, 2015; Mollink *et al.*, 2017; Sato *et al.*, 2017; Schilling *et al.*, 2018, 2019).

Grussu and colleagues (Grussu *et al.*, 2017) used *post mortem* specimens of thoracic and lumbar spinal cord tissue from multiple sclerosis patients and controls. They acquired NODDI and DTI sequences, while the histological procedure consisted of the staining for neurofilaments, myelin, astrocytes and

microglia, and the assessment of circular variance. In the multiple sclerosis patients' specimens, they found two chronic lesions, both with reduced circular variance, but one with scarce axonal loss and pronounced myelin loss and astrogliosis, the other with the opposite behaviour. They confirmed ODI specificity for orientation dispersion as this metric was found consistently reduced in the lesions with decreased circular variance. Interestingly, NDI was reduced in both lesions, even in the first one without axonal loss, so the authors concluded that myelin density would also contribute to NDI values. They suggest that myelin loss increases the amount of MRI-visible water, thus causing NDI to decrease. However, histological samples are dehydrated in their preparation so that this relationship may be different *in vivo*.

Another study, using an animal model of demyelination, showed that, in remyelinating lesions, ODI decreased and NDI increased over time, suggesting that NODDI may track remyelination (Luo *et al.*, 2019)

Finally, Yi and colleagues showed that ODI is also affected by the increased occupancy in the extra-neurite space happening during neuro-inflammation. Specifically, they found a direct correlation between ODI and microglial density, suggesting that ODI can be a marker of parenchymal inflammation (Yi *et al.*, 2019).

However, in grey matter, NODDI may not retain the same specificity for inflammatory changes as in white matter. A recent study investigated the hippocampus of EAE mice compared to disease-free mice. While NODDI was able to distinguish between the different hippocampal layers, it failed to capture the dendritic alterations and microglia activation occurring in the EAE hippocampus, whereas DTI metrics were significantly altered (Crombe *et al.*, 2018).

4.1.2.2 NODDI in multiple sclerosis

NODDI has been successfully used in multiple sclerosis patients to assess microstructural alterations in lesions, normal-appearing white matter, and grey matter. In patients, all studies reported reduced NDI in both the white matter lesions, compared with normal-appearing white matter, and in the normal-

appearing white matter itself, compared with healthy controls' white matter. ODI, instead, was found to be altered predominantly in white matter lesions with different directions depending on the study.

In a pilot-study, Schneider and colleagues compared the white matter of five relapsing-remitting multiple sclerosis patients and five healthy controls. The normal-appearing white matter of patients showed lower NDI and higher ODI than controls. White matter lesions had lower NDI and ODI compared with patients' normal-appearing white matter (Schneider *et al.*, 2017).

Granberg and colleagues combined 3 T and 7 T MRI to study white matter and, particularly, cortical pathology in early multiple sclerosis patients. This first study on the grey matter showed lower NDI in cortical lesions compared with the contralateral normal-appearing cortex, which, instead, did not show global alterations in NODDI metrics. A voxel-based morphometry analysis revealed topographical organization of NDI and ODI with an apparent banding of the metrics in the sensorimotor cortex where higher orientation dispersion on the left side was associated with increased Expanded Disability Status Scale (EDSS). The normal-appearing white matter in multiple sclerosis subjects had diffusely lower NDI than the white matter in controls. White matter lesions, besides a reduced NDI, also showed higher ODI than the contralateral normal-appearing white matter (Granberg *et al.*, 2017).

Spanò and colleagues recruited patients with different multiple sclerosis phenotypes: relapsing-remitting and secondary progressive multiple sclerosis. They analysed NODDI maps voxel-wise in the brain tissues, excluding the white matter lesions with probability maps. In comparison to the study by Granberg and colleagues, they assessed more extensively patients' disability including, not only the EDSS, but also the multiple sclerosis functional composite (MSFC) score, a test battery for cognitive, upper and lower limb function. In patients, they found decreased NDI in several white matter and grey matter areas more pronounced in secondary progressive than relapsing-remitting patients. ODI instead showed mixed behaviour, being higher or lower than healthy controls depending on the area. In some areas, the NDI and ODI alterations significantly correlated with disability scores (Spanò *et al.*, 2018).

A recent study evaluated the distribution of white matter damage in 24 relapsing-remitting multiple sclerosis patients compared with 24 healthy controls. They combined NODDI, DTI, and myelin volume fraction and analysed white matter tracts using Tract-Based Spatial Statistics (TBSS). In the TBSS analysis, they focused on FA, ISOVf, and myelin volume fraction changes. They demonstrated lower FA, lower myelin volume fraction and higher ISOVf values in the corpus callosum, cingulate gyri, and corona radiata of patients compared with controls. In the region of interest analysis, they analysed all metrics and found higher ODI in the normal-appearing white matter and lower ODI in the white matter lesions compared to healthy controls' white matter. None of their findings correlated with disability scores (Hagiwara *et al.*, 2019).

Finally, a pilot study assessed NODDI metrics in the spinal cord of multiple sclerosis patients. By and colleagues applied NODDI, DTI and DKI-derived mean kurtosis in the cervical spinal cord of six multiple sclerosis patients and eight controls. In patients, they found a difference between spinal cord lesions and normal-appearing white matter that was not detected by the other two techniques. Specifically, they found lower NDI in the white matter lesions, compared with normal-appearing white matter, and higher ODI in patients' normal-appearing white matter when compared with healthy controls (By *et al.*, 2017).

4.1.2.3 NODDI in neurological diseases and ageing

Since its development for *in vivo* applications, NODDI has been used in approximately 75 studies to investigate alterations in the CNS during neurological, psychiatric, and systemic diseases.

Studies on neurodegenerative diseases provide interesting cues on possible NODDI interpretations. In these conditions, microstructural changes in the CNS are more homogeneous than in neuro-inflammatory conditions, such as multiple sclerosis. In Parkinson's disease, a reduction in NDI and ODI in the pars compact of the substantia nigra correlated negatively with clinical severity (Andica *et al.*, 2018); in pre-manifest Huntington's disease, several white matter tracts, including the corpus callosum, showed reductions in NDI and

ODI and correlated with disability (Zhang *et al.*, 2018) ; in Alzheimer's disease, reduction in NDI and ODI was seen in several relevant cortical areas, with lower NDI in patents more cognitive impaired (Parker *et al.*, 2018), while in a mouse model of the disease, a low NDI correlated with the tau protein burden in the cortex and corpus callosum (Colgan *et al.*, 2016); finally, in amyotrophic lateral sclerosis, patients showed NDI reduction in cortical-spinal tracts up to the motor cortex and across the corpus callosum, while they had both increased and decreased ODI, depending on the area, with the reduced ODI in the motor cortex correlating with longer disease duration (Broad *et al.*, 2019)

NODDI has also been used to investigate changes in brain white matter development and normal ageing. During brain development, the NDI increases rapidly in childhood and more slowly in adulthood, while ODI shows the opposite behaviour (Chang *et al.*, 2015). In adulthood, ODI and ISOVf increase with age in the brain white matter, while NDI only shows small variations restricted to the frontal white matter (Billiet *et al.*, 2015).

Concerning the cortex, a recent study showed how NODDI parameters changed according to cortical microstructure. Fukutomi and colleagues (Fukutomi *et al.*, 2018) analysed NODDI metrics in 505 subjects from the Human Connectome Project. Firstly, they found that NDI had a strong correlation with the cortical myelin content. The histological studies discussed before also reported this association. However, since both axon and neuron density strongly correlate with myelin content (Schmierer *et al.*, 2007; Collins *et al.*, 2010; Glasser and van Essen, 2011; Glasser *et al.*, 2014), the authors concluded that the strongest contributor to NDI values in the cortex is the density of myelinated axons and not myelin itself. Secondly, they found that in the healthy cortex ODI and NDI maps were strongly correlated ($R= 0.60$, $p < 0.00001$), except for the primary motor cortex, where ODI was low-moderate and NDI high. Finally, they found that ODI captures the cortical myeloarchitecture: it is high in the granular cortex, which possesses tangential myelinated fibre bands, and low in the agranular areas, such as the insula and cingulate cortex. Moreover, ODI showed a strong negative correlation with cortical thickness, so, for example, the early sensory areas showed high ODI and thin cortex.

4.2 ^{23}Na MRI

4.2.1 Sodium

Sodium (^{23}Na) is one of the most abundant cations in the human body, and it is involved in several cellular activities. In the brain, as well in most of the body tissues, ^{23}Na concentration is 140 mmol/L in the extracellular space and 10-15 mmol/L in the intracellular space.

One of the most critical roles is in the sodium-potassium exchanger (or Na+/K+ATPase), as discussed in paragraph 3.1.1.6, that guarantees a higher concentration of sodium in the extracellular space than inside the cells. This pump maintains the cell membrane potential, and it is particularly crucial for excitable cells, such as neurons.

After protons, which are used in conventional MRI scans, ^{23}Na is the second most abundant MRI active nuclei. Moreover, after protons and fluorine-19(^{19}F), ^{23}Na also yields the strongest nuclear magnetic resonance signal, again. In 1984, Maudsley and Hilal applied ^{23}Na MRI in living tissues (Maudsley and Hilal, 1984). Initially, ^{23}Na MRI applications were limited by its poor signal to noise ratio, causing long acquisitions and low spatial resolution, and by the limited availability of MRI scanners with sodium coils. Moreover, ^{23}Na has a bi-exponential relaxation time and its major component of the T2 signal can be very difficult to detect because of a short T2.

Over the years, however, MRI hardware and software developments, together with the introduction of high and ultra-high-field scanners, have allowed better spatial resolutions and shorter acquisition times. Therefore, ^{23}Na MRI has been used in animals, ex vivo human brain tissues, and, finally, *in vivo* showing quantitative ^{23}Na measurements equivalent to the ones determined with ex vivo methods (Thulborn *et al.*, 1999).

In multiple sclerosis, as discussed in chapter 2, demyelination and inflammation can lead to increased intracellular sodium concentration, which triggers, in turn, toxic calcium influx damaging the neuron and the axolemma.

However, one limitation of ^{23}Na MRI is that it cannot differentiate between the intracellular and extracellular sodium concentrations. Although the intracellular compartment is larger (80-85%) than the extracellular one (15-20%), processes such as oedema and necrosis increase the extracellular space and can result in high sodium concentration captured by the ^{23}Na MRI. However, recent advances, using multiple quantum filters, inversion recovery pulses, and diffusion-based techniques can allow researchers to distinguish between intracellular and extracellular sodium accumulation (Nagel *et al.*, 2011; Fleysher *et al.*, 2013).

4.2.2 ^{23}Na MRI in multiple sclerosis

^{23}Na MRI was first applied to multiple sclerosis patients by Inglese and colleagues in 2010. In this study, they assessed the brain total sodium concentration (TSC) in a small cohort of relapsing-remitting multiple sclerosis patients compared to controls (Inglese *et al.*, 2010). They selected small regions of interest (range 2–8 pixels) of white matter (splenium of the corpus callosum, cerebellar, periventricular, frontal, and occipital lobes) and cortical grey matter. In patients, they also assessed TSC in white matter lesions larger than 5 mm and divided them in enhancing, T1 hypo- and isointense. They found that TSC was higher in the normal-appearing white matter and the frontal grey matter of patients than in controls, and it was associated with lesion volumes (T2-hyperintense and T1-hypointense) and moderately with EDSS. In the lesions, T1 hypointense lesions and enhancing lesions exhibited similar TSC that was still higher than patients' normal-appearing white matter and correlated moderately with EDSS.

Zaaraoui and colleagues investigated differences in TSC between relapsing-remitting multiple sclerosis patients with short (<5 years from onset) and long disease duration (Zaaraoui *et al.*, 2012). They found that early patients displayed only local TSC alterations in the brainstem, cerebellum, and left medial temporal lobe. In contrast, the global TSC values in the normal-appearing white and grey matter were similar to healthy controls. Advanced patients, instead, not only showed higher TSC in the normal-appearing white and grey matter than controls but also a higher TSC in the splenium of the

corpus callosum and the grey matter when compared to early patients. Interestingly, however, the TSC in white matter lesions, which was higher than the controls' white matter, was similar between early and advanced patients. They confirmed the previous findings of a correlation between TSC in the normal-appearing white matter and T2-hyperintense lesion volume, but not the association with EDSS, which was, instead, only associated with the grey matter TSC. These results suggest that TSC increase in early patients may be confined to local areas while becoming more widespread during the disease, involving both white and grey matter.

Pailing and colleagues extended these findings by assessing TSC in the brains of different multiple sclerosis phenotypes: relapsing-remitting, secondary, and primary progressive multiple sclerosis patients (Paling *et al.*, 2013). They found that patients had higher TSC in both normal-appearing white and grey matter than controls and that TSC was lower in lesions, particularly in the T1 hypointense ones. However, when grouping patients according to the disease phenotypes, they found that the secondary-progressive group was driving these results since they had higher TSC in the brain tissues compared not only with controls but also with relapsing-remitting patients. For disability, they found that TSC in deep grey matter was independently associated with EDSS and walking speed. Additionally, TSC in T1-hypointense lesions was associated with MSFC tests: 9-Hole Peg Test and paced auditory serial addition test (PASAT). Interestingly, primary-progressive and relapsing-remitting patients did not show significant differences in TSC.

The findings of Maarouf and colleagues, who also investigated TSC in primary- and secondary-progressive multiple sclerosis patients, may provide an explanation for this result (Maarouf *et al.*, 2014). They applied statistical mapping analysis to assess the topography of TSC alterations in the brain. They found that whilst secondary-progressive patients had widespread TSC alterations in the cortex, primary-progressive patients had high TSC confined to specific cortical areas, the motor, prefrontal and somatosensory cortices, pons, and cerebellum. The high TSC in the premotor cortex was associated with high EDSS score and in the prefrontal cortex with high MSFC. Therefore,

primary-progressive patients seem to have more localised TSC increases than secondary-progressive ones.

Furthermore, these findings suggested a correlation between disability and TSC in eloquent cortical areas. The same author explored this further by studying 58 patients with early relapsing-remitting multiple sclerosis who underwent detailed neuropsychological testing (Maarouf *et al.*, 2017). The cognitively impaired patients showed higher TSC in grey matter and normal-appearing white matter compared with cognitively preserved patients. Moreover, in a multivariable model, grey matter TSC explained more of the variability in cognition that grey matter atrophy. This result suggests that metabolic abnormalities in the cortex are relevant to cognitive impairment in multiple sclerosis and precede tissue loss.

Brownlee and colleagues recently confirmed these findings — the correlation between cortical TSC and disability and the increase in TSC in the secondary phase of multiple sclerosis — in the 15-year follow-up Queen Square CIS cohort (Brownlee *et al.*, 2019*b*). They found that patients with multiple sclerosis had higher TSC in all tissues compared not only to controls but also to patients who had remained CIS over the 15 years. Similar to previous studies, the differences were driven by patients with secondary-progressive multiple sclerosis. Finally, a higher cortical TSC was associated with worse scores at EDSS, MSFC, and cognitive tests, independently of grey matter atrophy.

As discussed before, one of the main issues with ^{23}Na MRI studies is to differentiate sodium increases in the intracellular and extracellular compartment as they may underlie different pathological processes. Petracca and colleagues used single quantum and triple-quantum filtered ^{23}Na MRI at 7 T to quantify intracellular and extracellular sodium concentration in the brain of 19 relapsing-remitting multiple sclerosis patients and 17 healthy volunteers (Petracca *et al.*, 2016). Interestingly, they found that in patients, the normal-appearing white matter had both intracellular and extracellular sodium concentrations higher than controls. However, only the increase of extracellular sodium concentration was related to high T1 lesion volume, high EDSS, and low normalised grey matter volume. Moreover, higher extracellular

sodium concentration was associated with longer disease duration, whilst the intracellular sodium concentration showed the opposite relationship. Therefore, the authors suggest that the extracellular sodium concentration may be an expression of structural damage, while the intracellular sodium concentration may represent a compensatory mechanism.

A recent study supported this interpretation of the variability of sodium concentration in the brain not only as a marker of neuro-axonal damage but also as an expression of functional metabolic changes by assessing the brain function with functional-^{23}Na MRI (Gandini Wheeler-Kingshott *et al.*, 2018). They showed, indeed, that functional-^{23}Na MRI successfully detected changes in activation between finger tapping and rest across the entire brain.

Additionally, ^{23}Na MRI in multiple sclerosis can not only differentiate between different types of white matter lesions, but also show meaningful correlations with disability, suggesting higher specificity for pathological substrates than conventional MRI lesion metrics.

Eisele and colleagues, looking at lesions individually, further explored this. In the first study, they combined ^{23}Na MRI and DWI to explore the heterogeneity of acute multiple sclerosis lesions (Eisele *et al.*, 2016). They confirmed higher TSC in acute enhancing lesions, but they found that hyperacute non-enhancing lesions with low apparent diffusion coefficient did not show alterations in TSC. This result suggests that TSC alterations appear with loss of tissue and BBB integrity. In a second study, they confirmed these findings by following up on these hyperacute lesions over time (Eisele *et al.*, 2019). They found indeed that the apparent diffusion coefficient increased over time along with the TSC increase and the development of vasogenic oedema and contrast-enhancement. After four weeks, TSC values decreased, and vasogenic oedema and contrast-enhancement resolved. These findings are in line with studies on TSC during stroke: sodium elevations are not seen during the phase when the DWI changes delineate the area of the acute ischemia, but after this, following tissue damage. Table 4.2 shows the pathological correlates of NODDI and ^{23}Na MRI.

Table 4.2 Pathological specificity of MRI measurements

MRI technique	MRI metric	Pathological substrate	
		White matter	Grey matter
NODDI	NDI	Loss of large myelinated axons	Neuro-axonal loss
NODDI	ODI	Dispersion of neurites orientation Microglia activation	Changes in cytoarchitecture Loss of fibers perpendicular to the cortex
NODDI	ISOVf	Axonal loss Oedema	Neuro-axonal loss
^{23}Na MRI	TSC	Neuro-axonal dysfunction Neuro-axonal loss Oedema	Neuro-axonal dysfunction Neuro-axonal loss

MRI techniques	MRI metric alterations	Hypothesised pathological substrate
NODDI and ^{23}Na MRI	↓NDI ↑TSC	Neuro-axonal loss
NODDI	↓NDI ↓ODI	Neuro-axonal loss
NODDI	↓NDI ↑ODI	Neuro-axonal damage and dispersion of neurites orientation or microglia activation

Abbreviations: NODDI: Neurite Orientation and Density Index; NDI: neurite density index; ODI: orientation dispersion index; ISOVf: Isotropic volume fraction; TSC: total sodium concentration

4.3 Structural Cortical Networks

Different MRI techniques can be used to study the CNS network. Researchers study the white matter tracts using DTI and tractography techniques (Conturo *et al.*, 1999). They can use functional MRI that measures brain activity, in the resting state or during a task, using blood-oxygen-level dependent contrast: when a cortical area of the brain is in use the blood flow and the oxygen levels increases (Frahm *et al.*, 1993). Finally, since functional changes in the brain can lead to related morphological modification in cortical areas (Maguire *et al.*, 2000; Golestani *et al.*, 2002), they can describe these coordinated patterns of cortical morphology with network parameters and build structural cortical networks (SCNs) (Lerch *et al.*, 2006; Tijms *et al.*, 2012). This is the method used in this thesis in Chapter 8.

Furthermore, when applying each of these techniques, the CNS network can be analysed using a mathematical framework called “graph theory”, which models the CNS as a mathematical structure composed of vertices (also called nodes or points) which are connected by edges (also called links or lines). In SCNs, the nodes correspond to cortical areas considered connected by edges that are weighted by structural similarity in thickness or volume across subjects (Lerch *et al.*, 2006) or within single subjects (Tijms *et al.*, 2012)

I chose to analyse single-subject SCNs, because, in comparison with other brain graphs (e.g., structural graphs derived from DTI or functional graphs derived from synchronic activation of brain areas), SCNs present the unique advantage of being derived from anatomical MRI acquisitions, such as a 3D T1-weighted sequence, frequently available in acquired datasets and even in routine clinical protocols. Moreover, SCNs have shown clinically relevant changes in many brain diseases (e.g., Bassett *et al.*, 2008; Tijms *et al.*, 2013; van Duinkerken *et al.*, 2016). However, few studies so far have investigated SCNs in multiple sclerosis (He *et al.*, 2009; Tewarie *et al.*, 2014; Muthuraman *et al.*, 2016; Rimkus *et al.*, 2018).

SCN analysis has revealed in multiple sclerosis patients, disruption of physiological small-world network topology of the brain: an efficient organization, shared by most of the complex systems in nature, including brain networks, that is neither completely regular nor completely random, because it combines a dense local clustering with relatively sparse long-distance connections (Watts and Strogatz, 1998) (Figure 4.3). Whilst multiple sclerosis patients can shift in either direction, either towards a more regular (Tewarie *et al.*, 2014; Muthuraman *et al.*, 2016) or a more random network (He *et al.*, 2009; Rimkus *et al.*, 2018), the only study including a small cohort of CIS patients (Muthuraman *et al.*, 2016) demonstrated increased clustered organization of SCNs in CIS subjects compared with healthy controls. Regular networks, such as lattices, are highly clustered, but with long path length: nodes are densely connected with their clique of neighbours, whereas they are linked to distant nodes only through several intermediate steps, causing a decrease in the global network efficiency. However, the SCNs were extracted at group level in the CIS cohort, and so it is still unclear whether and how these disruptions are associated with individual measures of disability.

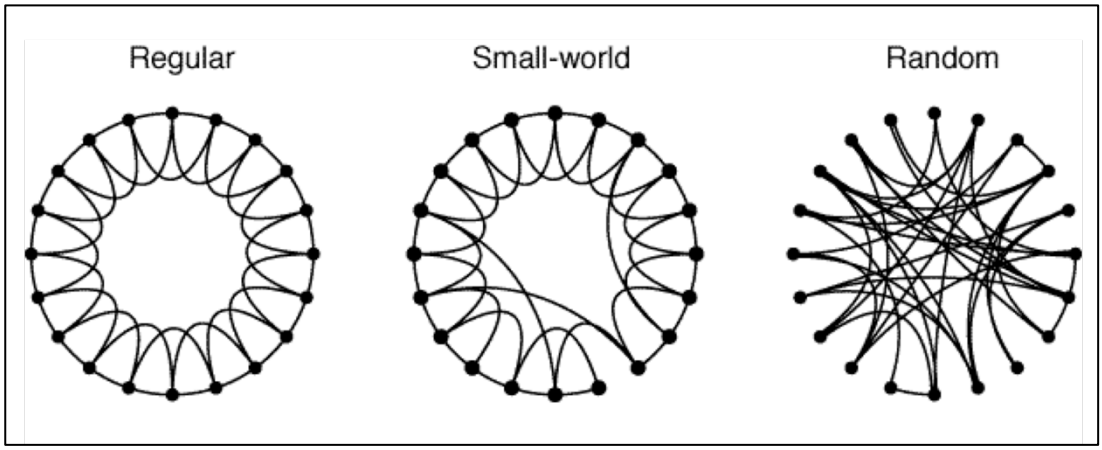

Figure 4.3 The small-world network (adapted from (Watts and Strogatz, 1998)

4.4 Optical coherence tomography

4.4.1 Principles

Optical Coherence Tomography (OCT) is a non-invasive technique that works similarly to B mode ultrasound, but, instead of acoustic waves, it uses light reflections to acquire images of retinal and nerve tissue at a very high resolution so that it can be defined an “optical biopsy” (Blumenthal *et al.*, 2009).

Briefly, low-coherence light is generated by using super luminescent diodes or short pulse lasers and scanned across the retina. Then, the echo time delay and magnitude of the backscattered light are measured. However, the direct detection of light echoes is not possible, because of their high speed, so interferometry techniques are used. The backscattered light is split into two arms, a sample and a reference beam (usually a mirror), traveling different routes. They are recombined before arriving at a detector. If light from both arms has travelled the same optical distance, it gives rise to an interference pattern. The image is acquired by measuring the amplitude of this interference signal: the higher the light reflected back, the greater the interference. Frequencies outside the short coherence length do not interfere.

The basic reflectivity profile is the axial-scan (A-scan) that contains spatial information about the dimension and location of the retinal structures. By laterally combining a series of A-scans, we obtain a B-scan: a cross-sectional image where amplitudes of reflections are represented in a grey scale or a false-colour scale

The first OCT models were time-domain: the range of depth was sampled one point at a time by moving the reference mirror. This mechanism made the acquisition long and spatial resolution low. In 2002, the OCT technology was improved, allowing the detection of reflections from the entire depth range simultaneously. This new technique is called spectral-domain or Fourier-domain OCT. The reference mirror is fixed, and the interference between the

sample and reference beams is detected as a spectrum and have a Fourier transformation to produce an A-scan (Figure 4.4).

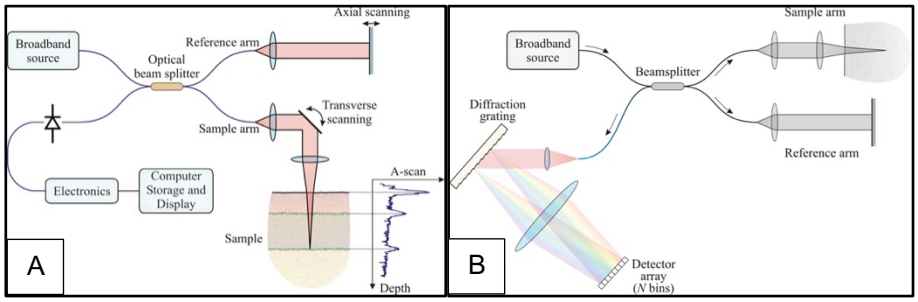

Figure 4.4 A) Time-Domain OCT; (B) Spectral-Domain OCT (image modified from uwa.edu.au)

The algorithm to combine multiple images which have been captured in the same location is called automatic real time (ART) mean. Single OCT images are averaged in real-time to decrease noise and enhance contrast within the final OCT image.

Spectral-domain OCT became commercially available in 2006 and superseded time-domain OCT for its faster acquisition (approximately 25,000 axial scans per second) and higher resolution (approximately 5-7μm). I have used a spectral-domain OCT instrument (Heidelberg Spectralis) in this thesis (chapter 8).

In the following paragraphs, I shall summarise the retinal structure focusing on the layers that are of interest for multiple sclerosis studies and analysed in chapter 8.

4.4.2 Retinal layers

In multiple sclerosis, the retinal OCT parameters are taken from the central area of the retina, the macula.

The retina is a unique CNS structure as it contains axons and glia in the absence of myelin. The macula is a circular area, approximately 1.5 mm diameter, located 17 degrees from the centre of the optic disc. In its centre there is the fovea, an oval-shaped depression that confers the greatest visual acuity thanks to its highest density of cone receptors (199,000/mm^2) (Curcio *et al.*, 1990).

The retina consists of three layers of nerve cell bodies and two layers of synapses (Figure 4.5) The outermost layer is the photoreceptor layer. The innermost layer is the ganglion cell layer (GCL), proximal to the lens and anterior chamber of the eye.

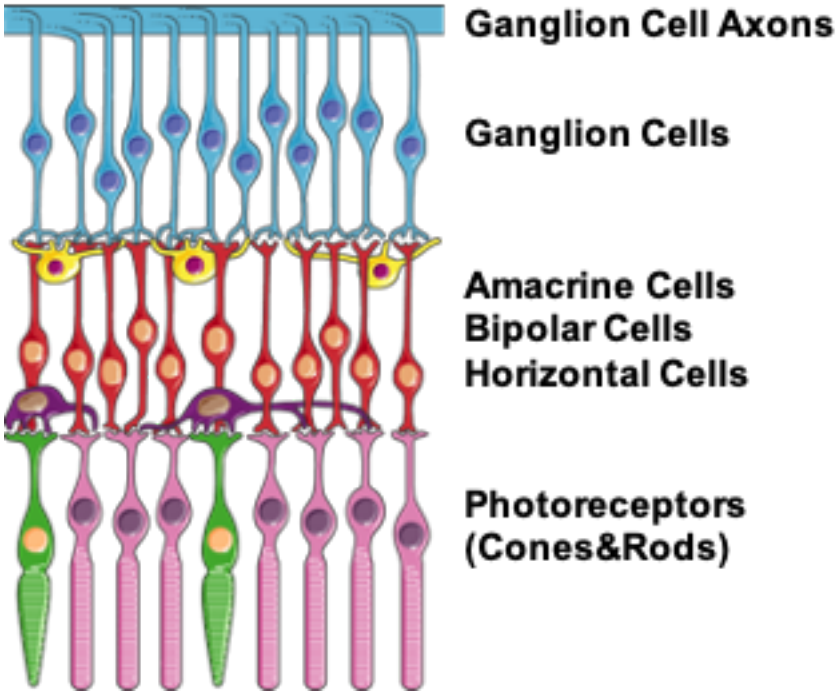

Figure 4.5 Retinal Layers

Photoreceptors are rods and cones that convert photons of light into electrochemical signals. Humans have a rod: cone ratio of 20:1, and approximately 50% of cones are located within the macular area (Curcio *et al.*, 1990).

The photoreceptors form synaptic connections with bipolar and horizontal cells in the outer plexiform layer. Here the initial processing of the visual signal begins.

After there are three layers usually investigated in multiple sclerosis studies: the inner nuclear layer (INL), the inner plexiform layer (IPL), and the GCL.

4.4.2.1 Inner nuclear layer

This layer consists of bipolar, horizontal, and amacrine cells. These cells form complex neuroretinal connections in the inner and outer plexiform layers that modify the photoreceptor signal and transmit it to the ganglion cells.

4.4.2.2 Inner plexiform layer

This is responsible for the second stage of retinal processing. In this layer, bipolar cells synapse with the dendrites of ganglion cells. Moreover, it consists of horizontally and vertically directed amacrine cells that integrate and influence bipolar cell outputs (Kolb et al., 1995).

4.4.2.3 Ganglion cell layer

The ganglion cells transfer visual information from the retina to the brain. Adults have, on average, 1.2 million retinal ganglion cells, and approximately 70% serves central vision (Curcio and Allen, 1990).

There are different types of ganglion cells. The most common (80% of the ganglion cells) and prominent in the foveal area are the midget, parvocellular cells. They confer high spatial acuity, stereopsis, and colour vision (specifically, red or green colour signal).

The ganglion cell layer also contains displaced amacrine cells and astrocytes.

Between the GCL and the inner limiting membrane, there is the retinal nerve fibre layer containing the axons projecting to the optic nerve head.

4.4.2.4 Retinal nerve fiber layer

Ganglion cell axons travel towards the optic nerve head within the retinal nerve fibre layer separated into bundles.

The unmyelinated axons of the foveal ganglion cells project directly to the temporal part of the optic disc via the papillomacular bundle (Figure 4.6). The remaining axons from the temporal retina form the arcuate bundles around the papillomacular bundle and enter the superior temporal and inferior temporal sections of the optic disc. Axons that originate from the nasal retina project directly to the nasal aspect of the optic disc in a radial pattern. Due to the high density of parvocellular ganglion cells in the fovea, the diameter of the nerve fibres in the temporal retina is smaller than in the nasal region or vertical disc poles (Jonas and Dichtl, 1996). Ganglion cell axons enter the optic nerve head or disc at a 90--degree angle, and they are still unmyelinated at this point.

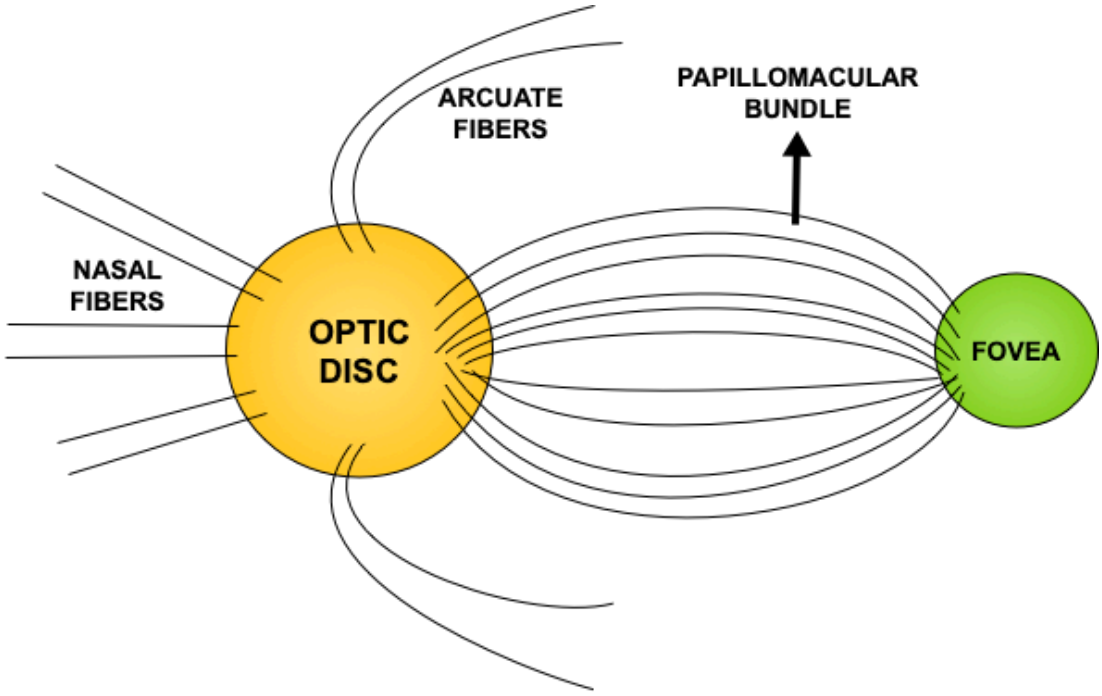

Figure 4.6 The papillomacular bundle

The optic disc, which does not contain photoreceptors ("blind spot"), is approximately 1 mm deep and 1.5 mm in diameter. It keeps a topographic organization of nerve fibres for the origin of axons: fibres from the fovea occupy a large proportion of the temporal aspect, whereas arcuate fibres occupy a peripheral position (Fitzgibbon and Taylor, 1996).

In ON, the inflammatory-demyelinating lesion of the optic nerve is followed by retrograde axonal degeneration along the retinal nerve fibre layer (RNFL)

culminating in the loss of retinal ganglion cells. Given the optic disc and retinal anatomy, the temporal sector of the disc and the papillomacular bundle, with their high density of thin axons, are understandably the most affected.

Besides axons, in the RNFL, there are astrocytes, retinal vessels, and Muller cells. Astrocytes and Muller cells form a neuroglial system that provides structural and nutritional support to the nerve fibres. The astrocytic processes partially envelop all nerve fibres and also cover the retinal capillaries isolating the axons from retinal blood flow. In the healthy eye, these cells can occupy 18% to 42% of the RNFL, depending on the retinal area (Ogden, 1983), but this percentage may increase with the disease (Green *et al.*, 2010). Therefore, after ON, the RNFL thickness is not purely accounting for axonal loss, but also gliosis. Consequently, the measure of the GCL, which is not confounded by this process, may reflect more the degenerative processes after ON. Indeed, Saidha et al. a superior structure--function correlation between the combined GCL-IPL (GCIPL) layer thickness and measures of visual function compared to RNFL (Saidha *et al.*, 2011).

4.4.3 Applications in multiple sclerosis

OCT was initially used for the diagnosis and management of ophthalmological conditions, but, over the last decades, it has been increasingly used in multiple sclerosis. Although not routinely used in clinical practice, OCT can help with the diagnosis of ON and exclude other ophthalmological conditions presenting with acute visual symptoms, such as maculopathy or ischaemic optic neuropathy.

We can recognise two significant applications in research.

Firstly, the inflammatory lesion in the optic nerve is similar to the acute plaques seen elsewhere in the CNS in multiple sclerosis. Therefore, OCT provides a unique opportunity to non-invasively quantify the structural effects of an inflammatory lesion, particularly in terms of axonal loss. The combination of OCT metrics with visual function (see Paragraph 5.7) allows the construction of a structural-functional paradigm of CNS injury in multiple sclerosis that can be used to study neurodegeneration and neuroprotection.

It is estimated that the average loss of RNFL in ON eyes is of -20.38 μm compared to controls (Petzold *et al.*, 2010). This process is particularly striking as the general healthy population appears to lose -20 μm over 60 years (Kanamori *et al.*, 2003).

The loss of retinal nerve fibre layer after ON follows an exponential model: it starts at 1-2 months, and, by three, maximum six months from the onset, 70-90% of the fibres are lost. Then, there is a slow, gradual decrease over time. The temporal sector is the affected early (Costello *et al.*, 2008; Henderson *et al.*, 2010).

On the other hand, the retina and optic nerve are an accessible site of the CNS and they offer the opportunity to study neuronal and axonal degenerative processes in multiple sclerosis, irrespective of the presence of ON.

RNFL and GCIPL show a higher rate of thinning in multiple sclerosis patients than healthy controls. In a longitudinal study of 299 multiple sclerosis patients, with and without ON, Talman and colleagues demonstrated a reduction of RNFL thickness of 1.7% at 1-2 yrs, 3.2% at 2-3 yrs, and 6.7% at >3 yrs of follow-up. Healthy controls' eyes, instead, decreased only 0.5% over 3 yrs (Talman *et al.*, 2010).

Different factors may be involved. On the one hand, the possible subclinical involvement of the optic nerve (London *et al.*, 2019) and trans-synaptic retrograde degeneration from lesions in the posterior visual pathway (Gabilondo *et al.*, 2014) may influence retinal thinning in the absence of ON. On the other hand, the loss of retinal ganglion cells and axons in the RNFL may mirror the brain atrophy as an expression of the same pathological mechanisms (Saidha *et al.*, 2015). GCIP and RNFL thinning are indeed seen also in neurodegenerative disorders such as Alzheimer's disease (Szegedi *et al.*, 2020). In this scenario, it is essential to note that a previous history of ON may interfere with the correlations between MRI parameters and RNFL thickness in patients with multiple sclerosis (Zimmermann *et al.*, 2013).

Atrophy within specific retinal layers has been associated with concomitant brain atrophy, both cross-sectionally (Gordon-Lipkin *et al.*, 2007; Grazioli *et al.*,

2008; Dörr *et al.*, 2011) and longitudinally (Saidha *et al.*, 2015). Particularly, GCIP atrophy seems to mirror global and GM atrophy in multiple sclerosis and it becomes marked in secondary progressive forms (Saidha *et al.*, 2015).

In the past, there have been conflicting findings on the correlation between overall disability, as measured by EDSS, and RNFL thickness. In a meta--analysis, Petzold and colleagues found six out of 12 studies reporting an association (Petzold *et al.*, 2010). A possible explanation is that this relationship may be more robust in early multiple sclerosis patients than advanced cases due to the presence of a "ceiling effect" for OCT. This effect has been shown for another ocular disease, glaucoma, which causes severe retinal atrophy (Rao *et al.*, 2015). Patients with a severe RNFL atrophy corresponding to the lowest values the OCT can detect may continue to deteriorate, but this decrease is not captured anymore by the OCT. Moreover, a recent study has shown a non-linear relationship with EDSS scores that could explain the lack of correlations in previous studies that used linear models (Martinez-Lapiscina *et al.*, 2016).

Chapter 5 Methodology

This chapter outlines the study design and methodology used in the projects of this thesis.

5.1 Recruitment

The study was approved by the institutional ethics committees at the National Hospital for Neurology and Neurosurgery and Moorfields Eye Hospital.

Since June 2014, patients presenting at Moorfields Eye Hospital and the National Hospital for Neurology and Neurosurgery for the onset of neurological symptoms suggestive of demyelination were invited to take part in the study. Once identified, potential participants were given the participant information sheet and allowed adequate time (a minimum of 24 hours) to decide if they wished to take part. Healthy controls were also recruited by posting information on the multiple sclerosis Society website and by word of mouth.

Inclusion criteria were: onset within three months from the recruitment (for patients), age between 18 and 65 years, the ability to give written informed consent in English, and to have an MRI scan. Exclusion criteria were: known neurological disease (other than CIS for patients), presence of anti-aquaporin-4 or anti-MOG antibodies, pregnancy or breastfeeding (assessed by asking the participant), and presence of magnetically sensitive or otherwise MRI incompatible implants.

The study protocol was approved by the local ethical committee and all subjects gave written informed consent (Study Ref: 13/LO/1762; 13/0231-CIS2013).

5.2 MRI protocol

5.2.1 Acquisition

The MRI scans were done at a 3T Achieva TX scanner (Philips Healthcare, Best, The Netherlands) with radiofrequency multi-transmit technology and Quasar Dual gradient set of 40/80 mT/m. The scanner has a 32–channel coil

for brain acquisition and a 16-channel neurovascular receive-only radiofrequency coil for the spinal cord. There was no major hardware or software upgrade during this study period. The protocol is summarised in Table 5.1.

Table 5.1 MRI protocol

Sequences	Slice orientation	Measured voxel size (mm)	TR (ms)	TE (ms)	Inversion time (ms)
^{1}H Head					
3D T1	Sag	1.0x1.0x1.0	6.9	3.1	821
3D FLAIR	Sag	1.2x1.2x1.2	8000	388	2400
PD/T2 TSE	Ax	1.0x1.3x3.0	3500	15/85	
T1 TSE +Gd††	Ax	1.0x1.3x3.0	625	10	
DWI	Ax	2.5x2.5x2.5	12	82	
^{23}Na Head					
3D gradient echo	Ax	3.0x3.0x3.0	1200	27	
T2 dual echo †	Ax	1.0x1.0x4.0	3875	11/85	
^{1}H Spinal Cord					
T1 TSE + Gd††	Sag	1.0x1.8x3.0	600	8	
PD/T2 TSE	Sag	1.0x1.8x3.0	3500	22/78	

† acquired in the sodium coil; †† patients only.
Abbreviations: FLAIR: fluid-attenuated inversion recovery; PD: proton density; TSE: turbo spin echo; Gd: gadolinium; DWI: diffusion-weighted image; TR: repetition time; TE: echo time

For the NODDI protocol, multi-shell DW images were acquired using a 2D echo-planar imaging sequence (2.5 mm isotropic voxels; field-of-view: 192x222 mm^2 ; repetition time: 12000 ms; echo time: 91 ms; b=300 s/mm^2, 8 directions; b=711 s/mm^2, 15 directions; b=2000 s/mm^2, 30 directions). Eight interleaved non-diffusion-weighted (b=0) images were also acquired.

On the same scanner, using a single tuned ^{23}Na coil (RAPID BioMed), I acquired ^{23}Na images (3 mm isotropic voxels; field-of-view: 240x200 mm^2; repetition time 120 ms; echo time of 0.27 ms). For the TSC quantification, calibration phantoms of 80 mM and 40 mM sodium concentration were fixed to the subject's head during the scan (Figure 5.1). A ^{1}H T2-weighted dual-echo scan (3mm isotropic voxels; repetition time 3875 ms; echo time 19 and 85 ms) was also acquired while the subject was in the sodium coil, using the scanner body coil. I used then this T2-weighted image for the sodium imaging post-processing.

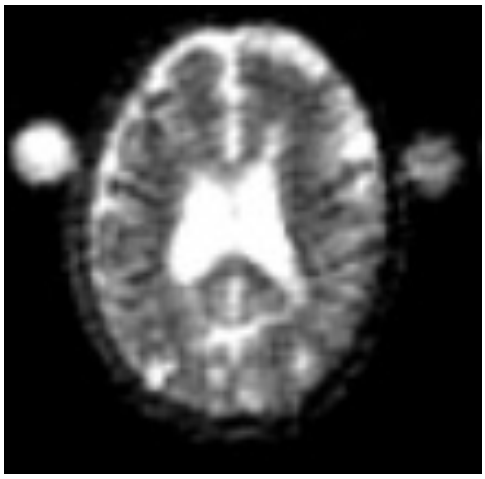

Figure 5.1 ^{23}Na MRI

Axial image at the level of the lateral ventricles obtained using a sodium coil. Two phantoms are visible at the lateral edges of the field of view with differing sodium concentrations indicated by differences in the signal intensity.

5.2.2 Post-processing

5.2.2.1 Lesion and tissue segmentation

I outlined the T2-hyperintense lesions in the white matter, for each patient, on the 2D proton density (PD) image also using the T2-weighted and 3D-FLAIR

sequences as references. I used the semi-automated edge finding tool from JIM v6.0 (Xinapse systems, Aldwincle, UK) and I then computed the lesion volume (ml).

Then, PD/T2 and 3D T1-images were rigidly registered and lesion masks were resampled in 3D T1 space. Subsequently, the 3D T1-weighted images were filled using a non-local patch-match lesion filling algorithm (Prados *et al.*, 2016*b*). The filled 3D T1-weighted images were then parcellated and segmented into grey matter (cortical and deep grey matter) and white matter using the Geodesic Information Flows (GIF)(Cardoso *et al.*, 2015) method v3.0 (niftyweb) (Prados *et al.*, 2016*a*) following the Desikan-Killiany-Tourville brain parcellation protocol (Klein and Tourville, 2012). All segmentations were quality checked. Afterwards, I obtained grey matter and normal-appearing white matter volumes and fractions for all subjects.

5.2.2.2 Diffusion-weighted data processing

Each DWI was corrected for eddy current-induced distortions and subject motion using "eddy" in FSL 6.0 (FMRIB, Oxford, UK) (Andersson and Sotiropoulos, 2016) and the original (not lesion-filled) 3D T1-weighted image was co-registered to the mean b=0 images using NiftyReg software package. All undistorted DWI data, as well as their anatomical 3D T1 alignment, were quality checked. For NODDI fitting, the Matlab (The MathWorks, Inc., Natick, Massachusetts, USA) NODDI toolbox (http://nitrc.org/projects/noddi_toolbox) using default settings was used to generate ODI and NDI maps. The brain tissue masks, as well as the lesion masks for patients, were then warped to each subject's DWI space to allow individual characterization of NODDI metrics in normal-appearing white and grey matter compartments and in white matter lesions.

5.2.2.3 ^{23}Na MRI data processing

TSC was quantified on a voxel-by-voxel basis using a linear method, dependent on the calibration phantoms.

A fully automated pipeline was used to quantify TSC on a voxel-by-voxel basis in brain tissues using the calibration phantoms as references. A linear method,

consistent of a series of registration steps was used: (1) the sodium scan was registered to the PD/T2-weighted scan obtained using the body coil; (2) the PD/T2-weighted scan obtained using the body coil was registered to the PD/T2-weighted scan obtained using the 32-channel head coil; and (3) the PD/T2-weighted scan obtained using the 32-channel head coil was registered to the 3D T1-weighted sequences. Each of these registration steps were then reversed in order to transform the segmented tissue masks (cortical grey matter, deep grey matter, normal-appearing white matter, white matter lesions) into sodium space and calculate the TSC (mM).

Total sodium concentration is higher in CSF than brain tissues. As a result small amounts of CSF partial volume may cause an artefactual increase in brain total sodium concentration. We used an automatic voxel-by-voxel partition-based correction method that removed the contribution of CSF sodium from sodium concentration maps in native sodium space (Paling *et al.*, 2013). The CSF volume fraction maps from GIF were registered to native sodium space. Then, CSF total sodium concentration was calculated on a subject-by-subject basis. Only voxels with at least 20% tissue volume fraction were used, and to reject unrealistically high total sodium concentrations, a threshold was set of two standard deviations above the mean of the sodium concentration in voxels with at least 95% tissue volume. Therefore, this correction was not applied in hypo-intense T1 lesions and enhancing lesions with high amounts of free water (<20% tissue volume fraction). This exclusion allowed total sodium concentration to reflect pathological processes such as neuro-axonal loss and oedema.

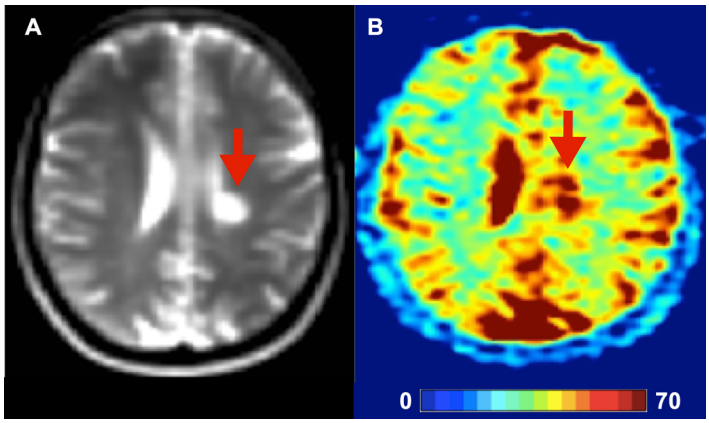

Figure 5.2 Total sodium concentration map

Example of a TSC map from a patient of this cohort. (A) a T2 image showing the presence of a periventricular T2-hyperintense lesion showing high total sodium concentration in the ^{23}Na MRI map (B). Abbreviations:

5.3 OCT

For OCT, I used spectral-domain OCT machine (Spectralis v.1.7.1.0, Heidelberg Engineering, Heidelberg, Germany) with the eye-tracking function for achieving measurement accuracy.

The examination was carried out in a dark room without using pharmacological pupil dilatation. I performed three 3.4mm peri-papillary circular scans (diameter: 12°; 1536 A-scans; 1 B-scan; ART: 100) manually centred around the optic nerve, and the scan with the highest quality was chosen for the analysis (in case of equal quality, an arbitrary scan was selected). From this scan, I took the global average of the RNFL thickness.

For the macular volume scan, I manually centred the scan around the fovea (20° × 20° volume scan; 1024 A-scans per B-scan; 25 B-scans; vertical alignment; ART: 10-25). The individual macular layers were then obtained with an automated segmentation software (HRA/Spectralis Viewing Module version 5.6.4.0). I used a 1, 3, and 6 mm grid on the thickness map selecting the 3 mm ring values for the analysis (Figure 5.3).

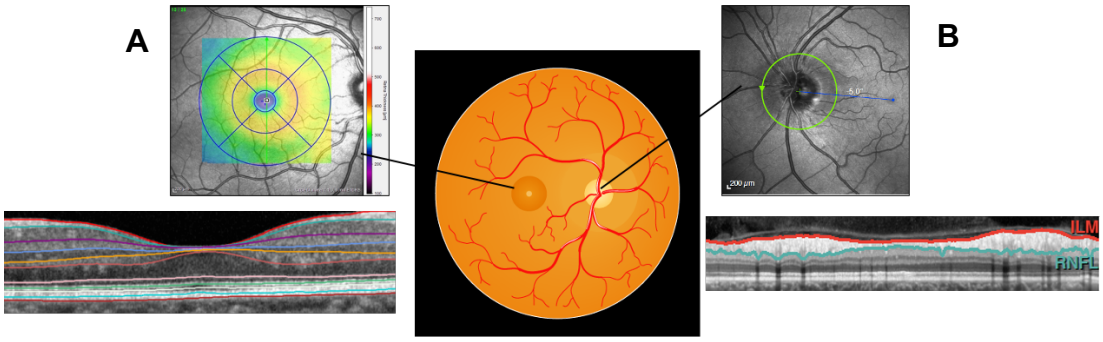

Figure 5.3 OCT Scan (A) Macula Grid; (B) Optic Nerve Head Circular Scan

5.4 The Kurtzke Expanded Disability Status Scale

The Kurtzke EDSS is the most widely used measure of disability (Kurtzke, 1983). The EDSS score is calculated by rating the degree of neurological disability across seven functional systems evaluated in the neurological exam (visual, brainstem, pyramidal, cerebellar, sensory, sphincter, and cerebral). The results are combined with the measured walking distance and independence with activities of daily living. A final score of 0 – 10 is given with higher scores indicating more severe disability (Table 5.2). It used both in the clinical as well as in the research setting.

However, EDSS has several disadvantages. Firstly, because scores are based on the results of the neurological examination, there is intra- and inter-observer variability. Secondly, it is heavily weighted towards ambulatory disability, not giving equal representation to other disabling aspects of multiple sclerosis, such as cognitive impairment and upper limb function. Finally, in the research setting, statistical models for EDSS are difficult because of the non-parametric nature of this variable.

Table 5.2 Expanded Disability Status Scale (EDSS) score (Kurtzke, 1983)

0	Normal neurological examination

1.0	No disability, minimal signs in one functional system (FS)
1.5	No disability, minimal signs on two or more FS
2.0	Minimal disability in one FS
2.5	Minimal disability in two FS
3.0	Moderate disability in one FS or mild disability in three or four FS
3.5	Moderate disability in two FS or mild disability in five FS
4.0	Able to walk ≥ 500 m but not unrestricted; severe disability in one FS or combinations of less severe disability in other FS
4.5	Able to walk ≥ 300 m unaided
5.0	Able to walk ≥ 200 m unaided
5.5	Able to walk ≥ 100 m unaided
6.0	Able to walk ≥ 100 m with unilateral assistance
6.5	Able to walk ≥ 20 m with bilateral assistance
7.0	Unable to walk 5 m with an aid, essentially restricted to a wheelchair but independent
7.5	Unable to take more than a few steps, restricted to a wheelchair
8.0	Restricted to wheelchair with effective use of the arms and retains many self-care functions
8.5	Restricted to bed much of the day, some use of the arms
9.0	Bedbound, able to communicate and eat
9.5	Bedbound, unable to communicate or swallow
10	Death due to multiple sclerosis

5.5 Multiple Sclerosis Functional Composite score

The MSFC was developed to address some of the limitations of the EDSS (Cutter *et al.*, 1999).

The MSFC explores three clinical dimensions: the upper limb function, the 9-hole peg test, one for the lower limb function, the timed 25-foot walk test, and a cognitive measure, PASAT, for attention and information processing speed. It is a well-validated battery and correlates well with disease stage, EDSS score, MRI metrics, health-related quality of life, and employment (Fischer *et al.*, 1999*a*)

The 9-hole peg test and timed 25-foot walk test can be expressed as a measure of time or speed. In this thesis, they will be used as a measure of time (Chapter 7). Raw scores can be used, or z-scores can be calculated from a reference population or normative values (Fischer *et al.*, 1999*a*).

However, it does not assess the visual function, so researchers have suggested adding visual tests, such as the Sloan low-contrast visual acuity (Balcer *et al.*, 2003).

5.6 Brief Cognitive Assessment for Multiple Sclerosis

The Brief Cognitive Assessment for Multiple Sclerosis (BICAMS) has been developed to overcome the issues related to previous batteries of neuropsychological tests validated in multiple sclerosis (Langdon *et al.*, 2012). The Brief Repeatable Battery of Neuropsychological tests and Minimal Assessment of Cognitive Function in multiple sclerosis, although comprehensive, require long administration time, 45 min and 90 min, respectively, specialised equipment, and trained staff.

BICAMS, instead, takes 15 min to complete and requires no specialist equipment or expertise in cognitive assessment. It comprises three tests to assess the three cognitive domains most affected during multiple sclerosis. The Symbol Digit Modalities Test (SDMT) for assessing attention and information processing speed, the California Verbal Learning Test-II (CVLTII)

for testing verbal memory, and the Brief Visuospatial Memory Test-Revised (BVMTR) for testing visual memory.

BICAMS has been widely validated across 11 languages and demonstrated the ability to identify significantly cognitive deficits in adults with multiple sclerosis compared to healthy controls (Corfield and Langdon, 2018).

5.7 Visual tests

Visual test scores were used in Chapter 8. For this study, all visual tests were assessed with the habitual refraction correction used by patients.

5.7.1 High contrast letter acuity

High Contrast Letter Acuity (HCLA) provides a reasonable assessment of visual function. HCLA is the identification of black letters (100% contrast) on a white background. In this study, I used the early treatment diabetic retinopathy study (ETDRS) charts, the gold standard in ophthalmology clinical trials. They contain lines of an equal number of letters that decrease in equal logarithmic steps and provide visual acuity in the form of Logarithm of minimum angle of resolution (LogMar). HCLA, however, is not related to the quality of vision and reflects the integrity of the entire anterior visual pathway, thus resulting in nonspecific to the ON damage.

Some studies have reported a linear relationship between HCLA and RNFL thickness (Trip *et al.*, 2005; Henderson *et al.*, 2010). Other authors (Costello *et al.*, 2006) did not find a linear correlation: only below the cut-off point of 70 μm RNFL thickness was significantly associated with visual acuity. They suggested this was due to a "functional reserve" of the visual system whereby visual function is preserved until a critical level of axonal loss is reached. However, others argue that this can be due to the different variability allowed by the two measuring systems. OCT measures of RNFL thickness have smaller confidence intervals, and less variability than functional tests, so small reductions in thickness may not be captured (Garway-Heath *et al.*, 2002; Hood and Kardon, 2007).

HCLA was measured in LogMar on retro illuminated ETRDS charts at 4m in a dark room. Best acuity was obtained with the correction used by patients and the use of a pinhole occluder, an opaque disk with small holes through it, that, as in a pinhole camera, can temporarily remove refractive errors due to myopia. If no letters were identified, a score of 1.7 was given.

5.7.2 Low contrast letter acuity

Low Contrast Letter Acuity (LCLA) is the identification of grey letters on a white background. It measures the contrast sensitivity, the difference in lightness between an object and its background (Richman et al., 2013).

Here, patients were assessed with Sloan charts at 1.25% and 2.5% of the contrast level. These charts have the same format as the ETDRS visual acuity charts (Figure 5.4). Each line of letters gets progressively smaller whilst the contrast remains the same. The LCLA score is calculated as the number of letters the patient can identify correctly at a specific contrast level. The maximum score is 70. The lighting levels of the testing environment were the same for all patients.

LCLA is more sensitive to visual impairment than HCLA and related to subjective visual complaints and quality of life (Sabadia *et al.*, 2016). A 7-letter reduction in LCLA is associated with a significant worsening of quality of life and RNFL thickness by OCT (Talman *et al.*, 2010).

In multiple sclerosis, LCLA has also been associated with measures of disability (Balcer *et al.*, 2017) and CNS damage, such as T2 lesion volume (Wu *et al.*, 2007) and brain atrophy (Reich *et al.*, 2009).

In this study, Sloan letter charts were tested at 2 meters in a dark room. Numbers of letters were recorded for each eye separately.

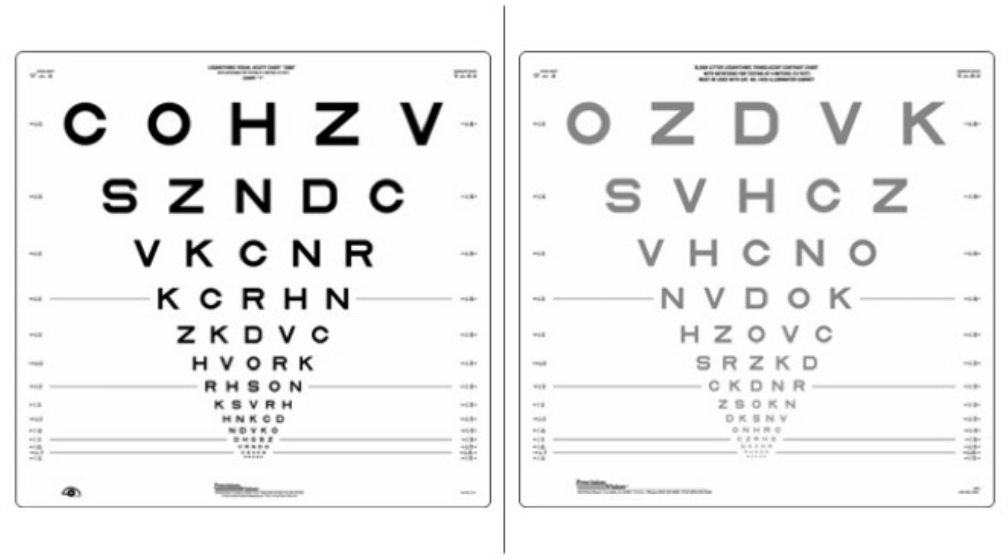

Figure 5.4 ETDRS HCLA (right) and LCLA (left) charts (image modified from a vendor website)

5.7.3 Colour vision

The macula mainly serves colour vision. As reported before, the thin axons from the ganglion cells converge to the temporal part of the optic disc through the papillomacular bundle. By affecting these fibres, the ON process causes deficits in colour vision (Henderson *et al.*, 2011). There is not a single type of colour defect, but all the spectrum may be involved after ON (Beck *et al.*, 1992). Here, I used the Farnsworth Munsell 100 hue test to measure colour vision Figure 5.5. This test consists of 85 coloured caps that need to be placed by the patient in the perceived order of hue. The error score is then calculated (Ménage *et al.*, 1993).

Figure 5.5 Farnsworth Munsell 100 Hue Test (munsell.com)

At baseline and three months after ON, colour vision seems to be associated with RNFL atrophy measured by OCT (Henderson *et al.*, 2011).

Abnormalities in colour vision can be detected in up to 70% of multiple sclerosis patients, even without a history of ON (Yuksel *et al.*, 2019), and they are present in all multiple sclerosis subtypes, but more pronounced in the progressive disease (Villoslada *et al.*, 2012). Colour vision deficits have been related to disability (Martínez-Lapiscina *et al.*, 2014).

In this study, the 85 coloured caps were presented under standard lighting levels (fluorescent office lighting at standard daylight). Each eye was tested separately.

Chapter 6 Reduced neurite density in the brain and cervical spinal cord in relapsing-remitting multiple sclerosis: a preliminary NODDI study

6.1 Introduction

In this Chapter, I present research I have done on the application of NODDI to the neuroaxis in relapsing-remitting multiple sclerosis patients.

As outlined in Paragraph 3.1.3, neurodegeneration represents a major component of multiple sclerosis pathology and it can affect the whole neuroaxis (Criste *et al.*, 2014).

We have seen in Paragraph 4.1 that NODDI is more specific than DTI in capturing the microstructural substrates possibly underpinning neurodegeneration (Timmers *et al.*, 2016) and the application of NODDI to multiple sclerosis revealed significant alterations in NDI and ODI in the brains of multiple sclerosis patients compared with healthy controls (Granberg *et al.*, 2017; Schneider *et al.*, 2017; Spanò *et al.*, 2018) . Furthermore, alterations in NODDI indices were correlated with physical disability, measured by EDSS (Granberg *et al.*, 2017; Spanò *et al.*, 2018). However, before this project, no one had investigated correlations between NODDI alterations and cognitive function, a clinical aspect in which I was interested as it has been associated with neurodegeneration (Zivadinov *et al.*, 2001)[15] and can affect multiple sclerosis patients from onset (see Paragraph 2.1.1.2) (Brochet and Ruet, 2019). Furthermore, the impact of white matter lesions on the observed NODDI abnormalities in multiple sclerosis was still unknown. Finally, one of the previous studies (Granberg *et al.*, 2017) used a unique 3T scanner with gradient strength up to 300 mT/m, a technology not widely available in the clinical setting, whose results are difficult to compare and/or to replicate.

Another key question was whether NODDI can be used to investigate *in vivo* neurodegeneration in the spinal cord of multiple sclerosis patients. Grussu and colleagues had previously demonstrated the feasibility of NODDI application

to the healthy spinal cord (Grussu *et al.*, 2015) and a preliminary study in six multiple sclerosis patients suggested the presence of abnormal NODDI metrics in the cervical spinal cord of patients not present in healthy controls (By *et al.*, 2017). However, characterization of NDI and ODI along the neuroaxis of multiple sclerosis patients, brain and spinal cord, was lacking, although this would have contributed understanding if these CNS structures share common pathological abnormalities.

Therefore, I have applied NODDI to the brain and cervical cord of relapsing-remitting multiple sclerosis patients and healthy controls, using a clinical 3T scanner. To determine if the underlying abnormalities in the neurite morphology, as captured by NODDI, contributed to disability, I assessed the correlations between NODDI indices and physical and cognitive disability.

6.2 Materials and methods

6.2.1 Patients' characteristics and clinical assessments

Twenty-eight consecutive patients were enrolled in this study with the following inclusion criteria: diagnosis of relapsing-remitting multiple sclerosis, age between 18 and 65 years, absence of relapses or corticosteroid treatment in the three months before imaging and no other known medical condition affecting the CNS. Twenty age- and sex-matched healthy controls were also recruited.

Patients' disability was assessed with EDSS. All subjects, patients and healthy controls, underwent the MSFC as well as the Brlef Cognitive Assessment for Multiple Sclerosis (BICAMS). See Chapter 5 for a full characterization of these tests.

Anxiety and depression were tested as possible confounders with the Hospital Anxiety and Depression Scale (HADS)(Pais Ribeiro *et al.*, 2018).

For MSFC total score, z-scores were calculated according to the National Multiple Sclerosis Society Task Force guidelines (Fischer *et al.*, 1999*a*).

Written informed consent, approved by the local research ethics committee, was obtained for all participants.

6.2.2 MRI protocol

Brain and spinal cord MRI scans were performed in the same session using a 3T Philips Achieva MRI system (Table 6.1). The spinal cord protocol was acquired before the brain protocol in all subjects to reduce the risk of movement artefacts in the spinal cord sequences.

Brain NODDI cardiac-gated diffusion-weighted images were acquired using a 2D spin-echo echo-planar imaging sequence. The diffusion protocol consisted of 3 b-shells and gradient directions isotropically distributed: b-value=300s/mm^2 and 8 directions; b value=1000 s/mm^2 and 30 directions; b value=2855s/mm^2 and 60 directions. Eight interleaved non-diffusion-weighted (b=0) images were also acquired.

The cervical cord was imaged in the axial-oblique plane (i.e., slices perpendicular to the longitudinal axis of the cord) with the centre of the imaging volume positioned at the level of C2-3 intervertebral disc. Moreover, to reduce motion artefacts during scanning and improve image quality, an MRI compatible cervical collar was worn by all subjects (Yiannakas *et al.*, 2012).

For NODDI of the spinal cord, the acquisition protocol for all scans relied on a reduced field-of-view, cardiac gated PGSE ZOOM-EPI sequence, acquiring two diffusion-weighted high angular resolution imaging (Tuch *et al.*, 2002) b-shells of thirty measurements at b=1000s/mm^2 and sixty measurements at b=2855s/mm^2 and three interleaved b=0 measurement, respectively. A total of 20 slices were acquired with a total acquisition time of approximately 35 min. Previous simulations conducted by Grussu and colleagues revealed that 3 b=0 measurements suffice to estimate the correct b=0 offset level 95% of times, with a precision of 7.8%, against precision of 4.9%, with eight b=0 measurements, with realistic spinal cord signal-to-noise ratio (Grussu *et al.*, 2015, 2019) (Figure 6.1).

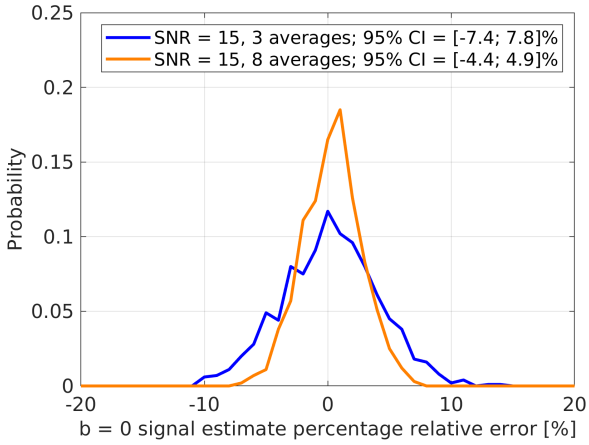

Figure 6.1 Distributions of percentage relative errors in b = 0 signal level estimation obtained by averaging three vs. eight noisy measurements.

The distributions were obtained over 1000 unique random instantiations of Rician noise at a realistic spinal cord signal-to-noise ratio of 15. Abbreviations: SNR: signal-to-noise ratio

Table 6.1 MRI protocol

	FOV (mm^2)	Voxel size (mm^3)	TR (ms)	TE (ms)	Inversion time (ms)
	BRAIN				
3D-T1	256x256	1.0x1.0x 1.0	6.9	3.1	836.46
PD/T2	240x180	1.0x1.0x 3.0	4900	15/85	
DWI[a]	192x222	2.5x2.5x 2.5	12000	91	
	SPINE				
3D-FFE	240x240x50[b]	0.5x0.5x 5.0	23	5	
DWI[c]	64x64	1.0x1.0x 5.0	12000	65.50	

[a] b-values 300/1000/2855s/mm^2 with 6/30/60 isotropically distributed gradient directions; is approximate being the sequence cardiac gated (TR=12 heart beats)
[b] mm^3
[c] b-values 1000/2855s/mm^2. TR is approximate being the sequence cardiac gated (TR=12 heart beats).
Abbreviations: DWI: diffusion-weighted image; FFE: fast field echo; FOV: field-of-view; TR: repetition time; TE: echo time

6.2.3 Conventional MRI post-processing

For the brain images, I outlined the T2-hyperintense lesions in the white matter, for each patient, on the 2D proton density (PD) image using the semi-automated edge finding tool from JIM v6.0 (Xinapse systems, Aldwincle, UK) and I then computed the lesion volume (ml).

The upper cervical cord cross-sectional area (CSA) was measured on the 3D-FFE scans of the cervical cord: an active surface model was applied using JIM v6.0 to obtain the CSA by averaging the area of three contiguous 5mm axial slices, centred on C2/3 disc (Horsfield *et al.*, 2010; Cawley *et al.*, 2018). Spinal cord lesions were identified as delineated areas of hyperintensity on the 3D-FFE sequence and counted.

6.2.4 Diffusion-weighted data processing

6.2.4.1 Brain

The method is described in Paragraph 5.2.2.2. Briefly, each DWI was corrected for eddy current-induced distortions and subject motion using "eddy" in FSL 6.0 (FMRIB, Oxford, UK) (Andersson and Sotiropoulos, 2016) and the original (not lesion-filled) 3D T1-weighted image was co-registered to the mean b=0 images using NiftyReg software package. All undistorted DWI data, as well as their anatomical 3D T1 alignment, were quality checked. For NODDI fitting, the Matlab (The MathWorks, Inc., Natick, Massachusetts, USA) NODDI toolbox (http://nitrc.org/projects/noddi_toolbox) using default settings was used to generate ODI and NDI maps. The brain tissue masks, as well as the lesion masks for patients, were then warped to each subject's DWI space to allow individual characterization of NODDI metrics in normal-appearing white and grey matter compartments and in white matter lesions.

6.2.4.2 Spinal cord

Diffusion-weighted data were pre-processed and corrected for motion (Grussu *et al.*, 2015). For each subject, the whole cord was segmented on the mean b=0 volume by using a semi-automatic active surface method (Horsfield *et al.*, 2010) implemented in JIM V6.0. The cord mask was then eroded slice-by-slice and cropped to the six central slices creating the whole-cord mask.

Subsequently, the spinal cord grey matter and white matter, as well as dorsal, lateral and ventral white matter sub-regions masks, were manually outlined in each subject on the average DWI, which was obtained by averaging the DWIs acquired for gradient directions at angle less or equal to 50 degrees with respect to the longitudinal axis of the spinal cord, according to the procedure described by Kearney and colleagues (Kearney *et al.*, 2015) (Figure 6.2).

a) Mean *b*= 0 image b) Average DW Image c) Segmentation from (b)

Figure 6.2 Examples of spinal cord grey matter and dorsal, lateral and ventral white matter sub-regions masks in one subject

An example of a b 0 image is given (a); for the segmentation, I used images obtained by averaging the DWIs acquired for gradient directions at angle less or equal to 50 degrees with respect to the longitudinal axis of the spinal cord (b); the masks were manually drawn using a semi-automated tool in the JIM V.6.0 software (c).

The NODDI model was fitted within the whole cord mask (before slice wise erosion) by using the NODDI MATLAB toolbox. NODDI indices were then calculated within the manually segmented spinal cord tissue masks. Voxels with ISOVf >0.99 (i.e. CSF voxels) were excluded from the analysis.

I quality checked all the brain and spinal cord NODDI images and excluded those with motion artefacts or noticeable signal drifts on the b=0 signal.

Examples of the brain and spinal cord NODDI maps are given in Figure 6.3.

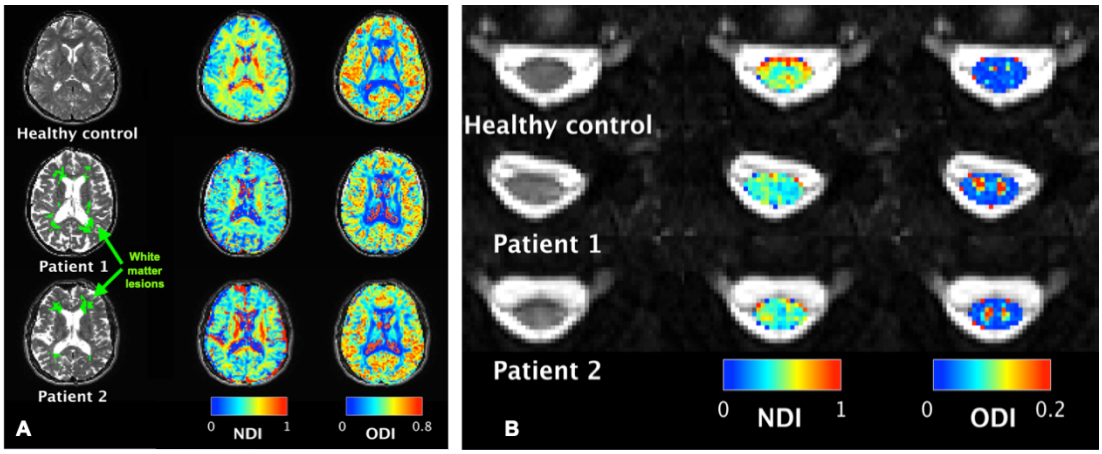

Figure 6.3 Example of NODDI maps

A) Example of brain NODDI maps from one healthy control (top row) and two patients: patient 1 (age 51, EDSS 3) and patient 2 (age 42, EDSS 3.5).
The first column shows the corresponding T2 weighed images and the lesion masks drawn for the two patients. The right panel shows the NODDI metrics: neurite density index (NDI) and orientation dispersion index (ODI). Visually, there is a reduction in NDI in multiple sclerosis lesions compared to the normal-appearing white matter in the two patients, and there are evident reduced NDI in the normal-appearing white matter of the two patients when compared to the healthy control.
B) Example of spine NODDI maps obtained from the same subjects. The first column shows the non-diffusion weighted image derived from the DWI. The right panel shows the NODDI metrics. Visually, there is a reduction in NDI in the white matter of the two patients when compared to the healthy control. The NDI reduction in the spinal cord outline depends in part from the partial volume effect from the CSF. Voxels with >0.99 ISOVf were excluded from the final analysis.

6.2.5 Statistical analysis

Group differences in demographic characteristics were assessed using the two-sample t-test for continuous variables and the chi-square test for categorical variables.

I applied linear regression to investigate the differences between patients and healthy controls for brain tissue volumes (i.e., white matter and GM tissue volumes), CSAs, clinical tests and NODDI metrics, adjusting for age and sex. When looking for differences in NODDI metrics, the models were repeated including specific brain tissue volumes (when brain comparisons were tested) or CSA (when spinal cord comparisons) to account for the possible influence of atrophy.

In patients, I used linear regression to investigate associations between NODDI metrics and brain volumes and spinal cord CSA, and disability (i.e., MSFC and BICAMS), adjusting for age and sex. Only the NODDI metrics and the clinical tests that showed significant differences between patients and healthy controls were entered in these models. In case of significant associations between NODDI metrics and disability scores, the regression models were re-estimated adjusting for the brain parenchymal fraction and the spinal cord CSA.

Since the EDSS score and lesion loads (brain lesion volume and spinal cord lesion count) are not normally distributed, I used the Spearman's rho correlation coefficient for the associations between NODDI metrics and these parameters.

Stata v. 14.1 (Stata Corporation, College Station, Texas, USA) was used. Results associated with a $p<0.05$ were considered statistically significant and reported. Due to the exploratory nature of the study, the statistical inference of multiple comparisons was not performed.

6.3 Results

Out of 28 patients and 20 healthy controls who underwent the MRI protocol, I included into the analysis the brain MRI data of 24 patients and 16 healthy controls and the spinal cord data of 27 patients and 18 healthy controls (the remainder scans were discarded after quality checks and/or for incomplete MRI protocol).

In comparison to healthy controls, relapsing-remitting multiple sclerosis patients showed brain and spinal cord atrophy (Table 6.2) as well as lower scores on the BICAMS, and MSFC (Table 6.3). The BICAMS and PASAT scores did not correlate with the HADS scores.

Table 6.2 Demographic and clinical characteristics of relapsing-remitting multiple sclerosis patients and healthy controls.

	RRMS patients (N=28)	Healthy controls (N=20)	p-values
Age (years)	39.4 ± 6.6	36.6 ± 12.5	0.21
Gender (female: male; % female)	23:5 (82)	13:7 (65)	0.17
Disease duration (years)	8 ± 5.6	-	-
DMDs (N, %)	15 (54)	-	-
Brain GM volume (ml)	624.7 ± 41.1	705.6 ± 80.8	**0.001**[a]
Brain WM volume (ml)	422 ± 33.9	482.7± 80.7	**0.012**[a]
BPF	0.7 ± 0.02	0.8 ± 0.01	**<0.0001**[a]
Spinal cord CSA (mm^2)	75.8 ± 6.7	83.6 ± 8.7	**0.009**[a]
Brain WM T2 lesion volume (ml) (median, range)	11.3 (0.3-41.3)	-	
WM spinal cord lesion count (median, range)	2 (0-8)		

[a] linear regression model correcting for age and gender.
Note. Data are means ± standard deviation, unless otherwise indicated. *Abbreviations:* RRMS: relapsing-remitting multiple sclerosis; DMDs: disease modifying drugs; GM: grey matter; BPF brain parenchymal fraction; CSA: cross-sectional area; WM: white matter

Table 6.3 Disability scales and cognitive tests in relapsing-remitting multiple sclerosis patients and healthy controls.

	RRMS patients (N=28)	Healthy controls (N=20)	p-value[a]
EDSS (median, range)	2.5 (1-6.5)		
HADS Anxiety (median, range)	4 (0-21)		
HADS Depression (median, range)	3 (0-10)		
Mean 9-HPT (sec.)	23 ± 5.3	18.4 ± 5.1	**0.006**
T25FW (sec.)	5.8 ± 3.1	3.9 ± 0.5	**0.03**
PASAT	38.8 ± 16	48.6 ± 9.4	0.053
MSFC (z-score[b])	0.03 ± 0.6	0.4 ± 0.4	**0.016**
SDMT	54.6 ± 11.2	62.1 ± 10.2	**0.027**
BVMT-R	22.3 ± 7.5	28.3 ± 3.9	**0.002**
CVLT-II	57.8 ± 11.3	63.3 ± 8.2	**0.016**

[a] A linear regression model was used adjusting for age and sex.
[b] Z-scores were computed according to the National multiple sclerosis Society's Clinical Outcomes Assessment Task Force indications using as a reference population our healthy control cohort.
Note. Data are means ± standard deviation, unless otherwise indicated.
Abbreviations: RRMS: Relapsing-Remitting Multiple Sclerosis; 9-HPT: 9-hole Peg Test; T25FW: timed 25-foot walk; PASAT: Paced Auditory Serial Addition Test; MSFC: Multiple Sclerosis Functional Composite; SDMT: Symbol Digit Modality Test; BVMT-R: Brief Visuospatial Memory Test-Revised; CVLT-II Californian Verbal Learning Test II.

Patients showed lower NDI in the brain normal-appearing white matter than healthy controls (B= -0.021, 95% confidence interval (CI): -0.041 to -0.002, p=0.032). In the spinal cord, patients showed lower NDI in the whole white matter (B= -0.07, 95%CI:-0.11 to -0.03, p=0.001), particularly in the dorsal and lateral white matter sub-regions, and a lower ODI in the dorsal white matter (B=-0.04, 95%CI:-0.07 to -0.1) than healthy controls (Figure 6.4). These differences remained significant after adjusting for white matter brain tissue volume and CSA, respectively (Table 6.4). NDI was lower in the spinal cord GM of relapsing-remitting multiple sclerosis patients than healthy controls (B= -0.04, 95%CI: -0.07 to -0.006, p=0.021), but this difference became not significant when adjusting for CSA.

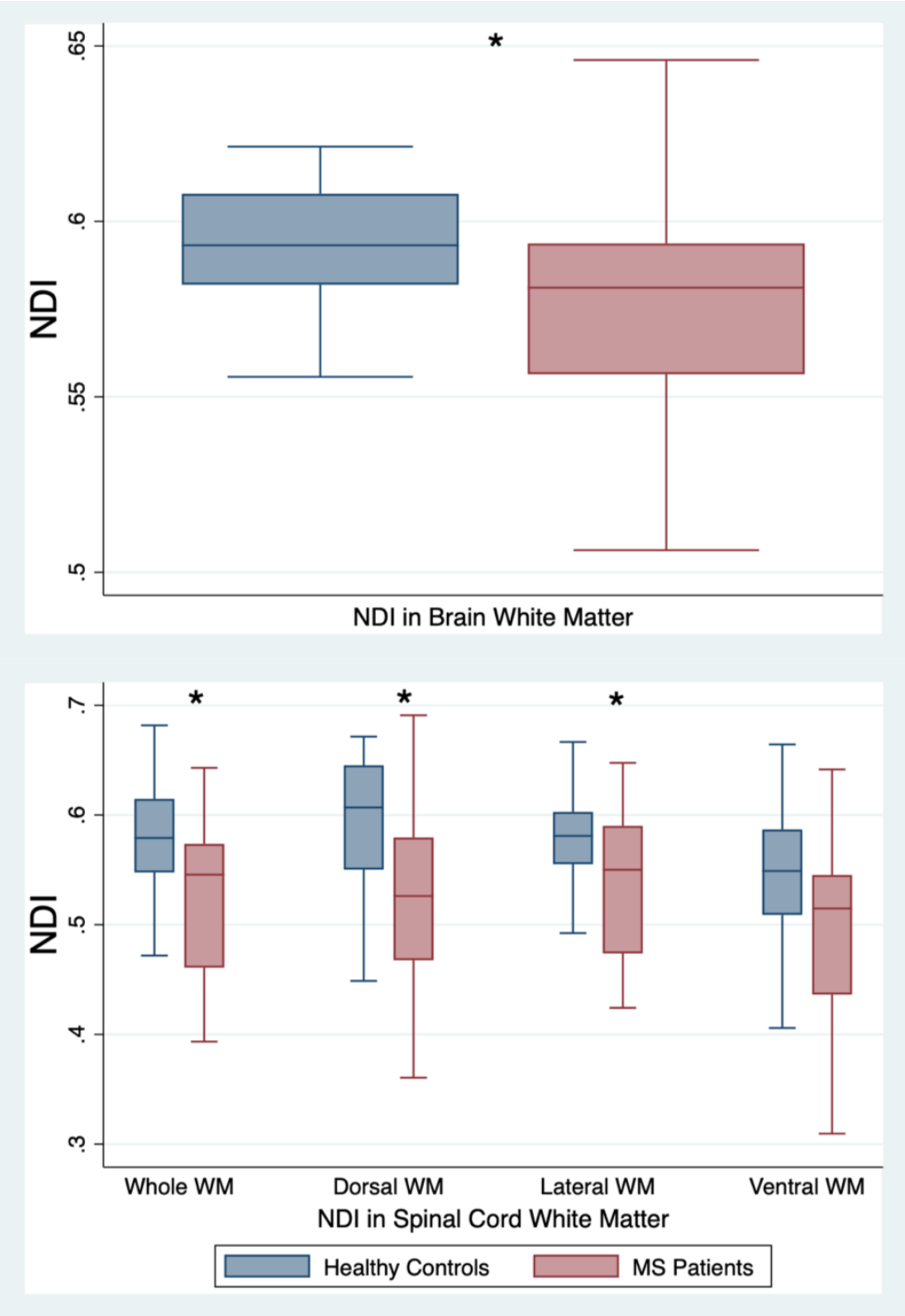

Figure 6.4 Boxplots of the NODDI metrics showing differences between patients and healthy controls.

Top: Neurite density index (NDI) values in the brain normal-appearing white matter of multiple sclerosis patients compared to healthy controls.*p-value<0.05

Table 6.4 NODDI measures in relapsing-remitting multiple sclerosis patients and healthy controls.

NODDI metric	RRMS patients	Healthy controls	Standardized B coefficient (β)	P-value[a]
		Brain		
N of subjects	24	16		
NDI WM	0.57 ± 0.03	0.60 ± 0.03	-0.35	**0.032**
ODI WM	0.27± 0.02	0.27 ± 0.02	0.02	0.60
NDI GM	0.44 ± 0.02	0.44 ± 0.01	-0.25	0.24
ODI GM	0.47 ± 0.01	0.47 ± 0.01	0.22	0.73
		Spinal cord		
N of subjects	27	18		
NDI Whole WM	0.52 ± 0.07	0.58 ± 0.06	-0.45	**0.015**
NDI Lateral WM (N voxels in the mask 134±47)	0.53 ± 0.07	0.58 ±0.06	-0.38	**0.021**
NDI Dorsal WM (N voxels in the mask 106±28)	0.52 ±0.09	0.59 ±0.06	-0.38	**0.020**
NDI Ventral WM (N voxels in the mask 47±19)	0.48 ±0.09	0.55 ±0.07	-0.27	0.095
ODI Whole WM	0.16 ±0.05	0.19 ±0.04	-0.28	0.12
ODI Lateral WM (N voxels in the mask 134±47)	0.16±0.06	0.18 ±0.04	-0.15	0.4

NODDI metric	RRMS patients	Healthy controls	Standardized B coefficient (β)	P-value[a]
ODI Dorsal WM (N voxels in the mask 106±28)	0.14 ±0.05	0.18 ±0.04	-0.39	**0.024**
ODI Ventral WM (N voxels in the mask 47±19)	0.19±0.07	0.21±0.05	-0.21	0.23
NDI GM (N voxels in the mask 190±26)	0.46 ± 0.06	0.49 ± 0.04	-0.20	0.20
ODI GM (N voxels in the mask 190±26)	0.09 ±0.04	0.1 ±0.03	-0.07	0.97

[a] A linear regression model was used adjusting for age, sex and specific tissue volumes (brain) or cervical cord cross-sectional area (spinal cord).
Note. Data are means ± standard deviations. *Abbreviations:* RRMS: relapsing-remitting multiple sclerosis; NDI: neurite dispersion index; ODI: orientation dispersion index; WM: white matter; GM: grey matter

In patients, lower NDI in the whole white matter and dorsal sub-region of the spinal cord correlated with higher EDSS score ($r_{s=}$-0.46 p=0.015 and $r_{s=-}$0.48, p=0.012, respectively) (Figure 6.5), while there was a weak correlation between lower ODI in the dorsal column and higher EDSS ($r_{s=}$-0.39 p=0.045).

In patients, lower NDI in the brain normal-appearing white matter was associated with a higher brain lesion load ($r_{s=-}$0.52, p=0.009) (Table 6.5; Table 6.6).

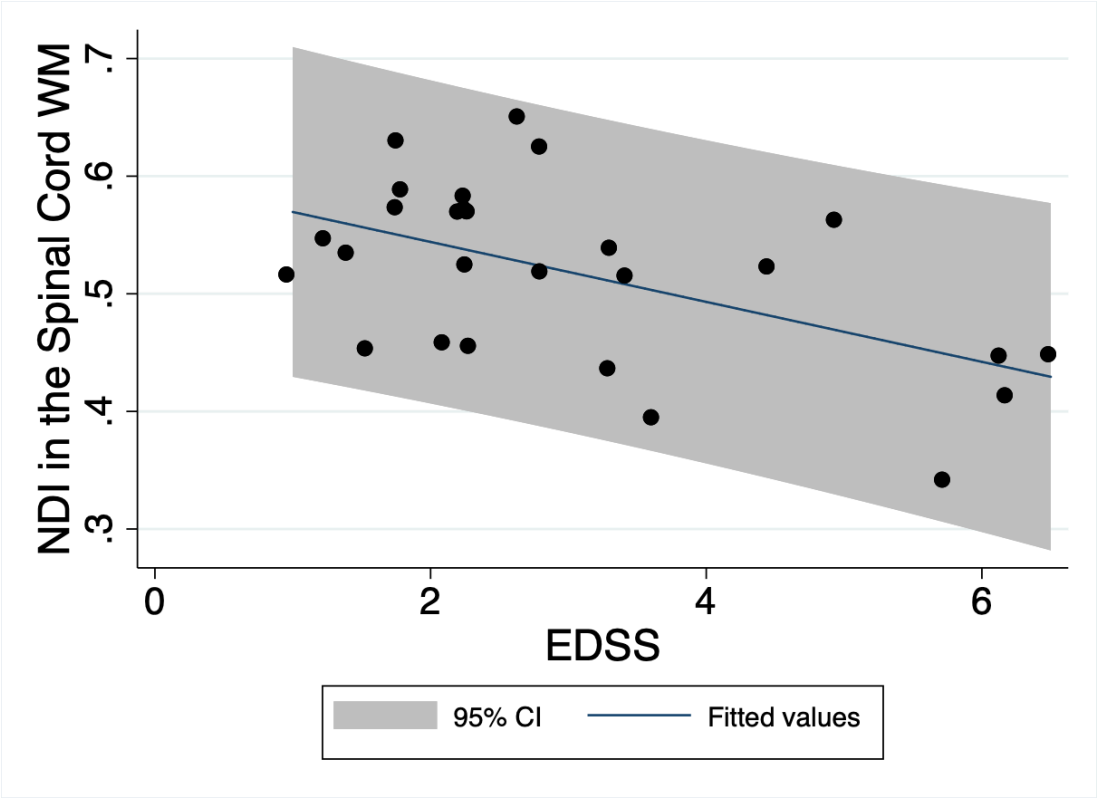

Figure 6.5 Relationship between the EDSS and the neurite density index (NDI) in the spinal cord white matter in relapsing-remitting multiple sclerosis patients (scatterplot).

Data are shown with confidence intervals computed the standard error of forecast due to the non-parametric variable. In relapsing-remitting multiple sclerosis patients the EDSS score was correlated a lower neurite density (NDI) in the spinal cord white matter (r_s=-0.46 p=0.015).
Abbreviations: EDSS: Expanded Disability Status Scale; NDI: neurite density index; WM: white matter.

Table 6.5 Associations of NODDI metrics with clinical outcomes (a) and Expanded Disability Status Scale (b)

a)

Dependent variable	Independent variable	Standardized B coefficient	p-value
BRAIN			
MSFC	NDI WM	-0.09	0.56
CVLT-II	NDI WM	-0.12	0.51
BVMT-R	NDI WM	-0.1	0.56
SDMT	NDI WM	0.04	0.82
MSFC	Brain lesion volume	-0.42	0.06
CVLT-II	Brain lesion volume	-0.1	0.6
BVMT-R	Brain lesion volume	-0.09	0.68
SDMT	Brain lesion volume	-0.17	0.4
MSFC	BPF	0.53	**0.034**
CVLT-II	BPF	0.28	0.49
BVMT-R	BPF	0.33	0.28
SDMT	BPF	0.28	0.25
SPINAL CORD			
MSFC	NDI Whole WM	0.26	0.25
MSFC	NDI Lateral WM	0.17	0.46
MSFC	NDI Dorsal WM	0.23	0.30
MSFC	NDI Dorsal WM	0.23	0.27
MSFC	CSA	0.20	0.39

b)

Dependent variable	Independent variable	r_s coefficient	p-value
	BRAIN		
EDSS	NDI WM	-0.14	0.51
	SPINAL CORD		
EDSS	NDI Whole WM	-0.46	**0.015**
EDSS	NDI Lateral WM	-0.30	0.13
EDSS	NDI Dorsal WM	-0.48	**0.012**
EDSS	ODI Dorsal WM	-0.39	**0.045**
EDSS	CSA	-0.19	0.4
EDSS	SC lesion count	0.48	**0.018**
MSFC	SC lesion count	-0.27	0.17

a) Results are from linear regression models adjusted for age and sex.
Abbreviations: MSFC: Multiple Sclerosis Functional Composite; CVLT-II: California Verbal Learning Test-II; BVMT-R: Brief Visuospatial Memory Test-Revised; SDMT: Symbol Digit Modality Test; NDI: Neurite Density Index; WM: White Matter; BPF: brain parenchymal fraction; CSA: cervical cord cross-sectional area; SC: spinal cord.
b) Results are from Spearman's correlation test. As EDSS was correlated with the NDI in the spinal cord, associations between EDSS and measure of spinal cord atrophy and lesion load were assessed.
Abbreviations: EDSS: Expanded Disability Status Scale; NDI: Neurite Density Index; WM: White Matter.

Table 6.6 Associations between NODDI metrics in the brain and spinal cord and associations with atrophy measures (a) and lesion load (b)

a)

Dependent variable	Independent variable	Standardized B coefficient	p-value
NDI WM Brain	BPF	0.32	0.26
NDI WM Spine	CSA	0.30	0.19
NDI WM Brain	NDI WM Spine	0.04	0.84

b)

Dependent variable	Independent variable	r_s coefficient	p-value
NDI WM Brain	Brain lesion volume	-0.52	**0.009**
NDI WM Spine	SC lesion count	-0.33	0.10

a) Results are from linear regression models adjusted for age and gender.
Abbreviations: NDI: Neurite Density Index; WM: White Matter; BPF: brain parenchymal fraction; CSA: cervical cord cross-sectional area**.**
b) Results are from Spearman's correlation test.
Abbreviations: NDI: Neurite Density Index; WM: White Matter; SC: spinal cord.

6.4 Discussion

Using a 3T clinical scanner, I found evidence of neurite integrity loss, as captured by NDI, in both the spinal cord and the brain of patients with multiple sclerosis when compared to healthy controls.

In the cervical cords of multiple sclerosis patients, reduced density of nerve fibres (NDI) was detected in the whole cord, especially in the lateral and dorsal white matter columns. I also found lower dispersion of neurites (ODI) in the dorsal columns of patients when compared to controls, as opposed to the finding of a different research group, which studied only six multiple sclerosis patients (By *et al.*, 2017). A low ODI value may be related to a reduction in the angular variations of axons, possibly caused by demyelination for the contribution of white matter lesions, not excluded in this project, that have shown low ODI values in previous studies (Grussu *et al.*, 2017; Schneider *et al.*, 2017) and are often present in the dorsal columns of multiple sclerosis patients (Bag *et al.*, 2011).

The results of the brain NODDI comparisons between groups mirrored the spinal cord findings, with lower NDI in the brain normal-appearing white matter of patients when compared to healthy controls. In the brain, I found a relationship between lower NDI and higher lesion load, thus extending the findings of previous studies (Granberg *et al.*, 2017; Spanò *et al.*, 2018). As alterations in the normal-appearing white matter in multiple sclerosis can be characterised by diffuse axonal injury (Kutzelnigg *et al.*, 2005), this results may support the hypothesis that degeneration of axons transected in focal lesions contributes to the axonal damage (Dziedzic *et al.*, 2010).

The most interesting result of this study is that lower NDI in the spinal cord white matter is associated with greater disability, as measured by EDSS. This suggests that reduced neurite density, which is a known component of neurodegeneration, may contribute to neurological impairment in multiple sclerosis. When reflecting on the absence of a significant correlation between low neurite density and increased disability in the brain, it is important to consider that long axons are highly compacted in the white matter columns of

the spinal cord, where they mediate neurological functions. Therefore, the alterations in the axon microstructure detected by NODDI in the spinal cord white matter are more likely to correlate with the EDSS, which is heavily weighted towards walking ability, than the global reduced NDI observed in the brain normal-appearing white matter. This interpretation is supported by a previous study carried out in multiple sclerosis which reported that the EDSS was related to reduced NDI only in specific brain white matter regions, such as the corpus callosum and internal capsule, where long-tract axons are found (Spanò *et al.*, 2018).

Finally, for the first time, I investigated possible correlations between cognitive performance and NODDI metrics. However, measures of cognition did not correlate with abnormal NODDI parameters. Since patterns of orientation abnormalities detected by diffusion imaging in the cortex seem to be related to cognitive functions (Muhlert *et al.*, 2013), further studies analysing NODDI in specific cortical regions and linking them with the corresponding cognitive domains are needed.

Given these considerations, in the following chapter, I analyse NODDI metrics in specific cortical regions and white matter areas.

6.4.1 Limitations

A possible limitation of this analysis is that I could not exclude multiple sclerosis lesions from the spinal cord NODDI maps; therefore, it is expected that NDI from the lesional tissue contributes to the observed reduced NDI. However, the relationship between spinal cord NDI and disability was independent of spinal cord lesion load, suggesting that NODDI may reflect clinically meaningful alterations in the white matter independently of visible lesions.

Furthermore, in the spinal cord, the relatively coarse resolution may have led to high levels of within-voxel partial volume effects, and the presence of highly anisotropic voxels may increase partial volume along the superior-inferior direction, thereby leading to higher values of ODI, as compared to brain white matter areas with similar fibre organization. Nonetheless, previous works

(Zhang *et al.*, 2012; De Santis *et al.*, 2019) have demonstrated that the echo times used in this study suffices to obtain an image quality suitable for group comparisons at the relatively low resolution employed here. Future work aiming at clinical translation is warranted to improve signal-to-noise ratio and hence achieve a better resolution and mitigate partial volume effects.

6.5 Conclusion

In conclusion, both brain and spinal cord white matter in multiple sclerosis showed reduced NDI in comparison to healthy controls that could indicate neurite integrity loss, a crucial element of neurodegeneration. Interestingly, I found that mainly when affecting the cervical cord, reduced NDI contributed to physical disability. This raises the potential of using spinal cord NDI metric as a marker of disability in multiple sclerosis so that it can be used to assess the efficacy of neuroprotective treatments and to provide insights into the mechanisms of disability in multiple sclerosis.

My findings highlight the ability of NODDI to detect clinically relevant alterations not captured by conventional MRI. However, we do not know the pathological mechanisms possibly behind these alterations. Therefore, in Chapter 7, while investigating with NODDI the presence microstructure abnormalities in patients at their onset, I also assessed the presence of TSC alterations with ^{23}Na MRI. As discussed in Paragraph 3.1.1.6 a status of “virtual” hypoxia can cause a neuro-axonal dysfunction mediated by intracellular sodium increase.

Chapter 7 Brain microstructural and metabolic alterations detected in vivo at onset of the first demyelinating event.

7.1 Introduction

As discussed in Chapter 3, in multiple sclerosis, diffuse pathological changes affect brain tissues that exhibit normal appearances with conventional MRI (Kutzelnigg and Lassmann, 2014). *Post-mortem* studies have characterized these processes in advanced multiple sclerosis (Kutzelnigg *et al.*, 2005), but these studies are understandably rare in early patients, with very small cohorts and often atypical cases (Barnett and Prineas, 2004).

Quantitative MRI techniques can measure, *in vivo,* microstructural changes, and contribute to our understanding of multiple sclerosis from its early phases (Cortese *et al.*, 2019). Furthermore, when metabolic quantitative MRI is employed, further insights into causative mechanisms of these changes can be probed (Ciccarelli *et al.*, 2014). However, multi-parametric approaches including structural and metabolic quantitative MRI are rare and have not yet been performed in early patients, except for the study of specific brain structures (Ranjeva *et al.*, 2003; Audoin *et al.*, 2007).

In this study, I investigated microstructural and metabolic alterations in the brains of patients at the onset of their first neurological episode suggestive of demyelination. In this study, I combined, for the first time, NODDI (Zhang *et al.*, 2012) and ^{23}Na MRI (Maudsley and Hilal, 1984).

As regards NODDI, in Chapter 6, I confirmed previous findings of reduced NDI in the normal-appearing white matter of established multiple sclerosis patients (Granberg *et al.*, 2017; Schneider *et al.*, 2017; Spanò *et al.*, 2018). Other studies also found different patterns of NDI and ODI alterations in specific white matter and grey matter areas with a clinical relevance (Granberg *et al.*, 2017; Spanò *et al.*, 2018). Therefore, it would be crucial to investigate if these abnormalities are also present at the early stage of the condition.

As discussed in Paragraph 4.2.2, the application of ^{23}Na MRI to multiple sclerosis cohorts showed that, in the normal-appearing white matter, white matter lesions and grey matter, TSC was increased in comparison to healthy controls (Inglese *et al.*, 2010; Zaaraoui *et al.*, 2012; Paling *et al.*, 2013; Petracca *et al.*, 2016; Maarouf *et al.*, 2017) and this was associated with increased disability (Zaaraoui *et al.*, 2012; Paling *et al.*, 2013; Petracca *et al.*, 2016; Maarouf *et al.*, 2017). A recent study also investigated TSC in CIS patients, but after 15 years from the onset. Brownlee and colleagues showed that TSC in the white matter and grey matter was higher in patients who had developed multiple sclerosis than in patients who had remained CIS and in healthy controls (Brownlee *et al.*, 2019*b*). However, we do not know if TSC alterations can be present at the onset of CIS and multiple sclerosis.

The goal of this project was to prove that a multi-parametric quantitative MRI approach can detect alterations in the brain tissues of early CIS and multiple sclerosis patients not captured by conventional MRI. The specific aims were: (i) to quantify NDI, ODI and TSC in normal-appearing white, white matter lesions, and grey matter; (ii) to determine if microstructural and metabolic alterations are correlated with clinical outcomes.

7.2 Methods

7.2.1 Participants

I analysed the data of 42 patients and 16 healthy controls from the cohort described in Paragraph 5.1 (Study Ref: 13/LO/1762; 13/0231-CIS2013).

7.2.2 Clinical assessments

In patients, I evaluated the disability using the clinical tests described in Chapter 5: EDSS (Kurtzke, 1983) (Paragraph 5.4); the MSFC (Fischer *et al.*, 1999*b*) (Paragraph 5.5); and the BICAMS (Langdon *et al.*, 2012) (Paragraph 5.6).

I recorded the years of education for each patient and calculated z-scores for the cognitive tests using the BICAMS initiative dataset (https://www.bicams.net)(Parmenter *et al.*, 2010) and, for the PASAT, the National Multiple Sclerosis Society Task Force database (Fischer *et al.*, 1999*b*).

7.2.3 MRI acquisition

The scans were performed at the 3T Achieva system and all participants underwent the MRI protocol described in Paragraph 5.2.1.

Because of coil issues, 32 out of the 42 patients and 13 of 16 healthy controls underwent ^{23}Na MRI. I used the single tuned ^{23}Na coil (RAPID BioMed) to acquire ^{23}Na images and the scanner body coil to acquire a ^{1}H T2-weighted dual-echo scan with the same spatial resolution of the ^{23}Na sequence (Paragraph 5.2.1, Table 5.1).

7.2.4 MRI post-processing

Figure 7.1 summarises the MRI post-processing, which I have described in Paragraph 5.2.2. Additionally, for this study, I have also identified and outlined the T1-hypointense lesions and gadolinium-enhancing lesions using the pre- and post-gadolinium T1-weighted turbo spin-echo sequences. All lesion masks were checked and corrected through interobserver-agreement with myself and an experienced rater, Dr. Indran Davagnanam. Subsequently, I computed the volume of the T2-hyperintense and T1-hypointense (non-enhancing) lesions for each subject.

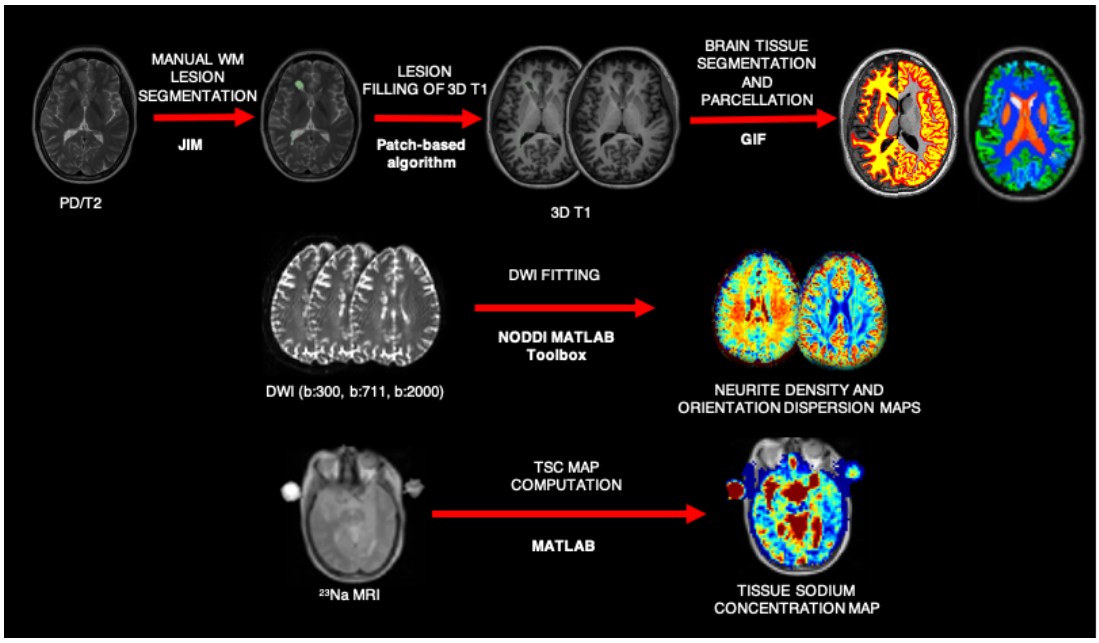

Figure 7.1 MRI post-processing

Abbreviations: WM: white matter; GIF: Geodesic Information Flow; DWI: Diffusion Weighted Imaging; NODDI: Neurite Orientation Dispersion and Density Imaging; TSC: total sodium concentration

Similarly to other projects of this thesis, using the non-local patch-match lesion filling algorithm (Prados *et al.*, 2016*b*), I filled the 3D T1-weighted images and then segmented into grey matter (cortical and deep grey matter) and white matter using GIF(Cardoso *et al.*, 2015) method v3.0 (Prados *et al.*, 2016*a*) (http://niftyweb.cs.ucl.ac.uk) following the Desikan-Killiany-Tourville brain parcellation protocol (Klein and Tourville, 2012). I obtained grey matter and white matter volumes and fractions for all subjects.

Both NODDI as well as ^{23}Na MRI have low spatial resolution (2.5mm and 3.0 mm isotropic voxels, respectively). Therefore, for the NDI, ODI and TSC estimation in the cortex, I grouped areas with anatomical proximity and functional similarity, as shown in Table 7.1. All segmentations were quality checked.

Table 7.1 Cortical and white matter areas in which neurite density index, orientation dispersion index and total sodium concentration have been computed

Areas	Structures	Side
	Grey Matter	
Cerebellum Grey Matter	Vermis, Lobes	L+R
Thalamus	Thalamus	L; R
Limbic Lobe	ACgG, MCgG, PCgG, PHG, Ent, Amigdala, Hippocampus	L; R
Hippocampus	Hippocampus	L; R
Insula	AIns, PIns	L; R
Orbitofrontal cortex	AOrG, POrG, MOrG, LOrG, GRe, SCA	L; R
Medial Frontal cortex	Medial Frontal cortex	L; R
Middle Frontal gyrus	Middle Frontal gyrus	L; R
Superior Frontal gyrus	SFG, MSFG	L; R
Inferior Frontal gyrus	OpIFG, OrIFG, TrIFG	L; R
Precentral gyrus	MPrG, PrG	L; R
Operculum	CO, FO, PO	L; R
Postcentral gyrus	PoG, MPoG	L; R
Cognitive Areas of the Parietal lobe	AnG, PCu, SMG, SPL	L; R
Superior-lateral Temporal lobe	MTG, TTG, STG, PP, PT	L; R
Medial-inferior Temporal lobe	FuG, ITG, TMP	L; R
Primary Visual cortex	Calc, Cun, OCP	L; R
Lingual gyrus	Lingual gyrus	L; R
Associative Areas of the Occipital lobe	IOG, MOG, SOG, OFuG	L; R
	White Matter	

Areas	Structures	Side
Cerebellar white matter		L+ R
Insular white matter		L+ R
Frontal white matter		L+R
Parietal white matter		L+ R
Temporal white matter		L+ R
Occipital white matter		L+ R
Corpus Callosum		**-**

Note: parcellations were based on the the Desikan-Killiany-Tourville protocol (Klein and Tourville, 2012)
Abbreviations: ACgG: anterior cingulate gyrus; MCgG: middle cingulate gyrus; PCgG: posterior cingulate gyrus; PHG: parahippocampal gyrus; Ent: entorhinal area; AIns: anterior insula; Pins: posterior insula; AOrG: anterior orbital gyrus; POrG: posterior orbital gyrus; MOrG: medial orbital gyrus; LOrG: lateral orbital gyrus; GRe: gyrus rectus; SCA:sub-callosal area; SFG: superior frontal gyrus; MSFG: superior frontal gyrus medial segment; OpIFG: opercular part of the inferior frontal gyrus; OrIFG: orbital part of the inferior frontal gyrus; TrIFG: triangular part of the inferior frontal gyrus; MPrG: precentral gyrus medial segment; PrG: precentral gyrus; CO: central operculum; FO: frontal operculum; PO: parietal operculum; PoG: postcentral gyrus; MPoG: postcentral gyrus medial segment; AnG: angular gyrus; PCu: pre-cuneus; SMG: supramarginal area; SPL: superior parietal lobule; MTG: middle temporal gyrus; TTG: transverse temporal gyrus; STG: superior temporal gyrus; PP: planum polare: PT: planum temporale; FuG: fusiform gyrus; ITG: inferior temporal gyrus; TMP: temporal pole; Calc: calcarine cortex; Cun: cuneus; OCP: occipital pole; IOG: inferior occipital gyrus MOG: middle occipital gyrus; SOG: superior occipital gyrus; OFuG: occipital fusiform gyrus.

The DW images post-processing is describe in detail in Paragraph 5.2.2. For each subject, I quality checked the NDI and ODI brain masks and, if necessary, I manually corrected them and recomputed NDI and ODI values. If this was unsuccessful, then that subject's brain area was discarded from further analysis.

TSC was quantified on a voxel-by-voxel basis using a linear method, dependent on the calibration phantoms, which is summarised in Paragraph 5.2.2.

7.2.5 Statistical analysis

I assessed group differences in demographic characteristics and brain tissue volumes using two-sample t-tests for continuous variables and chi-square tests for categorical variables.

I assessed differences between patients and controls in brain parenchymal fraction, normal-appearing white matter and global grey matter with linear regression, correcting for age and sex. Using the same model, I assessed the differences between patients and controls in the volume of the grey matter areas parcellated with GIF. Subsequently, group differences in NODDI metrics and TSC in the different brain areas were assessed with linear regression, adjusting for age and sex.

For grey matter, the corresponding volume of the parcellated area was added to the model as a predictor, if it was found significantly different between patients and controls.

To overcome the assessment of normality assumption for each area, I employed bootstrapping with 1000 repetitions.

In patients, I computed the differences in NDI, ODI and TSC between white matter lesions (all T2-hyperintense, T1-hypointense, and gadolinium-enhancing) and normal-appearing white matter with paired t-tests.

In patients, after identifying the areas where NDI, ODI and TSC were significantly different from healthy controls, I assessed their relationships with lesional and clinical variables.

For lesion parameters, I first log-transformed T2-hyperintense and T1-hypointense lesion volumes to allow parametric testing (Afifi *et al.*, 2007). Then, I used linear regression with bootstrapping to assess the relationship between NDI, ODI and TSC in brain areas with lesion volumes as well as with NDI, ODI and TSC in the T2-hyperintense lesions.

For the timed 25-foot walk and the 9-hole peg test, I used linear regression to assess associations between the altered NDI, ODI and TSC and these metrics.

Age and sex were kept as covariates in the model if significantly associated with these clinical variables. For cognitive tests, I used the z-scores adjusted for age, sex and education level. In case of significant associations between NDI, ODI and TSC and disability scores, I re-run the regressions entering the brain parenchymal fraction and the log-transformed T2-hyperintense lesion volume as independent variables to test the influence of conventional MRI metrics on my model.

Since the EDSS score is not normally distributed, I used the Spearman's rho correlation coefficient for the associations between NDI, ODI and TSC and EDSS scores.

Due to the exploratory nature of the study, I did not perform correction for multiple comparisons, but, for robust regression estimates, I used a significance level of 1% and provide 99% confidence intervals.

I4 performed statistical analyses with Stata v. 14.1 (Stata Corporation, College Station, Texas, USA).

7.3 Results

The demographic and clinical characteristics of the participants are shown in Table 7.2. After quality checking, I discarded two patients from the ^{23}Na MRI (failure of the calibration phantoms) and two patients from the NODDI analyses (movement artefacts).

Table 7.2 Demographic and clinical characteristics of patients and healthy controls.

		Patients (N=42)	Healthy controls (N=16)	p-values
Age (years)		33.1 ± 1.03	33.3 ± 1.7	0.89[a]
Sex (female: male; % female)		23:19 (55)	9:7 (56)	0.92[b]
Syndrome (N, %)	**Optic neuritis**	35 (83)	-	
	Myelitis	2 (5)	-	
	Brainstem syndrome	2 (5)	-	
	Supratentorial syndrome	2 (5)	-	
	Multifocal	1 (2)		
Steroids (N, %)		17 (40)	-	-
Grey matter volume (ml)		670.2 ± 52	670.8 ± 66.2	0.97[c]
White matter volume (ml)		454.7± 39.6	467.04± 50.6	0.33[c]
Brain parenchymal fraction		0.76± 0.009	0.76± 0.02	0.64[c]
White matter T2-hyperintense lesion volume (ml) (median, range)		3.18 (0-42.18)	-	
White matter T1-hypointense lesion volume (ml) (median, range)		0.27 (0-6.2)	-	

[a] two-sample t -tests
[b] Pearson's chi-squared test
[c] linear regression model correcting for age and sex.
Note. Data are means ± standard deviations, unless otherwise indicated. *Abbreviations:* CIS: clinically isolated syndrome

Patients and healthy controls did not differ significantly for age, sex, brain parenchymal fraction, normal-appearing white matter and grey matter volume (Table 7.2), and local grey matter volumes.

Thirty-six patients had T2-hyperintense white matter lesions, twenty-two of whom also had T1-hypointense lesions and thirteen had gadolinium-

enhancing lesions. Thirty patients had dissemination in space and nine of them also fulfilled the 2017 McDonald criteria for multiple sclerosis with additional dissemination in time (Thompson *et al.*, 2018).

Table 7.3 reports the clinical characteristics of the cohort. Table 7.4 reports the significant (p≤0.01) results in normal-appearing white matter and grey matter, which are detailed below.

Table 7.3 Clinical scores in patients

Tests	Raw means	Z-scores[a]
EDSS (median, range)	1.5 (0-3)	-
9-hole peg test (s)	20.42 ± 2.5	-
Timed 25-foot walk test (s)	4.4 ± 0.6	-
PASAT	-0.23 ± 1.2	-0.23 ± 1.2
SDMT	57.26 ± 9.6	-0.9 ± 1.1
BVMT-R	25.1± 5.9	-0.47 ± 1.06
CVLT-II	60.33± 9.2	1.13 ± 1.1

[a] Z-scores calculated from normative values displayed in the National Multiple Sclerosis Society Task Force database and from the normative data provided by the Brief International Cognitive Assessment for MS initiative.
Note. Data are means ± standard deviations, unless otherwise indicated. *Abbreviations:* CIS: clinically isolated syndrome; EDSS: the Expanded Disability Status Scale; PASAT: paced auditory serial addition test; SDMT: symbol digit modalities test. BVMT-R: brief visuospatial memory test-revised; CVLT-II Californian verbal learning test II.

Table 7.4. Differences between patients and healthy controls in NDI, ODI and TSC across different white matter and grey matter areas.

	Unstandardized coefficient (B)	Bootstrap sample CI 99%	p-value
NDI			
Normal-appearing white matter			
Corpus callosum	-0.03	-0.06 to -0.006	0.004
Grey matter			
Right primary visual cortex	-0.02	-0.04 to -0.001	0.010
Left associative areas of occipital lobe	-0.016	-0.03 to -0.002	0.005
Left cognitive areas of parietal lobe	-0.014	-0.03 to -0.0007	0.009
Left superior-lateral temporal lobe	-0.012	-0.02 to -0.0006	0.009
ODI			
Normal-appearing white matter			
White matter (all)	0.008	0.002 to 0.02	0.003
Corpus callosum	0.008	0.00007 to 0.016	0.010
White matter occipital	0.02	0.006 to 0.001	0.003
White matter frontal	0.008	0.0007 to 0.016	0.007
White matter temporal	0.02	0.006 to 0.02	<0.0001
Grey matter			
Left middle frontal gyrus	-0.012	-0.02 to -0.0007	0.004
Left superior-lateral temporal lobe	-0.008	-0.01 to -0.0005	0.006
Right cognitive areas of parietal lobe	-0.01	-0.02 to -0.0003	0.009
Right operculum	-0.02	-0.04 to -0.001	0.010
TSC			
Normal-appearing white matter			
Corpus callosum	3.5	0.25 to 6.32	0.004
Grey matter			
Left middle frontal gyrus	5.81	0.51 to 11.21	0.006
Left limbic lobe	2.8	0.25 to 5.22	0.005
Right orbitofrontal cortex	2.40	0.11 to 4.88	0.009

Note: results from linear regression models adjusted for age and sex. For grey matter areas, local volume were included in the model if significantly different between patients and controls. *Abbreviations*: CI: confidence interval; NDI: neurite density index; ODI: orientation dispersion index; TSC: total sodium concentration.

7.3.1 NODDI and TSC in White Matter

Compared with healthy controls, patients showed lower NDI in the corpus callosum. ODI was higher in the normal-appearing white matter of patients compared with healthy controls. In particular, ODI was increased bilaterally in occipital, frontal and temporal white matter as well as in the corpus callosum. TSC was higher in the corpus callosum of patients than healthy controls (Figure 7.2; Figure 7.3 ; Table 7.4).

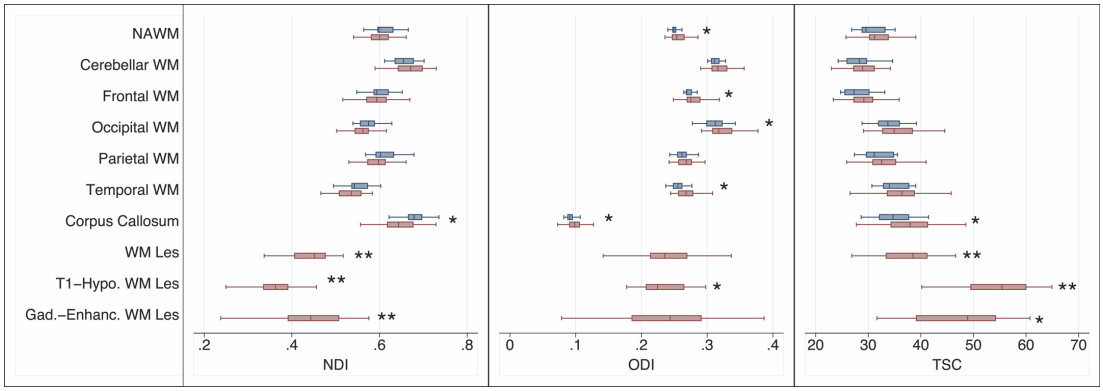

Figure 7.2. Neurite density index, orientation dispersion index and total sodium concentration in the normal-appearing white matter and white matter lesions of patients (red boxplots) and healthy controls (blue boxplots).

*p<0.01; ** p<0.0001 Abbreviations: NDI: Neurite Density Index; ODI: Orientation Dispersion Index; TSC: Total Sodium Concentration; NAWM: Normal-Appearing White Matter; WM: White Matter; Les: Lesion; Hypo.: Hypointense; Gad.: Gadolinium; Enhanc.: Enhancing

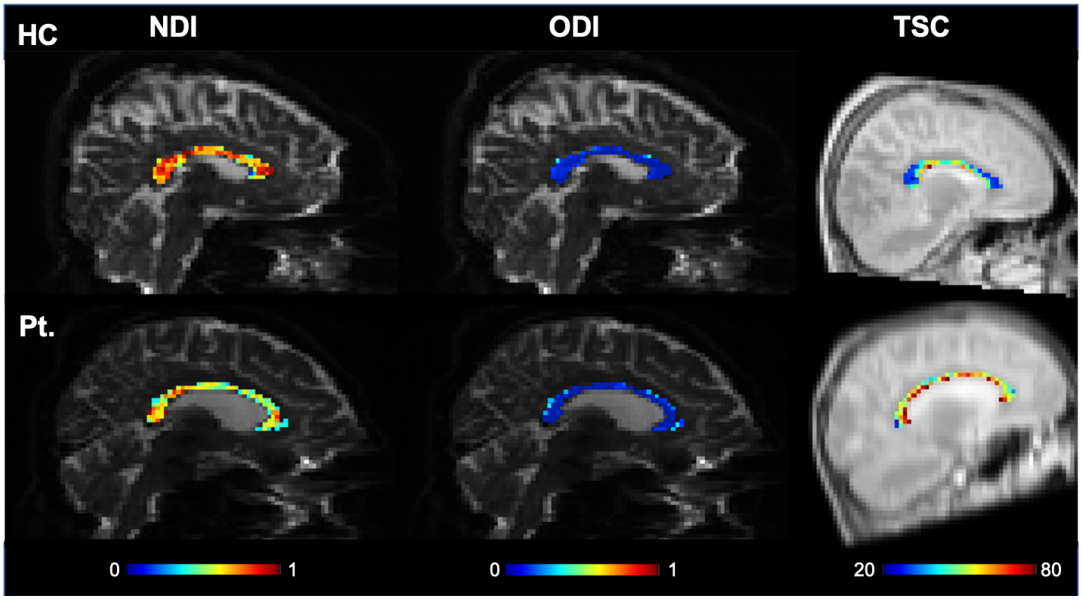

Figure 7.3.Neurite density index, orientation dispersion index and total sodium concentration in the corpus callosum of a healthy control (top) and a patient (bottom).

Abbreviations: HC: Healthy Control; NDI: Neurite Density Index; ODI: Orientation Dispersion Index; TSC: Total Sodium Concentration (values in mM); Pt.: Patient.

T2-hyperintense white matter lesions showed higher TSC (B=7.8; CI [4.8, 10.6], p<0.0001) and lower NDI (B=-0.16; CI [- 0.18, -0.14], p<0.0001) compared with normal-appearing white matter. A lower lesional NDI was associated with a higher lesional TSC (B= -0.05, CI [-0.01, -0.0006], p<0.0001). T1-hypointense white matter lesions had higher TSC (14 patients; B=25.41; CI[18.72, 32.10], p<0.0001), lower NDI (21 patients; B=-0.21; CI[-0.25, -0.18], p<0.0001) and lower ODI (B=-0.02; CI [-0.04, -0.004], p=0.002) compared with normal-appearing white matter. Gadolinium-enhancing lesions had higher TSC (eight patients; B=16.5; CI [3.8, 29.10], p=0.002) and lower NDI (13 patients; B=-0.16; CI [-0.22, -0.09], p<0.0001) compared with normal-appearing white matter (Figure 7.2)

7.3.2 NODDI and TSC in Grey Matter

Compared with healthy controls, patients showed lower NDI in the right primary visual cortex, left occipital associative and parietal cognitive areas and left superior-lateral temporal lobe. The ODI was significantly decreased in the left superior-lateral temporal lobe, the left frontal middle gyrus and the right

parietal cognitive areas. In patients, TSC was higher in the left frontal middle gyrus, left limbic lobe and right orbitofrontal cortex compared with healthy controls (Table 7.4; Figure 7.4).

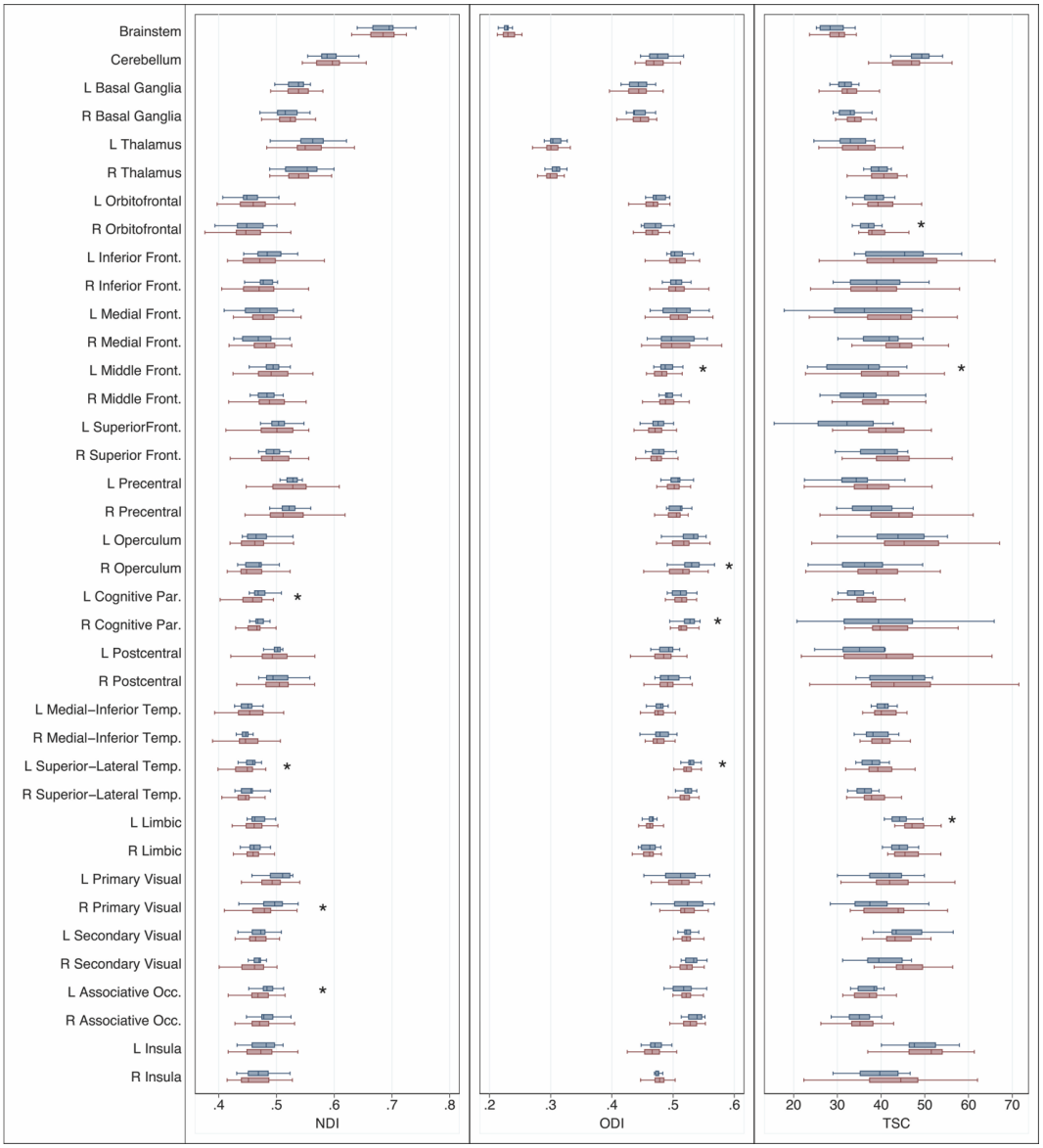

Figure 7.4. Neurite density index, orientation dispersion index and total sodium concentration in the grey matter of patients (red boxplots) and healthy controls (blue boxplots).

*p<0.01. Linear regression, corrected for age and sex and local volumes, if found significantly different between patients and controls.
Abbreviations: L: Left; R: Right; Front.: Frontal; Par.: Parietal; Temp.: Temporal; Occ.: Occipital.

7.3.3 NODDI and TSC associations with Lesion Parameters

In patients, NDI, ODI and TSC found altered in white matter and grey matter areas did not correlate with T1-hypointense and T2-hyperintense white matter lesion volumes. As only eight patients had gadolinium-enhancing lesions, I did not assess the associations with the volume of this subgroup of lesions.

A lower NDI in the corpus callosum was associated with a lower NDI on the T2-hyperintense white matter lesions, even after adjustment for T2-hyperintense white matter lesion volume (B=0.51, CI [0.27, 0.84], p<0.0001) (Figure 7.5).

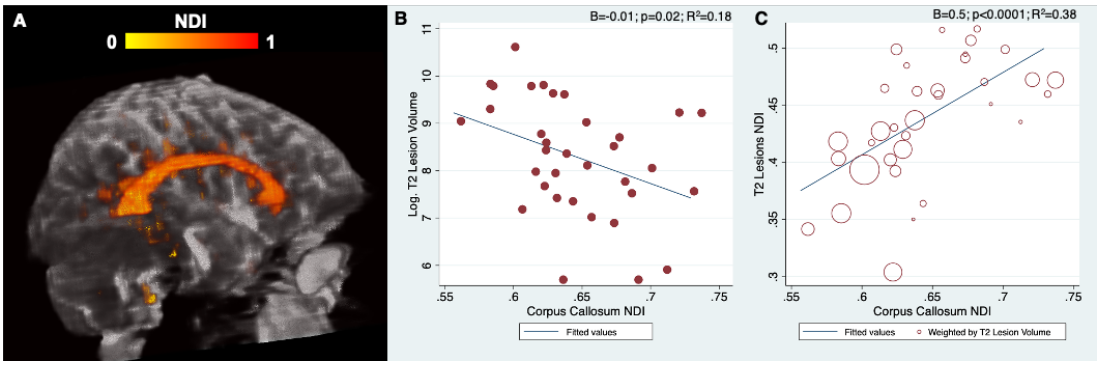

Figure 7.5 Relationships between the neurite density index in the T2-hyperintense lesions and corpus callosum.

(a) Example of neurite density index in the corpus callosum and T2-hyperintense lesions of a patient; (b) Relationship between the logarithmic transformation of the T2-hyperintense lesion volume and the neurite density index in the corpus callosum; (c) Relationship between the neurite density index in the T2-hyperintense lesions and corpus callosum (markers are weighted by the T2-hyperintense lesion volume). Abbreviations: NDI: Neurite Density Index; Log.: Logarithmic.

7.3.4 NODDI and TSC associations with Clinical Parameters

The brain parenchymal fraction, the T2-hyperintense and T1-hypointense lesion volumes did not correlate with the clinical variables.

A longer timed 25-foot walk test was associated with higher ODI in the corpus callosum (B=0.01, 99% CI= 0.003-0.02, p=0.009, R^2=0.17). The brain parenchymal fraction was not significantly correlated to this the timed 25-foot walk test. It did not influence its relationship with ODI, while the T2-hyperintense lesion volume, which did not correlate with the test, had a modest

effect on the model (ODI-B=0.01, p=0.013 R^2=0.18). Higher disability, measured by EDSS, correlated with higher TSC in the left frontal middle gyrus (r=0.5, p=0.005).

I found a borderline significance (0.01<p-value<0.05) for the association between NDI, ODI and TSC in cortical areas and the 9-hole peg test, CVLT-II, SDMT, and BVMT-R (Table 7.5).

Table 7.5. Borderline significant association (0.01<p-value<0.05) between clinical parameters and neurite density index, orientation dispersion index and total sodium concentration

Dependent Variable	Independent Variable	Unstandardized coefficient (B)	Confidence Interval 95%	p-value	R^2
9-hole peg test	Left limbic lobe TSC	0.52	0.12 to 0.93	0.012	0.19
SDMT (z-score)	Left frontal middle gyrus ODI	0.06	0.0004 to 0.01	0.038	0.11
CVLT-II (z-score)	Right primary visual cortex NDI	-0.09	-0.02 to -0.0004	0.039	0.12
BVMT-R (z-score)	Right operculum ODI	-0.01	-0.02 to -0.001	0.028	0.12
With T2-hyprintese lesion volume as covariate					
9-hole peg test	Left limbic lobe TSC	0.52	0.12 to 0.93	0.012	0.19
SDMT (z-score)	Left frontal middle gyrus ODI	0.06	0.0003 to 0.01	0.04	0.11
CVLT-II (z-score)	Right primary visual cortex NDI	-0.09	-0.02 to -0.0006	0.037	0.12
BVMT-R (z-score)	Right operculum ODI	-0.01	-0.02 to -0.0009	0.031	0.12
With brain parenchymal fraction as covariate					
9-hole peg test	Left limbic lobe TSC	0.52	0.12 to 0.93	0.012	0.19
SDMT (z-score)	Left frontal middle gyrus ODI	0.06	-0.000009 to 0.01	0.05	0.11

Dependent Variable	Independent Variable	Unstandardized coefficient (B)	Confidence Interval 95%	p-value	R^2
CVLT-II (z-score)	Right primary visual cortex NDI	-0.08	-0.02 to 0.0003	0.057	0.12
BVMT-R (z-score)	Right operculum ODI	-0.009	-0.02 to -0.00009	0.048	0.12

Note: results are from linear regression model
Abbreviations: SDMT: symbol digit modality test; CVLT-II: California Verbal Learning Test-II; BVMT-R: brief visuospatial memory test-revised

7.4 Discussion

In this study, using quantitative MRI, I have demonstrated that CIS and early multiple sclerosis patients have microstructural and metabolic alterations in the brain not detectable by conventional MRI. Moreover, this novel multi-parametric approach shows early signs of axonal damage in the corpus callosum and sheds light on possible pathobiological mechanisms underlying this process.

7.4.1 Fibre disorganization in normal-appearing white matter and axonal loss in white matter lesions

In the normal-appearing white matter of patients, I found widespread increases in ODI, particularly affecting the frontal, temporal and occipital lobes. I believe this could reflect inflammation and early fibre disorganization.

In multiple sclerosis, diffuse inflammation with lymphocytic infiltration and microglial activation can be observed in the normal-appearing white matter (Kutzelnigg *et al.*, 2005). These tissue changes are not seen with conventional MRI, as small alterations in the blood-brain barrier permeability do not permit the extravasation of gadolinium into the interstitium (Vos *et al.*, 2005). As the presence of an activated microglial status may increase ODI (Yi *et al.*, 2019), I hypothesise that the increased occupancy in the extra-neurite space related to inflammation could have driven the higher ODI in the normal-appearing white matter of this cohort.

Besides inflammation, axonal loss also dominates the pathology of normal-appearing white matter in multiple sclerosis, which may be a sequela of direct inflammation and, also, secondary Wallerian degeneration from white matter plaques (Kutzelnigg *et al.*, 2005). Previous NODDI studies (Granberg *et al.*, 2017; Schneider *et al.*, 2017; Spanò *et al.*, 2018), including the one presented in the previous chapter, enrolled established multiple sclerosis patients, who, compared with this early cohort, may have had more advanced neuroaxonal injury resulting in a consistent finding of decreased NDI in the normal-appearing white matter that I did not find. ODI, instead, has shown variable behaviour: it has been either higher in multiple sclerosis than healthy controls

(Schneider *et al.*, 2017; Hagiwara *et al.*, 2019) or both higher and lower, depending on the area examined (Spanò *et al.*, 2018), or unaltered, as Granberg and colleagues (Granberg *et al.*, 2017) and I have found. I believe the discrepancies of these previous studies may result from different degrees of axonal loss and inflammation in the tissue. In this study, normal-appearing white matter inflammatory processes may have been prevalent and caused initial degenerative changes in the axonal structure resulting in an increased fanning and/or dispersion of the fibres (i.e., high ODI) without yet a significant decrease in axonal density (i.e., low NDI). Longitudinal studies will help to understand how NODDI metrics can mirror pathological changes in the disease evolution.

In lesional white matter (i.e., T2-hyperintense lesions), I confirmed findings from previous multiple sclerosis studies (Inglese *et al.*, 2010; Zaaraoui *et al.*, 2012; Paling *et al.*, 2013; Eisele *et al.*, 2016; Petracca *et al.*, 2016; Granberg *et al.*, 2017; Maarouf *et al.*, 2017; Schneider *et al.*, 2017): lesions exhibit lower NDI and higher TSC compared with normal-appearing white matter, particularly in the T1-hypointense lesions. Interestingly, low lesional NDI correlated with high lesional TSC supporting the hypothesis that TSC and NDI together can be potential biomarkers of axonal damage because of demyelination and inflammation. For gadolinium-enhancing lesions in this study, NDI and TSC show similar directional behaviour to T1 black holes, compared with normal-appearing white matter, i.e., lower NDI and higher TSC. This could indicate both acute axonal loss as well as oedema (Trapp *et al.*, 1998). In the T1-hypointense lesions ODI was low, supporting the hypothesis that in the presence of marked neuroaxonal loss, this index is low as the dispersion is estimated from relatively few axons(Grussu *et al.*, 2017; Schneider *et al.*, 2017).

7.4.2 Early signs of axonal damage in the corpus callosum

NDI correlates primarily with axonal density and also with their degree of myelination (Sepehrband *et al.*, 2015; Grussu *et al.*, 2017). Therefore, I propose the low NDI in the corpus callosum may reflect early axonal damage, particularly at the expense of large myelinated axons. The high corpus callosal

ODI may not only be related to inflammation, as discussed before, but also be consequent to this reduced density of large axons. In a highly coherent structure, which, in health, has very low ODI, the orientation dispersion of the surviving axons can increase with neuroaxonal degeneration.

The ^{23}Na MRI findings of higher TSC in the corpus callosum support the hypothesis of early axonal damage within this structure and are consistent with a previous study in established multiple sclerosis (Petracca *et al.*, 2016). As seen in Paragraph 3.1.1.6, demyelination and inflammation drive neuroaxonal damage through a cascade of events marked by an increased sodium influx in the axolemma due to at least two mechanisms. Firstly macrophages attack can damage mitochondria with consequent energy failure and sodium influx (Mahad *et al.*, 2009; Lassmann, 2016). In addition, demyelination can lead to a redistribution of ^{23}Na channels along the axons to maintain ionic potentials (Craner *et al.*, 2004). The consequences of these processes would be a toxic calcium influx, which leads to neuroaxonal death (Trapp and Stys, 2009). The co-existence of low NDI and high ODI suggests that TSC may be increased consequent to both increased extracellular volume, due to axonal loss, and increased intracellular concentration, due to axonal metabolic dysfunction.

This study shows that a lower NDI in the corpus callosum correlates with lower NDI in white matter lesions, thus suggesting that retrograde neurodegeneration from the transected axons of the affected white matter could influence axonal integrity in the corpus callosum (Haider *et al.*, 2016). This structure may be particularly susceptible to Wallerian degeneration having a high density of fibres, all in the same direction, that could degenerate secondarily from the same distant demyelinating lesion.

Overall, my novel results show the presence of axonal damage, not captured by conventional MRI techniques, in the corpus callosum of patients within three months of symptom onset.

The presence of demyelinating plaques in the corpus callosum is a distinctive feature of multiple sclerosis, shared by few other conditions (Aliaga and Barkhof, 2014), and disease-related corpus callosal atrophy has been

documented in *post-mortem* cases (Barnard and Triggs, 1974). Therefore, researchers have investigated changes in the corpus callosum of CIS patients. Using DTI, they showed increased mean diffusivity (Bommarito *et al.*, 2018) and reduced fractional anisotropy (Bester *et al.*, 2008; Raz *et al.*, 2010) in this area. However, DTI indices are less specific than NODDI at differentiating neurodegeneration from other microstructural substrates and a decreased fractional anisotropy may be just related to an increased ODI (Timmers *et al.*, 2016; Grussu *et al.*, 2017). Other studies using DTI parameters of axial and radial diffusivity demonstrated increased axial diffusivity (Huang *et al.*, 2018; Schneider *et al.*, 2019), an index that has been associated with axonal damage (Alexander *et al.*, 2007). However, the lesions were excluded only with probability maps (Schneider *et al.*, 2019) or not excluded at all (Huang *et al.*, 2018) from the analysis, so that they could have influenced their findings. Two studies, from the same group, assessed possible metabolic alterations in the corpus callosum using MR spectroscopy (Ranjeva *et al.*, 2003; Audoin *et al.*, 2007). In the first study, the authors concluded that only demyelination, and not neurodegeneration, occurred in the corpus callosum because they found the N-acetyl aspartate/Creatine ratio not significantly altered. However, they reported MRI spectroscopy results as metabolite ratios and this stability could have been caused by a similar change in the two metabolites. In the latter study, they found decreased N-acetyl aspartate, as a sign of axonal dysfunction, in the corpus callosum, but callosal lesions were included in the analysis.

7.4.3 Metabolic and microstructural alterations in cortical grey matter

In grey matter, I found metabolic and microstructural alterations in several cortical regions. In the previous chapter, I did not find significant differences in the NDI and ODI of the whole grey matter between patients and healthy controls, similar to previous studies (Granberg *et al.*, 2017). However, when analysing local areas, authors found NDI and NDI alterations in certain areas (Spanò *et al.*, 2018). This is not surprising as, compared to white matter, significant alterations in the whole cortex may be more difficult to detect given its non-homogenous microstructure: NDI and ODI can vary according to the

specific myelo- and cyto-architecture of different cortical areas (Fukutomi *et al.*, 2018).

Topographically, these early patients, most of them with optic neuritis, had low NDI in the visual areas. The presence of retrograde axonal degeneration following the optic nerve damage has been described (Tur *et al.*, 2016). This may suggest a possible relationship with damage to the anterior visual pathway that deserves further investigation in future studies.

The finding of low ODI in certain grey matter areas could indicate complex tissue changes in the cortex, sensitive to mechanisms such as changes in dendritic arborization (Fukutomi *et al.*, 2018; Wang *et al.*, 2019).

In patients, I found higher TSC in some grey matter areas compared with healthy controls. TSC has been generally increased in studies of established multiple sclerosis (Zaaraoui *et al.*, 2012; Paling *et al.*, 2013; Petracca *et al.*, 2016, Brownlee *et al.*, 2019*b*). In early multiple sclerosis/CIS, alterations due to microstructural pathology may still be only localized to a few areas and, over time, may become more diffuse. Moreover, functional and dynamic metabolic changes can also contribute to an increase in TSC (Gandini Wheeler-Kingshott *et al.*, 2018).

7.4.4 Associations with clinical parameters

This cohort of patients had, as expected, low disability, limiting the likelihood of detecting correlations with clinical outcomes. Nevertheless, even though I restricted the analysis only to the areas where significant alterations were found, my results offer interesting insights.

Firstly, I found that higher ODI in the corpus callosum correlated with a longer timed 25-foot walk test ($p=0.009$). As this area is the largest interconnecting fibre tract in the brain, it is probable that is involved in gait regulation (Bhadelia *et al.*, 2009). Secondly, although I performed ^{23}Na MRI in a cohort of patients early after symptom onset, I could confirm previous findings of associations between cortical TSC and physical disability (Petracca *et al.*, 2016, Brownlee *et al.*, 2019*b*). Although this correlation was restricted to a specific gyrus,

nevertheless, it suggests that ^{23}Na MRI can detect pathological abnormalities relevant to physical disability even in early patients.

Finally, as hypothesis-generating results ($0.01<p<0.05$), I observed that lower ODI in grey matter areas involved in attention and language (i.e., the left middle frontal gyrus) and cognition (i.e., the right operculum) was associated with worse cognitive performance. This suggests that early changes in cortical morphology may affect cognition.

Interestingly, no significant clinical associations were found for brain parenchymal fraction or T2-hyperintense lesion volume, implying that NODDI and ^{23}Na MRI may offer more sensitive and clinically relevant markers of tissue pathology in early MS than conventional MRI metrics.

7.4.5 Limitations

I acknowledge several limitations of this study. Firstly, not all the subjects who underwent NODDI also completed the ^{23}Na MRI protocol. However, being the first study on ^{23}Na MRI in very early patients and the first one combining this technique with NODDI, I believe that the current sample size (32 patients and 13 controls) can justify the exploratory aims of this research.

Secondly, the discussion of results for NODDI is based on previous histological findings in animal models and observational studies in neurological disorders, and for ^{23}Na MRI, on previous observational studies in multiple sclerosis. I cannot directly demonstrate that these measures are sensitive to the different pathophysiological substrates. Only pathological studies can provide this evidence, and, for early patients, they are rare and performed in small and/or atypical cohorts.

This study performed NODDI on a clinical scanner. This clinical implementation requires echo times longer than ones achievable at ultra-high gradient strength, theoretically implying lower signal-to-noise levels. Nonetheless, previous work (Zhang *et al.*, 2012; De Santis *et al.*, 2019) has demonstrated that the echo time used in this study is sufficient to produce image quality suitable for group comparisons.

Finally, the low ^{23}Na sensitivity at 3T means that I could derive only TSC, rather than intracellular and extracellular sodium concentrations. Nevertheless, using NODDI, I could identify areas of low NDI where it is likely that an increased extracellular volume due to axonal loss contributed to the TSC increase. High field scanners (e.g., 7T) are required to disentangle the intracellular and extracellular component of the TSC changes (Petracca *et al.*, 2016) and could be considered in future studies (Fleysher *et al.*, 2013).

7.5 Conclusions

In summary, I found that CIS and multiple sclerosis patients at symptom onset have diffuse axonal dispersion in normal-appearing white matter, potentially related to inflammation, whilst they exhibit alterations consistent with axonal pathology and dysfunction in the corpus callosum, a typical site for multiple sclerosis involvement, and in cortical areas. This study suggests that the combined use of NODDI and ^{23}Na MRI can detect and provide insights, *in vivo,* into early multiple sclerosis pathology. My results report clinical associations with NODDI and ^{23}Na imaging, not evident with more conventional measures of the brain or T2-hyperintense lesion volumes. Future longitudinal studies can assess whether these changes correlate with disability accumulation

Chapter 8 Single-subject structural cortical networks in clinically isolated syndrome

8.1 Introduction

In the previous chapter, we saw that patients at their first demyelinating episode can show microstructural and metabolic alterations in the normal-appearing white and gray matter. These alterations were related to physical disability, but I only found trends regarding the correlation with the cognitive function.

As seen in the Paragraph 3.4, beyond the structural changes in the CNS tissues, patients with multiple sclerosis may have alterations of the CNS seen as a network. We have seen in Paragraph 4.3 that there are several techniques to study the CNS as a network and SCNs offer the advantage of the use of anatomical sequences in already acquired dataset.

SCNs are altered in multiple sclerosis. Briefly, multiple sclerosis patients can shift in either direction, either towards a more regular (Tewarie *et al.*, 2014; Muthuraman *et al.*, 2016) or a more random network (He *et al.*, 2009; Rimkus *et al.*, 2018), the only study including a small cohort of CIS patients (Muthuraman *et al.*, 2016) demonstrated increased clustered organization of SCNs in CIS subjects compared with healthy controls.

So I decided to use this technique to see if there were alterations of SCNs in this early phase and to use a single-subject technique (Tijms *et al.*, 2012) to find clinical correlations, in particular with information processing speed, which, as discussed before, is often altered in patients with multiple sclerosis and clinically isolated syndrome since the early phases (Brochet and Ruet, 2019).

My aim was to investigate SCNs alterations in a larger cohort of patients at onset. Moreover, since SCNs have been studied exclusively in single-center studies before, my secondary aim was to evaluate the impact of between-scanner variability on single-subject SCN analysis. Consequently, I have

added to the cohort recruited in London data from patients and healthy controls recruited with the same characteristics in other centres in Europe.

8.2 Materials and methods

8.2.1 Participants

This study represents an analysis of the baseline data acquired as part of a prospective MAGNIMS (www.magnims.eu) 3-year multi-center, multi-vendor project, conducted in six multiple sclerosis Centres (Table 8.1). Previous studies using the same cohort addressed a different issue and are unrelated to this analysis (Hagens *et al.*, 2018*b*, *a*).

Sixty patients experiencing symptoms suggestive of a CIS (age 18 to 59 years at baseline) were recruited from the six participating centres within six months of symptom onset. Thirty-eight age and gender-matched healthy controls were also recruited (Table 8.1). Exclusion criteria for all participants were a history of other known medical conditions that could have affected the brain (vascular, malignant, neurological) and MRI related contra-indications.

Table 8.1 Demographic characteristics of clinically isolated syndrome patients and healthy controls

	CIS patients	Healthy Controls	p-value
No.	60	38	-
Age (years)	34 ± 8	35 ± 9	0.22
Gender (female: male; % female)	40:20 (67)	23: 15 (61)	0.46
Center group sizes No. (%)			
VU University Medical Center	0 (0)	8 (20)	
University Hospital Basel	13 (22)	8 (21)	-
St. Josef Hospital	4 (7)	3 (8)	-
UCL Queen Square Institute	25 (42)	19 (50)	-
Hospital Clínico San Carlos	10 (16)	0 (0)	-
Sapienza University of	10 (16)	2 (5)	-
Cortical GM volume (ml)	512 ± 47	523 ± 52	0.26
WM lesion volume (ml)	0.8 (0-19.4)	-	-
MS according to the 2017	8 (13)	-	-
0-1 WM lesion No. (%)	11 (18)	-	-
2-10 WM lesion No. (%)	23 (38)	-	-
> 10 WM lesion No. (%)	26 (43)	-	-
EDSS	1.5 (0-3)	-	-
SDMT [a]	54.9±14.5	-	-

[a] Available in 47 patients. Data are means ± standard deviation; EDSS and WM lesion volume are median with minimum and maximum. Abbreviations: CIS: clinically isolated syndrome; CGM: cortical gray matter; WM: white matter; EDSS: Expanded Disability Status Scale; SDMT: Symbol Digit Modality Test

8.2.2 Clinical examination

At baseline, CIS patients underwent neurological examination and EDSS was assessed by a trained physician. Forty-seven patients were also tested for information processing speed with SDMT.

8.2.3 Image acquisition and post-processing

All subjects underwent a baseline MRI scan of the brain and spinal cord at a 3T scanner, and CIS patients additionally underwent administration of intravenous contrast. The scanning parameters were based on local protocols and followed the MAGNIMS guidelines (Rovira *et al.*, 2015). The acquisition protocols for the different vendors are reported in Table 8.2: they included brain 3D T1-weighted (1 mm isotropic) and 3D fluid-attenuated inversion recovery (FLAIR); proton density/T2 and post-contrast T1-weighted sequences for brain and spinal cord.

White matter lesion number and location (periventricular, juxtacortical, deep white matter, infratentorial and spinal) were recorded. Subsequently, dissemination in space and time, as well as multiple sclerosis diagnosis, were determined according to the revised 2017 McDonald criteria (Thompson *et al.*, 2018).

In this project, I performed white matter lesion segmentation with a semi-automated process using the 3D FLAIR and 3D T1-weighted MRI sequences (Sudre *et al.*, 2015) and then I checked, and manually corrected, the lesion masks if necessary. Subsequently, I obtained the lesion volumes.

Afterwards, I use the same methodology described in previous chapters to lesion fill the 3D-T1 (Prados *et al.*, 2014) and automatically segment the cortical gray matter (CGM) with GIF method v3.0 (Prados *et al.*, 2016*a*) . Additionally, ninety-eight cortical areas were identified in the native-space bilateral CGM according to the Desikan-Killiany-Tourville protocol (Klein and Tourville, 2012). I quality checked all segmentations and in case I discarded the scans. Finally, for computational reasons, CGM segmentation on the 3D T1-weighted images was resliced to 2.0 mm isotropic voxels to reduce the dimensionality of the data (Tijms *et al.*, 2012).

Table 8.2 MRI sequence parameters per centre

Center	Vendor	Parameters	3D T1	3D FLAIR	2D PD/T2	T1 SE +c	T1	PD/T2
				Head				Spinal Cord
VU University Medical Center Amsterdam	GE Discovery MR750	Slice orientation	Sag	Sag	Ax	Ax	Sag	Sag
		Measured voxel size (mm)	1.0x1.0x1.0	1.1x1.1x1.2	0.65x1.0x3.0	0.78x1.0x3.0	0.93x1.5x3.0	0.93x1.5x3.0
		TR (ms)	8.2	8000	9415	660	589	3598/3400
		TE (ms)	3.2	130	20/112	9	8.7	9.6/80
		Flip angle (degrees)	12	90	90	70	90	90
		Inversion time (ms)	450	2340				
University Hospital Basel	Siemens Verio	Slice orientation	Sag	Sag	Ax	Ax	Sag	Sag
		Measured voxel size (mm)	1.0x1.0x1.0	1.0x1.0x1.0	1.0x1.0x3.0	1.0x1.0x3.0	0.67x0.84x3.0	0.67x0.84x3.0
		TR (ms)	1570	5000	3570	650	500	2500/3450
		TE (ms)	2.67	402	9.3/93	8.4	10	8.1/102

Center	Vendor	Parameters	3D T1	3D FLAIR	2D PD/T2	T1 SE +c	T1	PD/T2
		Flip angle (degrees)	9	Variable	140	75	140	160/140
		Inversion times (ms)	900	1800				
St. Josef Hospital Bochum	Philips Achieva	Slice orientation	Sag	Sag	Ax	Ax	Sag	Sag
		Measured voxel size (mm)	1.1x1.1x1.0	1.0x1.3x1.0	1.0x1.0x3.0	1.0x1.0x3.0	0.48x0.48x3.0	0.48x0.48x3.0
		TR (ms)	10	5000	3000	635	462	3696
		TE (ms)	4.2	354	118	17	8	120
		Flip angle (degrees)	15	180	150	90	90	90
		Inversion times (ms)	1100	1900				
Hospital Clínico San Carlos Madrid	GE Signa HDxt	Slice orientation	Sag	Sag	Ax	Ax	Sag	Sag
		Measured voxel size (mm)						
		TR (ms)	10	6000	2500	540	500	2240
		TE (ms)	4.2	135	10/100	7.5	8.5	18/119

Center	Vendor	Parameters	3D T1	3D FLAIR	2D PD/T2	T1 SE +c	T1	PD/T2
		Flip angle (degrees)	12	90	90	90	90	90
		Inversion times (ms)	450	1840				
Sapienza University of Rome	Siemens Verio	Slice orientation	Sag	Sag	Ax	Ax	Sag	Sag
		Measured voxel size (mm)	1.0x1.0x1.0	1.0x1.0x1.0	0.6x0.6x3.0	1.0x0.8x3.0	1.0x0.8x3.0	1.0x0.8x3.0
		TR (ms)	1900	5000	5970	628	600	2500/3000
		TE (ms)	2.93	395	10/103	9.8	9.4	7.8/107
		Flip angle (degrees)	9		150	120	140	160
		Inversion times (ms)	900	1800				

Abbreviations: Ax = axial, DIR = double inversion recovery, FLAIR = fluid-attenuated inversion recovery, GE = General Electric, NA= not applicable, PD = proton density, Sag = sagittal, SE = spin-echo, T = Tesla, TE = echo time, TR = repetition time

8.2.4 Single-subject gray matter graphs

SCNs were extracted at subject level using software developed by B.M. Tijms (https://github.com/bettytijms/) in Matlab v7.12.0.635. Briefly, first, the SCNs' nodes were defined as regions-of-interest in the native space CGM segmentation, corresponding to 3x3x3 voxel cubes. This was chosen because a 3-voxel size can capture the thickness and folding of the cortex (Kiselev *et al.*, 2003) without generating large matrices of cubes.

The similarity between all the cubes (nodes) in the network was determined with the correlation coefficient, which was collected in a matrix that was subsequently thresholded and binarized, so that the chance of having spurious correlations for all single-subject SCNs was < or = to 5%. The obtained graphs were undirected with nodes connected each other by edges, only if their similarity matrix survived this threshold (Figure 8.1).

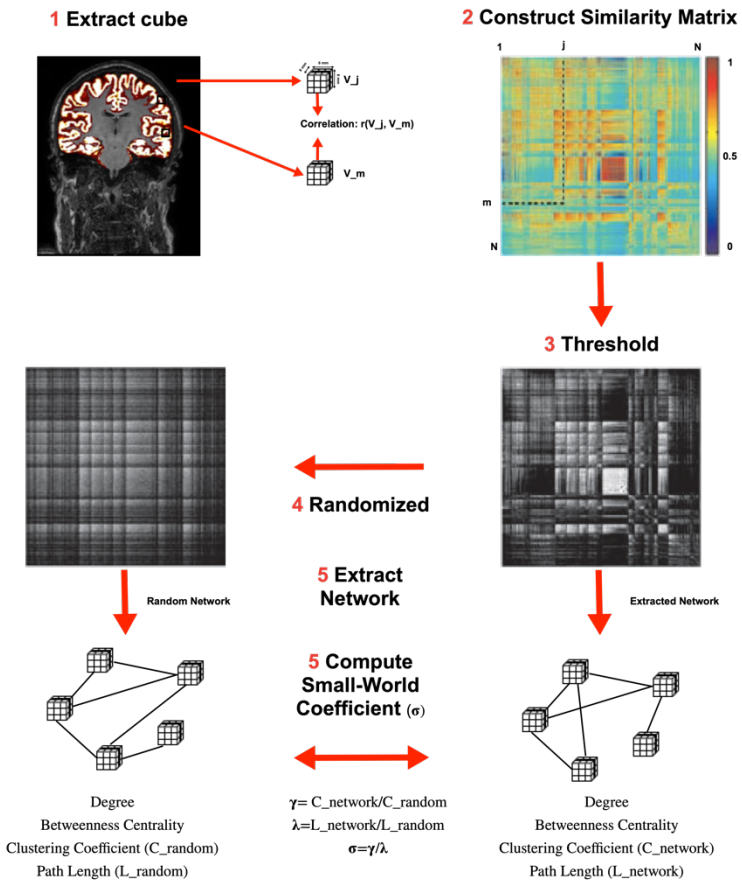

Figure 8.1 SCNs extraction (adapted from (Tijms *et al.*, 2012))

8.2.5 Graph properties

First, I determined the following global graph-defining properties: the size of the SCNs (i.e., the number of cubes), the average degree (i.e., the number of edges) and the connectivity density (i.e., the proportion of existing connections to the maximum number of possible connections). Then, I computed the global graph parameters averaged across all cubes: the characteristic path length (Rubinov and Sporns, 2010), the clustering coefficient (Watts and Strogatz, 1998), the betweenness centrality (Zuo *et al.*, 2012) and the eigenvector centrality (Joyce *et al.*, 2010) (Figure 8.2). In addition, the clustering coefficient and characteristic path length of each graph were normalised with those of 20 randomised reference graphs of identical size and degree distribution (Tijms *et al.*, 2012). The small-world coefficient was then obtained from the ratio between the normalised clustering coefficient (γ) and the normalised characteristic path length (λ) (Watts and Strogatz, 1998). A network shows a small-world properties when its nodes are highly clustered, as in regular lattices, but they can also be reached from every other node in a small number of steps, e.g. in random graphs, resulting in a ratio between γ and λ greater than one (Bullmore and Sporns, 2009).

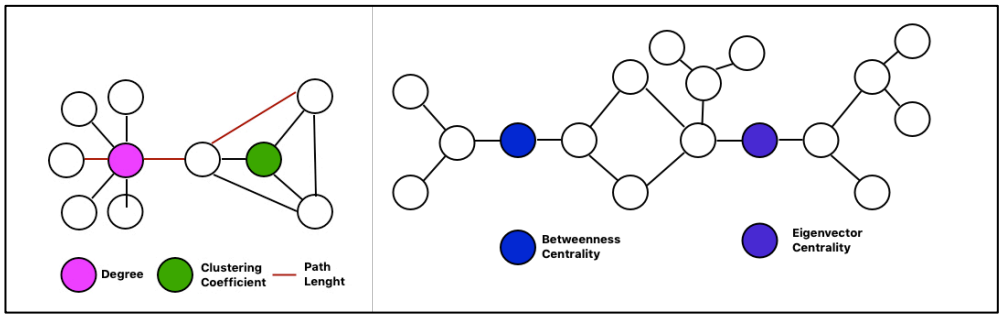

Figure 8.2 Network properties

At regional level, I averaged the local graph parameters across the nodes within each of the 98 cortical areas, which had been parcellated with GIF in each individual subject, in order to reduce the dimensionality of the SCNs and increase the comparability between subjects, across centers and possibly with previous studies (van Wijk *et al.*, 2010).

8.2.6 Statistical analysis

Group differences in demographic characteristics and CGM volume were assessed using two-sample t-tests for continuous variables and chi-square tests for categorical variables.

I initially applied a multivariate linear regression model to compare graph properties between groups, adjusting for age, gender and CGM volume. Since non-normalised global graph parameters (betweenness centrality, eigenvector centrality, clustering coefficient and path length) are dependent on graph-defining properties (size, connectivity density and degree), I included any of these graph-defining properties when they were significantly different between groups as additional independent variables to the model. I tested possible nonlinear effects of age with quadratic regression analysis imputing graph parameters as dependent variables.

Since the analysis of the global graph parameters was meant to be exploratory, I did not perform multiple comparison adjustments.

Group differences in local graph parameters in the 98 CGM areas were assessed with linear regression, correcting for age, gender and local CGM volume). Due to concerns about residual variance heterogeneity across centers, the regression was estimated using the Hubert-White (Huber, 1967; White, 1980) standard error, which is known to be robust to residual heterogeneity. Significant P values were identified correcting for multiple comparisons using a False Discovery Rate (FDR) of 5% for multiple hypothesis testing (Genovese *et al.*, 2002).

White matter lesion volumes were log transformed to allow parametric testing (Afifi *et al.*, 2007) and the relationships between these and global/local graph metrics as well as clinical parameters (EDSS, SDMT, multiple sclerosis diagnosis according to the 2017 McDonald criteria) were assessed using linear regression adjusting for age and gender. Associations between local/global graph metrics changes and clinical parameters were assessed with linear regression adjusting for age and gender. The white matter lesion volume was

included as an additional independent variable to the model if associated with the clinical parameters.

Since patients are heterogeneous in terms of the number of white matter lesions, an established risk factor for conversion to multiple sclerosis, I also divided patients into distinct groups according to the number of intracranial white matter lesions: 0-1, 2-9 and >10 lesions. This allowed further comparisons between healthy controls and patients at different risk stage of developing MS (Tintoré *et al.*, 2006).

Not all centers provided both healthy controls and patients, hence I investigated and controlled for centre effects in the following manner. In addition to entering the centre as a covariate in a linear regression including all centers, with graph metrics as dependent variables and age, gender and CGM volume as the other covariates, I performed a further analysis restricted to those centers contributing both patients and healthy controls (Basel, Bochum and London). If the between-group graph parameter differences or p-values were materially altered by inclusion of center in either the full or the restricted analyses, center was retained as covariate in the unrestricted model over all centers.

Statistical analyses were performed with Stata v. 14.1 (Stata Corporation, College Station, Texas, USA).

8.3 Results

8.3.1 Subject characteristics

The clinical and radiological characteristics of the participants (60 patients and 38 healthy controls) are provided in Table 8.3. Patients and healthy controls did not show significant differences in age, gender and CGM volumes. Patients had low disability and were cognitively preserved. Out of the entire sample of 60 patients, eight fulfilled the 2017 McDonald criteria for multiple sclerosis.

Participants' characteristics across centers are detailed in Table 8.3.

Table 8.3 Participants' characteristics across centers.

	Amsterdam		Basel			Bochum			London			Madrid		Rome	
Group	CIS patients	HCs	CIS patients	HCs	P value	CIS patients	HCs	P value	CIS patients	HCs	P value	CIS patients	HCs	CIS patients	HCs
No.	0	8	13	7		4	3		25	19		10	0	8	1
Age	-	36.3 ± 8	34.2 ± 6	34.3 ± 7	0.99[a]	31 ± 8	45.3± 13	0.11[a]	34.2 ± 8	33.8 ± 7	0.86[a]	31.2 ± 3	-	35.5± 13	49
Female No. (%)	-	5 (63)	9 (69)	4 (57)	0.59[b]	4 (100)	3 (100)	-	14 (56)	11 (58)	0.9[b]	5 (50)	-	8 (100)	0 (0)
CGM Vol. ml	-	527.8 ± 48	521.6 ± 61	532.3 ± 62	0.96[a]	513.4 ± 29	531.8 ± 44	0.86[a]	512.3 ± 41	516.4 ±56	0.71[a]	519 ± 46	-	478.5 ± 45	520.1
Lesion Vol. ml	-	-	0.1 (0-9)	-		2.5 (0.7-19)	-		1.8 (0-19)	-		0.3 (0.07-6)	-	1.4 (0.2-4)	-
0-1 les. No. (%)	-	-	5 (40)	-		0 (0)	-		5 (20)	-		1 (10)	-	0 (0)	-
2-10 les.	-	-	4 (30)	-		1 (25)	-		6 (24)	-		7 (70)	-	5 (63)	-
>10 les.	-	-	4 (30)	-		3 (75)	-		14 (56)	-		2 (20)	-	3 (37)	-
MS No. (%)	-	-	2 (15)	-		0 (0)	-		1 (4)	-		0 (0)	-	5 (63)	-
EDSS	-	-	2 (0-3)	-		2 (1.5-	-		1.5 (0-3)	-		1 (0-3)	-	2 (0-2)	
SDMT	-	-	55.8 ± 7	-		64.3 ± 3	-		60.3 ± 9	-		-	-	24.7 ± 6	

[a] Group differences in age and cortical grey matter volume were assessed using two-sample t-tests
[b] Group differences in sex distribution were assessed with chi-square test for categorical variables
Note. Data are means ± standard deviations, medians with minimum and maximum or absolute numbers with percentages. Volumes are in ml.
Abbreviations. CIS: clinically isolated syndrome; HCs: healthy controls; CGM: cortical grey matter; Vol.: Volume; Les.: lesion; MS: multiple sclerosis; EDSS: Expanded Disability Status Scale; SDMT: Symbol Digit Modality Test.

8.3.2 Global graph metrics

All single-subject SCNs did not exhibit disconnected nodes.

Both CIS and HC groups retained small-world topology (γ/λ>1), but in patients the multivariate regression analysis (R^2=0.06, F(4, 92)=2.38, p<0.05) showed a higher γ than healthy controls (B= 0.01, 95% CIs=0.003-0.02, p=0.012) . Patients showed also (R^2=0.11, F (4, 92) =3.41, p<0.05) a higher small-world coefficient than healthy controls (B= 0.01, 95% CIs=0.004-0.02, p=0.003).

Age and age squared did not have any effects on the global graph metrics.

After correction for center effect, the differences between patients and healthy controls for small-world coefficient remained significant (p=0.024) but not for γ.

For global graph-defining properties, patients had smaller network sizes compared with healthy controls (Table 8.4); therefore, to compare SCNs between patients and healthy controls, I adjusted the analysis of the non-normalised global graph parameters for the network size. patients initially showed higher eigenvector centrality than controls (B=0.07, 95% CIs=0.01-0.1, p=0.02), but this difference lost significance after adjusting for network size.

Table 8.4 Global graph parameters

	CIS patients	Healthy Controls	Unstandard. coefficient (B)	95% Confidence Interval	p-value
Size (No. of cubes)	6984 ± 256	7104 ± 248	-123.15	-226.44 to -19.86	0.02
Connectivity Density (%)	24.86 ± 1.35	25.03 ± 1.23	-0.31	-0.8 to 0.2	0.19
Degree (mean/1000)	1.74 ±0.12	1.78 ± 0.12	-0.02	-0.05 to 0.01	0.39
Characteristic Path Length	1.81 ± 0.02	1.81 ± 0.02	0.0007	-0.003 to 0.005	0.73
Clustering Coefficient	0.55 ± 0.02	0.55 ± 0.01	-0.002	-0.007 to 0.003	0.45
Betweenness Centrality	0.6 ± 0.18	0.51± 0.24	0.005	-0.02 to 0.03	0.71
Eigenvector Centrality	0.39 ± 0.19	0.46 ± 0.2	0.004	-0.02 to 0.03	0.75
Gamma (γ)	1.41 ± 0.024	1.40 ± 0.021	0.008	-0.0006 to 0.017	0.07
Lambda (λ)	1.04 ± 0.006	1.04 ± 0.004	-0.00009	-0.001 to 0.001	0.89
Small-world coefficient	1.36 ± 0.02	1.35 ± 0.01	0.009	0.001 to 0.02	0.024

Statistical differences in global graph parameters between CIS patients and healthy controls tested with multivariate linear regression. All analyses were adjusted for age, gender, CGM volume and center. Size was used as an additional independent variable in the linear regression model for the non-normalised global graph parameters (characteristic path length, clustering coefficient, betweenness centrality, eigenvector centrality). Betweenness and eigenvector centrality values were rescaled to 0 to 1 value. Data are reported as unadjusted means ± standard deviation. Abbreviations: CIS: clinically isolated syndrome; unstandard.: unstandardized.

Center/scanner effect was also significant for connectivity density ($p<0.0001$) and for all global graph parameters ($p<0.0001$). Therefore, center was retained as covariate in the multivariate regression analysis. Table 8.5 shows the SCNs parameters across centers.

In patients, a higher small-world coefficient was associated ($R^2=0.17$, $F(3, 55)=3.64$, $p<0.05$) with higher white matter lesion volume (= 0.36, $p=0.007$), after adjusting for age (= 0.03, $p=0.832$) and gender (= -0.18, $p=0.162$); additionally, patients with higher lesion counts (>10 lesions) showed higher gamma and greater small-world coefficients compared with healthy controls and with patients with lower lesion numbers (Figure 8.3). The small-world coefficient in CIS patients and the white matter lesion location were not significantly associated.

Table 8.5 Structural cortical networks parameters across centers.

	Amsterdam		Basel			Bochum			London			Madrid		Rome	
Group	CIS patients	HCs	CIS patients	HCs	P[a]	CIS patients	HCs	P[a]	CIS patients	HCs	P[a]	CIS patients	HCs	CIS patients	HCs
No.	0	8	13	7		4	3		25	19		10	0	8	1
Size	-	7143 ±171	7022 ±237	7031 ±357	0.9	6951 ±133	7254 ±233	**0.001**	6945 ±303	7102 ±242	**0.04**	7141 ±219	-	6867 ±99	6923
CD	-	24.86 ±0.98	25.73 ±1.48	25.79 ±1.45	0.6	25.76 ±0.58	25.36 ±1.04	0.6	24.3 ±1.02	24.86 ±1.22	**0.02**	24.17 ±1.4	-	25.61 ±1.02	23.29
Degree	-	1.78 ±0.08	1.81 ±0.12	1.82 ±0.17	0.6	1.79 ±0.04	1.84 ±0.13	**0.05**	1.69 ±0.12	1.77 ±0.11	**0.015**	1.73 ±0.12	-	1.76 ±0.06	1.61
BC	-	0.59 ±0.2	0.56 ±0.2	0.38 ±0.28	0.9	0.54 ±0.14	0.66 ±0.16	0.2	0.57 ±0.2	0.49 ±0.25	0.5	0.73 ±0.15	-	0.61 ±0.11	0.61
EC	-	0.42 ±0.15	0.42 ±0.19	0.61 ±0.25	0.8	0.49 ±0.15	0.37 ±0.07	**0.03**	0.37 ±0.2	0.43 ±0.2	**0.04**	0.22 ±0.14	-	0.52 ±0.13	0.45
CL	-	0.55 ±0.01	0.56 ±0.02	0.56 ±0.02	0.6	0.56 ±0.004	0.55 ±0.01	0.08	0.54 ±0.01	0.55 ±0.02	0.9	0.54 ±0.02	-	0.57 ±0.01	0.54
PL	-	1.82 ±0.02	1.80 ±0.02	1.80 ±0.02	0.7	1.81 ±0.01	1.81 ±0.01	0.2	1.81 ±0.01	1.81 ±0.01	0.5	1.82 ±0.01	-	1.84 ±0.01	1.83
gamma (γ)	-	1.41 ±0.02	1.40 ±0.02	1.41 ±0.02	0.7	1.41 ±0.01	1.41 ±0.01	0.9	1.40 ±0.02	1.38 ±0.02	**0.018**	1.40 ±0.01	-	1.45 ±0.02	1.44
lambda (λ)	-	1.04 ±0.002	1.04 ±0.002	1.04 ±0.003	0.5	1.04 ±0.003	1.04 ±0.001	0.5	1.03 ±0.002	1.03 ±0.003	0.8	1.03 ±0.003	-	1.05 ±0.005	1.04
s-w coeff.	-	1.36 ±0.01	1.35 ±0.02	1.36 ±0.02	0.8	1.36 ±0.01	1.36 ±0.01	0.9	1.35 ±0.02	1.34 ±0.01	**0.02**	1.35 ±0.01	-	1.38 ±0.02	1.38

[a] Group differences were assessed with linear regression models adjusting for age, sex and cortical grey matter volume. If graph-defining properties (i.e. size, connectivity density and degree) were significantly different between groups they were included as predictors in the analysis

Note. Data are means ± standard deviations. 2 patients and 2 HCs were discarded during the quality assurance of the scans. **Abbreviations.** P: p-value; CD: connectivity density; BC: betweenness centrality; EC: eigenvector centrality; CL: clustering coefficient; PL: path length; S-w Coeff.: small-world coefficient.

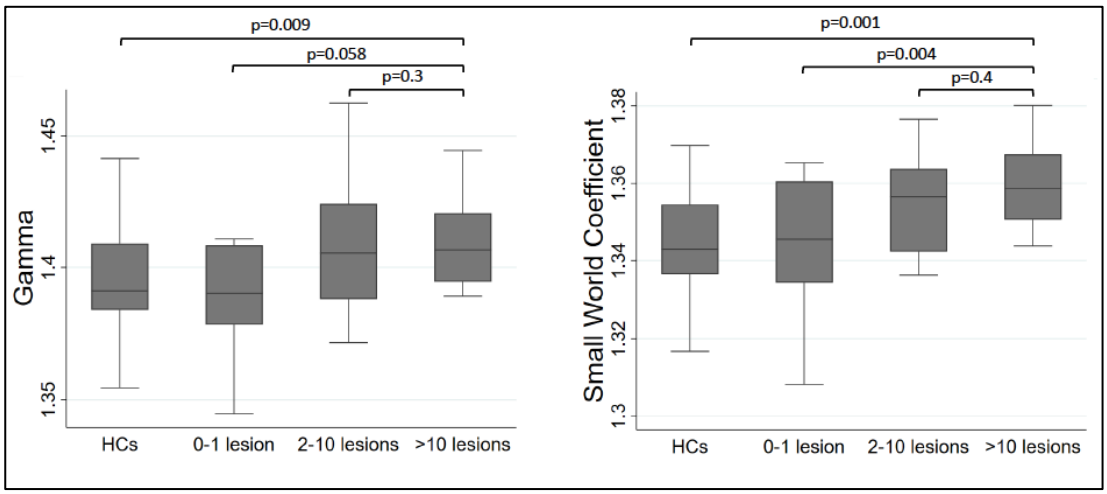

Figure 8.3 Differences in gamma and small-world coefficient between healthy controls and clinically isolated syndrome patients.

Boxplots of the values of gamma and small-world coefficient over healthy controls and clinically isolate syndrome patients divided in three categories according to the number of white matter lesions. P values from regression analysis adjusted for age, gender and center. Abbreviations: HCs: healthy controls.

Amongst the 47 patients with SDMT scores available, a higher small-world coefficient was associated (R^2=0.21,F(3,43)=3.86, p<0.05) with a lower SDMT score (i.e. slower information processing speed) (= -0.39, p=0.008) after adjusting for age (= -0.81, p=0.42) and gender (= 0.85, p=0.4) (Figure 8.4). There were too few multiple sclerosis patients (n=9) in my cohort to allow comparisons with healthy controls and other CIS patients not diagnosed with multiple sclerosis.

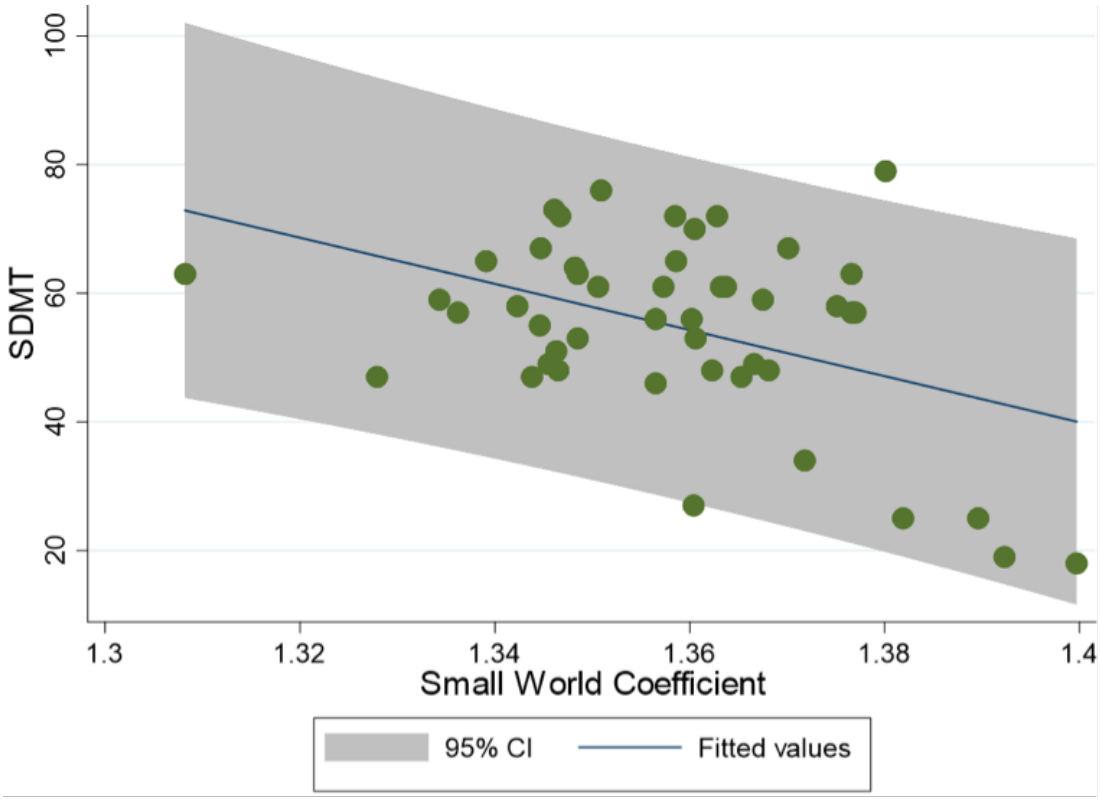

Figure 8.4 Scatterplot of Symbol Digit Modality Test on the small-world coefficient in clinically isolated syndrome patients.

Abbreviations: SDMT: Symbol Digit Modality Test.

8.3.3 Local graph metrics

I investigated whether differences between CIS patients and healthy controls were specific to cortical areas. Patients and controls showed similar volumes in the 98 CGM areas and there were no significant differences in degree. Several cortical areas showed significant differences for betweenness centrality, clustering coefficient and path length ($p<0.05$), but only three survived correction for multiple testing (Table 8.6).

Table 8.6 Significant differences in structural cortical networks local graph metrics.

Cortical Area	Metric	CIS Patients	HCs	p-value*
		L Hemisphere		
L middle frontal gyrus	BC	0.46±0.2	0.58±0.3	0.01
L posterior orbital gyrus	BC	0.45±0.2	0.53±0.2	0.02
L inferior temporal	BC	0.53±0.2	0.61±0.2	0.04
L parahippoca	CL	0.52±0.2	0.53±0.2	0.02
L superior frontal gyrus	CL	0.51±0.2	0.52±0.2	0.02
L pre-central gyrus	EC	0.48±0.3	0.52±0.2	0.003
L pre-central gyrus	PL	1.79±0.2	1.81±0.2	0.02
L middle frontal gyrus	PL	1.83±0.02	1.83±0.02	0.03
L parietal operculum	PL	1.84±0.03	1.83±0.03	0.04
L superior frontal gyrus	PL	1.80±0.02	1.80±0.02	0.02
		R Hemisphere		
R cuneus	BC	0.39±0.2	0.49±0.2	0.01
R entorhinal area	BC	0.33±0.2	0.42±0.2	0.02
R superior frontal gyrus	BC	0.30±0.2	0.33±0.2	<0.0001[a]
R middle cingulate	BC	0.27±0.2	0.35±0.2	0.02
R medial frontal cortex	BC	0.37±0.2	0.46±0.2	0.04
R posterior cingulate	BC	0.35±0.2	0.49±0.3	0.01
R supplementar	BC	0.32±0.2	0.42±0.2	0.04
R entorhinal area	CL	0.53±0.02	0.54±0.02	0.007
R cuneus	CL	0.48±0.03	0.48±0.03	0.03
R inferior occipital	CL	0.51±0.02	0.52±0.02	0.03

R gyrus rectus	CL	0.51±0.03	0.52±0.04	0.02
R posterior cingulate	CL	0.51±0.03	0.51±0.03	0.02
R post-central gyrus	CL	0.51±0.04	0.53±0.03	<0.0001[a]
R supplementar	CL	0.52±0.03	0.53±0.03	0.03
R precuneus	CL	0.49±0.03	0.50±0.02	0.04
R supplementar	EC	0.39±0.2	0.47±0.2	0.02
R post-central gyrus	EC	0.39±0.2	0.48±0.2	0.02
R superior frontal gyrus	EC	0.25±0.2	0.41±0.2	0.04
R entorhinal area	EC	0.48±0.2	0.55±0.2	0.02
R cuneus	PL	1.88±0.02	1.87±0.03	0.008
R entorhinal area	PL	1.80±0.03	1.79±0.03	0.002
R inferior occipital	PL	1.82±0.02	1.81±0.03	0.02
R anterior cingulate	PL	1.81±0.05	1.79±0.05	0.02
R medial orbital gyrus	PL	1.80±0.03	1.79±0.03	0.007
R post-central gyrus	PL	1.82±0.04	1.80±0.04	0.02
R gyrus rectus	PL	1.81±0.05	1.78±0.04	0.01
R superior frontal gyrus	PL	1.81±0.05	1.79±0.05	0.01
R precuneus	PL	1.86±0.03	1.84±0.03	0.006
R supplementar	PL	1.79±0.05	1.77±0.05	0.004
R posterior cingulate	PL	1.83±0.03	1.82±0.04	0.04

[a] Significant P values after the correction for multiple comparisons using a False Discovery Rate (FDR) of 5% for multiple hypothesis testing.

Note**.** Group differences in local graph parameters were assessed with linear regression, correcting for age, gender and local CGM volume.

Data are means ± standard deviations. Abbreviations**:** L: left; R: right; seg.: segment; BC: betweenness centrality; CL: clustering coefficient; EC: eigenvector centrality; PL: path length.

Patients showed lower betweenness centrality in the right superior frontal gyrus (0.300.01 vs 0.330.01, p<0.0001; p_{FDR}<0.05) and lower clustering coefficient in the right postcentral gyrus (0.510.04 vs 0.540.03, p<0.0001; p_{FDR}<0.05) in comparison to healthy controls (Figure 8.5). Among patients, these alterations were not correlated with clinical parameters or white matter lesion volume.

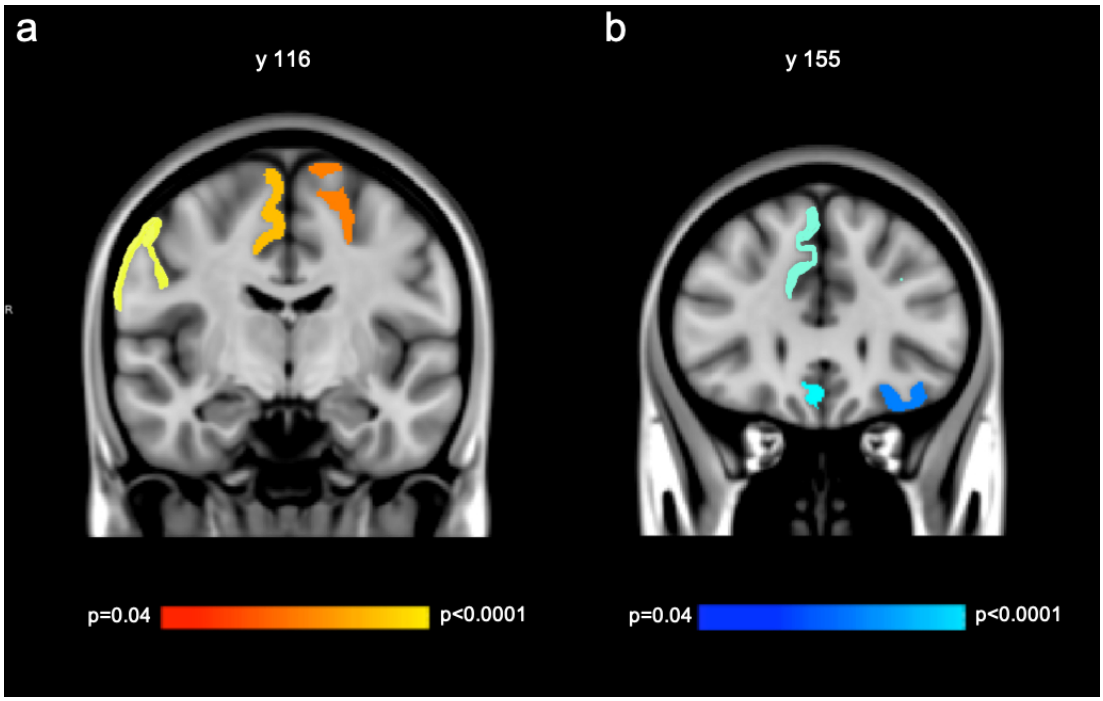

Figure 8.5 Local structural cortical network differences in clinically isolated syndrome patients.

Local network differences in clinically isolated syndrome (CIS) patients are shown in selected slices in the Montreal Neurological Institute (MNI) space. (a) cortical areas with lower clustering coefficient in CIS patients compared to controls with a yellow to red colour scale according to the statistical significance; (b) cortical areas with lower betweenness centrality in CIS patients compared to controls with a light-blue to blue colour scale according to the statistical significance.

Finally, patients with >10 white matter lesions had lower betweenness centrality in the right postcentral gyrus (0.290.01 0.330.01, p_{FDR}<0.05) and lower clustering coefficient in the right medial orbital gyrus (0.510.04 vs 0.530.03, p_{FDR}<0.05), compared with healthy controls.

There was significant (p_{FDR}<0.05) variability across centers in the following local graph properties: characteristic path length in the bilateral anterior insula,

left inferior and middle temporal gyrus, left parahippocampal gyrus; clustering coefficient in the right inferior and middle occipital gyrus; betweenness centrality in the left posterior cingulate cortex and eigenvector centrality in the right middle occipital gyrus.

8.4 Discussion

In this study, using single-subject SCN analysis, I showed that in patients at the onset of a demyelinating episode, graph alterations are related to disease burden. At the global level, patients possess altered small-world topology characterised by a shift towards a more regular network. These findings are in line with previous studies on SCNs in CIS patients (Muthuraman *et al.*, 2016). A regular network tends to possess dense local connections (i.e. high clustering) between nodes at the expense of the long-distance ones (i.e. low path length), thus compromising the efficient balance between short and long-range information transfer, distinctive of small-world networks (Watts and Strogatz, 1998).

When comparing the whole patient cohort with healthy controls, the difference in small-world coefficient was significant, although small. This small difference could be because patients were at the very onset of the disease, some of them with little white matter damage. When patients were stratified according to the number of white matter lesions, this difference in the small-world coefficient increased: subjects with higher lesion load at onset showed higher small-world coefficient values compared not only with healthy controls, but also with the group of patients with 0-1 lesion.

This altered topology was correlated with a high lesion load. Moreover, I did not find any significant differences in cortical volumes between groups: in patients the tendency to lose long-distance connections could be a consequence of altered connectivity due to lesional disruption of white matter tracts more than to alterations in cortical areas (Figure 8.6).

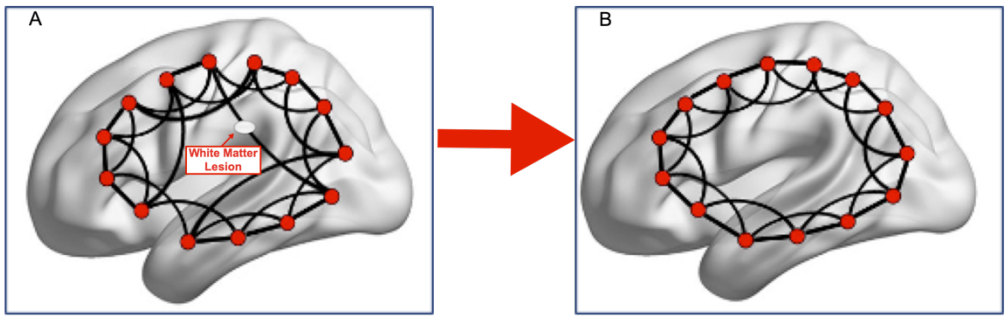

Figure 8.6 (A) White matter lesions disrupt the long-distance connections in the small-world network resulting in a regular network (B)

The increase in the small-world coefficient, in this study, was associated with worse cognitive performance. Noteworthy, the analysis of single-subject SCNs in established multiple sclerosis (Rimkus *et al.*, 2018), similar to studies conducted with the same methodology in dementia (Tijms *et al.*, 2013), showed that cognitively impaired patients tend to possess random SCN topology. However, unlike individuals in my cohort, those patients already had evidence of definite gray matter atrophy. This suggests that small-world topology alterations of the SCNs may have different characteristics at different stages of the disease, being more regular in the early phases and more random when neurodegeneration starts to occur.

At local level, patients had altered network properties in several cortical region, including low clustering coefficient in areas relevant to cognition. These alterations do not seem to affect the global SCNs properties and the clinical phenotype. However, studies with further cognitive assessments and longitudinal follow-up could investigate the clinical relevance of these findings.

In this study, SCNs differed in size between CIS patients and healthy controls, although the two groups did not show any difference in CGM volume. It is possible that the smaller size of patients' SCNs could result from the different MRI pre-processing, particularly the white matter lesion segmentation in patients, or from the presence of intra-cortical lesions. Most studies use methods that constrain networks into identical sizes (i.e. parcellated cortical areas), whereas, here, I chose to extract SCNs from native space

segmentations, thus preserving the inter-individual variability. Therefore, the network size may also depend on the head size as well as on the 3D-T1 characteristics (i.e., the position in the scanner, the different contrast at the grey matter-CSF interface).

It is still not clear how to compare graphs with different sizes and/or connectivity densities (van Wijk *et al.*, 2010). Here, I adjusted for SCN size in my statistical models, but after this, I could not detect any differences in non-normalised global graph-parameters between patients and healthy controls.

One final consideration is the multi-center setting of this study giving rise to inter-center variability. Inter-scanner variations had significant effects on the global graph parameters. This may have been due to differences in white matter-grey matter interface contrast across different scanners that influenced the CGM segmentation outcomes. These findings suggest that it is important to account for inter-center variability for single-subject SCN extraction from multi-center neuroimaging datasets. The advantage of multi-center settings though is the putative increase in statistical power and, although variance heterogeneity across centers may be a potential problem for this analysis, the relative robustness of the small-world result suggests this may not in my case be a major limitation.

8.5 Conclusions

In this study, I applied, for the first time, a recently developed method to extract single-subject SCNs in CIS. Using clinical scans, I was able to demonstrate altered small-world topology in CIS patients SCNs that was associated with cognitive processing.

Chapter 9 Visual function and Brlef Cognitive Assessment for Multiple Sclerosis (BICAMS) in optic neuritis clinically isolated syndrome patients

9.1 Introduction

As seen in Paragraph 2.1.1.1, ON is a frequent presentation of demyelinating CIS (Jenkins and Toosy, 2017). Research studies often include cognitive outcomes when investigating disability accrual and risk for multiple sclerosis conversion in CIS cohorts. Whilst most studies have found cognitive deficits in information processing speed and visuospatial memory (Reuter *et al.*, 2011; Uher *et al.*, 2014; Ruano *et al.*, 2017), the prevalence of cognitive impairment in CIS patients, as we have seen, varies from one study to another (Brochet and Ruet, 2019). One possible explanation is that researchers do not always assess vision and damage in the visual pathways when testing cognition in CIS patients with ON. In this study, I hypothesise these factors can influence vision-dependent cognitive tests in ON-CIS patients.

MS researchers have shown relationships between visual function and cognitive performance, for tests depending both on visual (Bruce *et al.*, 2007; Davis *et al.*, 2009; Feaster and Bruce, 2011; Wieder *et al.*, 2013; Nguyen *et al.*, 2018) and non-visual inputs (Feaster and Bruce, 2011; Wieder *et al.*, 2013; Nguyen *et al.*, 2018). However, none of these studies took past ON history into account. Furthermore, they assessed patients with long disease duration and different multiple sclerosis phenotypes (i.e., relapsing-remitting and progressive) (Wieder *et al.*, 2013; Nguyen *et al.*, 2018). Therefore, they may have observed the effects of the CNS damage accrual on both vision and cognitive functions.

Markers of retinal damage derived from OCT, such as RNFL and GCIPL, have inconsistent associations with cognitive outcomes (Toledo *et al.*, 2008; Anhoque *et al.*, 2013; Wieder *et al.*, 2013; Coric *et al.*, 2018; Nguyen *et al.*,

2018; Bsteh *et al.*, 2019). Some studies included patients with previous ON (Anhoque *et al.*, 2013; Wieder *et al.*, 2013; Nguyen *et al.*, 2018) hence, their findings may have been affected by pre-existing retinal layer changes. Other studies excluded eyes with previous ON (Toledo *et al.*, 2008; Bsteh *et al.*, 2019) but, by including patients with long disease duration, other factors, such as brain atrophy or white matter lesion accrual, may have influenced their results. A recent study grouped the patients according to ON history and reported an association between GCIPL thinning and cognitive impairment evident only in the group without a history of ON (Coric *et al.*, 2018).

Many patients recruited for this study presented with ON. Therefore, in this study, I included only those patients with unilateral ON and analysed affected and non-affected eyes separately. I assessed patients at baseline (I.e., within three months from onset) and also at six months. By this time, it has been shown in the literature that most of the visual recovery has occurred (Beck *et al.*, 1994), and the ON-related retinal thinning is already evident (Balk *et al.*, 2016; Sanchez-Dalmau *et al.*, 2018). I used the MRI data to evaluate the possible contribution of damage to the posterior visual pathways, the non-affected eye and the CNS. For the cognitive assessment, I used the BICAMS because it includes both visually and non-visually dependent tests.

9.2 Materials and Methods

9.2.1 Participants

In this study, I included 42 patients with ON recruited consecutively from the National Hospital of Neurology & Neurosurgery and the Moorfields Eye Hospital, London, United Kingdom. They fulfil the criteria indicated in Paragraph 5.1 . Additionally, patients with high refractive errors (> -6.0 or +6.0 dpt.) were excluded from this project. I also included 13 healthy controls.

9.2.2 Clinical assessments

The clinical assessments (patients only) included EDSS, BICAMS, HCLA, LCLA and colour vision with the methodology detailed in Paragraphs 5.4-5.6 For the Farnsworth-Munsell test, I used the total error score (TES) for

statistical analysis. In all tests, participants used their habitual distance corrective lenses. Assessments were performed at baseline and six months.

9.2.3 Image acquisition and post-processing

OCT and MRI were both performed at baseline and after six months.

For the OCT, as discussed in Paragraph 5.3, I used the spectral-domain OCT (Spectralis v.1.7.1.0, Heidelberg Engineering, Heidelberg, Germany) to acquire the peripapillary circular scans and the macular volume scans with the methodology described in the paragraph. The baseline peripapillary and macular scans were used as a reference for the follow-up scans.

After obtaining the individual macular layers with the automated segmentation software, I performed a quality control of the scans according to the OSCAR-IB criteria (Tewarie *et al.*, 2012) and the scans that failed the quality control were excluded. In the case of minor failures of the automated segmentation, whenever possible, they were manually corrected.

The OCT metrics used for this study were the RNFL thickness, the GCIPL, and the INL. In the ON cohort, for each patient, I used the OCT measurements from affected and non-affected eyes, while, for healthy controls, I computed the binocular average of these measurements.

The MRI scans were performed at 3T Philips Achieva system and, at both time points, included: 3D T1-weighted turbo field echo, 3D fluid-attenuated inversion recovery, 2D PD/T2-weighted turbo spin-echo of the brain; and sagittal PD/T2-weighted images of the spinal cord; pre- and post-gadolinium T1-weighted images of the brain and spinal cord (baseline only) (for parameters see Paragraph 5.2.1). Additionally, at baseline, I used also a 2D STIR coronal sequences of the orbits to exclude other conditions mimicking demyelinating ON (26 slices; slice thickness: 2 mm; field of view: 220 mm x 220 mm; echo time: 75 ms; repetition time: 4643 ms).

White matter lesion numbers and location were recorded for each time point and, subsequently, dissemination in space and time were determined according to the revised 2017 McDonald criteria (Thompson *et al.*, 2018).

For the white matter lesion segmentation, I used the same approach of Chapter 6 and 7 (see Paragraph 5.2.2.1). Lesion volumes were then computed for T2-hyperintense and T1-hypointense white matter lesions.

For brain tissue segmentation, as in previous chapters, I used the non-local patch-match lesion filling technique (Prados *et al.*, 2014) and GIF (Cardoso *et al.*, 2015), described in Paragraph 5.2.2.1. Additionally, in this project, after registering the 3D-T1 images in the Montreal Neurological Institute (MNI152) space, I used the Juelich Histological Atlas (https://fsl.fmrib.ox.ac.uk/fsl/fslwiki/Atlases/Juelich) to create binary optic radiation masks. I then obtained the volume of the white matter lesions in the optic radiations.

MRI volumetric analyses were performed only for baseline scans assuming that (i) CIS patients do not usually show significant changes of brain volumes at six months; (ii) after CIS onset lesions can lose volume recovering from inflammation and oedema, thus the number of lesions at six months can be more informative than the lesion load.

9.2.4 Statistical analysis

Group differences between ON-CIS patients and healthy controls for demographic characteristics were assessed using the two-sample t-test for continuous variables and the chi-square test for categorical variables.

Three statistical analyses were conducted.

1) At baseline, I used mixed effect models to assess the differences at baseline in OCT metrics between affected eyes and non-affected eyes in patients as well as between non-affected eyes and HCs' eyes. The models were adjusted for age, sex, months from onset and administration of steroid treatment (affected eye only). For patients, I used the same model for the differences in visual outcomes between the two eyes.

2) Longitudinally, I applied a similar mixed effect model, adjusted for the same covariates, to assess changes over time in OCT metrics, visual and cognitive outcomes. However, I also added time and Group x Time interaction as explanatory variables (group was defined either as affected eyes vs. non-affected eyes or non-affected eyes vs. HCs). For BICAMS, I used raw scores, as they attain the same significance level of z-scores (Parmenter *et al.*, 2010), adjusting for age, sex and education. Z-scores were used for descriptive purposes.

If a variable *x* was showing a significant change over time, I calculated the difference between six months and baseline (labelled as *x*).

3) I applied multiple linear regression models, adjusted for age, sex and months from onset, to examine associations between OCT metrics and MRI parameters (brain and WM lesion volumes) with baseline and cognitive and visual scores, each test entered as a response variable separately.

Statistical analyses were performed with Stata v.14.1 (Stata Corporation, College Station, Texas, USA).

Only results associated with $p<0.05$ were considered statistically significant and subsequently reported in this paper. Due to the exploratory nature of the study, correction for multiple comparisons was not performed.

9.3 Results

Thirty patients and 13 HCs completed the study at six months. Patients and HCs did not differ significantly for age, sex and brain volumes (Table 9.1).

Table 9.1 Demographic characteristics and brain volumes of patients and healthy controls at baseline

	Patients	HCs	p-value
N	42	13	-
Age years, mean (SD)	33(7)	33(6)	0.78[a]
Sex, N female (%)	25(59.5)	7(53.9)	0.88[b]
Months from onset, mean	2 (1.2)	-	-
Grey matter vol. ml, mean (SD)	662.5(47.4)	675.9(67)	0.53[c]
White matter vol. ml, mean	449.8(38.2)	466.5(49.6)	0.12[c]
Brain Parenchymal	0.760.009)	0.76(0.01)	0.64[c]

Abbreviations: HCs: healthy controls; SD: standard deviation; Gm: grey matter; vol.: volume; Wm: white matter; ORs: optic radiations
[a] two-sample t-test
[b] chi-square test
[c] linear regression adjusting for age and sex

Thirty-six (86%) out of forty-two baseline CIS patients presented with brain lesions and thirty of them had lesions involving the optic radiations (Table 9.2).

Following quality control of OCT acquisitions, I discarded the following patients' OCT data: 9/84 (11%) baseline and 4/60 (7%) 6-month RNFL; 8/84 (10%) baseline and 3/60 (6%) 6-month macular scans. HCs' OCT scans passed the QC.

At baseline, while all patients performed in the normative average for CVLTII, 10 (24%) patients and 4 (9.5%) showed deficits (<1.5 z-score) for SDMT and BVMT-R, respectively. Two (5%) patients had <1.5 z-score in both tests matching the definition for cognitive impairment. Over time, only BVMT-R and CVLTII scores improved significantly (Table 9.3).

Table 9.2 Clinical and MRI characteristics of patients at baseline and six months

	BASELINE	6 MONTHS	p-value
N	42	35	-
Months from onset, mean	2 (1.2)	-	-
MS, N (%)	9(21)	11(31)	-
T1-hypointense lesion vol. ml,	0.6(1.1)	-	-
T1-isointense lesion vol. ml,	21.4(99.8)	-	-
Optic radiations lesion vol. ml,	0.4(0.6)		
Total lesion number, median	16(59)	13(62)	0.058 [a]
EDSS, median (IQR)	1.5 (0.5)	1(1.5)	-
Steroids, N (%)	15(36)	0(0)	-
DMDs, N (%)	0(0)	7(30)	-

NOTE: Multiple Sclerosis diagnosed according to McDonald Criteria 2017 revision
Abbreviations: IQR: inter-quartile range; MS: multiple sclerosis; EDSS: Expanded Disability Status Scale; DMDs: disease modifying drugs
[a] paired-sample t-test

Table 9.3 BICAMS scores in patients

	BASELINE		6 MONTHS		P value
	Raw score	Z-score	Raw score	Z-score	
SDMT mean (SD)	57.9(9.3)	-0.86(1.1)	59.7(8.5)	-0.55(0.6)	0.32[a]
BVMT-R mean (SD)	25.6(5.4)	-0.39(1)	28.4(3.1)	0.17(1)	0.001[a]
CVLTII mean (SD)	60.6(9)	1.2(1.2)	67(6)	2.08(1)	0.01[a]

NOTE: Z-scores (age-, sex- and education-adjusted) were calculated using the dataset provided by the BICAMS initiative (https://www.bicams.net).
Abbreviations: SDMT: Symbol Digit Modalities Test; BVMT-R: Brief Visuospatial Memory Test-Revised; CVLTII: California Verbal Learning Test II; SD: standard deviation
[a] mixed effect model adjusted for age, sex and education.

At baseline, affected eyes had significant deficits for HCLA (=0.12, p<0.0001), 2.5% and 1.25% LCLA (=-15.3 and =-10.2, respectively; p<0.0001) and colour vision TES (=100, p<0.0001) compared with non-affected eyes. Over time, all the visual scores in the affected eyes improved (Table 9.4; Figure 9.1).

Table 9.4 Visual Outcomes in Patients

Metrics		Affected Eye	Non-affected Eye	Coef. (95% CI)	p-value[a]
HCLA	BL LogMar, mean (SD)	0.1(0.2)	-0.02(0.1)	0.12(0.06 to 0.18)	<0.0001
	6M LogMar, mean (SD)	0.04(0.2)	-.06(0.1)	0.06(-.007 to 0.14)	0.08
	Coeff.(95%CI)	4.5 (0.6 to 8.4)	0.8(-3.04 to 4.7)	-	-
	p-value[b]	0.023	0.68	-	-
LCLA 2.5%	BL, mean (SD)	11(12)	26(11)	-15.3 (-19.6 to -10.9)	<0.0001
	6M, mean (SD)	17(12)	28.6(7.9)	-9.4(-14.6 to -4.3)	<0.0001
	Coeff.(95%CI)				
	p-value[b]				
LCLA 1.25%	BL, mean (SD)	4(7)	14(11)	-10.1(-13.6 to -6.7)	<0.0001
	6M, mean (SD)	8(8)	15(8.5)	-6.5 (-10.6 to -2.3)	0.002
	Coeff.(95%CI)	8.2(3.3 to 13)	2.3(-2.5 to 7.2)	-	-
	p-value[b]	0.001	0.34	-	-
TES	BL, mean (SD)	209.4(176)	109.4(56.6)	3.4(2.2 to 4.6)	<0.0001
	6M, mean (SD)	129(178.5)	108.3 (56.7)	1.02(-.43 to 2.5)	0.43
	Coeff.(95%CI)	-2.4(-3.7 to -1)	0.04(-1.3 to 1.4)	-	-
	p-value[b]	0.001	0.95	-	-

Abbreviations: CI: confidence interval; SD: standard deviation; HCLA: high-contrast letter acuity; LCLA: low-contrast letter acuity; TES: total error score.
[a] mixed effect model adjusted for age, sex, months from onset and steroids comparing affected eyes and non-affected eyes.
[b] mixed effect model adjusted for age, sex and months from onset and steroids comparing baseline with 6-month values

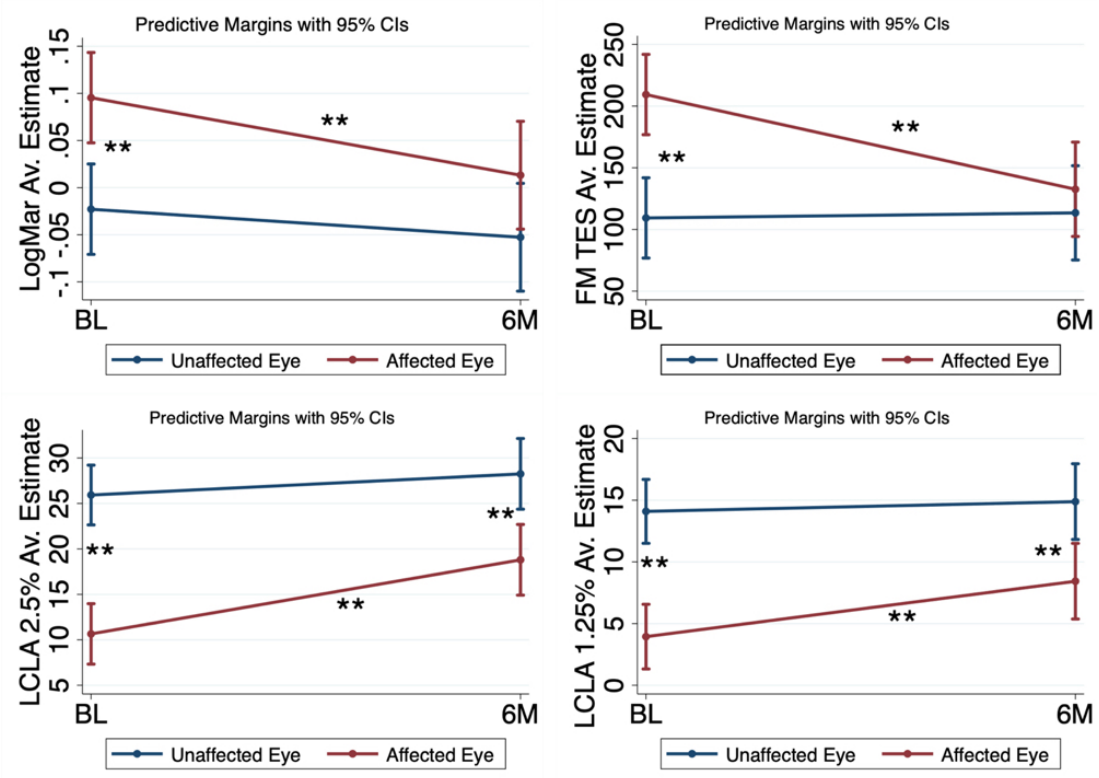

Figure 9.1 Visual Outcomes

**p<0.0001
Results from mixed effect models adjusted for age, sex, steroids intake and months from onset. For changes overtime, an interaction GroupxTime was used.
Abbreviations: Av: Average; BL: baseline; 6M: six months; FM: Farnsworth-Munsell test; TES: total error score; LCLA: low-contrast letter acuity

At baseline, the affected eye GCIPL was significantly lower than the non-affected eye GCIPL (=-11.5, p<0.0001), which was lower than in HCs (=-8, p=0.002) (Figure 9.2). Over time, the RNFL decreased significantly in the affected eyes while the GCIPL did not change significantly (Table 9.5; Figure 9.3).

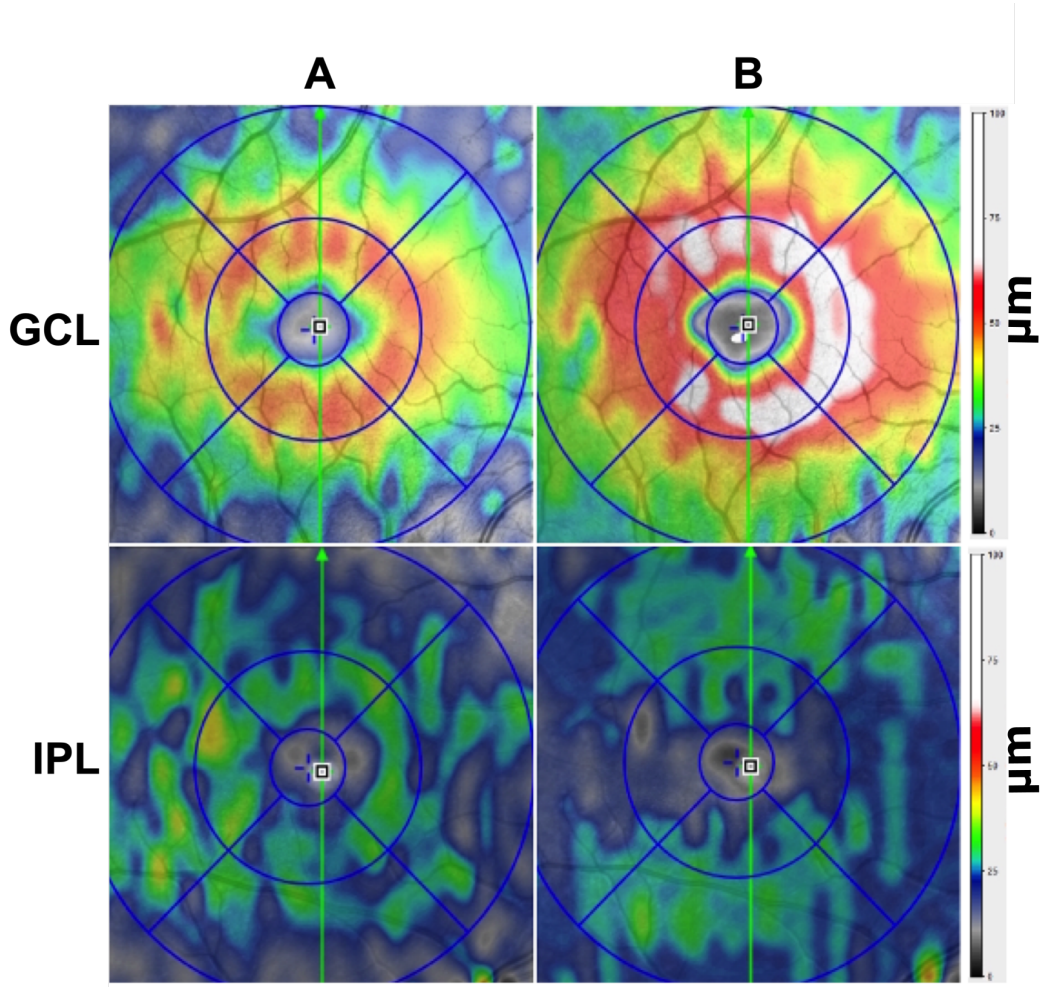

Figure 9.2 Examples of ganglion cell layer (GCL) and inner plexiform layer (IPL) thickness maps at baseline in a healthy control (A) and an optic neuritis patient's affected eye (B)

Table 9.5 Optical Coherence Tomography Metrics in patients and healthy controls

Metrics		Affected Eye	Non-affected Eye	Coef. (95% CI)	p-value[a]	HCs (average)	Coef. (95% CI)	p-value[b]
RNFL	BL μm, mean (SD)	95.4 (30.5)	95.4 (12.7)	0.32 (-7.3 to 7.9)	0.93	101.7 (9.9)	-5.6 (-12.7- 1.5)	0.12
	6M μm, mean (SD)	81.2 (13.8)	99.4 (11.4)	-14.7 (-23.6 to -5.9)	0.001	101.6 (10.1)	-5.2 (-12.6 to 2.07)	0.16
	Coeff. (95%CI) BL vs. 6M	-13.05 (-21.5 to -4.6)	2(-6.4 to 10.3)	-	-	1.2(-1.9 to 4.2)	-	-
	p-value[c]	0.02	0.65	-	-	0.46	-	-
GCIPL	BL μm, mean (SD)	76.8 (10.2)	88.4 (8.6)	-11.5 (-14.8 to -8.2)	<0.0001	96.4 (7)	-8 (-12.9 to -3.05)	0.002
	6M μm, mean (SD)	75.3 (12.5)	90.7 (8.9)	-11.8 (-15.6 to -7.9)	<0.0001	95.7(9.4)	-7.5(-12.6 to -2.5)	0.004
	Coeff. (95%CI) BL vs. 6M	-0.67 (-4.4 to 3)	-0.44 (-4.1 to 3.2)	-	-	-1.4 (-3.1 to 0.4)	-	-
	p-value[c]	0.72	0.81	-	-	0.13	-	-
INL	BL μm, mean (SD)	39.4 (3.3)	39.5 (3.6)	.003 (-0.8 to 0.8)	0.98	39 (3)	0.61 (-0.8 to 1.9)	0.63
	6M μm, mean (SD)	39.7 (4)	39 (3.6)	0.9 (-.08 to 1.8)	0.07	39.7 (3.7)	-0.36 (-1.5 to 0.8)	0.7

	Affected Eye	Non-affected Eye	Coef. (95% CI)	p-value[a]	HCs (average)	Coef. (95% CI)	p-value[b]
Coeff. (95%CI) BL vs. 6M	0.4(-0.6 to 1.3)	-0.5 (-1.4 to 0.4)	-	-	0.6 (-0.8 to 2)	-	-
p-value[c]	0.45	0.29	-	-	0.38	-	-

Abbreviations: CI: confidence interval; HCs: healthy controls; SD: standard deviation; BL: baseline; RNFL: peripapillary retinal nerve fiber layer; GCIPL: combined ganglion cell and inner plexiform layers; INL: inner nuclear layer

[a] mixed effect model adjusted for age, sex, steroids months from onset and steroids comparing affected eyes and non-affected eyes.

[b] mixed effect model adjusted for age, sex and months from onset comparing patients' non-affected eyes with the average of healthy controls eyes

[c] mixed effect model adjusted for age, sex, steroids and months from onset comparing baseline with 6-month values

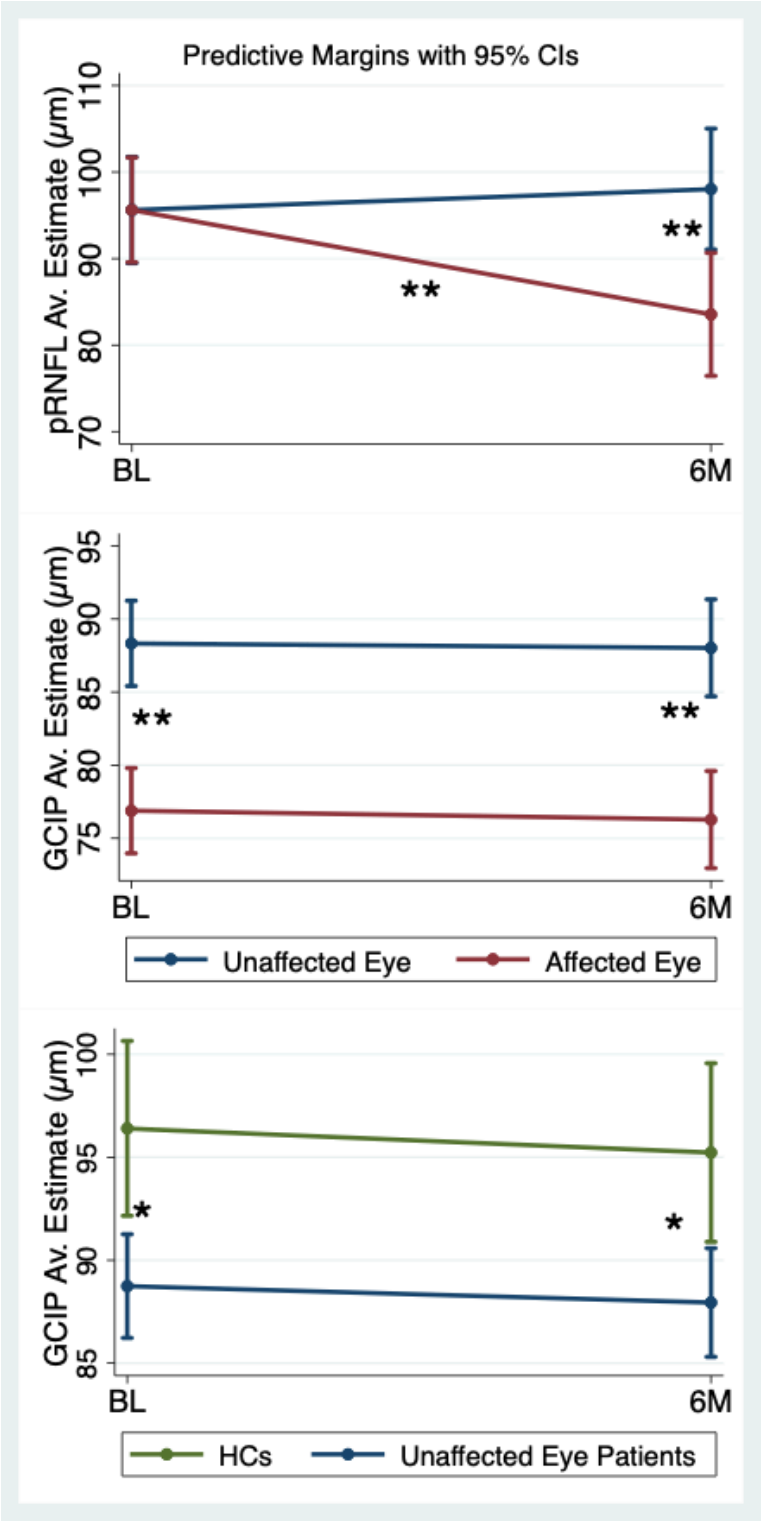

Figure 9.3 Optical Coherence Tomography Metrics

**p<0.0001 *p<0.05
Results from mixed effect models adjusted for age, sex, steroids intake and months from onset. For changes overtime, an interaction GroupxTime was used.
Abbreviations: Av: Average; BL: baseline; 6M: six months; pRNLF: peripapillary retinal nerve fiber layer; GCIPL: combined ganglion cell and inner plexiform layers: INL: inner nuclear layer

The LCLA 1.25% improvement was predicted by thicker baseline GCIPL in the affected eyes (B=0.33, CI95=0.07-0.58, p=0.015) (Figure 9.4).

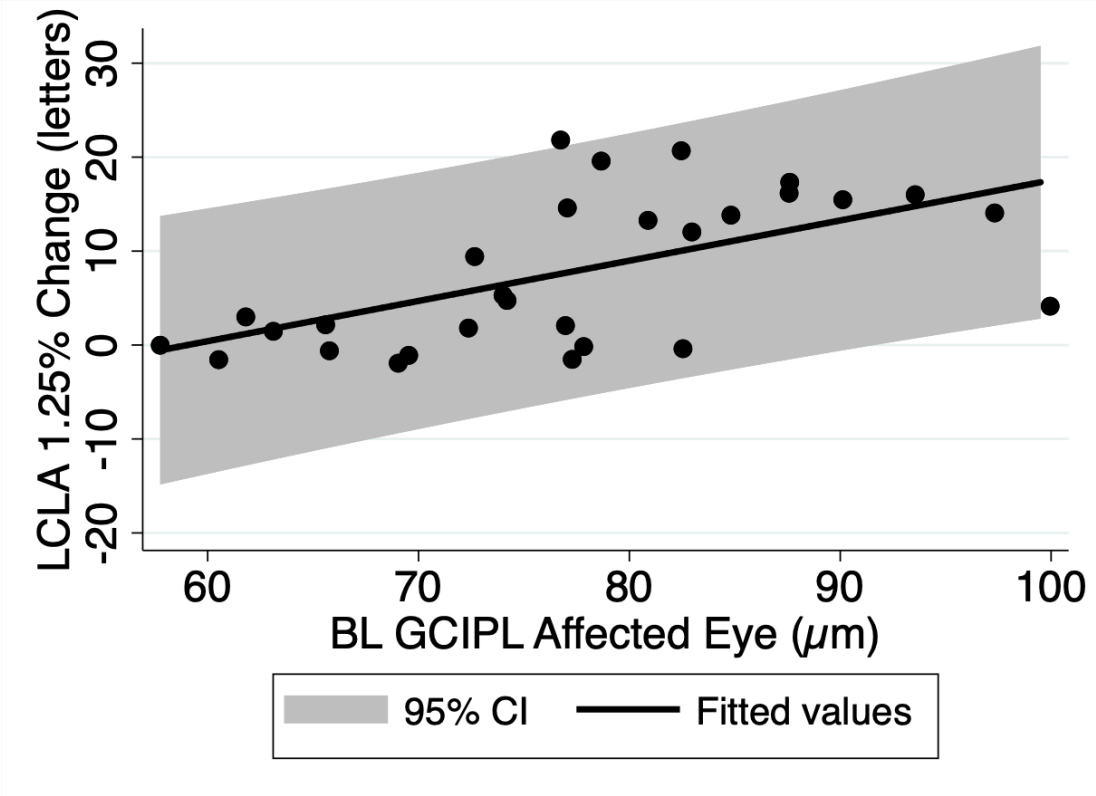

Figure 9.4 OCT Metrics and Visual Outcomes in Patients

ΔLCLA was predicted by the baseline GCIPL in the affected eyes (p=0.015). Results from linear regression adjusted for age, sex and months from onset.
Abbreviations: LCLA: low-contrast letter acuity; BL: baseline; GCIPL: combined ganglion cell and inner plexiform layers.

An improvement in affected eye HCLA between baseline and six months was significantly associated with an improvement in the BVMT-R score (R^2 = 0.17; B=-19.9; CI95=-38.3 to -1.5, p=0.03) (Figure 9.5).

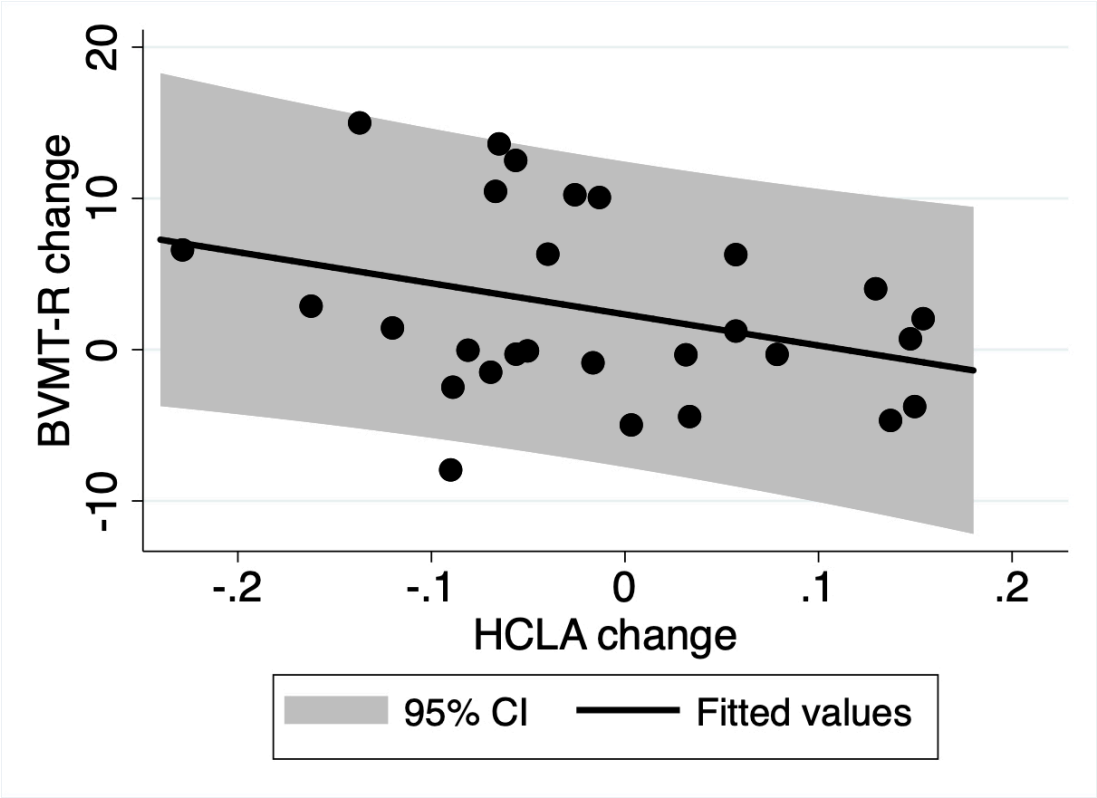

Figure 9.5 Visual Outcomes and Brief Visuospatial Memory Test-Revised

∆BVMT-R was associated with the ∆HCLA in the affected eyes (p=0.03). Results from linear regression adjusted for age, sex and months from onset.
Abbreviations: LCLA: low-contrast letter acuity; BVMT-R: Brief Visuospatial Memory Test-Revised (BVMT-R).

I did not find any correlations between OCT metrics, white matter and optic radiation lesion volumes, white matter lesion number and BICAMS scores at baseline or over time.

9.4 Discussion

Patients with clinically isolated, unilateral ON performed worse in BICAMS visually dependent tests (BVMT-R and SDMT) than in CVLTII (visually non-dependent).

Over time, both the CVLTII and the BVMT-R had an improvement possibly influenced by the training effect and the general recovery from the relapse. However, only the BVMT-R improvement was associated with the recovery of visual function (HCLA).

The correlation between BVMT-R improvement and affected eye HCLA recovery is very interesting as the non-affected eye remains visually non-compromised. This did not depend on the measures of structural damage of the posterior visual pathway or CNS. It is possible, however, that higher visual processing, tested in this study by BVMT-R, depends on binocular afferent stability and/or symmetry and when this is disrupted, there is impairment of visually dependent cognitive performance. As the affected eye improves, binocular visual symmetry is restored, and visual cognitive performance normalizes. The mechanisms for this are speculative but may include higher visual neuroplastic changes. Furthermore, bidirectional relationships between vision and cognition may occur and cognitive status may influence the performance in the visual tests (Wieder *et al.*, 2013). These findings suggest that visual acuity should be considered when BICAMS is administered to ON patients to help interpret BVMT-R scores. This can have implications in clinical trials, where often cognitive scores are used, and vision is not measured.

LCLA, although recovering significantly, remained impaired in patients' affected eyes, but I could not find correlations with SDMT or BVMT-R, in contrast to previous studies (Wieder *et al.*, 2013; Nguyen *et al.*, 2018). These studies, however, showed a correlation between LCLA and cognition, independently of ON history. As LCLA has been related to CNS damage (Balcer *et al.*, 2017), particularly global and regional brain atrophy (Frohman *et al.*, 2009), in multiple sclerosis patients with long disease duration, LCLA may be related to cognitive performance as a surrogate marker of neurodegeneration and not just of visual impairment. This would also explain similar results in neurodegenerative diseases (e.g., Rizzo *et al.*, 2000; Crucian and Okun, 2003). In this early cohort, instead, in the absence of brain atrophy, LCLA could reflect visual pathway damage more than CNS alterations, as shown by the correlation with GCIPL.

No associations were found between BICAMS scores and OCT metrics. The presence of demyelination, inflammation and neuro-axonal damage at baseline may have different and possibly opposing effects on OCT masking potential correlations with BICAMS. Longitudinal studies are required to assess if, with the disease progression, relationships arise.

Finally, SDMT did not improve over time. Deficits in information processing speed are known to characterise CIS cognitive impairment. SDMT did not correlate with visual function or damage to visual pathways. This suggests that other mechanisms, possibly related to brain function, drive SDMT performances, as previously described in Chapter 8. My previous results suggest that information processing speed may be altered when long-range connections are lost and cortical areas are disconnected. Multiple sclerosis is indeed recognised as a "disconnection syndrome" (Dineen *et al.*, 2009). However, there is not a definite evidence in literature on the relationship between brain connectivity disruptions and impaired information processing speed (Manca *et al.*, 2018). Therefore, further studies are needed.

In non-affected eyes, although GCIPL was thinner than in HCs, it did not correlate with BICAMS scores. At present, there is no gold-standard for detecting sub-clinical nerve involvement (Hoch *et al.*, 2017). However, as non-affected eyes' RNFL and orbit MRI was normal, I do not believe this was a sign of subclinical nerve involvement. GCIPL was not significantly related to brain volume either. It is possible that the thinner GCIPL of the non-affected eye may be represent a manifestation of early MS neurodegeneration that is not yet detectable in other brain compartments. This could be investigated with further longitudinal analyses on the same cohort.

9.4.1 Limitations

This study has several limitations. I could not assess at six months the whole cohort as few patients were lost to follow-up. However, using mixed effect models, I could adjust for the missing data.

I could not use a non-ON CIS cohort to assess the generalisability of my findings. However, ON is a frequent CIS onset and I believe that my results may be of interest for neurologist and researchers assessing cognition in CIS patients.

Finally, I did not use diffusion imaging to segment the optic radiations. However, as I aimed to the assess the lesion location, and not the white matter tract properties, this methodology should be adequate.

9.5 Conclusion

In conclusion, after ON, reduced performance in BVMT-R is observed and improves six months later. This improvement is associated with the recovery of HCLA in the affected eye independently of visual pathway and CNS damage suggesting that higher visual processing may be involved in the improvement of visuospatial memory. This study also suggests that vision should be assessed in ON patients to help interpret BVMT-R.

Chapter 10 Conclusions and future directions

10.1 Introduction

In this thesis, I have assessed patients at their first neurological episode suggestive of demyelination with four main goals: (i) the measurement with quantitative MRI of the microstructural damage in the central nervous system and its possible association with pathological processes involving sodium homeostasis; (ii) the assessment of the clinical relevance, in terms of physical and cognitive disability, of the possible findings; (iii) the valuation of the influence of pathophysiological changes in the cortical morphology on clinical outcomes; (iv) the determination of the relationship between the structural and functional damage in the visual pathway and the assessment of cognitive performances.

My work gives insights over existing information in the literature.

The preliminary study presented in Chapter 6 adds methodological elements to the existing literature. It demonstrates the feasibility of NODDI application in the brain and spinal cord at the same time. Besides, it suggests that it is important to include the spinal cord in advanced imaging studies: the spinal cord may show more clinically significant changes than the brain ones, even in the presence of similar findings in the two CNS compartments.

The other studies included in this thesis demonstrate microstructural, metabolic, and SCNs alterations at the early stage of the disease. Particularly, I found alterations in the normal-appearing brain tissues that are better characterized than in similar studies with DTI (Gallo *et al.*, 2005; Rovaris *et al.*, 2008; Cappellani *et al.*, 2014; Kolasa *et al.*, 2015), which could not distinguish between orientation dispersions and neuro-axonal loss, and MR spectroscopy (Ranjeva *et al.*, 2003), which could only study single areas. In addition, I showed early neuro-axonal damage to the corpus callosum not found in previous studies (see Paragraph 7.4.2)

SCNs, which were altered in more advanced multiple sclerosis populations, show alterations even in early cases and, therefore, can be used at this stage. Also, methodologically, this lays the foundations for SCNs analysis even in multi-centric contexts with appropriate adjustments.

Finally, in the field that explores relationships between vision and cognition, my study shows that there is a relationship between vision and specific cognitive domains in optic neuritis patients regardless of the structural damage in the brain and visual pathways. This finding implies that more complex alterations in cortical functions may be involved in this relationship, as discussed in the previous paragraph.

My thesis also gives insights to understanding cognitive changes in multiple sclerosis.

The cohort recruited for this thesis was characterised by low cognitive disability, as expected from patients at an early stage of the disease. Indeed, only a few patients performed below the threshold for cognitive deficits (≤-1.5 standard deviation). This relatively cognitive preservation can have contributed to the results in Chapter 7, where I could only find trends in associations between microstructural and metabolic alterations in brain tissues and cognitive performance while I found significant associations between these alterations and physical disability.

Interestingly, in the larger cohort analysed in Chapter 8, I found that SCNs alterations impacted information processing speed, a cognitive domain typically affected in multiple sclerosis (Brochet and Ruet, 2019). This result may suggest that more global changes, such as the ones in coordinated cortical morphology patterns, can have more significant effects on cognition than localised structural or metabolic alterations. Since this was not a comparative study, these are only speculations, and studies using both SCNs, microstructural and metabolic imaging are needed to verify this hypothesis.

On the other hand, the fact that vision also affects visuospatial memory in patients with optic neuritis suggests that visual acuity should be measured

when testing these patients with BICAMS and confirm that complex cortical processes are involved in determining cognitive performance.

The lack of correlations with structural abnormalities may be due to the absence of significant damage in the cohort assessed, such as brain atrophy. Nevertheless, I could not find correlations between NODDI metrics in the grey matter and cognition in the multiple sclerosis cohort assessed in Chapter 6 either. However, NODDI alterations have not been analysed in single cortical regions, but globally. Like previous studies (Granberg *et al.*, 2017), these patients had no alterations of NODDI in the gray matter, which could contribute to the lack of associations with cognitive parameters.

The major findings related to each of these aims are summarised here along with future directions.

10.2 Microstructural and metabolic alterations

As shown in Chapter 3, over the years, studies on autoptic cases and biopsy samples from multiple sclerosis patients have revolutionised the way we think about this disease pathology. From the notion that in multiple sclerosis damage was restricted to demyelinated plaques (Charcot, 1880), to the knowledge that the normal-appearing white matter outside the lesions is highly abnormal (Kutzelnigg *et al.*, 2005); from the concept that inflammation was just restricted to active lesions (Nesbit *et al.*, 1991), to the discovery that lymphocytes infiltration can be hindered behind the intact BBB (Vos *et al.*, 2005) and meningeal follicle-like structures constitute a reservoir of encephalitogenic cells (Magliozzi *et al.*, 2007).

These advances are mainly related to established multiple sclerosis patients, while little is known about very early patients. There is the suggestion that neuro-axonal loss can be present from the beginning (Barnett and Prineas, 2004), but the opportunity to collect a large cohort of early autopsy cases to confirm this hypothesis is unlikely. Therefore, advanced imaging studies can assume a crucial role not only by detecting CNS abnormalities at an early stage, but also by generating new hypothesis on the genesis of these abnormalities.

As such, this thesis adds important elements to the field. The choice of a multi-parametric MRI approach allowed me to investigate not only the presence of microstructural damage in the SCN in early cases but also associated pathogenetic processes. In particular, I employed ^{23}NA MRI that can detect alterations in sodium homeostasis (Paragraph 3.1.1.6) can be related to axonal dysfunction and eventually loss.

Hence, I was able to demonstrate that patients at their first episode of demyelination already possess microstructural abnormalities in the brain tissues not captured by conventional MRI. These changes seem to affect normal-appearing white matter diffusely and the grey matter focally. Some structures, such as the corpus callosum, appear to be particularly affected by these alterations. In the context of diffuse axonal dispersion (increased ODI) in the normal-appearing white matter, the corpus callosum additionally shared features with white matter lesions having signs of axonal dysfunction (increased TSC) and initial axonal loss (decreased NDI). This is relevant because this structure may be the focus of future clinical trials for neuroprotection. Single-centre clinical trials have indeed started to use both NODDI and ^{23}Na MRI for the test of neuroprotective drugs in progressive multiple sclerosis (https://clinicaltrials.gov/PROXIMUS). In the future, also trials on early patients may adopt these techniques.

Another subject of reflection is the comparison between the preliminary study I conducted with NODDI in established relapsing-remitting multiple sclerosis patients and the study in the early cohort. In the former, I found diffuse signs of the possible loss of large myelinated axons (decreased NDI), while in the latter neuro-axonal loss was only restricted to specific structures, such as the corpus callosum and some cortical areas. Since, additionally, brain volumes in the early cohort were normal, this may indicate that in early patients we have to look for focal alterations in the CNS more than for widespread changes. The longitudinal follow-up of this cohort, which is still ongoing, will clarify if the local alterations can result in manifest atrophy over time.

10.3 Clinical relevance of microstructural and metabolic alterations

During my PhD, I had the opportunity to work with a heterogeneous cohort of patients at their first demyelinating episode: some of them were diagnosed with multiple sclerosis at the first scan, some of them fulfilled only the criteria of dissemination in space or time, some had a high lesion volume, some had no lesions at all. Yet, despite their different characteristics, as a neurologist, the only clinical information I was able to provide to these patients was the diagnosis of CIS or multiple sclerosis, and, in case of CIS diagnosis, the risk of having a relapse in the following decades categorised as “high”, in the presence of white matter lesions, and “low”, in the absence of them.

One of the reasons is that, at present, the “snapshot” taken at onset is based on conventional MRI images whose metrics have poor specificity for pathological processes. As seen in Chapter 2 and Chapter 3, lesion parameters measured at baseline have only a modest correlation with clinical outcomes. Brain volumes may hold higher clinical significance than white matter lesion metrics, but they are usually normal at this early stage, as it was in my cohort.

In this thesis, I showed that alterations found in the corpus callosum and specific cortical areas had clinical relevance independently of white matter lesions and brain volumes. Thus, NODDI and ^{23}Na MRI may have higher specificity to CNS pathology than conventional MRI metrics. The longitudinal follow-up of this cohort will determine if these changes are also related to future disability accrual.

At the moment, the length of the protocol does not allow the use of NODDI and ^{23}Na MRI in routine clinical practice. However, changes in scanner hardware and acquisition protocols may lead to faster acquisition time, with the possibility of translating this technique from research centres to the clinical setting.

10.4 Structural cortical networks

My findings on SCNs suggest that they can be affected early in multiple sclerosis. Specifically, the efficient brain network topology, the small-world, seems altered possibly as a consequence of the disruption of long-range connections, a process that is likely to happen in multiple sclerosis where plaques can interrupt connections through white matter tracts. Interestingly, SCNs alterations were correlated with cognitive performance.

These results are important to help understand the pathophysiological mechanisms at the onset of the disease. They support the idea that it is not only primary structural damage, directly related to inflammation, demyelination and neuro-axonal loss, which I investigated in Chapter 7, influencing clinical outcomes, but also the functional and structural arrangements consequent to this damage, in this case, expressed by changes in patterns of cortical morphology.

There is extensive literature on network alterations in patients with multiple sclerosis, from early cases, such as the ones studied in this thesis, to advanced patients. Although we are still far from the application of these techniques in the clinical practice, yet metrics from functional MRI or DTI-tractography studies have started to be used as outcomes in clinical trials (McKee *et al.*, 2015). In the future, their results will help to understand the contribution of brain network disruptions in the disease evolution.

My contribution to this promising field is to have demonstrated, for the first time, the feasibility of single-subject SCNs investigation in a multi-centre setting and their potential in patients at the onset of demyelinating symptoms. As initiatives collecting MRI and clinical data from large cohorts of multiple sclerosis patients are becoming more frequent and extensive, the single-subject SCNs analysis can have an important role in the study of network disruptions in multiple sclerosis since they can be derived from anatomical sequences, such as the 3D T1, frequently available even in clinical scans. Since SCNs alterations showed clinical relevance at the onset of CIS and multiple sclerosis, future longitudinal analyses will assess if the observed

changes in SCNs can predict conversion to multiple sclerosis during the follow-up.

10.5 Visual function and BICAMS assessment

In this thesis, I have assessed cognitive function in early patients. The reason is that, as seen in Paragraph 2.1.1.2, cognition can be early impaired in multiple sclerosis patients. Furthermore, the EDSS, which is the standard way to score disability, is biased towards ambulation and motor function, which, in this early stage of the disease, can still be normal. Thus, a cognitive battery such as BICAMS can offer the opportunity to further assess brain functions in early patients.

Here, I demonstrated, however, that the assessment of BVMT-R, a standard test for visuospatial memory used not only in BICAMS, but also in the Minimal Assessment of Cognitive Function in Multiple Sclerosis, can be affected by the visual impairment determined by ON. Interestingly, however, this correlation neither was influenced by the amount of damage in the affected eye, expressed as atrophy of the RNFL or GCIPL, nor seems affected by the amount of damage in the visual pathways and in the CNS. So, my hypothesis is that higher visual processing, not studied in this context, may be involved.

This finding not only has a practical implication, the suggestion of assessing visual function in the clinical and research setting when using BICAMS in ON-CIS patients, but also yields new insights into the pathophysiological mechanisms behind the clinical manifestation of early patients. ON, besides determining visual symptoms, may have an effect also in other clinical aspects, such as visuospatial memory.

10.6 Future directions

The projects I have carried out during my PhD have tried to investigate the pathophysiological mechanisms behind the damage in the CNS of early patients using advanced imaging techniques. The results presented in this thesis help in part to fill the gap left by pathological studies, which are rarely done in early cohorts, and observational studies with conventional MRI

metrics, which cannot investigate the pathological substrates. Furthermore, they add important elements to the body of research that have used advanced imaging techniques to study CIS and multiple sclerosis patients at the onset.

NODDI can detect areas of neuro-axonal loss from the onset of the disease. Although multi-centre studies may not be feasible at the moment for the high inter-vendor variability, in the future, NODDI can help to identify potential targets for early neuroprotective agents in single-centre trials. Specifically, in this thesis, I have confirmed that the loss of large myelinated axons in the white matter may be associated with sodium accumulation. Thus, this cation may play a crucial role in the pathogenesis of the damage since the beginning. Future studies will have to focus if these changes are at the expense of those patients who eventually develop a high disability.

The extraction of SCNs is a novel method in the panorama of the techniques used for the brain network study. However, it has already found many applications in various disorders because it explores further the cortical changes during medical conditions, and it has the enormous advantage or requiring just an anatomical MRI image. Hence, it is crucial to have shown here that SCNs can find applications so early in multiple sclerosis.

I demonstrated SCNs abnormalities that were clinically relevant. The finding of patterns of synchronous cortical changes so early in the disease reminds us that there is a whole part of structural and functional adaptation that must be taken into account even when studying multiple sclerosis onsets. Future analysis will reveal if these changes correlate with multiple sclerosis conversion.

I also showed that SCNs analysis is feasible, with the appropriate adjustments, in a multi-centre setting. Therefore, this technique can be used in large sets of early patients and thus give more robust results.

Finally, my last results chapter invites colleagues to consider ON not just as one of the different types of CIS but as a complex syndrome whose CNS

involvement goes beyond the visual system. Visual acuity impairment seems to have an impact on cognitive performance at the onset. Future research will have to clarify whether this is an exclusive preserve of ON patient or if it can be generalised to other syndromes with a subclinical involvement of the optic nerve.

Furthermore, my thesis outputs are hypothesis generating and can be tested and developed in future studies.

The first study reported in Chapter 6 not only served as a preliminary work for my research in Chapter 7, but also provided interesting hypothesis to verify with future studies. I found that although signs of neurodegeneration showed by the low NDI were present both in the brain and spinal cord white matter, it was in the spinal cord that the low NDI was related to disability. The hypothesis is that neurodegeneration in the spinal cord may drive disability in multiple sclerosis. This will be verified with a future study comparing the same cohort of patients with patients with post-traumatic cervical myelopathy that underwent MRI scans and clinical assessments with the same protocol of Chapter 6. This way I could confirm if NDI is reflecting neurodegeneration and is related to physical disability, i.e., I would expect low NDI in the myelopathy cohort correlated with physical disability in the limbs.

As regards Chapter 7, I hypothesised that microstructural changes are present in the brain of early patients and are clinically significant while at this early stage brain volumes may be not. I will further verify this hypothesis with the analysis of the longitudinal data that are generating from this cohort. Specifically, I will assess if the alterations described in Chapter 7 relate to disability accrual more than the percentual of brain volume change over time. The other hypothesis is that the corpus callosum has early neurodegeneration. With the follow up of the cohort, I will verify this hypothesis checking if patients who have at baseline lower NDI and higher TSC than others develop callosal atrophy over time.

For the SCNs, my main conclusion was that lesions can alter long range connections and cause a shift towards a regular and clustered small-world network. In my study, this organisation seems not efficient as it is related to a poor performance at the SDMT. I will test this hypothesis in the same cohort demonstrating that with lesion accumulation over time the shift towards the regular small-world network will be maintained.

Finally, the last study in Chapter 9 generated the hypothesis that the performance in the BVMT-R among optic neuritis patients is influenced by the visual recovery. Future studies can test this hypothesis by comparing patients with optic neuritis with patients with other type of onsets that do not impair the vision and check if the two groups have a similar improvement in the BVMT-R.

Finally, the 2017 revision of the McDonald criteria for multiple sclerosis suggested domains to further explore, such as the impact of the optic nerve involvement and the evidence of cortical lesions on the diagnosis. Since the studies included in this thesis are cross-sectional, these points have not been investigated. However, my thesis offers interesting insights regarding the use of MRI in patients' initial assessment at their first demyelinating event. Firstly, my thesis suggests that advanced imaging can show clinically relevant pathological alterations not detected by conventional MRI. Therefore, in the future, advanced techniques could be used to assess the presence of damage to demonstrate dissemination in space. Obviously, this must be first developed in longitudinal studies investigating if these alterations are at the expense of patients converting to multiple sclerosis. Secondly, my thesis suggests that the study of higher cortical functions, which are excluded from the criteria, may impact patients' final clinical phenotype.

References

Aboul-Enein F, Rauschka H, Kornek B, Stadelmann C, Stefferl A, Brück W, et al. Preferential Loss of Myelin-Associated Glycoprotein Reflects Hypoxia-Like White Matter Damage in Stroke and Inflammatory Brain Diseases. J Neuropathol Exp Neurol 2003; 62: 25–33.

Afifi AA, Kotlerman JB, Ettner SL, Cowan M. Methods for improving regression analysis for skewed continuous or counted responses. Annu Rev Public Health 2007; 28: 95–111.

Aktas O, Prozorovski T, Zipp F. Death Ligands and Autoimmune Demyelination. Neurosci 2006; 12: 305–316.

Alexander AL, Lee JE, Lazar M, Field AS. Diffusion Tensor Imaging of the Brain. Neurotherapeutics 2007; 4: 316–329.

Aliaga ES, Barkhof F. MRI mimics of multiple sclerosis. In: Handbook of Clinical Neurology. Elsevier B.V.; 2014. p. 291–316

Allen I V., McKeown SR. A histological, histochemical and biochemical study of the macroscopically normal white matter in multiple sclerosis. J Neurol Sci 1979; 41: 81–91.

Andersen O, Lygner PE, Bergström T, Andersson M, Vablne A. Viral infections trigger multiple sclerosis relapses: a prospective seroepidemiological study. J Neurol 1993; 240: 417–422.

Andersson JLR, Sotiropoulos SN. An integrated approach to correction for off-resonance effects and subject movement in diffusion MR imaging. Neuroimage 2016; 125: 1063–1078.

Andica C, Kamagata K, Hatano T, Okuzumi A, Saito A, Nakazawa M, et al. Neurite orientation dispersion and density imaging of the nigrostriatal pathway in Parkinson's disease: Retrograde degeneration observed by tract-profile analysis. Park Relat Disord 2018; 51: 55–60.

Andica C, Kamagata K, Hayashi T, Hagiwara A, Uchida W, Saito Y, et al. Scan-

rescan and inter-vendor reproducibility of neurite orientation dispersion and density imaging metrics. Neuroradiology 2020; 62: 483–494.

Androdias G, Reynolds R, Chanal M, Ritleng C, Confavreux C, Nataf S. Meningeal T cells associate with diffuse axonal loss in multiple sclerosis spinal cords. Ann Neurol 2010; 68: 465–476.

Anhoque CF, Biccas-Neto L, Domingues SCA, Teixeira AL, Domingues RB. Cognitive impairment and optic nerve axonal loss in patients with clinically isolated syndrome. Clin Neurol Neurosurg 2013; 115: 1032–1035.

Ascherio A, Munger KL, White R, Köchert K, Simon KC, Polman CH, et al. Vitamin D as an early predictor of multiple sclerosis activity and progression. JAMA Neurol 2014; 71: 306–314.

Assaf Y, Cohen Y. Structural Information in Neuronal Tissue as Revealed by Q-Space Diffusion NMR Spectroscopy of Metabolites in Bovine Optic Nerve. NMR Biomed 1999; 12: 335–44.

Audoin B, Ibarrola D, Malikova I, Soulier E, Confort-Gouny S, Au Duong M V., et al. Onset and underpinnings of white matter atrophy at the very early state of multiple sclerosis - A two-year longitudinal MRI/MRSI study of corpus callosum. Mult Scler 2007; 13: 41–51.

Babbe H, Roers A, Waisman A, Lassmann H, Goebels N, Hohlfeld R, et al. Clonal expansions of CD8+ T cells dominate the T cell infiltrate in active multiple sclerosis lesions as shown by micromanipulation and single cell polymerase chain reaction. J Exp Med 2000; 192: 393–404.

Babinski J. Recherches sur l'anatomie pathologique de la sclerose en plaque et etude comparative des diverses varietes de la scleroses de la moelle. Arch Sci Physiol (Paris) 1885; 5–6: 186–207.

Bag AK, Patel BN, Osman S, Roberson GH. Clinico-Radiologic Profile of Spinal Cord Multiple Sclerosis in Adults. Neuroradiol J 2011; 24: 511–518.

Balcer LJ, Baier ML, Cohen JA, Kooijmans MF, Sandrock AW, Nano-Schiavi

ML, et al. Contrast letter acuity as a visual component for the Multiple Sclerosis Functional Composite. Neurology 2003; 61: 1367–1373.

Balcer LJ, Raynowska J, Nolan R, Galetta SL, Kapoor R, Benedict R, et al. Validity of low-contrast letter acuity as a visual performance outcome measure for multiple sclerosis. Mult Scler 2017; 23: 734–747.

Balk LJ, Cruz-Herranz A, Albrecht P, Arnow S, Gelfand JM, Tewarie P, et al. Timing of retinal neuronal and axonal loss in MS: a longitudinal OCT study. J Neurol 2016; 263: 1323–31.

Barkhof F, Brück W, De Groot CJA, Bergers E, Hulshof S, Geurts J, et al. Remyelinated lesions in multiple sclerosis: Magnetic resonance image appearance. Arch Neurol 2003; 60: 1073–1081.

Barnard RO, Triggs M. Corpus callosum in multiple sclerosis. J Neurol Neurosurg Psychiatry 1974; 37: 1259–1264.

Barnett MH, Prineas JW. Relapsing and remitting multiple sclerosis: Pathology of the newly forming lesion. Ann Neurol 2004; 55: 458–468.

Basser PJ, Mattiello J, LeBihan D. MR diffusion tensor spectroscopy and imaging. Biophys J 1994; 66: 259–267.

Bassett DS, Bullmore E, Verchinski BA, Mattay VS, Weinberger DR, Meyer-Lindenberg A. Hierarchical Organization of Human Cortical Networks in Health and Schizophrenia. J Neurosci 2008; 28: 9239–9248.

Beck RW, Chandler DL, Cole SR, Simon JH, Jacobs LD, Kinkel RP, et al. Interferon β-1a for early multiple sclerosis: CHAMPS trial subgroup analyses. Ann Neurol 2002; 51: 481–490.

Beck RW, Cleary PA, Anderson MM, Keltner JL, Shults WT, Kaufman DI, et al. A randomized, controlled trial of corticosteroids in the treatment of acute optic neuritis. N Engl J Med 1992; 326: 581–588.

Beck RW, Cleary PA, Backlund JC. The Course of Visual Recovery after Optic Neuritis. Ophthalmology 1994; 101: 1771–1778.

Ben-Nun A, Wekerle H, Cohen IR. The rapid isolation of clonable antigen-specific T lymphocyte lines capable of mediating autoimmune encephalomyelitis. Eur J Immunol 1981; 11: 195–199.

Berger J, Moser HW, Forss-Petter S. Leukodystrophies: Recent developments in genetics, molecular biology, pathogenesis and treatment. Curr Opin Neurol 2001; 14: 305–312.

Bermel RA, Innus MD, Tjoa CW, Bakshi R. Selective caudate atrophy in multiple sclerosis: A 3D MRI parcellation study. Neuroreport 2003; 14: 335–339.

Bester M, Heesen C, Schippling S, Martin R, Ding XQ, Holst B, et al. Early anisotropy changes in the corpus callosum of patients with optic neuritis. Neuroradiology 2008; 50: 549–557.

Bhadelia RA, Price LL, Tedesco KL, Scott T, Qiu WQ, Patz S, et al. Diffusion tensor imaging, white matter lesions, the corpus callosum, and gait in the elderly. Stroke 2009; 40: 3816–3820.

Bielekova B, Goodwin B, Richert N, Cortese I, Kondo T, Afshar G, et al. Encephalitogenic potential of the myelin basic protein peptide (amino acids 83-99) in multiple sclerosis: Results of a phase II clinical trial with an altered peptide ligand. Nat Med 2000; 6: 1167–1175.

Bielekova B, Martin R. Development of biomarkers in multiple sclerosis. Brain 2004; 127: 1463–1478.

Le Bihan D, Breton E, Lallemand D, Grenier P, Cabanis E, Laval-Jeantet M. MR imaging of intravoxel incoherent motions: Application to diffusion and perfusion in neurologic disorders. Radiology 1986; 161: 401–407.

Billiet T, Vandenbulcke M, Mädler B, Peeters R, Dhollander T, Zhang H, et al. Age-related microstructural differences quantified using myelin water imaging and advanced diffusion MRI. Neurobiol Aging 2015; 36: 2107–2121.

Bitsch A, Schuchardt J, Bunkowski S, Kuhlmann T, Brück W. Acute axonal

injury in multiple sclerosis Correlation with demyelination and inflammation. Brain 2000; 123: 1174–1183.

Bjartmar C, Kidd G, Mörk S, Rudick R, Trapp BD. Neurological disability correlates with spinal cord axonal loss and reduced N-acetyl aspartate in chronic multiple sclerosis patients. Ann Neurol 2000; 48: 893–901.

Blumenthal EZ, Parikh RS, Pe'er J, Naik M, Kaliner E, Cohen MJ, et al. Retinal nerve fibre layer imaging compared with histological measurements in a human eye. Eye 2009; 23: 171–175.

Bommarito G, Bellini A, Pardini M, Solaro C, Roccatagliata L, Laroni A, et al. Composite MRI measures and short-term disability in patients with clinically isolated syndrome suggestive of MS. Mult Scler 2018; 24: 623–631.

Bramow S, Frischer JM, Lassmann H, Koch-Henriksen N, Lucchinetti CF, Sørensen PS, et al. Demyelination versus remyelination in progressive multiple sclerosis. Brain 2010; 133: 2983–2998.

Breij ECW, Brink BP, Veerhuis R, van den Berg C, Vloet R, Yan R, et al. Homogeneity of active demyelinating lesions in established multiple sclerosis. Ann Neurol 2008; 63: 16–25.

Brex PA, Ciccarelli O, O'Riordan JI, Sailer M, Thompson AJ, Miller DH. A longitudinal study of abnormalities on MRI and disability from multiple sclerosis. N Engl J Med 2002; 346: 158–164.

Broad RJ, Gabel MC, Dowell NG, Schwartzman DJ, Seth AK, Zhang H, et al. Neurite orientation and dispersion density imaging (NODDI) detects cortical and corticospinal tract degeneration in ALS. J Neurol Neurosurg Psychiatry 2019; 90: 404–411.

Brochet B, Ruet A. Cognitive Impairment in Multiple Sclerosis With Regards to Disease Duration and Clinical Phenotypes. Front Neurol 2019; 10

Brosnan CF, Raine CS. Mechanisms of Immune Injury in Multiple Sclerosis. Brain Pathol 1996; 6: 243–257.

Brownlee WJ, Altmann DR, Alves Da Mota P, Swanton JK, Miszkiel KA, Wheeler-Kingshott CAMG, et al. Association of asymptomatic spinal cord lesions and atrophy with disability 5 years after a clinically isolated syndrome. Mult Scler 2017; 23: 665–674.

Brownlee WJ, Altmann DR, Prados F, Miszkiel KA, Eshaghi A, Gandini Wheeler-Kingshott CAM, et al. Early imaging predictors of long-term outcomes in relapse-onset multiple sclerosis. Brain 2019; 142: 2276–2287.

Brownlee WJ, Solanky B, Prados F, Yiannakas M, Da Mota P, Riemer F, et al. Cortical grey matter sodium accumulation is associated with disability and secondary progressive disease course in relapse-onset multiple sclerosis. J Neurol Neurosurg Psychiatry 2019: jnnp-2018-319634.

Bruce JM, Bruce AS, Arnett PA. Mild visual acuity disturbances are associated with performance on tests of complex visual attention in MS. J Int Neuropsychol Soc 2007; 13: 544–548.

Brück W, Kuhlmann T, Stadelmann C. Remyelination in multiple sclerosis. J Neurol Sci 2003; 206: 181–185.

Brück W, Porada P, Poser S, Rieckmann P, Hanefeld F, Kretzschmarch HA, et al. Monocyte/macrophage differentiation in early multiple sclerosis lesions. Ann Neurol 1995; 38: 788–796.

Bsteh G, Hegen H, Teuchner B, Amprosi M, Berek K, Ladstätter F, et al. Peripapillary retinal nerve fibre layer as measured by optical coherence tomography is a prognostic biomarker not only for physical but also for cognitive disability progression in multiple sclerosis. Mult Scler J 2019; 25: 196–203.

Von Büdingen HC, Tanuma N, Villoslada P, Ouallet JC, Hauser SL, Genain CP. Immune responses against the myelin/oligodendrocyte glycoprotein in experimental autoimmune demyelination. J Clin Immunol 2001; 21: 155–170.

Bullmore E, Sporns O. Complex brain networks: Graph theoretical analysis of structural and functional systems. Nat Rev Neurosci 2009; 10: 186–198.

By S, Xu J, Box BA, Bagnato FR, Smith SA. Application and evaluation of NODDI in the cervical spinal cord of multiple sclerosis patients. NeuroImage Clin 2017; 15: 333–342.

Campbell GR, Mahad DJ. Mitochondrial changes associated with demyelination: consequences for axonal integrity. Mitochondrion 2012; 12: 173–9.

Campbell J, Rashid W, Cercignani M, Langdon D. Cognitive impairment among patients with multiple sclerosis: Associations with employment and quality of life. Postgrad Med J 2017; 93: 143–147.

Cantorna MT. Vitamin D and autoimmunity: Is vitamin D status an environmental factor affecting autoimmune disease prevalence? Proc Soc Exp Biol Med 2000; 223: 230–233.

Cappellani R, Bergsland N, Weinstock-Guttman B, Kennedy C, Carl E, Ramasamy DP, et al. Diffusion tensor MRI alterations of subcortical deep gray matter in clinically isolated syndrome. J Neurol Sci 2014

Cardoso MJ, Modat M, Wolz R, Melbourne A, Cash D, Rueckert D, et al. Geodesic Information Flows: Spatially-Variant Graphs and Their Application to Segmentation and Fusion. IEEE Trans Med Imaging 2015; 34: 1976–1988.

Cawley N, Tur C, Prados F, Plantone D, Kearney H, Abdel-Aziz K, et al. Spinal cord atrophy as a primary outcome measure in phase II trials of progressive multiple sclerosis. Mult Scler J 2018; 24: 932–941.

Cepok S, Zhou D, Srivastava R, Nessler S, Stei S, Büssow K, et al. Identification of Epstein-Barr virus proteins as putative targets of the immune response in multiple sclerosis. J Clin Invest 2005; 115: 1352–1360.

Cercignani M, Gandini Wheeler-Kingshott C. From micro- to macro-structures in multiple sclerosis: what is the added value of diffusion imaging. NMR Biomed 2019; 32: e3888.

CHAMPIONS STUDY Group. IM interferon β-1a delays definite multiple

sclerosis 5 years after a first demyelinating event. Neurology 2006; 66: 678–684.

CHAMPS STUDY GROUP. Interferon β-1a for optic neuritis patients at high risk for multiple sclerosis. Am J Ophthalmol 2001; 132: 463–471.

Chang A, Tourtellotte WW, Rudick R, Trapp BD. Premyelinating oligodendrocytes in chronic lesions of multiple sclerosis. N Engl J Med 2002; 346: 165–173.

Chang YS, Owen JP, Pojman NJ, Thieu T, Bukshpun P, Wakahiro MLJ, et al. White matter changes of neurite density and fiber orientation dispersion during human brain maturation. PLoS One 2015; 10

Charcot J. Lecons sur les maladies du systeme nerveux faites a la Salpetriere. Lect about Dis Nerv Syst done Salpetriere 1880; 1A

Charo IF, Ransohoff RM. Mechanisms of disease: The many roles of chemokines and chemokine receptors in inflammation. N Engl J Med 2006; 354: 610–621.

Chiaravalloti ND, DeLuca J. Cognitive impairment in multiple sclerosis. Lancet Neurol 2008; 7: 1139–51.

Chung AW, Seunarine KK, Clark CA. NODDI reproducibility and variability with magnetic field strength: A comparison between 1.5 T and 3 T. Hum Brain Mapp 2016; 37: 4550–4565.

Chung KK, Altmann D, Barkhof F, Miszkiel K, Brex PA, O'Riordan J, et al. A 30-Year Clinical and Magnetic Resonance Imaging Observational Study of Multiple Sclerosis and Clinically Isolated Syndromes. Ann Neurol 2020; 87: 63–74.

Ciccarelli O, Barkhof F, Bodini B, De Stefano N, Golay X, Nicolay K, et al. Pathogenesis of multiple sclerosis: insights from molecular and metabolic imaging. Lancet Neurol 2014; 13: 807–822.

Ciccarelli O, Giugni E, Paolillo A, Mainero C, Gasperini C, Bastianello S, et al.

Magnetic resonance outcome of new enhancing lesions in patients with relapsing-remitting multiple sclerosis. Eur J Neurol 1999; 6: 455–459.

Cifelli A, Arridge M, Jezzard P, Esiri MM, Palace J, Matthews PM. Thalamic neurodegeneration in multiple sclerosis. Ann Neurol 2002; 52: 650–653.

Cleary PA, Beck RW, Bourque LB, Backlund JC, Miskala PH. Visual symptoms after optic neuritis. Results from the Optic Neuritis Treatment Trial. J Neuroophthalmol 1997; 17: 18–23; quiz 24–8.

Cole SR, Beck RW, Moke PS, Gal RL, Long DT. The National Eye Institute Visual Function Questionnaire: Experience of the ONTT. Investig Ophthalmol Vis Sci 2000; 41: 1017–21.

Colgan N, Siow B, O'Callaghan JM, Harrison IF, Wells JA, Holmes HE, et al. Application of neurite orientation dispersion and density imaging (NODDI) to a tau pathology model of Alzheimer's disease. Neuroimage 2016; 125: 739–744.

Collins CE, Airey DC, Young NA, Leitch DB, Kaas JH. Neuron densities vary across and within cortical areas in primates. Proc Natl Acad Sci U S A 2010; 107: 15927–15932.

Coman I, Aigrot MS, Seilhean D, Reynolds R, Girault JA, Zalc B, et al. Nodal, paranodal and juxtaparanodal axonal proteins during demyelination and remyelination in multiple sclerosis. Brain 2006; 129: 3186–3195.

Comi G, Filippi M, Barkhof F, Durelli L, Edan G, Fernández O, et al. Effect of early interferon treatment on conversion to definite multiple sclerosis: A randomised study. Lancet 2001; 357: 1576–1582.

Comi G, Martinelli V, Rodegher M, Moiola L, Bajenaru O, Carra A, et al. Effect of glatiramer acetate on conversion to clinically definite multiple sclerosis in patients with clinically isolated syndrome (PreCISe study): a randomised, double-blind, placebo-controlled trial. Lancet 2009; 374: 1503–1511.

Comi G, Martinelli V, Rodegher M, Moiola L, Leocani L, Bajenaru O, et al. Effects of early treatment with glatiramer acetate in patients with clinically

isolated syndrome. Mult Scler J 2013; 19: 1074–1083.

Confavreux C, Vukusic S, Adeleine P. Early clinical predictors and progression of irreversible disability in multiple sclerosis: an amnesic process. Brain 2003; 126: 770–782.

Conturo TE, Lori NF, Cull TS, Akbudak E, Snyder AZ, Shimony JS, et al. Tracking neuronal fiber pathways in the living human brain. Proc Natl Acad Sci U S A 1999; 96: 10422–10427.

Corcione A, Aloisi F, Serafini B, Capello E, Mancardi GL, Pistoia V, et al. B-cell differentiation in the CNS of patients with multiple sclerosis. In: Autoimmunity Reviews. Elsevier; 2005. p. 549–554

Corfield F, Langdon D. A Systematic Review and Meta-Analysis of the Brief Cognitive Assessment for Multiple Sclerosis (BICAMS). Neurol Ther 2018; 7: 287–306.

Coric D, Balk LJ, Verrijp M, Eijlers A, Schoonheim MM, Killestein J, et al. Cognitive impairment in patients with multiple sclerosis is associated with atrophy of the inner retinal layers. Mult Scler J 2018; 24: 158–166.

Cortese R, Collorone S, Ciccarelli O, Toosy AT. Advances in Brain Imaging in Multiple Sclerosis. Ther Adv Neurol Disord 2019; 12: 1756286419859722.

Costello F, Coupland S, Hodge W, Lorello GR, Koroluk J, Pan YI, et al. Quantifying axonal loss after optic neuritis with optical coherence tomography. Ann Neurol 2006; 59: 963–969.

Costello F, Hodge W, Pan YI, Eggenberger E, Coupland S, Kardon RH. Tracking retinal nerve fiber layer loss after optic neuritis: A prospective study using optical coherence tomography. Mult Scler 2008; 14: 893–905.

Cotton F, Weiner HL, Jolesz FA, Guttmann CRG. MRI contrast uptake in new lesions in relapsing-remitting MS followed at weekly intervals. Neurology 2003; 60: 640–6.

Craner MJ, Newcombe J, Black JA, Hartle C, Cuzner ML, Waxman SG.

Molecular changes in neurons in multiple sclerosis: altered axonal expression of Nav1.2 and Nav1.6 sodium channels and Na+/Ca2+ exchanger. Proc Natl Acad Sci U S A 2004; 101: 8168–73.

Criste G, Trapp B, Dutta R. Axonal loss in multiple sclerosis. Causes and mechanisms. In: Handbook of Clinical Neurology. Elsevier B.V.; 2014. p. 101–113

Crombe A, Planche V, Raffard G, Bourel J, Dubourdieu N, Panatier A, et al. Deciphering the microstructure of hippocampal subfields with in vivo DTI and NODDI: Applications to experimental multiple sclerosis. Neuroimage 2018; 172: 357–368.

Crucian GP, Okun MS. Visual-spatial ability in Parkinson's disease. Front Biosci 2003; 8: s992-7.

Cua DJ, Sherlock J, Chen Y, Murphy CA, Joyce B, Seymour B, et al. Interleukin-23 rather than interleukin-12 is the critical cytokine for autoimmune inflammation of the brain. Nature 2003; 421: 744–748.

Curcio CA, Allen KA. Topography of ganglion cells in human retina. J Comp Neurol 1990; 300: 5–25.

Curcio CA, Sloan KR, Kalina RE, Hendrickson AE. Human photoreceptor topography. J Comp Neurol 1990; 292: 497–523.

Cutter GR, Baier ML, Rudick RA, Cookfair DL, Fischer JS, Petkau J, et al. Development of a multiple sclerosis functional composite as a clinical trial outcome measure. Brain 1999; 122 (Pt 5): 871–82.

Cuzner ML, Opdenakker G. Plasminogen activators and matrix metalloproteases, mediators of extracellular proteolysis in inflammatory demyelination of the central nervous system. J Neuroimmunol 1999; 94: 1–14.

Dalton CM, Chard DT, Davies GR, Miszkiel KA, Altmann DR, Fernando K, et al. Early development of multiple sclerosis is associated with progressive grey matter atrophy in patients presenting with clinically isolated syndromes. Brain

2004; 127: 1101–1107.

Davis AS, Hertza J, Williams RN, Gupta AS, Ohly JG. The Influence of Corrected Visual Acuity on Visual Attention and Incidental Learning in Patients with Multiple Sclerosis. Appl Neuropsychol 2009; 16: 165–168.

Dietemann JL, Beigelman C, Rumbach L, Vouge M, Tajahmady T, Faubert C, et al. Multiple sclerosis and corpus callosum atrophy: Relationship of MRI findings to clinical data. Neuroradiology 1988; 30: 478–480.

Dineen RA, Vilisaar J, Hlinka J, Bradshaw CM, Morgan PS, Constantinescu CS, et al. Disconnection as a mechanism for cognitive dysfunction in multiple sclerosis. Brain 2009; 132: 239–249.

Dobson R, Ramagopalan S, Giovannoni G. The effect of gender in clinically isolated syndrome (CIS): A meta-analysis. Mult Scler J 2012; 18: 600–604.

Dörr J, Wernecke KD, Bock M, Gaede G, Wuerfel JT, Pfueller CF, et al. Association of retinal and macular damage with brain atrophy in multiple sclerosis. PLoS One 2011; 6

Duddy ME, Alter A, Bar-Or A. Distinct Profiles of Human B Cell Effector Cytokines: A Role in Immune Regulation? J Immunol 2004; 172: 3422–3427.

van Duinkerken E, Ijzerman RG, Klein M, Moll AC, Snoek FJ, Scheltens P, et al. Disrupted subject-specific gray matter network properties and cognitive dysfunction in type 1 diabetes patients with and without proliferative retinopathy. Hum Brain Mapp 2016; 37: 1194–1208.

Dutta R, McDonough J, Yin X, Peterson J, Chang A, Torres T, et al. Mitochondrial dysfunction as a cause of axonal degeneration in multiple sclerosis patients. Ann Neurol 2006; 59: 478–489.

Dziedzic T, Metz I, Dallenga T, König FB, Müller S, Stadelmann C, et al. Wallerian degeneration: A major component of early axonal pathology in multiple sclerosis. Brain Pathol 2010; 20: 976–985.

Eisele P, Konstandin S, Griebe M, Szabo K, Wolf ME, Alonso A, et al.

Heterogeneity of acute multiple sclerosis lesions on sodium (23Na) MRI. Mult Scler 2016; 22: 1040–1047.

Eisele P, Konstandin S, Szabo K, Ebert A, Roßmanith C, Paschke N, et al. Temporal evolution of acute multiple sclerosis lesions on serial sodium (23Na) MRI. Mult Scler Relat Disord 2019; 29: 48–54.

Engelhardt B, Wolburg H. Mini review: Transendothelial migration of leukocytes: Through the front door or around the side of the house? Eur J Immunol 2004; 34: 2955–2963.

Eriksson M, Andersen O, Runmarker B. Long-term follow up of patients with clinically isolated syndromes, relapsing-remitting and secondary progressive multiple sclerosis. Mult Scler 2003; 9: 260–274.

Eshaghi A, Marinescu R V, Young AL, Firth NC, Prados F, Jorge Cardoso M, et al. Progression of regional grey matter atrophy in multiple sclerosis. Brain 2018; 141: 1665–1677.

Eshaghi A, Prados F, Brownlee WJ, Altmann DR, Tur C, Cardoso MJ, et al. Deep gray matter volume loss drives disability worsening in multiple sclerosis. Ann Neurol 2018; 83: 210–222.

Evans CF, Horwitz MS, Hobbs M V., Oldstone MBA. Viral infection of transgenic mice expressing a viral protein in oligodendrocytes leads to chronic central nervous system autoimmune disease. J Exp Med 1996; 184: 2371–2384.

Feaster HT, Bruce JM. Visual acuity is associated with performance on visual and non-visual neuropsychological tests in multiple sclerosis. Clin Neuropsychol 2011; 25: 640–51.

Ferguson B, Matyszak MK, Esiri MM, Perry VH. Axonal damage in acute multiple sclerosis lesions. Brain 1997; 120: 393–399.

Ferizi U, Schneider T, Panagiotaki E, Nedjati-Gilani G, Zhang H, Wheeler-Kingshott CAM, et al. A ranking of diffusion MRI compartment models with in

vivo human brain data. Magn Reson Med 2014; 72: 1785–1792.

Feuillet L, Reuter F, Audoin B, Malikova I, Barrau K, Ali Cherif A, et al. Early cognitive impairment in patients with clinically isolated syndrome suggestive of multiple sclerosis. Mult Scler 2007; 13: 124–127.

Filippi M, Rocca MAA. Functional MR Imaging in Multiple Sclerosis. Elsevier; 2009

Filippi M, Wolinsky JS, Sormani MP, Comi G. Enhancement frequency decreases with increasing age in relapsing-remitting multiple sclerosis. Neurology 2001; 56: 422–423.

Fischer JS, Rudick RA, Cutter GR, Reingold SC. The Multiple Sclerosis Functional Composite measure (MSFC): an integrated approach to MS clinical outcome assessment. Mult Scler J 1999; 5: 244–250.

Fischer JS, Rudick RA, Cutter GR, Reingold SC. The Multiple Sclerosis Functional Composite Measure (MSFC): An Integrated Approach to MS Clinical Outcome Assessment. National MS Society Clinical Outcomes Assessment Task Force. Mult Scler 1999; 5: 244–250.

Fisniku LK, Brex PA, Altmann DR, Miszkiel KA, Benton CE, Lanyon R, et al. Disability and T2 MRI lesions: a 20-year follow-up of patients with relapse onset of multiple sclerosis. Brain 2008; 131: 808–817.

Fitzgibbon T, Taylor S. Retinotopy of the Human Retinal Nerve Fibre Layer and Optic Nerve Head. J Comp Neurol 1996; 375

Fleysher L, Oesingmann N, Brown R, Sodickson DK, Wiggins GC, Inglese M. Noninvasive quantification of intracellular sodium in human brain using ultrahigh-field MRI. NMR Biomed 2013; 26: 9–19.

Frahm J, Merboldt K -D, Hänicke W. Functional MRI of human brain activation at high spatial resolution. Magn Reson Med 1993; 29: 139–144.

Friese MA, Fugger L. Autoreactive CD8 + T cells in multiple sclerosis: a new target for therapy? Brain 2005; 128: 1747–1763.

Frischer JM, Bramow S, Dal-Bianco A, Lucchinetti CF, Rauschka H, Schmidbauer M, et al. The relation between inflammation and neurodegeneration in multiple sclerosis brains. Brain 2009; 132: 1175–89.

Frischer JM, Weigand SD, Guo Y, Kale N, Parisi JE, Pirko I, et al. Clinical and pathological insights into the dynamic nature of the white matter multiple sclerosis plaque. Ann Neurol 2015; 78: 710–721.

Frohman EM, Dwyer MG, Frohman T, Cox JL, Salter A, Greenberg BM, et al. Relationship of optic nerve and brain conventional and non-conventional MRI measures and retinal nerve fiber layer thickness, as assessed by OCT and GDx: a pilot study. J Neurol Sci 2009; 282: 96–105.

Frohman EM, Racke MK, Raine CS. Medical progress: Multiple sclerosis - The plaque and its pathogenesis. N Engl J Med 2006; 354: 942–955.

Fukutomi H, Glasser MF, Zhang H, Autio JA, Coalson TS, Okada T, et al. Neurite imaging reveals microstructural variations in human cerebral cortical gray matter. Neuroimage 2018; 182: 488–499.

Gabilondo I, Martínez-Lapiscina EH, Martínez-Heras E, Fraga-Pumar E, Llufriu S, Ortiz S, et al. Trans-synaptic axonal degeneration in the visual pathway in multiple sclerosis. Ann Neurol 2014; 75: 98–107.

Gallo A, Rovaris M, Riva R, Ghezzi A, Benedetti B, Martinelli V, et al. Diffusion-Tensor Magnetic Resonance Imaging Detects Normal-Appearing White Matter Damage Unrelated to Short-term Disease Activity in Patients at the Earliest Clinical Stage of Multiple Sclerosis. Arch Neurol 2005; 62: 803.

Gandini Wheeler-Kingshott CAM, Riemer F, Palesi F, Ricciardi A, Castellazzi G, Golay X, et al. Challenges and Perspectives of Quantitative Functional Sodium Imaging (fNaI). Front Neurosci 2018; 12: 810.

Garway-Heath DF, Holder GE, Fitzke FW, Hitchings RA. Relationship between electrophysiological, psychophysical, and anatomical measurements in glaucoma. Investig Ophthalmol Vis Sci 2002; 43: 2213–2220.

Genovese CR, Lazar NA, Nichols T. Thresholding of statistical maps in functional neuroimaging using the false discovery rate. Neuroimage 2002; 15: 870–8.

Geurts JJG, Bö L, Roosendaal SD, Hazes T, Daniëls R, Barkhof F, et al. Extensive Hippocampal Demyelination in Multiple Sclerosis. J Neuropathol Exp Neurol 2007; 66: 819–827.

Gilmore C, Geurts J, Evangelou N, Bot J, van Schijndel R, Pouwels P, et al. Spinal cord grey matter lesions in multiple sclerosis detected by post-mortem high field MR imaging. Mult Scler J 2009; 15: 180–188.

Gilmore CP, Donaldson I, Bö L, Owens T, Lowe J, Evangelou N. Regional variations in the extent and pattern of grey matter demyelination in multiple sclerosis: A comparison between the cerebral cortex, cerebellar cortex, deep grey matter nuclei and the spinal cord. J Neurol Neurosurg Psychiatry 2009; 80: 182–187.

Glanz BI, Holland CM, Gauthier SA, Amunwa EL, Liptak Z, Houtchens MK, et al. Cognitive dysfunction in patients with clinically isolated syndromes or newly diagnosed multiple sclerosis. Mult Scler 2007; 13: 1004–1010.

Glasser MF, van Essen DC. Mapping human cortical areas in vivo based on myelin content as revealed by T1- and T2-weighted MRI. J Neurosci 2011; 31: 11597–11616.

Glasser MF, Goyal MS, Preuss TM, Raichle ME, Van Essen DC. Trends and properties of human cerebral cortex: Correlations with cortical myelin content. Neuroimage 2014; 93: 165–175.

Golestani N, Paus T, Zatorre RJ. Anatomical correlates of learning novel speech sounds. Neuron 2002; 35: 997–1010.

Gordon-Lipkin E, Chodkowski B, Reich DS, Smith SA, Pulicken M, Balcer LJ, et al. Retinal nerve fiber layer is associated with brain atrophy in multiple sclerosis. Neurology 2007; 69: 1603–1609.

Granberg T, Fan Q, Treaba CA, Ouellette R, Herranz E, Mangeat G, et al. In vivo characterization of cortical and white matter neuroaxonal pathology in early multiple sclerosis. Brain 2017; 140: 2912–2926.

Grazioli E, Zivadinov R, Weinstock-Guttman B, Lincoff N, Baier M, Wong JR, et al. Retinal nerve fiber layer thickness is associated with brain MRI outcomes in multiple sclerosis. J Neurol Sci 2008; 268: 12–17.

Green AJ, Mcquaid S, Hauser SL, Allen I V, Lyness R. Ocular pathology in multiple sclerosis: retinal atrophy and inflammation irrespective of disease duration. Brain 2010; 133: 1591–1601.

Greter M, Heppner FL, Lemos MP, Odermatt BM, Goebels N, Laufer T, et al. Dendritic cells permit immune invasion of the CNS in an animal model of multiple sclerosis. Nat Med 2005; 11: 328–334.

De Groot JA, Bergers E, Kamphorst W, Ravid R, Polman CH, Barkhof F, et al. Post-mortem MRI-guided sampling of multiple sclerosis brain lesions Increased yield of active demyelinating and (p)reactive lesions. 2001

Grussu F, Ianuş A, Tur C, Prados F, Schneider T, Kaden E, et al. Relevance of time-dependence for clinically viable diffusion imaging of the spinal cord. Magn Reson Med 2019; 81: 1247–1264.

Grussu F, Schneider T, Tur C, Yates RL, Tachrount M, Ianuş A, et al. Neurite dispersion: a new marker of multiple sclerosis spinal cord pathology? Ann Clin Transl Neurol 2017; 4: 663–679.

Grussu F, Schneider T, Zhang H, Alexander DC, Wheeler-kingshott CAMAM, Wheeler–Kingshott CAM. Neurite orientation dispersion and density imaging of the healthy cervical spinal cord in vivo. Neuroimage 2015; 111: 590–601.

Hafler DA, Compston A, Sawcer S, Lander ES, Daly MJ, De Jager PL, et al. Risk alleles for multiple sclerosis identified by a genomewide study. N Engl J Med 2007; 357: 851–862.

Hagens MH, Burggraaff J, Kilsdonk ID, Ruggieri S, Collorone S, Cortese R, et

al. Impact of 3 Tesla MRI on interobserver agreement in clinically isolated syndrome: A MAGNIMS multicentre study. Mult Scler 2018: 1352458517751647.

Hagens MHJ, Burggraaff J, Kilsdonk ID, de Vos ML, Cawley N, Sbardella E, et al. Three-Tesla MRI does not improve the diagnosis of multiple sclerosis. Neurology 2018; 91: e249–e257.

Hagiwara A, Kamagata K, Shimoji K, Yokoyama K, Andica C, Hori M, et al. White matter abnormalities in multiple sclerosis evaluated by quantitative synthetic MRI, diffusion tensor imaging, and neurite orientation dispersion and density imaging. Am J Neuroradiol 2019; 40: 1642–1648.

Hagström IT, Schneider R, Bellenberg B, Salmen A, Weiler F, Köster O, et al. Relevance of early cervical cord volume loss in the disease evolution of clinically isolated syndrome and early multiple sclerosis: a 2-year follow-up study. J Neurol 2017; 264: 1402–1412.

Haider L, Zrzavy T, Hametner S, Höftberger R, Bagnato F, Grabner G, et al. The topograpy of demyelination and neurodegeneration in the multiple sclerosis brain. Brain 2016; 139: 807–15.

Halliwell B. Oxidative stress and neurodegeneration: where are we now? J Neurochem 2006; 97: 1634–1658.

Hart PH, Gorman S, Finlay-Jones JJ. Modulation of the immune system by UV radiation: More than just the effects of vitamin D? Nat Rev Immunol 2011; 11: 584–596.

Hauser SL, Oksenberg JR, Lincoln R, Garovoy J, Beck RW, Cole SR, et al. Interaction between HLA-DR2 and abnormal brain MRI in optic neuritis and early MS. Neurology 2000; 54: 1859–1861.

He Y, Dagher A, Chen Z, Charil A, Zijdenbos A, Worsley K, et al. Impaired small-world efficiency in structural cortical networks in multiple sclerosis associated with white matter lesion load. Brain 2009; 132: 3366–3379.

Hemmer B, Archelos JJ, Hartung HP. New concepts in the immunopathogenesis of multiple sclerosis. Nat Rev Neurosci 2002; 3: 291–301.

Henderson APD, Altmann DR, Trip SA, Miszkiel KA, Schlottmann PG, Jones SJ, et al. Early factors associated with axonal loss after optic neuritis. Ann Neurol 2011; 70: 955–963.

Henderson APD, Barnett MH, Parratt JDE, Prineas JW. Multiple sclerosis: Distribution of inflammatory cells in newly forming lesions. Ann Neurol 2009; 66: 739–753.

Henderson APD, Trip SA, Schlottmann PG, Altmann DR, Garway-Heath DF, Plant GT, et al. A preliminary longitudinal study of the retinal nerve fiber layer in progressive multiple sclerosis. J Neurol 2010; 257: 1083–1091.

Henry RG, Shieh M, Amirbekian B, Chung SW, Okuda DT, Pelletier D. Connecting white matter injury and thalamic atrophy in clinically isolated syndromes. J Neurol Sci 2009; 282: 61–66.

Hensiek AE, Sawcer SJ, Feakes R, Deans J, Mander A, Akesson E, et al. HLA-DR 15 is associated with female sex and younger age at diagnosis in multiple sclerosis. J Neurol Neurosurg Psychiatry 2002; 72: 184–187.

Hoch MJ, Bruno MT, Shepherd TM. Advanced MRI of the Optic Nerve. J Neuro-Ophthalmology 2017; 37: 187–196.

Hood DC, Kardon RH. A framework for comparing structural and functional measures of glaucomatous damage. Prog Retin Eye Res 2007; 26: 688–710.

Horsfield MA, Sala S, Neema M, Absinta M, Bakshi A, Sormani MP, et al. Rapid semi-automatic segmentation of the spinal cord from magnetic resonance images: application in multiple sclerosis. Neuroimage 2010; 50: 446–55.

Huang J, Liu Y, Zhao T, Shu N, Duan Y, Ren Z, et al. White matter microstructural alterations in clinically isolated syndrome and multiple

sclerosis. J Clin Neurosci 2018; 53: 27–33.

Huber PJ. The behavior of maximum likelihood estimates under non-standard conditions. In: Proceedings of the Fifth Berkeley Symposium on Mathematical Statistics and Probability. University of California Press, Berkeley; 1967. p. 221–233

Inglese M, Madelin G, Oesingmann N, Babb JS, Wu W, Stoeckel B, et al. Brain tissue sodium concentration in multiple sclerosis: a sodium imaging study at 3 tesla. Brain 2010; 133: 847–57.

Jacobs LD, Beck RW, Simon JH, Kinkel RP, Brownscheidle CM, Murray TJ, et al. Intramuscular interferon beta-1a therapy initiated during a first demyelinating event in multiple sclerosis. N Engl J Med 2000; 343: 898–904.

Jenkins TM, Toosy AT. Optic neuritis. Curr Opin Neurol 2017; 30: 61–66.

Jensen JH, Helpern JA, Ramani A, Lu H, Kaczynski K. Diffusional kurtosis imaging: The quantification of non-Gaussian water diffusion by means of magnetic resonance imaging. Magn Reson Med 2005; 53: 1432–1440.

JH van W, W K, CJ DG, MA van W, JA C, R R, et al. Axonal Loss in Multiple Sclerosis Lesions: Magnetic Resonance Imaging Insights Into Substrates of Disability. Ann Neurol 1999; 46

Jonas JB, Dichtl A. Evaluation of the retinal nerve fiber layer. Surv Ophthalmol 1996; 40: 369–378.

Joyce KE, Laurienti PJ, Burdette JH, Hayasaka S. A new measure of centrality for brain networks. PLoS One 2010; 5: e12200.

Kanamori A, Escano MFT, Eno A, Nakamura M, Maeda H, Seya R, et al. Evaluation of the effect of aging on retinal nerve fiber layer thickness measured by optical coherence tomography. Ophthalmologica 2003; 217: 273–278.

Kappos L, Freedman MS, Polman CH, Edan G, Hartung HP, Miller DH, et al. Effect of early versus delayed interferon beta-1b treatment on disability after a first clinical event suggestive of multiple sclerosis: a 3-year follow-up analysis

of the BENEFIT study. Lancet 2007; 370: 389–397.

Kappos L, Moeri D, Radue EW, Schoetzau A, Schweikert K, Barkhof F, et al. Predictive value of gadolinium-enhanced magnetic resonance imaging for relapse rate and changes in disability or impairment in multiple sclerosis: A meta-analysis. Lancet 1999; 353: 964–969.

Kappos L, Polman CH, Freedman MS, Edan G, Hartung HP, Miller DH, et al. Treatment with interferon beta-1b delays conversion to clinically definite and McDonald MS in patients with clinically isolated syndromes. Neurology 2006; 67: 1242–1249.

Kearney H, Schneider T, Yiannakas MC, Altmann DR, Wheeler-Kingshott CAM, Ciccarelli O, et al. Spinal cord grey matter abnormalities are associated with secondary progression and physical disability in multiple sclerosis. J Neurol Neurosurg Psychiatry 2015; 86: 608–614.

Kiselev VG, Hahn KR, Auer DP. Is the brain cortex a fractal? Neuroimage 2003; 20: 1765–74.

Kitley J, Woodhall M, Waters P, Leite MI, Devenney E, Craig J, et al. Myelin-oligodendrocyte glycoprotein antibodies in adults with a neuromyelitis optica phenotype. Neurology 2012; 79: 1273–1277.

Klein A, Tourville J. 101 labeled brain images and a consistent human cortical labeling protocol. Front Neurosci 2012; 6

Kolasa M, Hakulinen U, Helminen M, Hagman S, Raunio M, Rossi M, et al. Longitudinal assessment of clinically isolated syndrome with diffusion tensor imaging and volumetric MRI. Clin Imaging 2015; 39: 207–212.

Kornek B, Lassmann H. Axonal Pathology in Multiple Sclerosis. A Historical Note. Brain Pathol 1999; 9: 651–656.

Koubiyr I, Deloire M, Coupé P, Dulau C, Besson P, Moroso A, et al. Differential Gray Matter Vulnerability in the 1 Year Following a Clinically Isolated Syndrome. Front Neurol 2018; 9: 824.

Krishnamoorthy G, Saxena A, Mars LT, Domingues HS, Mentele R, Ben-Nun A, et al. Myelin-specific T cells also recognize neuronal autoantigen in a transgenic mouse model of multiple sclerosis. Nat Med 2009; 15: 626–632.

Krumbholz M, Theil D, Cepok S, Hemmer B, Kivisäkk P, Ransohoff RM, et al. Chemokines in multiple sclerosis: CXCL12 and CXCL13 up-regulation is differentially linked to CNS immune cell recruitment. Brain 2006; 129: 200–211.

Krumbholz M, Theil D, Derfuss T, Rosenwald A, Schrader F, Monoranu CM, et al. BAFF is produced by astrocytes and up-regulated in multiple sclerosis lesions and primary central nervous system lymphoma. J Exp Med 2005; 201: 195–200.

Kugler A V., Deppe M. Non-lesional cerebellar damage in patients with clinically isolated syndrome: DTI measures predict early conversion into clinically definite multiple sclerosis. NeuroImage Clin 2018; 19: 633–639.

Kuhle J, Barro C, Andreasson U, Derfuss T, Lindberg R, Sandelius Å, et al. Comparison of three analytical platforms for quantification of the neurofilament light chain in blood samples: ELISA, electrochemiluminescence immunoassay and Simoa. Clin Chem Lab Med 2016; 54: 1655–1661.

Kuhle J, Disanto G, Dobson R, Adiutori R, Bianchi L, Topping J, et al. Conversion from clinically isolated syndrome to multiple sclerosis: A large multicantre study. Mult Scler 2015; 21: 1013–1024.

Kurtzke JF. Rating neurologic impairment in multiple sclerosis: an expanded disability status scale (EDSS). Neurology 1983; 33: 1444–52.

Kutzelnigg A, Faber-Rod JC, Bauer J, Lucchinetti CF, Sorensen PS, Laursen H, et al. Widespread demyelination in the cerebellar cortex in multiple sclerosis. Brain Pathol 2007; 17: 38–44.

Kutzelnigg A, Lassmann H. Neuropathology of Cognitive Dysfunction in Multiple Sclerosis. Handb Clin Neurol 2008; 89: 719–723.

Kutzelnigg A, Lassmann H. Pathology of multiple sclerosis and related inflammatory demyelinating diseases. Handb Clin Neurol 2014; 122: 15–58.

Kutzelnigg A, Lucchinetti CF, Stadelmann C, Brück W, Rauschka H, Bergmann M, et al. Cortical demyelination and diffuse white matter injury in multiple sclerosis. Brain 2005; 128: 2705–2712.

Lakhani DA, Schilling KG, Xu J, Bagnato F. Advanced Multicompartment Diffusion MRI Models and Their Application in Multiple Sclerosis. Am J Neuroradiol 2020; 41: 751–757.

Langdon DW, Amato MP, Boringa J, Brochet B, Foley F, Fredrikson S, et al. Recommendations for a brief international cognitive assessment for multiple sclerosis (BICAMS). Mult Scler 2012; 18: 891–898.

Lanzavecchia A. Receptor-Mediated Antigen Uptake and its Effect on Antigen Presentation to Class II-Restricted T Lymphocytes. Annu Rev Immunol 1990; 8: 773–793.

Lassmann H. Comparative Neuropathology of Chronic Experimental Allergic Encephalomyelitis and Multiple Sclerosis. Schriftenr Neurol 1983; 25

Lassmann H. Review: The architecture of inflammatory demyelinating lesions: Implications for studies on pathogenesis. Neuropathol Appl Neurobiol 2011; 37: 698–710.

Lassmann H. Demyelination and neurodegeneration in multiple sclerosis: The role of hypoxia. Ann Neurol 2016; 79: 520–521.

Lennon VA, Wingerchuk DM, Kryzer TJ, Pittock SJ, Lucchinetti CF, Fujihara K, et al. A serum autoantibody marker of neuromyelitis optica: Distinction from multiple sclerosis. Lancet 2004; 364: 2106–2112.

Lerch JP, Worsley K, Shaw WP, Greenstein DK, Lenroot RK, Giedd J, et al. Mapping anatomical correlations across cerebral cortex (MACACC) using cortical thickness from MRI. Neuroimage 2006; 31: 993–1003.

Libbey JE, McCoy LL, Fujinami RS. Molecular Mimicry in Multiple Sclerosis.

Int Rev Neurobiol 2007; 79: 127–147.

Lin F, Yu C, Liu Y, Li K, Lei H. Diffusion tensor group tractography of the corpus callosum in clinically isolated syndrome. Am J Neuroradiol 2011; 32: 92–98.

London F, Zéphir H, Drumez E, Labreuche J, Hadhoum N, Lannoy J, et al. Optical coherence tomography: a window to the optic nerve in clinically isolated syndrome. Brain 2019; 142: 903–915.

Lovas G, Szilágyi N, Majtényi K, Palkovits M, Komoly S. Axonal changes in chronic demyelinated cervical spinal cord plaques. Brain 2000; 123: 308–317.

Lucchinetti C, Brück W, Parisi J, Scheithauer B, Rodriguez M, Lassmann H. A quantitative analysis of oligodendrocytes in multiple sclerosis lesions A study of 113 cases. Brain 1999; 122: 2279–2295.

Lucchinetti C, Brück W, Parisi J, Scheithauer B, Rodriguez M, Lassmann H. Heterogeneity of multiple sclerosis lesions: implications for the pathogenesis of demyelination. Ann Neurol 2000; 47: 707–17.

Lumsden C. The neuropathology of multiple sclerosis. Handb Clin Neurol 1970; 9: 217–309.

Lünemann JD, Jelčić I, Roberts S, Lutterotti A, Tackenberg B, Martin R, et al. EBNA1-specific T cells from patients with multiple sclerosis cross react with myelin antigens and co-produce IFN-γ and IL-2. J Exp Med 2008; 205: 1763–1773.

Lünemann JD, Tintoré M, Messmer B, Strowig T, Rovira Á, Perkal H, et al. Elevated Epstein-Barr virus-encoded nuclear antigen-1 immune responses predict conversion to multiple sclerosis. Ann Neurol 2010; 67: 159–169.

Luo T, Oladosu O, Rawji KS, Zhai P, Pridham G, Hossain S, et al. Characterizing Structural Changes With Devolving Remyelination Following Experimental Demyelination Using High Angular Resolution Diffusion MRI and Texture Analysis. J Magn Reson Imaging 2019; 49: 1750–1759.

Maarouf A, Audoin B, Konstandin S, Rico A, Soulier E, Reuter F, et al.

Topography of brain sodium accumulation in progressive multiple sclerosis. Magn Reson Mater Physics, Biol Med 2014; 27: 53–62.

Maarouf A, Audoin B, Pariollaud F, Gherib S, Rico A, Soulier E, et al. Increased total sodium concentration in gray matter better explains cognition than atrophy in MS. Neurology 2017; 88: 289–295.

Magliozzi R, Howell O, Vora A, Serafini B, Nicholas R, Puopolo M, et al. Meningeal B-cell follicles in secondary progressive multiple sclerosis associate with early onset of disease and severe cortical pathology. Brain 2007; 130: 1089–104.

Maguire EA, Gadian DG, Johnsrude IS, Good CD, Ashburner J, Frackowiak RS, et al. Navigation-related structural change in the hippocampi of taxi drivers. Proc Natl Acad Sci U S A 2000; 97: 4398–403.

Mahad DJ, Ziabreva I, Campbell G, Lax N, White K, Hanson PS, et al. Mitochondrial changes within axons in multiple sclerosis. Brain 2009; 132: 1161–74.

Manca R, Sharrack B, Paling D, Wilkinson ID, Venneri A. Brain connectivity and cognitive processing speed in multiple sclerosis: A systematic review. J Neurol Sci 2018; 388: 115–127.

Marik C, Felts PA, Bauer J, Lassmann H, Smith KJ. Lesion genesis in a subset of patients with multiple sclerosis: a role for innate immunity? Brain 2007; 130: 2800–2815.

Martinelli V, Dalla Costa G, Colombo B, Dalla Libera D, Rubinacci A, Filippi M, et al. Vitamin D levels and risk of multiple sclerosis in patients with clinically isolated syndromes. Mult Scler 2014; 20: 147–155.

Martinez-Lapiscina EH, Arnow S, Wilson JA, Saidha S, Preiningerova JL, Oberwahrenbrock T, et al. Retinal thickness measured with optical coherence tomography and risk of disability worsening in multiple sclerosis: A cohort study. Lancet Neurol 2016; 15: 574–584.

Martínez-Lapiscina EH, Fraga-Pumar E, Gabilondo I, Martínez-Heras E, Torres-Torres R, Ortiz-Pérez S, et al. The multiple sclerosis visual pathway cohort: Understanding neurodegeneration in MS. BMC Res Notes 2014; 7

Masterman T, Ligers A, Olsson T, Andersson M, Olerup O, Hillert J. HLA-DR15 is associated with lower age at onset in multiple sclerosis. Ann Neurol 2000; 48: 211–219.

Maudsley AA, Hilal SK. Biological aspects of sodium-23 imaging. Br Med Bull 1984; 40: 165–166.

McKee JB, Elston J, Evangelou N, Gerry S, Fugger L, Kennard C, et al. Amiloride Clinical Trial In Optic Neuritis (ACTION) protocol: A randomised, double blind, placebo controlled trial. BMJ Open 2015; 5

McMahon EJ, Bailey SL, Castenada CV, Waldner H, Miller SD. Epitope spreading initiates in the CNS in two mouse models of multiple sclerosis. Nat Med 2005; 11: 335–339.

Ménage MJ, Papakostopoulos D, Dean Hart JC, Papakostopoulos S, Gogolitsyn Y. The Farnsworth-Munsell 100 hue test in the first episode of demyelinating optic neuritis. Br J Ophthalmol 1993; 77: 68–74.

Meuth SG, Herrmann AM, Simon OJ, Siffrin V, Melzer N, Bittner S, et al. Cytotoxic CD8+ T cell-neuron interactions: Perforin-dependent electrical silencing precedes but is not causally linked to neuronal cell death. J Neurosci 2009; 29: 15397–15409.

Mews I, Bergmann M, Bunkowski S, Gullotta F, Brück W. Oligodendrocyte and axon pathology in clinically silent multiple sclerosis lesions. Mult Scler 1998; 4: 55–62.

Miller DH, Chard DT, Ciccarelli O. Clinically isolated syndromes. Lancet Neurol 2012; 11: 157–169.

Minneboo A, Barkhof F, Polman CH, Uitdehaag BMJ, Knol DL, Castelijns JA. Infratentorial Lesions Predict Long-term Disability in Patients with Initial

Findings Suggestive of Multiple Sclerosis. Arch Neurol 2004; 61: 217–221.

Moccia M, Prados F, Filippi M, Rocca MA, Valsasina P, Brownlee WJ, et al. Longitudinal spinal cord atrophy in multiple sclerosis using the generalized boundary shift integral. Ann Neurol 2019; 86: 704–713.

Moccia M, Ruggieri S, Ianniello A, Toosy A, Pozzilli C, Ciccarelli O. Advances in spinal cord imaging in multiple sclerosis. Ther Adv Neurol Disord 2019; 12: 175628641984059.

Mollink J, Kleinnijenhuis M, Cappellen van Walsum AM van, Sotiropoulos SN, Cottaar M, Mirfin C, et al. Evaluating fibre orientation dispersion in white matter: Comparison of diffusion MRI, histology and polarized light imaging. Neuroimage 2017; 157: 561–574.

Montalban X, Tintoré M, Swanton J, Barkhof F, Fazekas F, Filippi M, et al. MRI criteria for MS in patients with clinically isolated syndromes. Neurology 2010; 74: 427–434.

Moroso A, Ruet A, Lamargue-Hamel D, Munsch F, Deloire M, Coupé P, et al. Microstructural analyses of the posterior cerebellar lobules in relapsing-onset multiple sclerosis and their implication in cognitive impairment. PLoS One 2017; 12

Moutsianas L, Jostins L, Beecham AH, Dilthey AT, Xifara DK, Ban M, et al. Class II HLA interactions modulate genetic risk for multiple sclerosis. Nat Genet 2015; 47: 1107–1113.

Mowry EM, Pesic M, Grimes B, Deen SR, Bacchetti P, Waubant E. Clinical predictors of early second event in patients with clinically isolated syndrome. J Neurol 2009; 256: 1061–1066.

Muhlert N, Sethi V, Schneider T, Daga P, Cipolotti L, Haroon HA, et al. Diffusion MRI-based cortical complexity alterations associated with executive function in multiple sclerosis. J Magn Reson Imaging 2013; 38: 54–63.

Munger KL, Fitzgerald KC, Freedman MS, Hartung HP, Miller DH, Montalbán

X, et al. No association of multiple sclerosis activity and progression with EBV or tobacco use in BENEFIT. Neurology 2015; 85: 1694–1701.

Muthuraman M, Fleischer V, Kolber P, Luessi F, Zipp F, Groppa S. Structural brain network characteristics can differentiate CIS from early RRMS. Front Neurosci 2016; 10: 1–12.

Nagel AM, Amarteifio E, Lehmann-Horn F, Jurkat-Rott K, Semmler W, Schad LR, et al. 3 Tesla sodium inversion recovery magnetic resonance imaging allows for improved visualization of intracellular sodium content changes in muscular channelopathies. Invest Radiol 2011; 46: 759–766.

Nagpal S, Na S, Rathnachalam R. Noncalcemic actions of vitamin D receptor ligands. Endocr Rev 2005; 26: 662–687.

Nesbit GM, Forbes GS, Scheithauer BW, Okazaki H, Rodriguez M. Multiple sclerosis: Histopathologic and MR and/or CT correlation in 37 cases at biopsy and three cases at autopsy. Radiology 1991; 180: 467–474.

Neumann H, Cavalié A, Jenne DE, Wekerle H. Induction of MHC class I genes in neurons. Science (80-) 1995; 269: 549–552.

Neumann H, Medana IM, Bauer J, Lassmann H. Cytotoxic T lymphocytes in autoimmune and degenerative CNS diseases. Trends Neurosci 2002; 25: 313–319.

Nguyen J, Rothman A, Fitzgerald K, Whetstone A, Syc-Mazurek S, Aquino J, et al. Visual Pathway Measures are Associated with Neuropsychological Function in Multiple Sclerosis. Curr Eye Res 2018; 43

Nielsen AS, Kinkel RP, Tinelli E, Benner T, Cohen-Adad J, Mainero C. Focal cortical lesion detection in multiple sclerosis: 3 tesla DIR versus 7 tesla FLASH-T2. J Magn Reson Imaging 2012; 35: 537–542.

Nikić I, Merkler D, Sorbara C, Brinkoetter M, Kreutzfeldt M, Bareyre FM, et al. A reversible form of axon damage in experimental autoimmune encephalomyelitis and multiple sclerosis. Nat Med 2011; 17: 495–499.

O'riordan JI, Thompson AJ, Kingsley DPE, Macmanus DG, Kendall BE, Rudge P, et al. The prognostic value of brain MRI in clinically isolated syndromes of the CNS A 10-year follow-up. Brain 1998; 121: 495–503.

Ogden TE. Nerve fiber layer of the owl monkey retina: retinotopic organization. Invest Ophthalmol Vis Sci 1983; 24: 265–9.

Optic Neuritis Study Group. Multiple Sclerosis Risk After Optic Neuritis. Arch Neurol 2008; 65: 727–32.

Optic Neuritis Study Group TONS. Multiple sclerosis risk after optic neuritis: final optic neuritis treatment trial follow-up. Arch Neurol 2008; 65: 727–732.

Pais Ribeiro JL, Martins da Silva A, Vilhena E, Moreira I, Santos E, Mendonça D. The hospital anxiety and depression scale, in patients with multiple sclerosis. Neuropsychiatr Dis Treat 2018; Volume 14: 3193–3197.

Paling D, Solanky BS, Riemer F, Tozer DJ, Wheeler-Kingshott CAM, Kapoor R, et al. Sodium accumulation is associated with disability and a progressive course in multiple sclerosis. Brain 2013; 136: 2305–17.

Parker TD, Slattery CF, Zhang J, Nicholas JM, Paterson RW, Foulkes AJM, et al. Cortical microstructure in young onset Alzheimer's disease using neurite orientation dispersion and density imaging. Hum Brain Mapp 2018; 39: 3005–3017.

Parmenter BA, Testa SM, Schretlen DJ, Weinstock-Guttman B, Benedict RHB. The utility of regression-based norms in interpreting the minimal assessment of cognitive function in multiple sclerosis (MACFIMS). J Int Neuropsychol Soc 2010; 16: 6–16.

Patrikios P, Stadelmann C, Kutzelnigg A, Rauschka H, Schmidbauer M, Laursen H, et al. Remyelination is extensive in a subset of multiple sclerosis patients. Brain 2006; 129: 3165–72.

Pender MP. The Essential Role of Epstein-Barr Virus in the Pathogenesis of Multiple Sclerosis. Neurosci 2011; 17: 351–367.

Perron H, Lang A. The human endogenous retrovirus link between genes and environment in multiple sclerosis and in multifactorial diseases associating neuroinflammation. Clin Rev Allergy Immunol 2010; 39: 51–61.

Peterson JW, Bö L, Mörk S, Chang A, Trapp BD. Transected neurites, apoptotic neurons, and reduced inflammation in cortical multiple sclerosis lesions. Ann Neurol 2001; 50: 389–400.

Petracca M, Vancea RO, Fleysher L, Jonkman LE, Oesingmann N, Inglese M. Brain intra- and extracellular sodium concentration in multiple sclerosis: a 7 T MRI study. Brain 2016; 139: 795–806.

Petzold A, de Boer JF, Schippling S, Vermersch P, Kardon R, Green A, et al. Optical coherence tomography in multiple sclerosis: A systematic review and meta-analysis. Lancet Neurol 2010; 9: 921–932.

Pierpaoli C, Barnett A, Pajevic S, Chen R, Penix LR, Virta A, et al. Water diffusion changes in wallerian degeneration and their dependence on white matter architecture. Neuroimage 2001; 13: 1174–1185.

Pitt D, Werner P, Raine CS. Glutamate excitotoxicity in a model of multiple sclerosis. Nat Med 2000; 6: 67–70.

Planche V, Ruet A, Coupé P, Lamargue-Hamel D, Deloire M, Pereira B, et al. Hippocampal microstructural damage correlates with memory impairment in clinically isolated syndrome suggestive of multiple sclerosis. Mult Scler J 2017; 23: 1214–1224.

Plumb J, McQuaid S, Mirakhur M, Kirk J. Abnormal Endothelial Tight Junctions in Active Lesions and Normal-appearing White Matter in Multiple Sclerosis. Brain Pathol 2006; 12: 154–169.

Polman C, Kappos L, Freedman MS, Edan G, Hartung HP, Miller DH, et al. Subgroups of the BENEFIT study: Risk of developing MS and treatment effect of interferon beta-1b. J Neurol 2008; 255: 480–487.

Polman CH, Reingold SC, Banwell B, Clanet M, Cohen JA, Filippi M, et al.

Diagnostic criteria for multiple sclerosis: 2010 Revisions to the McDonald criteria. Ann Neurol 2011; 69: 292–302.

Prados F, Cardoso MJ, Burgos N, Gandini Wheeler-Kingshott CAM, Ourselin S. NiftyWeb: web based platform for image processing on the cloud. Int Soc Magn Reson Med 24th Annu Meet Exhib 2016

Prados F, Cardoso MJ, Kanber B, Ciccarelli O, Kapoor R, Gandini Wheeler-Kingshott CAM, et al. A multi-time-point modality-agnostic patch-based method for lesion filling in multiple sclerosis. Neuroimage 2016; 139: 376–384.

Prados F, Cardoso MJ, MacManus D, Wheeler-Kingshott CAM, Ourselin S. A modality-agnostic patch-based technique for lesion filling in multiple sclerosis. Med Image Comput Comput Assist Interv 2014; 17: 781–8.

Probert L, Eugster H-P, Akassoglou K, Bauer J, Frei K, Lassmann H, et al. TNFR1 signalling is critical for the development of demyelination and the limitation of T-cell responses during immune-mediated CNS disease. Brain 2000; 123: 2005–2019.

Ranjeva JP, Pelletier J, Confort-Gouny S, Ibarrola D, Audoin B, Le Fur Y, et al. MRI/MRS of corpus callosum in patients with clinically isolated syndrome suggestive of multiple sclerosis. Mult Scler 2003; 9: 554–565.

Rao A, Singh AK, Mukherjee S, Chowdhury M. Comparing focal and global responses on multifocal electroretinogram with retinal nerve fibre layer thickness by spectral domain optical coherence tomography in glaucoma. Br J Ophthalmol 2015; 99: 500–507.

Raz E, Cercignani M, Sbardella E, Totaro P, Pozzilli C, Bozzali M, et al. Clinically Isolated Syndrome Suggestive of Multiple Sclerosis: Voxelwise Regional Investigation of White and Gray Matter 1. Radiology 2010; 254

Reiber H, Ungefehr S, Jacobi C. The intrathecal, polyspecific and oligoclonal immune response in multiple sclerosis. Mult Scler 1998; 4: 111–117.

Reich DS, Smith SA, Gordon-Lipkin EM, Ozturk A, Caffo BS, Balcer LJ, et al.

Damage to the optic radiation in multiple sclerosis is associated with retinal injury and visual disability. Arch Neurol 2009; 66: 998–1006.

Reith W, Steimle V, Durand B, Kobr M, Mach B. Regulation of MHC Class II Gene Expression. Immunobiology 1995; 193: 248–253.

Reuter F, Zaaraoui W, Crespy L, Faivre A, Rico A, Malikova I, et al. Cognitive impairment at the onset of multiple sclerosis: Relationship to lesion location. Mult Scler 2011; 17: 755–758.

Rimkus CM, Schoonheim MM, Steenwijk MD, Vrenken H, Eijlers AJC, Killestein J, et al. Gray matter networks and cognitive impairment in multiple sclerosis. Mult Scler J 2018

Rizzo M, Anderson SW, Dawson J, Nawrot M. Vision and cognition in Alzheimer's disease. Neuropsychologia 2000; 38: 1157–1169.

Rocca MA, Colombo B, Falini A, Ghezzi A, Martinelli V, Scotti G, et al. Cortical adaptation in patients with MS: A cross-sectional functional MRI study of disease phenotypes. Lancet Neurol 2005; 4: 618–626.

Rocca MA, Preziosa P, Filippi M. What role should spinal cord MRI take in the future of multiple sclerosis surveillance? Expert Rev Neurother 2020: 1–15.

Roosendaal SD, Schoonheim MM, Hulst HE, Sanz-Arigita EJ, Smith SM, Geurts JJG, et al. Resting state networks change in clinically isolated syndrome. Brain 2010; 133: 1612–1621.

Rovaris M, Judica E, Ceccarelli A, Ghezzi A, Martinelli V, Comi G, et al. A 3-year diffusion tensor MRI study of grey matter damage progression during the earliest clinical stage of MS. J Neurol 2008; 255: 1209–1214.

Rovira À, Wattjes MP, Tintoré M, Tur C, Yousry TA, Sormani MP, et al. Evidence-based guidelines: MAGNIMS consensus guidelines on the use of MRI in multiple sclerosis-clinical implementation in the diagnostic process. Nat Rev Neurol 2015; 11: 471–82.

Ruano L, Portaccio E, Goretti B, Niccolai C, Severo M, Patti F, et al. Age and

disability drive cognitive impairment in multiple sclerosis across disease subtypes. Mult Scler 2017; 23: 1258–1267.

Rubinov M, Sporns O. Complex network measures of brain connectivity: Uses and interpretations. Neuroimage 2010; 52: 1059–1069.

Sabadia SB, Nolan RC, Galetta KM, Narayana KM, Wilson JA, Calabresi PA, et al. 20/40 or Better Visual Acuity After Optic Neuritis. J Neuro-Ophthalmology 2016; 36: 369–376.

Saidha S, Al-Louzi O, Ratchford JN, Bhargava P, Oh J, Newsome SD, et al. Optical coherence tomography reflects brain atrophy in multiple sclerosis: A four-year study. Ann Neurol 2015; 78: 801–813.

Saidha S, Syc SB, Durbin MK, Eckstein C, Oakley JD, Meyer SA, et al. Visual dysfunction in multiple sclerosis correlates better with optical coherence tomography derived estimates of macular ganglion cell layer thickness than peripapillary retinal nerve fiber layer thickness. Mult Scler J 2011; 17: 1449–1463.

Sailer M, O'Riordan JI, Thompson AJ, Kingsley DP, MacManus DG, McDonald WI, et al. Quantitative MRI in patients with clinically isolated syndromes suggestive of demyelination. Neurology 1999; 52: 599–606.

Sanchez-Dalmau B, Martinez-Lapiscina EH, Torres-Torres R, Ortiz-Perez S, Zubizarreta I, Pulido-Valdeolivas I V, et al. Early retinal atrophy predicts long-term visual impairment after acute optic neuritis. Mult Scler 2018; 24: 1196–1204.

De Santis S, Bastiani M, Droby A, Kolber P, Zipp F, Pracht E, et al. Characterizing Microstructural Tissue Properties in Multiple Sclerosis with Diffusion MRI at 7 T and 3 T: The Impact of the Experimental Design. Neuroscience 2019; 403: 17–26.

Sato K, Kerever A, Kamagata K, Tsuruta K, Irie R, Tagawa K, et al. Understanding microstructure of the brain by comparison of neurite orientation dispersion and density imaging (NODDI) with transparent mouse brain. Acta

Radiol open 2017; 6: 2058460117703816.

Schilling KG, By S, Feiler HR, Box BA, O'Grady KP, Witt A, et al. Diffusion MRI microstructural models in the cervical spinal cord – Application, normative values, and correlations with histological analysis. Neuroimage 2019; 201

Schilling KG, Janve V, Gao Y, Stepniewska I, Landman BA, Anderson AW. Histological validation of diffusion MRI fiber orientation distributions and dispersion. Neuroimage 2018; 165: 200–221.

Schirmer L, Albert M, Buss A, Schulz-Schaeffer WJ, Antel JP, BrÃ¼ck W, et al. Substantial early, but nonprogressive neuronal loss in multiple sclerosis (ms) spinal cord. Ann Neurol 2009; 66: 698–704.

Schmierer K, Wheeler-Kingshott CAM, Boulby PA, Scaravilli F, Altmann DR, Barker GJ, et al. Diffusion tensor imaging of post mortem multiple sclerosis brain. Neuroimage 2007; 35: 467–477.

Schneider R, Genç E, Ahlborn C, Gold R, Lukas C, Bellenberg B. Temporal Dynamics of Diffusion Metrics in Early Multiple Sclerosis and Clinically Isolated Syndrome: A 2-Year Follow-Up Tract-Based Spatial Statistics Study. Front Neurol 2019; 10

Schneider T, Brownlee WJ, Zhang H, Ciccarelli O, Miller DH, Gandini Wheeler-Kingshott CAM, et al. Sensitivity of multi-shell NODDI to multiple sclerosis white matter changes: a pilot study. Funct Neurol 2017; 32: 97.

Seewann A, Vrenken H, Van Der Valk P, Blezer ELA, Knol DL, Castelijns JA, et al. Diffusely abnormal white matter in chronic multiple sclerosis: Imaging and histopathologic analysis. Arch Neurol 2009; 66: 601–609.

Sepehrband F, Clark KA, Ullmann JFP, Kurniawan ND, Leanage G, Reutens DC, et al. Brain tissue compartment density estimated using diffusion-weighted MRI yields tissue parameters consistent with histology. Hum Brain Mapp 2015; 36: 3687–3702.

Serafini B, Rosicarelli B, Magliozzi R, Stigliano E, Aloisi F. Detection of ectopic

B-cell follicles with germinal centers in the meninges of patients with secondary progressive multiple sclerosis. Brain Pathol 2004; 14: 164–74.

Sethi V, Yousry TA, Muhlert N, Ron M, Golay X, Wheeler-Kingshott C, et al. Improved detection of cortical MS lesions with phase-sensitive inversion recovery MRI. J Neurol Neurosurg Psychiatry 2012; 83: 877–82.

Shi R, Blight AR. Compression injury of mammalian spinal cord in vitro and the dynamics of action potential conduction failure. J Neurophysiol 1996; 76: 1572–1580.

Shields SD, Cheng X, Gasser A, Saab CY, Tyrrell L, Eastman EM, et al. A channelopathy contributes to cerebellar dysfunction in a model of multiple sclerosis. Ann Neurol 2012; 71: 186–194.

Simon JH. Brain and spinal cord atrophy in multiple sclerosis. Neuroimaging Clin N Am 2000; 10: 753–70 ,ix.

Smith KJ, Lassmann H. The role of nitric oxide in multiple sclerosis. Lancet Neurol 2002; 1: 232–241.

Sospedra M, Martin R. Immunology of multiple sclerosis. Annu Rev Immunol 2005; 23: 683–747.

Spanò B, Giulietti G, Pisani V, Morreale M, Tuzzi E, Nocentini U, et al. Disruption of neurite morphology parallels MS progression. Neurol - Neuroimmunol Neuroinflammation 2018; 5: e502.

De Stefano N, Giorgio A, Battaglini M, Rovaris M, Sormani MP, Barkhof F, et al. Assessing brain atrophy rates in a large population of untreated multiple sclerosis subtypes. Neurology 2010; 74: 1868–1876.

De Stefano N, Narayanan S, Francis SJ, Smith S, Mortilla M, Carmela Tartaglia M, et al. Diffuse axonal and tissue injury in patients with multiple sclerosis with low cerebral lesion load and no disability. Arch Neurol 2002; 59: 1565–1571.

Steiner I, Nisipianu P, Wirguin I. Infection and the etiology and pathogenesis

of multiple sclerosis. Curr Neurol Neurosci Rep 2001; 1: 271–276.

Strasser-Fuchs S, Enzinger C, Ropele S, Wallner M, Fazekas F. Clinically benign multiple sclerosis despite large T2 lesion load: Can we explain this paradox? Mult Scler J 2008; 14: 205–211.

Sudre CH, Cardoso MJ, Bouvy WH, Biessels GJ, Barnes J, Ourselin S. Bayesian model selection for pathological neuroimaging data applied to white matter lesion segmentation. IEEE Trans Med Imaging 2015; 34: 2079–102.

Sumowski JF, Rocca MA, Leavitt VM, Dackovic J, Mesaros S, Drulovic J, et al. Brain reserve and cognitive reserve protect against cognitive decline over 4.5 years in MS. Neurology 2014; 82: 1776–1783.

Swanton JK, Fernando KT, Dalton CM, Miszkiel KA, Altmann DR, Plant GT, et al. Early MRI in optic neuritis: The risk for disability. Neurology 2009; 72: 542–550.

Swanton JK, Fernando KT, Dalton CM, Miszkiel KA, Altmann DR, Plant GT, et al. Early MRI in optic neuritis: The risk for clinically definite multiple sclerosis. Mult Scler 2010; 16: 156–165.

Szegedi S, Dal-Bianco P, Stögmann E, Traub-Weidinger T, Rainer M, Masching A, et al. Anatomical and functional changes in the retina in patients with Alzheimer's disease and mild cognitive impairment. Acta Ophthalmol 2020

Talman LS, Bisker ER, Sackel DJ, Long DA, Galetta KM, Ratchford JN, et al. Longitudinal study of vision and retinal nerve fiber layer thickness in multiple sclerosis. Ann Neurol 2010; 67: 749–760.

Tavazzi E, Zivadinov R, Dwyer MG, Jakimovski D, Singhal T, Weinstock-Guttman B, et al. MRI biomarkers of disease progression and conversion to secondary-progressive multiple sclerosis. Expert Rev Neurother 2020

Tewarie P, Balk L, Costello F, Green A, Martin R, Schippling S, et al. The OSCAR-IB Consensus Criteria for Retinal OCT Quality Assessment. PLoS

One 2012; 7: e34823.

Tewarie P, Steenwijk MD, Tijms BM, Daams M, Balk LJ, Stam CJ, et al. Disruption of structural and functional networks in long-standing multiple sclerosis. Hum Brain Mapp 2014; 35: 5946–5961.

Thompson AJ, Banwell BL, Barkhof F, Carroll WM, Coetzee T, Comi G, et al. Diagnosis of multiple sclerosis: 2017 revisions of the McDonald criteria. Lancet Neurol 2018; 17: 162–173.

Thulborn KR, Davis D, Adams H, Gindin T, Zhou J. Quantitative tissue sodium concentration mapping of the growth of focal cerebral tumors with sodium magnetic resonance imaging. Magn Reson Med 1999; 41: 351–9.

Tijms BM, Möller C, Vrenken H, Wink AM, de Haan W, van der Flier WM, et al. Single-Subject Grey Matter Graphs in Alzheimer's Disease. PLoS One 2013; 8: 1–9.

Tijms BM, Seris P, Willshaw DJ, Lawrie SM. Similarity-based extraction of individual networks from gray matter MRI scans. Cereb Cortex 2012; 22: 1530–1541.

Timmers I, Roebroeck A, Bastiani M, Jansma B, Rubio-Gozalbo E, Zhang H. Assessing Microstructural Substrates of White Matter Abnormalities: A Comparative Study Using DTI and NODDI. PLoS One 2016; 11: e0167884.

Tintoré M, Rovira A, Arrambide G, Mitjana R, Río J, Auger C, et al. Brainstem lesions in clinically isolated syndromes. Neurology 2010; 75: 1933–1938.

Tintoré M, Rovira A, Brieva L, Grivé E, Jardí R, Borrás C, et al. Isolated demyelinating syndromes: comparison of CSF oligoclonal bands and different MR imaging criteria to predict conversion to CDMS. Mult Scler J 2001; 7: 359–363.

Tintoré M, Rovira A, Río J, Nos C, Grivé E, Téllez N, et al. Baseline MRI predicts future attacks and disability in clinically isolated syndromes. Neurology 2006; 67: 968–972.

Tintoré M, Rovira À, Río J, Otero-Romero S, Arrambide G, Tur C, et al. Defining high, medium and low impact prognostic factors for developing multiple sclerosis. Brain 2015; 138: 1863–1874.

Toledo J, Sepulcre J, Salinas-Alaman A, García-Layana A, Murie-Fernandez M, Bejarano B, et al. Retinal nerve fiber layer atrophy is associated with physical and cognitive disability in multiple sclerosis. Mult Scler J 2008; 14: 906–912.

Tomassini V, Matthews PM, Thompson AJ, Fuglø D, Geurts JJ, Johansen-Berg H, et al. Neuroplasticity and functional recovery in multiple sclerosis. Nat Rev Neurol 2012; 8: 635–46.

Trapp BD, Nave K-A. Multiple Sclerosis: An Immune or Neurodegenerative Disorder? Annu Rev Neurosci 2008; 31: 247–269.

Trapp BD, Peterson J, Ransohoff RM, Rudick R, Mörk S, Bö L. Axonal transection in the lesions of multiple sclerosis. N Engl J Med 1998; 338: 278–285.

Trapp BD, Stys PK. Virtual hypoxia and chronic necrosis of demyelinated axons in multiple sclerosis. Lancet Neurol 2009; 8: 280–291.

Trip SA, Schlottmann PG, Jones SJ, Altmann DR, Garway-Heath DF, Thompson AJ, et al. Retinal nerve fiber layer axonal loss and visual dysfunction in optic neuritis. Ann Neurol 2005; 58: 383–391.

Tuch DS, Reese TG, Wiegell MR, Makris N, Belliveau JW, Wedeen VJ. High angular resolution diffusion imaging reveals intravoxel white matter fiber heterogeneity. Magn Reson Med 2002; 48: 577–82.

Tur C, Goodkin O, Altmann DR, Jenkins TM, Miszkiel K, Mirigliani A, et al. Longitudinal evidence for anterograde trans-synaptic degeneration after optic neuritis. Brain 2016; 139: 816–828.

Uher T, Blahova-Dusankova J, Horakova D, Bergsland N, Tyblova M, Benedict RHB, et al. Longitudinal MRI and neuropsychological assessment of patients

with clinically isolated syndrome. J Neurol 2014; 261: 1735–1744.

Villoslada P, Cuneo A, Gelfand J, Hauser SL, Green A. Color vision is strongly associated with retinal thinning in multiple sclerosis. Mult Scler J 2012; 18: 991–999.

Viterbo RG, Iaffaldano P, Trojano M. Verbal fluency deficits in clinically isolated syndrome suggestive of multiple sclerosis. J Neurol Sci 2013; 330: 56–60.

Vos CMP, Geurts JJG, Montagne L, Van Haastert ES, Bö L, Van Der Valk P, et al. Blood-brain barrier alterations in both focal and diffuse abnormalities on postmortem MRI in multiple sclerosis. Neurobiol Dis 2005; 20: 953–960.

Wakefield AJ, More LJ, Difford J, McLaughlin JE. Immunohistochemical study of vascular injury in acute multiple sclerosis. J Clin Pathol 1994; 47: 129–133.

van Walderveen MA, Kamphorst W, Scheltens P, van Waesberghe JH, Ravid R, Valk J, et al. Histopathologic correlate of hypointense lesions on T1-weighted spin-echo MRI in multiple sclerosis. Neurology 1998; 50: 1282–8.

Wang N, Zhang J, Cofer G, Qi Y, Anderson RJ, White LE, et al. Neurite orientation dispersion and density imaging of mouse brain microstructure. Brain Struct Funct 2019; 224: 1797–1813.

Watts DJ, Strogatz SH. Collective dynamics of ‘small-world’ networks. Nature 1998; 393: 440–442.

Waxman SG. Nitric oxide and the axonal death cascade. Ann Neurol 2003; 53: 150–153.

Waxman SG. Mechanisms of disease: sodium channels and neuroprotection in multiple sclerosis-current status. Nat Clin Pract Neurol 2008; 4: 159–69.

Waxman SG, Craner MJ, Black JA. Na + channel expression along axons in multiple sclerosis and its models. Trends Pharmacol Sci 2004; 25: 584–591.

Wegner C, Esiri MM, Chance SA, Palace J, Matthews PM. Neocortical neuronal, synaptic, and glial loss in multiple sclerosis. Neurology 2006; 67:

960–967.

Wheeler-Kingshott CAM, Cercignani M. About “axial” and “radial” diffusivities. Magn Reson Med 2009; 61: 1255–1260.

White H. A Heteroskedasticity-Consistent Covariance Matrix Estimator and a Direct Test for Heteroskedasticity. Econometrica 1980; 48: 817–838.

Wieder L, Gäde G, Pech LM, Zimmermann H, Wernecke K-D, Dörr J-M, et al. Low contrast visual acuity testing is associated with cognitive performance in multiple sclerosis: a cross-sectional pilot study. BMC Neurol 2013; 13: 167.

van Wijk BCM, Stam CJ, Daffertshofer A. Comparing brain networks of different size and connectivity density using graph theory. PLoS One 2010; 5: e13701.

Wingerchuk DM, Banwell B, Bennett JL, Cabre P, Carroll W, Chitnis T, et al. International consensus diagnostic criteria for neuromyelitis optica spectrum disorders. Neurology 2015; 85: 177–189.

Wolswijk G. Oligodendrocyte survival, loss and birth in lesions of chronic-stage multiple sclerosis. Brain 2000; 123: 105–115.

Wolswijk G. Oligodendrocyte precursor cells in the demyelinated multiple sclerosis spinal cord. Brain 2002; 125: 338–349.

Wu GF, Schwartz ED, Lei T, Souza A, Mishra S, Jacobs DA, et al. Relation of vision to global and regional brain MRI in multiple sclerosis. Neurology 2007; 69: 2128–2135.

Wucherpfennig KW, Strominger JL. Molecular mimicry in T cell-mediated autoimmunity: Viral peptides activate human T cell clones specific for myelin basic protein. Cell 1995; 80: 695–705.

Wynford-Thomas R, Jacob A, Tomassini V. Neurological update: MOG antibody disease. J Neurol 2019; 266: 1280–1286.

Yi SY, Barnett BR, Torres-Velázquez M, Zhang Y, Hurley SA, Rowley PA, et

al. Detecting Microglial Density With Quantitative Multi-Compartment Diffusion MRI. Front Neurosci 2019; 13: 81.

Yiannakas MC, Kearney H, Samson RS, Chard DT, Ciccarelli O, Miller DH, et al. Feasibility of grey matter and white matter segmentation of the upper cervical cord in vivo: A pilot study with application to magnetisation transfer measurements. Neuroimage 2012; 63: 1054–1059.

Yuksel B, Dogan B, Koctekin B, Atis N, Erdal A, Kurtulus F, et al. Color vision testing versus pattern visual evoked potentials and optical coherence tomography parameters in subclinical optic nerve involvement in multiple sclerosis. J Clin Neurosci 2019; 61: 48–53.

Zaaraoui W, Konstandin S, Audoin B, Nagel AM, Rico A, Malikova I, et al. Distribution of Brain Sodium Accumulation Correlates with Disability in Multiple Sclerosis: A Cross-sectional 23 Na MR Imaging Study. Radiology 2012; 264: 859–867.

Zhang H, Schneider T, Wheeler-Kingshott CA, Alexander DC. NODDI: Practical in vivo neurite orientation dispersion and density imaging of the human brain. Neuroimage 2012; 61: 1000–1016.

Zhang J, Gregory S, Scahill RI, Durr A, Thomas DL, Lehericy S, et al. In vivo characterization of white matter pathology in premanifest huntington's disease. Ann Neurol 2018; 84: 497–504.

Zimmermann H, Freing A, Kaufhold F, Gaede G, Bohn E, Bock M, et al. Optic neuritis interferes with optical coherence tomography and magnetic resonance imaging correlations. Mult Scler J 2013; 19: 443–450.

Zipp F, Aktas O. The brain as a target of inflammation: common pathways link inflammatory and neurodegenerative diseases. Trends Neurosci 2006; 29: 518–527.

Zivadinov R, Sepcic J, Nasuelli D, De Masi R, Bragadin LM, Tommasi MA, et al. A longitudinal study of brain atrophy and cognitive disturbances in the early phase of relapsing-remitting multiple sclerosis. J Neurol Neurosurg Psychiatry

2001; 70: 773–80.

Zuo X-N, Ehmke R, Mennes M, Imperati D, Castellanos FX, Sporns O, et al. Network Centrality in the Human Functional Connectome. Cereb Cortex 2012; 22: 1862–1875.

3